Performance of drains in earthquake-induced liquefaction mitigation under new and existing buildings

Samy Garcia Torres

Department of Engineering
University of Cambridge

This dissertation is submitted for the degree of
Doctor of Philosophy

Murray Edwards College September, 2020

Declaration

This thesis is the result of my own work and includes nothing which is the outcome of work done in collaboration except as declared in the Preface and specified in the text. It is not substantially the same as any that I have submitted, or, is being concurrently submitted for a degree or diploma or other qualification at the University of Cambridge or any other University or similar institution except as declared in the Preface and specified in the text. I further state that no substantial part of my thesis has already been submitted, or, is being concurrently submitted for any such degree, diploma or other qualification at the University of Cambridge or any other University or similar institution except as declared in the Preface and specified in the text. It does not exceed the prescribed word limit for the relevant Degree Committee.

Samy Garcia Torres
September 2020

Abstract

Performance of drains in earthquake-induced liquefaction mitigation under new and existing buildings

Damage in buildings documented after recent earthquake-induced liquefaction events emphasises the importance of improving vulnerable regions using countermeasure techniques. Further investigations are required to evaluate the performance of currently available mitigation techniques. Vertical drains are an effective countermeasure technique, extensively utilised to reduce damage, as rapid dissipation of excess pore pressures can be achieved in case of liquefaction. However, further research using physical and numerical modelling techniques, centred on the behaviour of drain arrangements below structures is required in order to generate knowledge concerning the issue of their performance in the presence of buildings.

Dynamic centrifuge modelling has been employed in this work to improve understanding related to the performance of drain arrangements in earthquake-induced liquefaction below new and existing structures. The analysis considers the use of recycled material as an alternative to coarse gravel inside the drains and proposes a simplified technique for the accurate simulation of the drain behaviour during soil reconsolidation.

The influence of the foundation bearing pressure as an important factor in the performance of the drain arrangements was observed during and after the shaking, in the evaluation of a simplified arrangement of vertical drains under new buildings. Excess pore pressures were controlled and rapidly dissipated due to the significant confining pressure exerted by the foundation, enabling lower foundation settlement and great rotational response in the case of a heavy foundation. The “unit cell” and “infinite cell” behaviour of the internal and perimeter drains was accentuated in the presence of the structure.

The performances of different alternatives of rubble brick vertical drain arrangements were evaluated, with a focus on providing an optimal treatment to the vulnerable area below the foundation. Improved control and dissipation of excess pore pressures, including

enhanced foundation settlement response were achieved when adding edge drains below the foundation in a 13- vertical drain arrangement, due to the higher area replacement ratio in the soil. Moreover, the lower soil softening generated in the stratum with 17- vertical drain arrangement, enabled a great rotational response of the foundation. Countereffects in the effective performance of the arrangement of 17 drains were also presented during the reconsolidation stage, as a delay in the flow front arrivals of the external drain rings was registered. The foundation settlement improvement was lower than expected when adding the edge drains below the foundation, due to the bulging effect presented at the top of the drains. The alternative of replacing internal and edge drains utilizing aluminium encased vertical drains below the foundation showed an improved behaviour of the soil principally during dissipation compared to the original arrangement. Improved settlement response was obtained using this variation, together with a consequent greater seismic demand of the foundation due to the effective performance of the edge and internal drains and the greater shear reinforcement provided by the columns. In addition, a comparative analysis in which the 17- vertical drain arrangement and the single rubble brick column that covers the entire foundation footprint were evaluated, highlighted the importance of considering external drain rings in the arrangement, capable of reducing the “infinite cell” behaviour of a single drain during the shaking. The foundation settlement response obtained in all the tests, highlights the relevance of an optimal performance of the arrangement during the shaking, rather than only the soil reconsolidation stage.

Inclined rubble brick drain arrangement around existing buildings was evaluated as a feasible and economical alternative mitigation technique. Excess pore pressures were controlled and easily dissipated below the foundation due to the inclined columns radial proximity in the direction of the structure along the stratum depth. In addition, an improved settlement response of the foundation was obtained compared to that over an arrangement of vertical perimeter drains. A larger rotational response was also attained for the foundation in the case of inclined drains, in response to the relatively lower soil softening. Furthermore, the high-bearing pressure of the foundation significantly influenced the effective performance of the inclined drain arrangement, enabling a lower settlement response compared to a lighter foundation.

A simplified 3D finite element technique was developed using ABAQUS software to simulate principally the dissipation behaviour of a soil considering a drain arrangement below new and existing buildings. This simplified method allows to obtain the adequate permeability of the drain coarse material for an optimal response of the foundation in terms of settlement, becoming a valuable tool for practitioners. The models evaluated using centrifuge methodology were also analysed utilising this technique, thus, the validation of the proposed method was possible. The model calibration was performed by varying the soil stiffness and permeability parameters in order to obtain a correct simulation of the soil

during and after the shaking. Accurate simulation of excess pore pressure generation was achieved, particularly for traditional vertical arrangements, in small soil stratums. The constant soil stiffness and permeability during the reconsolidation stage, represent the principal limitation in the correct simulation of the soil behaviour, as a slower rate of soil reconsolidation was obtained after the shaking in the numerical model compared to the physical model. The proposed technique was considered satisfactory as a similar settlement response of the foundation was obtained in both the numerical and physical analyses.

Samy Garcia Torres

Acknowledgements

I am very grateful for the exceptional and unforgettable years I have spent at the Schofield Centre. First, I would like to express my gratitude to Professor Gopal Madabhushi for giving me the opportunity to develop research related to earthquake-induced liquefaction and for his encouragement and guidance during these years. I would like to also thank Dr Stuart Haigh and Dr Giulia Viggiani for their helpful advice and suggestions.

I acknowledge the support and kind help from technicians at the Schofield Centre in the development of the centrifuge tests. In particular, I would like to thank Mark Smith, Kristian Pether and John Chandler for their assistance with the preparation of the models and the running of tests. I am grateful to Richard for his support, Cris McGinnie for his help with instrumentation and Magda for her assistance regarding administrative issues.

I would like to thank the financial support of the Peruvian Council of Science, Technology and Technological Innovation (CONCYTEC). Also, special thanks go to Murray Edwards College and the Department of Engineering for the travel funding.

This research would not have been possible without the generous support and sincere friendship from the members of the research group at the Schofield Centre during these years. Fiona, Thejesh, Srikanth, Alessandro, Gianmario, Jad, Charalambos, Ahmed, Zacharoula, Andrei, Alexandra, Deryck, Chuhan, Mengchen, Ramesh, Domenico, Giorgio, Vikram, Laura, Gaetano thank you for your honest friendship and for sharing invaluable knowledge.

I would like to give special thanks to my friends at Murray Edwards College, CUED and Swirles Court accommodation, especially Naty, Ziqing and Alejandra. Also, thanks go to the amazing friends I made in London during the last year, particularly Loan, Kike and Maca. I am deeply grateful to the mentorship of my professors at PUCP, Dr Ramzy Kahhat in particular, and to all my wonderful friends in Peru for their vital support during these years.

I will forever be grateful to my family: Sony, Eva, Nora, and especially to my dear parents, Ana and Carlos, who inspired me to believe in my dreams and to whom I owe everything I have become. Finally, I am thankful to my beloved Juan Samuel, for his incredible heart.

¡Muchas gracias!

Table of contents

List of figures

List of tables

Nomenclature

N	Scaling factor
g	Acceleration of gravity
B	Foundation width
S	Settlement
D_L	Depth of liquefiable layer
D_r	Relative density
q	Bearing pressure
θ	Rotation
A_r	Area replacement ratio
τ_{A_r}	Additional drains shear reinforcement
σ	Stress
σ'	Effective stress
r_u	Excess pore pressure ratio
t	Time
Δu	Excess pore pressure
c	Concentration
μ	Dynamic viscosity
C_v	Coefficient of consolidation

k	Hydraulic conductivity
m_v	Compressibility
n	Porosity
E	Young's modulus
E_o	One-dimensional stiffness
G	Shear modulus
γ	Soil unit weight
ρ	Density
ν	Poisson's ratio
e	Void ratio
τ	Shear stress
φ	Friction angle
ψ	Dilation angle
c'	Cohesion

Chapter 1

Introduction

1.1 Recent earthquakes and liquefaction mitigation techniques

Remarkable structural damage has been registered after recent earthquakes due to earthquake-induced liquefaction. The Christchurch earthquakes in New Zealand in 2010 and 2011 caused significant damage to dwellings located in liquefiable areas (see Fig. 1.1). Settlement and tilting were documented, particularly of shallow foundations (Olarte *et al.*, 2017), necessitating the demolition of several houses as treatment would have been prohibitively expensive (Rasouli *et al.*, 2012). Additionally, numerous buildings were affected during the 2011 Tohoku earthquake in Japan (see Fig. 1.2). Tokyo Bay was damaged considerably by liquefaction, resulting in subsidence and tilting of a large number of houses (Towhata and Rasouli, 2013). More recently, liquefaction significantly impacted the neighbourhoods of Balaroa and Petobo in Palu city after the 2018 Sulawesi earthquake and tsunami in Indonesia. Large areas were affected, including 2050 and 1045 of damaged houses in Balaroa and Petobo, respectively (Widiyanto *et al.*, 2019) (Fig. 1.3). The significant impact on buildings due to earthquake-induced liquefaction, documented over the years, substantiates the relevance of adequate soil improvement and the demand for further research focused on the improved performance of buildings.

Countermeasure techniques against liquefaction damage have been studied since 1960 (Rasouli *et al.*, 2016). Densification, drainage and grouting are some of the well-known mitigation techniques that are used extensively by practitioners in the field. Although the principal objective is to improve the structural response, methods such as using vertical

drains consider a design based on free field conditions, which frequently represents an unreal context. The omission of deviatoric shear mechanisms imposed by the structure, provides an inaccurate estimation of the soil behaviour and structural response, resulting in an inexact estimation of the damage and imprecise design patterns for the mitigation techniques.

Fig. 1.1 Tilting of house, Christchurch earthquake (Towhata and Rasouli, 2013).

(a) Tilting of house caused by liquefaction, Tokyo Bay area (Towhata and Rasouli, 2013).

(b) Subsided structures, Itako city (Rasouli *et al.*, 2014).

(c) Settled building (Tokimatsu *et al.*, 2012).

Fig. 1.2 Damage to buildings, Tohoku earthquake

Remediation methods have been extensively installed below buildings; nevertheless, there are still existing structures located in liquefiable areas that have not received treatment, and are, therefore, highly vulnerable to suffering damage. Demolition of buildings is often considered a suitable option to improve the soil after the earthquake; however, this is not a viable alternative when no structural loss has occurred. Then again, enhancing the soil below existing structures could be more challenging compared to the mitigation of new structures, as additional complications arise in terms of installation (e.g. significant vibration is presented during densification). Recent techniques have been developed to prevent insidious interventions for the existing structures. One of these is chemical grouting; however, this could be a costly treatment for houses, as it is ten times more expensive than other techniques, such as reducing the ground water level (Rasouli *et al.*, 2016). Additionally, vertical perimeter drains represent an economical, easy-to-install option for existing constructions; nevertheless, limitations arise when large-plan areas are considered. Fortunately, technological advances in directional drilling have introduced new alternatives for drain installation below existing structures, such as inclined perimeter drains.

Fig. 1.3 Balaroa neighborhood in Palu city, prior to and after the Sulawesi earthquake and tsunami. (DigitalGlobe, via Associated Press)

The amount of construction waste resulting from the demolition of buildings or earthquake debris represents an environmental concern. The demolition of constructions has increased due to the faster urbanisation in many cities. Considerable amount of masonry or concrete waste from demolition of old buildings has been documented in the EU in recent years, with only a minor percentage of these following an adequate waste treatment (Ledesma *et al.*, 2015). Moreover, available landfills are not frequently sufficient to cope with the amount of waste (Nataatmadja and Tan, 2001), demonstrating the lack of adequate disposal areas for a proper end-of-life of the waste material. Clearly, an improved waste

management system is required, centred on recycling alternatives to reduce the amount of construction waste. In the same way, it is highly desirable that geotechnical procedures should be related to environmental conservation, providing economical and sustainable engineering solutions. Drainage improvement techniques integrated with the recycling of materials, may become the optimal alternative.

1.2 Research objectives

The structural damage registered in liquefiable regions after an earthquake, highlights the relevance of exhaustive research related to countermeasure techniques against liquefaction. Vertical drains have been widely utilised in recent decades as a mitigation method; nevertheless, insufficient research and unclear insight regarding the performance of drains below structures, make it difficult for engineers to select this technique as the preferred option.

Therefore, the aims of this thesis are:

- Improve understanding of the performance of vertical and inclined drains below new and existing buildings, considering the excess pore pressures generated due to an earthquake. The soil behaviour in terms of excess pore pressure generation and dissipation is analysed together with the foundation settlement and the dynamic response.
- Provide an alternative coarse material to be used inside the drains and increase knowledge of the related performance of recycled drains below new and existing buildings.
- Develop a simplified finite element technique to simulate the performance of vertical drains during the reconsolidation stage below new and existing structures, that could facilitate practitioners in the technical design.

1.3 Thesis outline

This thesis contains the following eight chapters:

Chapter 1: *Introduction*

The research motivation is presented in this chapter, focusing on the structural damage generated by earthquake-induced liquefaction and the remediation techniques utilised for new and existing buildings. In addition, the research objectives are defined.

Chapter 2: *Literature Review*

State of the art and critical analysis of the research is presented in this chapter. The soil liquefaction mechanism and the empirical approach for the estimation of liquefaction potential are presented in the initial sections. A review of the general mitigation techniques currently utilised in field, including drainage methods, is outlined together with some of the experimental work developed on this topic. The vertical drains technique is detailed, considering the empirical method utilised in the design and the physical and numerical work centred on the mitigation of new and existing buildings. A general review of the research that has been developed on recycled vertical drains is also presented. In addition, research related to the settlement of shallow foundations due to liquefaction is summarised.

Chapter 3: *Methodology*

Centrifuge and numerical modelling methodologies utilised in this thesis are detailed in this chapter. The resources and different processes required to carried out dynamic centrifuge tests, using the Schofield Centre facilities at University of Cambridge, are explained. In addition, the simplified FE technique, developed using ABAQUS to simulate the performance of vertical drains during the reconsolidation stage is detailed.

Chapter 4: *New buildings: Vertical drains performance in liquefaction mitigation*

The performance of a simplified arrangement of vertical drains under new buildings is evaluated as a base case study. The effectiveness of the technique is examined by a comparison with a similar shallow foundation over unimproved soil. In addition, the analysis considers the influence of different bearing pressures in the soil.

Chapter 5: *New buildings: Improved arrangement alternatives using sustainable materials as vertical drains*

The behaviour of different arrangements of rubble brick vertical drains below new buildings is examined. The drains configurations are designed, focusing on an improved mitigation of the area below the structure. Comparative analyses of 13- and 17- drain arrangements are presented in the initial section. A 17- drain arrangement, with aluminium encased drains below the foundation, is examined and compared with the original configuration with no encased drains. Finally, a single column that covers the complete foundation footprint is evaluated as a simplified alternative.

Chapter 6 : *Existing Buildings: Performance of inclined perimeter drains as liquefaction mitigation technique*

The performance of a rubble brick inclined drain arrangement, as an alternative to the traditional vertical drains configuration below existing buildings, is evaluated in this section.

The analysis considers a comparison with the vertical perimeter drain arrangement and the influence of different bearing pressures over the soil.

Chapter 7: *Numerical modelling of drain arrangements below new and existing buildings*

The simplified FE technique developed using ABAQUS software, to simulate the dissipation behaviour of the soil in the presence of vertical drains below new and existing buildings, is used to examine the drain arrangements previously tested using centrifuge modelling. The calibration and validation of the numerical model are developed considering results obtained from centrifuge tests. A discussion of the factors affecting the relationship among the numerical and physical models is presented. In the last section, a parametric analysis, considering the FE model of a simplified arrangement below new building, is developed to obtain the most favourable permeability factor for a minimal foundation settlement response.

Chapter 8: *Conclusions and future work*

The conclusions of this research are presented in this chapter. The limitations presented in this work are detailed, recommendations for designing engineers and further related research, to enhance the physical and numerical modelling procedures and improve the understanding of vertical and inclined drains performance below structures, are indicated.

Chapter 2

Literature Review

2.1 Mechanism of Liquefaction

Soil liquefaction refers to the loss of shear strength in the soil as a consequence of the excess pore pressure generated due to cyclic loading. In loose sand, a contractive behaviour of the soil is expected due to the rolling particles that drop into the voids in the presence of shear forces. Cyclic shear stresses induce a rise in the pressure of the pore fluid, as there is insufficient time for the fluid to be drained. The increment of excess pore pressures reaches high values, equal to the soil effective stress, enabling a complete loss of contact between particles in the soil. The excess pore pressure ratio (r_u), which is defined as the ratio between the excess pore pressure and the initial soil vertical stress (equation 2.1), specifies the state of the soil.

$$r_u = \frac{\bar{u}}{\sigma'_{vo}} \tag{2.1}$$

The term '*initial liquefaction'* was proposed by Seed and Lee (1966), after evaluating the soil behaviour when considering cyclic loading. Liquefaction initiation is expected when the effective stress in the soil reaches the same value as the excess pore pressures (r_u=1). According to Florin and Ivanov (1961), loose sand presents soil sedimentation state when reaching initial liquefaction. Complete liquefaction behaviour results from the considerable decrease in the soil shear strength. In the case of denser sand, a dilation response is expected following initial liquefaction, limiting shear strains in the soil. The straining-hardening behaviour enables a reduction of excess pore pressures and the regaining of soil stiffness.

This is denominated '*cyclic mobility'* by Castro (1975). According to Florin and Ivanov (1961), liquefaction starts at shallow layers and continues toward the bottom, where higher confining stresses are presented. In addition, Schofield (1981) emphasised the relevance of the hydraulic gradient in the occurrence of liquefaction, as well as the low confining stress in the soil. The opened fissures and fractures that are created in the unconfined soil due to the shearing can lead to exhibition of liquefaction phenomena such as sand boiling etc.

2.1.1 Theoretical framework

The '*critical'* or '*steady-state'* refers to the condition in which a continuous increment of strains is observed in the soil while no variation of the shear and confining stresses is presented (Schofield and Wroth, 1968; Castro, 1975). According to Castro (1975), the *steady-state line* can be defined from the relationship between the void ratio and the confining stress, representing the upper limit of a non-flow liquefiable behaviour of the soil. The steady state line provides knowledge about the exposure of the soil about to undergo liquefaction behaviour (Ishihara, 1993); however, when cyclic loading is considered, the theory of phase transformation appears to be more suitable. The '*phase transformation line'* represents the transition between the contractive and the dilative soil behaviour (Ishihara *et al.*, 1975). Figure 2.1 presents results for loose and dense sand from triaxial tests considering cyclic loading, in which the phase transformation line is noted for both cases. Above this line, the soil behaviour varies from contractive to dilative, showing a rise in the shear stress and a decrease of excess pore pressures. This line is also called the '*characteristic threshold line'* (Luong and Sidaner, 1981), which illustrates the state of transition in the soil. The dilative zone over the line is referred to as *`surcharacteristic domain'*, and the contractive zone beneath is referred to as the *`subcharacteristic domain'* (Fig. 2.2).

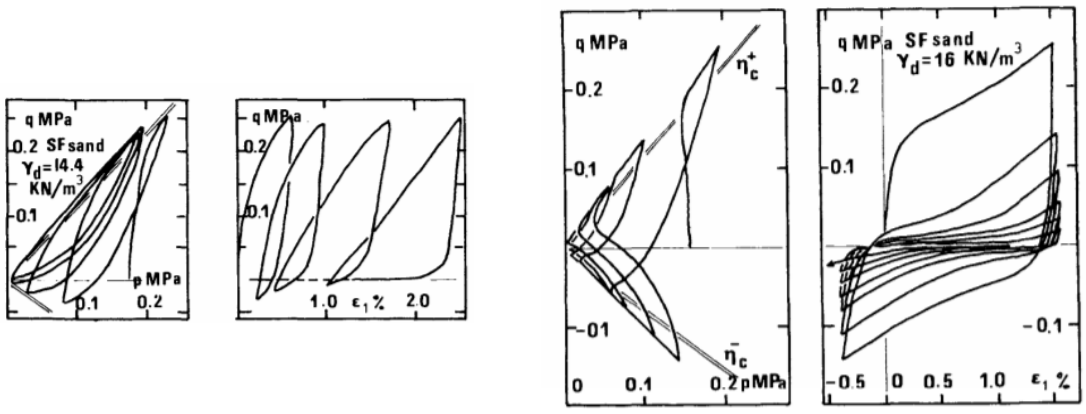

(a) Loose sand **(b) Dense sand**

Fig. 2.1 Undrained triaxial cyclic loading for loose and dense sand (Luong and Sidaner, 1981).

The undrained cyclic torsional tests developed by Ishihara (1985) illustrate the '*characteristic threshold lines'* for loose and dense sand (Fig. 2.3), in which the contractive and dilatancy regions can be observed. In case of the loose sand, the excess pore pressures reached higher values, while the effective stress in the soil decreased significantly by crossing the characteristic line, suggesting a complete liquefaction behaviour. By contrast, the dense soil presented a dilative behaviour with a regaining of strength, and limited strains in the soil. This behaviour can lead to a greater transference of the acceleration in the soil during the shaking (Lee, 1985).

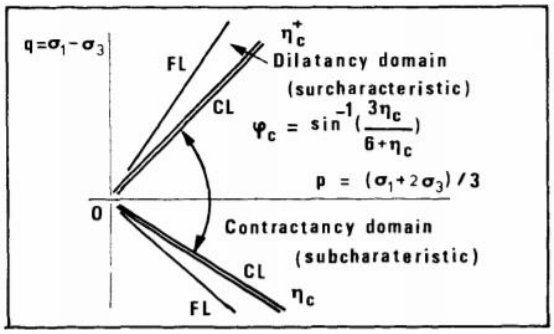

Fig. 2.2 Dilatancy (surcharacteristic) and Contractancy (subcharacteristic) domains (Luong and Sidaner, 1981).

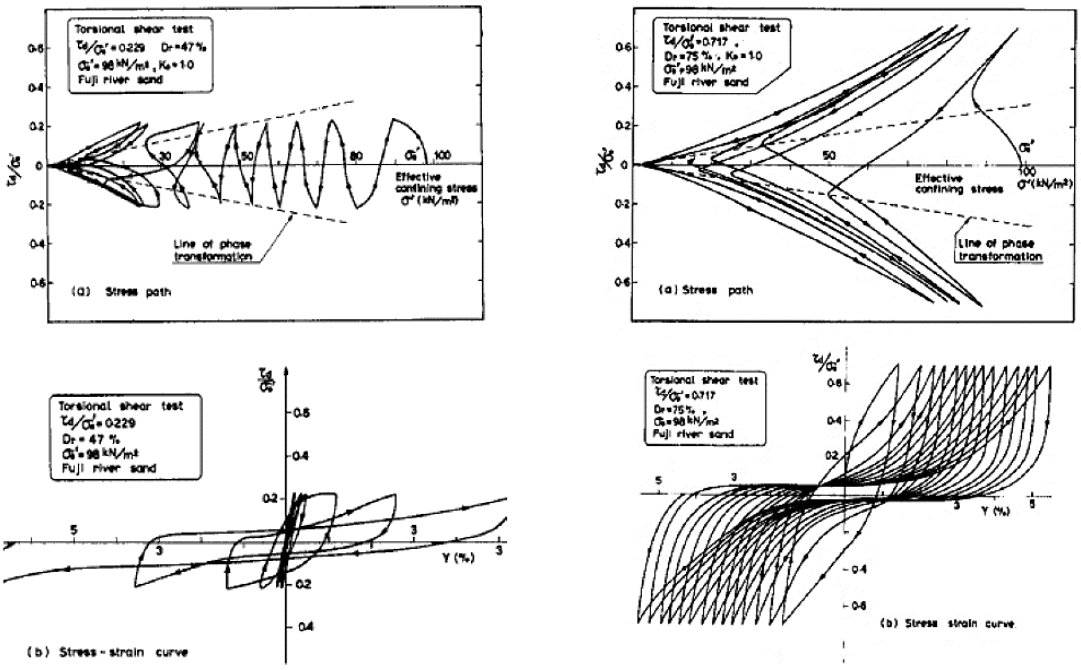

(a) Loose sand **(b) Dense sand**

Fig. 2.3 Stress path and stress-strain curves from cyclic torsional tests (Ishihara, 1985).

2.2 Liquefaction potential: simplified procedure

The evaluation of soil liquefaction potential is essential to estimate the risk to which a site is exposed during and after an earthquake. The 'simplified procedure' proposed by Seed and Idriss (1971) provides a semi-empirical method by which to estimate this.

In this procedure, the cyclic stress ratio *(CSR)* is obtained as a ratio of the cyclic shear stress at a specific depth (equation 2.2). The proposed equation for *CSR* considers the soil peak acceleration (α_p), soil initial effective stress (σ'_{v0}), soil total stress (σ_{v0}) and r_d. The last factor corresponds to the reduction coefficient, which is related to the decrease in the shear stress along the soil's depth. This factor was analysed by Youd and Idriss (2001), providing a trend of r_d variation along the stratum depth, and by Idriss and Boulanger (2004) who proposed reduction coefficient values for different earthquake magnitudes (Fig. 2.4a).

$$CSR = \left(\frac{\tau}{\sigma'}\right) = 0.65 \frac{\alpha_p}{g} \frac{\sigma_{v0}}{\sigma'_{v0}} r_d \tag{2.2}$$

Additionally, correction factors associated with the limitations of the procedure, in terms of the low static shear stress and low overburden pressures, were estimated by Seed (1981). Triaxial tests were performed to attain the K_σ ratio, which depicts the cyclic resistance ratio at great pressures. Moreover, the factor of K_α, that refers to the greater shear stresses for sloping soils, was estimated as a ratio of the peak shear stress and the normal effective stress.

The cyclic stress ratio *(CSR)* previously estimated is then compared with the liquefaction resistance ratio *(CRR).* The *CRR* can be obtained from laboratory tests; nevertheless, it can easily be determined using the chart for liquefaction triggering that illustrates the relationship between the cyclic stress ratio (*CSR*) and $(N_1)_{60}$ blow count (Fig. 2.4b). The curves illustrated in the graph, represent the dividing line between liquefaction and no liquefaction in the soil and the *CRR* magnitudes. These correlations have been performed by Seed (1979) using field data and were later updated by Idriss and Boulanger (2004).

The simplified procedure is utilised to estimate the liquefaction potential in free field conditions; therefore, it is expected to be an inaccurate approach when considering the presence of a structure. This limitation was analysed by Rollins and Seed (1990), suggesting that the variation of the vertical effective stresses due to additional bearing pressure represents a relevant factor, as it affects the cyclic stress ratio in the soil surrounding the structure. Additionally, the high confining pressure enables a reduction in the level of excess pore pressure generation, explained by the greater cycle resistance in the soil during the shaking (Liu and Dobry, 1997; Ghosh, 2003; Dashti *et al.*, 2010a; Adamidis, 2017). This suggests a lower potential of the soil to reach complete liquefaction in the foundation soil.

The bearing pressure influence on the soil behaviour during the shaking will be extensively discussed in Chapters 3 and 6, with consideration of the drainage mitigation in the soil.

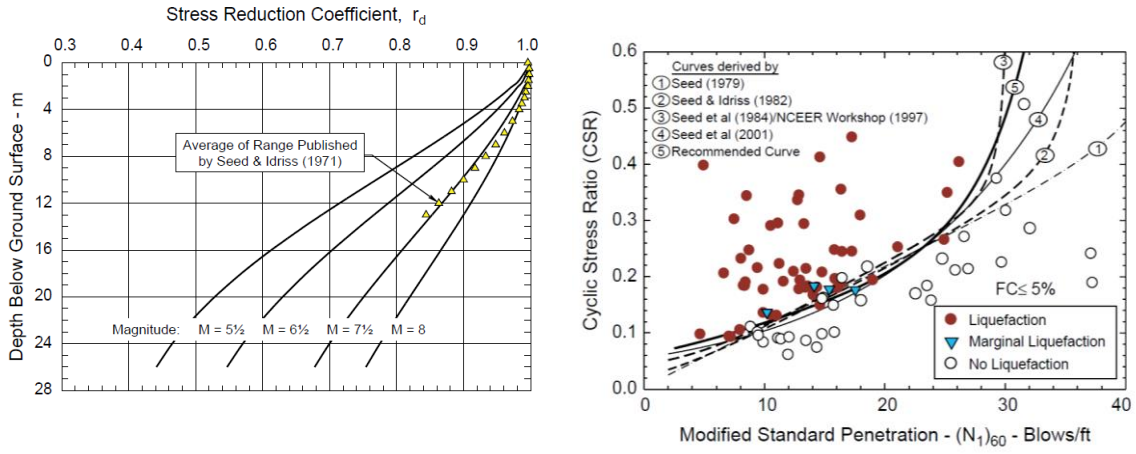

(a) **(b)**

Fig. 2.4 a) Variation of stress reduction coefficient (r_d) and b) curves relating *CRR* to $(N_1)_{60}$ for clean sands (*M*=7.5) (Idriss and Boulanger, 2004).

2.3 Liquefaction mitigation techniques

The installation of countermeasure techniques is vital in liquefiable regions. Mitigation methods aim to reduce the level of damage to the structure or to avoid liquefaction occurrence. General techniques utilised in field are:

- Densification
- Drainage
- Grouting
- Dewatering
- Reinforcement
- Replacement

Towhata (2008) presented statistics related to the employment of mitigation techniques in the field against liquefaction damage from 1993-2004. Soil densification was the most utilised method during this period; meanwhile, the use of drainage techniques decreased considerably. In addition, a significant increment in the employment of grouting methods was observed, this being the second most utilised measure at the end of this period. By contrast, reinforcement, reduction of the ground water level (GWL) and replacement techniques were less popular techniques implemented in the field.

Most of the mitigation techniques have been designed based on free field conditions; nevertheless, this represents a disadvantage for existing structures as not all of the current methods can be smoothly installed. For instance, the installation of densification techniques involves vibrations that may affect the stability of the soil below the structure (Yasuda, 2007). Therefore, enhanced countermeasure techniques for existing structures have been developed in recent decades (Fig. 2.5).

A series of existing structures located in liquefiable areas have been treated using these techniques (Yasuda, 2007). The dewatering method was utilised for a tank yard in Kawasaki by introducing 26 wells capable of reducing the water level. Also, the ground below a wharf was improved using the grouting technique, after damage was sustained in the 1989 Loma Prieta earthquake. Similarly, the Yokohama customs building was treated by installing this method from the building floor. Moreover, old tanks in Kawasaki were remediated employing the injection technique, in which inclined bore holes were dug below the structure and injected with highly permeable silica grouting. Finally, piles were installed around a timber house that had previously been affected by the Tokachi-oki earthquake in 2004 (Yasuda *et al.*, 2004).

Moreover, lowering the soil saturation degree, using air injection as a countermeasure technique against liquefaction damage, presents effective results below existing buildings. Zeybek and Madabhushi (2017) performed a series of centrifuge tests to improve the understanding of deformation mechanisms below structures when air injection is used in the soil. Results revealed that this method allowed for the reduction of excess pore pressure generation in the soil and structural settlement. Deviatoric deformations were significantly reduced in the presence of air bubbles and the soil liquefiable depth was considerable decreased. Similar results were previously observed by Okamura *et al.* (2012), highlighting that the reduction of soil liquefaction potential was a positive effect of the technique. In addition, the impact of sequential earthquakes on the performance of complete and partially saturated soils was also evaluated (Zeybek *et al.*, 2020). Considerable structural embedment was obtained in the case of fully saturated soil, while settlement was significantly lower in the case of partial saturated soil, which limited the structure embedment.

The effective performance of countermeasure techniques below buildings has been verified in the field after the occurrence of earthquakes. Mitchell *et al.* (1995) collected field data from regions that were previously improved with mitigation techniques in USA (California) and Japan. Different methods, such as drainage and grouting, were observed, highlighting the improved behaviour of the soil in the treated zones. In addition, the effectiveness of the in-ground walls was validated after the 1995 Hyogoeken-Nanbu earthquake, as an improved behaviour of the foundation had been registered (Hamada and Wakamatsu, 1996). In the work performed by Hausler and Sitar (2001), the efficacy of

ground remediation methods was measured in terms of the damage magnitude. Densification and drainage represented the most examined cases, exhibiting an optimal performance in the soil.

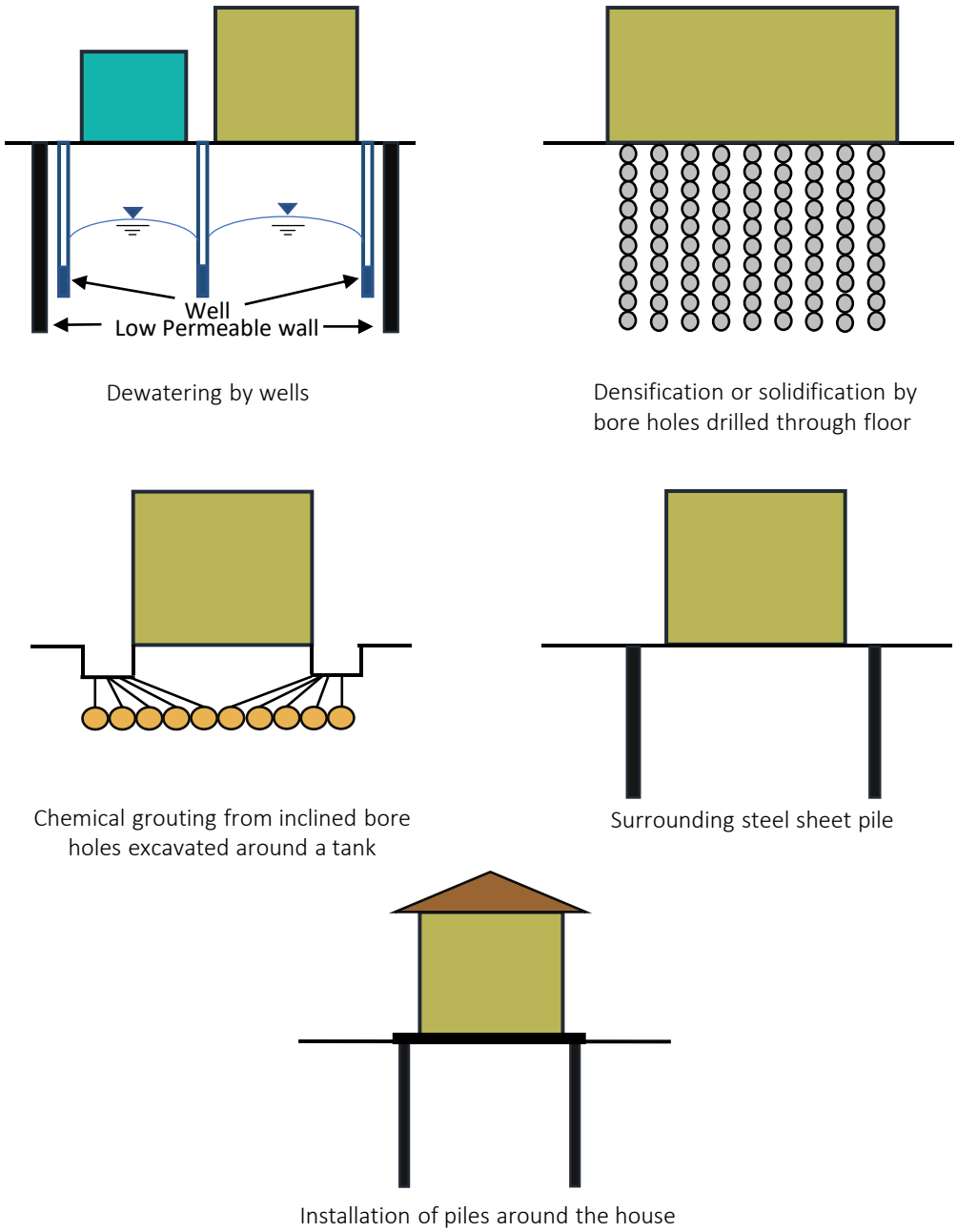

Fig. 2.5 Mitigation methods for existing foundations (Yasuda, 2007).

2.3.1 Physical modelling of countermeasure techniques

Extensive experimental work has been carried out to improve the understanding of the performance of mitigation techniques below structures.

Mitrani and Madabhushi (2005) assessed the effective performance of inclined micro-piles as a mitigation technique under existing structures through the comparison of untreated and treated soil, by using centrifuge modelling. The technique produced positive effects, as dilation in the soil surrounding the piles was observed. In addition, centrifuge modelling was utilised to evaluate the performance of a bridge foundation improved with densification mitigation technique (Coelho *et al.*, 2004). A significant reduction of the foundation settlement was obtained as well as a decrease in the rotational response. The effectiveness of the technique relies on soil dilation being exhibited below the foundation during the earthquake and the adequate migration of pore pressures during the reconsolidation stage.

The performance of soil densification, structural walls and prefabricated vertical drains (PVD) was examined by Olarte *et al.* (2017). Densification led to a reduction of the structural settlement and a decrease in excess pore pressure generation; however, an amplification of the seismic demand was registered for the superstructure. Vertical drains enabled a rapid dissipation of excess pore pressures and a significant reduction of structural settlement including the structure rotational response, while the acceleration in the structure was also increased. In the case of structural walls, their efficacy was highly dependent on the input motion, showing an ineffective performance for high magnitude earthquakes. In addition, Olarte *et al.* (2018) evaluated structures in liquefiable soil containing mixed techniques. Densification together with vertical drains and densification including latex barriers to prevent drainage were analysed. By considering only the densification technique, a decrease in the structural settlement was registered; however, this was greater than the tolerable value. Densification with the water barrier enabled a similar settlement response compared with the densification technique alone; nevertheless, a greater rotational response was obtained due to the rise of excess pore pressures near the structure's boundaries. Vertical drains, together with densification, enabled a significant reduction of structural settlement and rotation, as well as an increment in the superstructure seismic demand, representing a greater risk of damage.

The performance of rigid containment walls beneath structures was evaluated by Mitrani and Madabhushi (2012). The effectiveness of the technique was verified as the structure settlement decreased in response to the soil movement inhibition below the foundation. The blockage of fluid flow towards the area beneath the foundation (due to the wall being impermeable) had an important role in the structural response. In addition, the performances of sheet-pile walls and water barriers were evaluated by Dashti *et al.* (2010a). A latex water barrier in the soil around the foundation, enabled settlement reduction due to the inhibition of fluid flow below the foundation. On the other hand, sheet-pile walls limited shear strains in the soil, reducing deformations below the structure to a greater extent compared with the water barrier. Both techniques enabled a rise in the structure's acceleration. In these studies, although significant reduction was obtained for the settlement response, countereffects in

the superstructure performance were observed, highlighting the importance of analysing the structural response when considering countermeasure techniques. In addition to the work developed by researchers using centrifuge modelling, shaking table tests were carried out toward the same target. Sheet-pile walls and drains installed at the toe of a river dike to improve the soil behaviour were examined using shaking table tests (Mizutani *et al.*, 2001). A significant reduction in the structure subsidence was obtained by considering both techniques. Likewise, the effective work of sheet-piles below existing structures was verified using shaking table tests (Rasouli *et al.*, 2012). The stiffness provided by the walls in the soil generated a greater confinement strength, representing a relevant factor in the effectiveness of the technique. The use of sheet-piles walls, together with lowering the ground water level, led to a complete reduction of the settlement response (Rasouli *et al.*, 2014).

2.4 Vertical drains

Vertical drain arrangements are utilised as an effective mitigation method in liquefiable soil. The techniques main objective is to enable a rapid dissipation of the excess pore pressures generated during an earthquake, enabling limited deformation in the soil and minimising structural damage (Brennan, 2004; Howell, 2013).

Initial work, focused on the design of gravel columns, was elaborated by Seed and Booker (1977). In this study, the basic equation for generation and dissipation of excess pore pressures (equation 2.3) was modified with consideration, in the equation, of the term of excess pore pressure generation developed due to cyclic loading ($\partial u_g/\partial t$).

$$\frac{k}{\gamma_w}\left(\frac{\partial^2 u}{\partial x^2}+\frac{\partial^2 u}{\partial y^2}\right)=m_v\frac{\partial u}{\partial t} \tag{2.3}$$

In addition, the (u_g) term takes into account the number of cycles required for liquefaction (N_L), number of uniform cycles (N), alpha (α) as an empirical value of 0.7 and soil initial effective stress (σ'_{v0}) (equation 2.4).

$$\frac{u_g}{\sigma'_{v0}}=\frac{2}{\pi}arcsin\left(\frac{N}{N_L}\right)^{\frac{1}{2\alpha}} \tag{2.4}$$

The Liquefaction Analysis for Radial Flow (LARF) finite element program was elaborated by Seed and Booker (1977) to solve this equation, and different charts were

proposed for the design of gravel columns. The charts illustrate the relationship between the excess pore pressure (r_u) and the *a/b* (*a*: drain radius, *b*: half of spacing between drains) ratios, considering different N/N_L and T_{ad} (factor that relates the earthquake duration and the soil consolidation properties) values. The charts provide the drain spacing ratio for a maximum average r_u ratio and suggest an optimal performance of the arrangement when greater drain radius or lesser spacing between the drains are given.

Design charts provided by Seed and Booker (1977) are frequently utilised to avoid the risk of complete liquefaction in the soil. Nevertheless, assumptions such as sole radial flow and infinite permeability of the granular columns, are considered in this method, making its validity questionable.

The drains infinite permeability conjecture was debated by Onoue *et al.* (1987). Numerical and experimental analyses were carried out to evaluate the gravel drains performance for liquefaction inhibition, considering the well resistance (Onoue, 1988). The use of this parameter was verified as a relevant factor in the design of gravel columns and different charts were proposed to illustrate the relationship among the drain spacing and the well resistance for different N/N_L values (Fig. 2.6). Brennan (2004) validated the accuracy of the Onoue charts over the Seed and Booker (1977) curves for the free field, after performing a series of centrifuge tests.

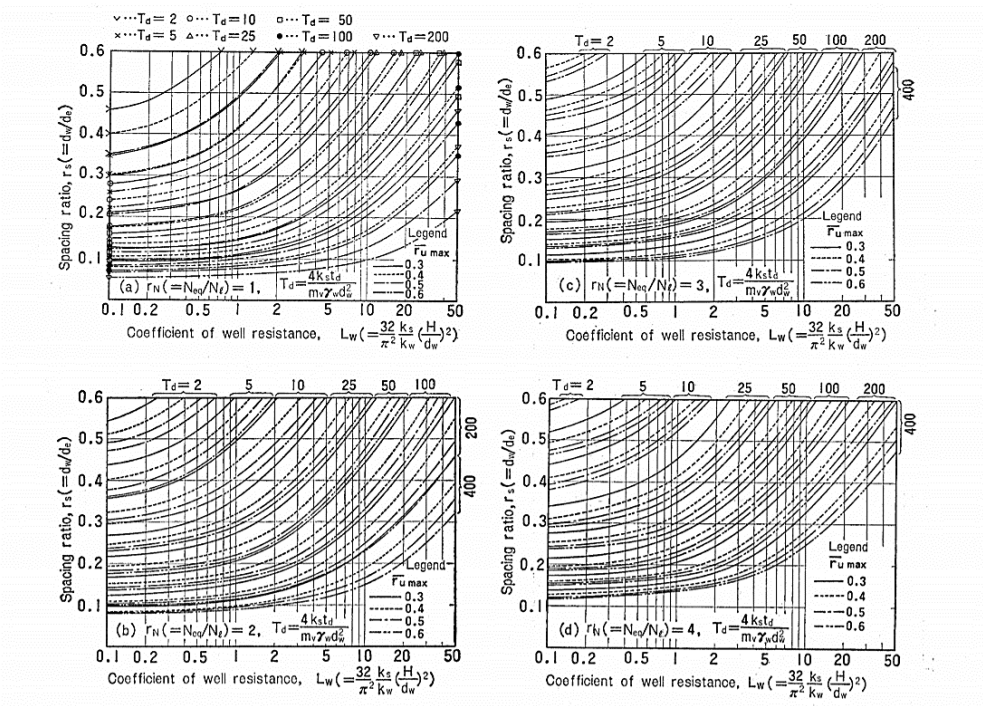

Fig. 2.6 Relationship between the coefficient of well resistance and spacing ratio (Onoue, 1988).

Although the updates of the original design charts allowed a more accurate design and an improved performance of the drain arrangement, the structural bearing pressure should have been considered. The design of vertical drain configuration below a structure based on theoretical procedures could involve an overestimation of the r_u ratio, implying higher costs. Therefore, a clear understanding of the bearing pressure influence in the vertical drains performance is required.

2.4.1 Vertical drains installation and performance in field

Vertical drains are installed in the field using vibratory or flight auger methods (Kirmani, 2004). The first technique involves the insertion of a steel case, containing a removeable shoe, inside the ground, which is then filled with highly permeable material before it is removed. On the other hand, the auger method permits a minor disturbance of the soil and reduces the smear effect. The auger is inserted into the soil and then starts to rotate. The coarse material is then added through the hollow stem, and the auger is withdrawn at the same time. In addition, recent advances in directional drilling have allowed an alternative option for installation: inclined drains (Fig. 2.7). Although conventional vertical drains have been widely employed against liquefaction, prefabricated vertical drains (PVD) have become a well-known alternative, as they consist of encased hollow pipes capable of preventing clogging (Howell, 2013).

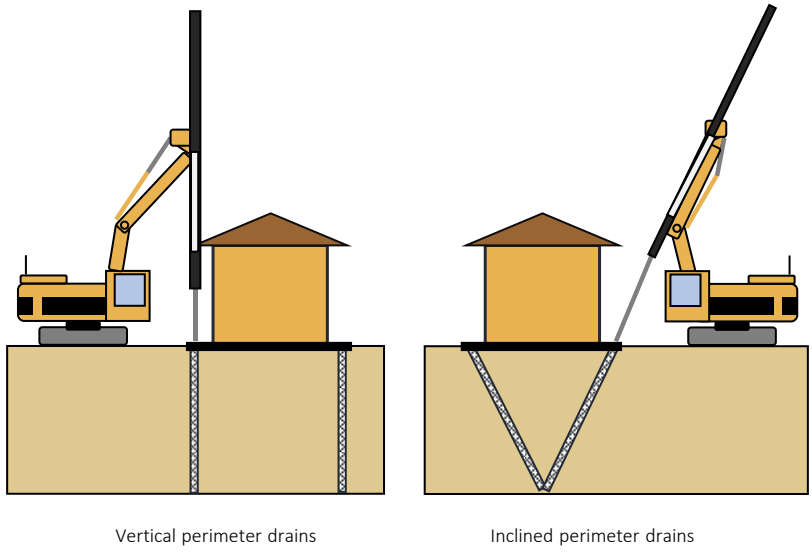

Fig. 2.7 Vertical and inclined perimeter drains

Regions treated with vertical drains and later struck by an earthquake have been surveyed to verify the effectiveness of gravel columns and vertical drains in the soil. Gravel drains were installed below a wharf in Tokyo Bay in 1978, following the design charts proposed by Seed and Booker (1977) (Sonu *et al.*, 1993). The drains were able to avoid the

occurrence of liquefaction during 1993 Hokkaido earthquake that hit the Port of Kushiro and mitigate damage, although this area was located close to the epicentre. Furthermore, in the work developed by Hausler and Sitar (2001), the field data of ninety sites treated with distinct countermeasure techniques and hit by different earthquakes, was collected. Buildings and shallow foundations were examined, showing an optimal response in the presence of gravel, vertical and wick drains.

Although field data is a useful tool with which to improve empirical methods and verify the optimal performance of a mitigation technique in field, the infrequent occurrence of earthquakes limits the acquisition of data. According to Howell (2013), prefabricated vertical drains have been installed in different sites in the US; nevertheless, these sites have not been exposed to earthquakes of the designed magnitudes, therefore, no field data is available for the validation of the PVD technique.

2.4.2 Physical modelling of vertical drains

Experimental tests have been carried out to analyse the soil behaviour and structural response in the presence of vertical drain and gravel column drainage techniques.

Brennan (2004) carried out a series of centrifuge tests considering different arrangements of vertical drains in order to evaluate the role of each drain ring in the soil. Definitions for the unit cell and infinite cell were stated in this work. The first term refers to the threshold in which the drain is in charge of the fluid flow. Infinite cell is described as the opposite; the drain is in control of infinite fluid flow from further places due to the absence of adjacent drains. Additionally, drain categories were determined based on the drain location (Fig. 2.8). Perimeter drains are drains in charge of infinite fluid flow from farther places. Sub-perimeter drains are located between the perimeter and internal drains and are responsible for the fluid that is not dissipated by the external ring. Finally, the internal drains present a unit cell behaviour, as they are surrounded by additional drain rings.

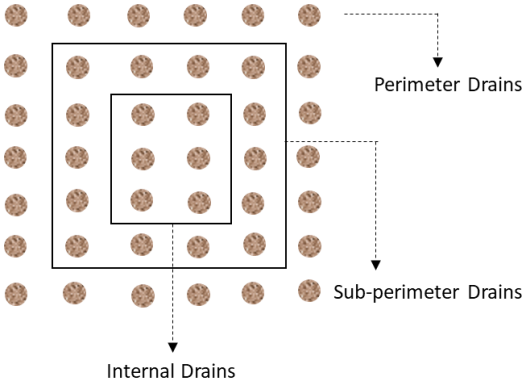

Fig. 2.8 Drain categories based on drains location

Vertical drains effectiveness was verified by Brennan and Madabhushi (2002), performing a series of dynamic centrifuge tests. The radial fluid flow toward the drains, and the flowfront behaviour, which represents the boundary division between soil influenced by the drain and soil not influenced by it, were examined in free field conditions. In this thesis, the flow front arrival time for the soil surrounding the drains was obtained graphically, from the pore pressure transducers recordings, following the method established by Brennan (2004). This point corresponds to the intersection of the line drawn along the straight horizontal part of the curve and the extrapolated line traced in the dissipation part, which follows the slope of the curve.

Howell *et al.* (2012) evaluated the behaviour of prefabricated vertical drains in slightly sloping soil by carrying out centrifuge tests. The enhanced behaviour of the soil revealed the advantages of using this technique, in terms of faster dissipation and reduction of strains. Excess pore pressure generation in the improved soil was not considerably reduced when compared with the unimproved region for certain input motions. Nevertheless, the soil deformation was always smaller in the treated region, suggesting that excess pore pressure generation is not a crucial factor in determining the effective performance of drains. This was also observed in Chapter 6.

The performance of granular columns in the free field was evaluated by Badanagki *et al.* 2018). Centrifuge tests were performed to analyse the behaviour of granular columns in terms of improved drainage, additional shear reinforcement and densification around the column. For an area replacement ratio (A_r) greater than 20%, significant reduction of settlement and lateral strains were obtained, principally due to the faster dissipation enabled by the columns. Moreover, a greater acceleration response around the columns was registered due to both the enhanced drainage and the shear reinforcement provided by the pillars, rather than only by the increment of shear strength. The rapid dissipation of excess pore pressures accelerated the regaining of the soil stiffness.

These studies were focused on the performance of vertical drains and granular columns in free field conditions. However, due to the need for evaluating vertical drains performance in a more real context, recent experimental tests have been centred on the analysis of drainage techniques below structures.

The behaviour of prefabricated vertical drains in liquefiable soil, below structures of different bearing pressures was analysed by performing a series of centrifuge tests (Paramasivam *et al.*, 2018). Lower excess pore pressures and faster dissipation were observed in the soil foundation, allowing a decrease of the structural settlement. In addition, an increase in the seismic demand of the structure was registered due to the great soil strength. Similarly, in Badanagki *et al.* (2019), the performance of granular columns below a structure of 180 kPa was examined. Granular columns reduced settlement and rotation of the structure when a high A_r was presented, as the extent and duration of excess pore pressures were controlled, and the shear strains were reduced. The columns allowed an increment in the soil stiffness, inducing a great transference of the input motion to the structure. The countereffects for the superstructure, when using granular columns, were noted, exposing the importance of analysing the foundation response in the case of soil improvement with vertical drains.

The performance and effectiveness of different configurations of drains, together with other methods such as lowering ground water level and sheet-pile walls, were evaluated in Rasouli *et al.* (2016). The utilisation of the last two techniques, together with shallow inclined drains below the foundation, enabled a greater reduction of the structural settlement compared with the response obtained using only one of these techniques. In addition, the configuration of shallow inclined drains presented an improved performance in terms of liquefaction occurrence, compared with using the full-depth inclined and vertical drains. The mitigation of shallow layers, considering a great proximity of drains to the foundation base area, provided a better response of the foundation, as observed in this work. Moreover, the different performances observed between the shallow and full-depth inclined drain configurations, highlight the need for further evaluation related to the factors that most influence the effective performance of inclined drains.

2.4.3 Numerical modelling of vertical drains

Numerical modelling of vertical drains has initially been developed considering free field conditions. Early work was performed by Seed and Booker (1977), in which the abovementioned LARF program was developed for the design of drains arrangement. In addition, Drains3D code was created by Brennan (2004) to evaluate the dissipation behaviour of vertical drains in the free field, based on the consolidation equation. The excess pore pressure generation obtained using this code showed similar results to the centrifuge

tests; however, the rise in compressibility of the soil at low effective stresses during liquefaction, was not observed, suggesting an inaccurate dissipation prediction. Similarly, Pestana *et al.* (1997) developed a program called FEQDrain, in which the Seed and Booker (1977) equation was utilised to model the excess pore pressure generation and dissipation. The drains permeability was considered a finite factor and the radial and vertical fluid flows were contemplated; nevertheless, only the drain zone of influence was considered in the analysis, impeding an accurate simulation of the soil lateral deformation (Howell, 2013).

The performance of drainage techniques has been analysed using different softwares able to model soil liquefaction (i.e.*Opensees, FLAC*) (Vytiniotis, 2009). Howell *et al.* (2015) performed a numerical simulation for unimproved and improved soil containing prefabricated vertical drains, utilising *Opensees* software. Simulations of vertical drains as unit cells and as a centrifuge model (considering the container boundary conditions) were analysed. Generation of excess pore pressures was well simulated in the last case, showing a similar soil deformation compared with the physical test. On the contrary, inaccurate results were obtained in terms of soil deformation by modelling drains as unit cells, due to the infinite slope simulated in the software. This study remarks the importance of validating the numerical model of vertical drains using experimental results.

In addition to the well-known software used for the simulation of vertical drains performance during liquefaction, researchers have worked with ABAQUS to assess the behaviour of drains in soft clays. In Ye *et al.* (2013), an embankment was treated with a mixed method that combined soil cement columns and vertical drains, enabling faster consolidation and enhancing the soil bearing capacity. Similarly, Tajudin *et al.*, (2015) examined the behaviour of PVDs, verifying the improved soil response due to the rapid excess pore pressure dissipation. Although dynamic and coupled pore pressure procedures cannot be modelled together in ABAQUS for liquefaction simulation, these studies guaranteed an adequate performance of the vertical drains in terms of excess pore pressure dissipation, when using this program.

2.4.4 Recycled vertical drains

Vertical drain arrangements containing recycled material as coarse sand have been evaluated in recent years, as these represent an economic and eco-friendly alternative. The performance of wall gravel drains containing recycled concrete was evaluated as a mitigation technique for buried structures, using shaking table tests (Orense *et al.*, 2003). A decrease in the structure uplift was obtained due to the rapid dissipation of excess pore pressures below the structure. Moreover, the high level of permeability of the wall gravel drains was verified as a relevant factor in the effective performance of the technique. In addition, shaking table tests were carried out to examine the behaviour of rubber and gravel

columns in liquefiable soil (Bahadori *et al.*, 2018) (Fig. 2.9). The granular columns provided a greater reduction of the free field deformation compared with the rubber columns; however, for a higher input motion and density, an improved performance of the rubber drains was observed. Furthermore, non-reinforced and reinforced backfill for a quay wall were analysed by Hazarika *et al.* (2007) using shaking table tests. The treated backfill considered a cushion and vertical drains made of tire chips. Results verified the effectiveness of the proposed mitigation method, as a decrease of the seismic load and structural displacement were registered. Soil improvement, considering vertical drains with coir dust and sea sand inside, was evaluated by Ghajj *et al.* (2008). A comparison between improved and unimproved soft clay was developed using laboratory consolidation tests. An enhanced rate of reconsolidation was obtained when mixed material, of coir and sea sand, inside the drains was considered, due to their high permeability.

Numerical modelling of drains containing reused material was performed by Abdullah and Hazarika (2016). A configuration composed of a horizontal layer and vertical drains containing tyre chips below a foundation was analysed. Significant improvement in the structural performance was registered because of the high permeability of the tyre chips, representing an acceptable alternative with which to replace the gravel material inside drains.

Although some recycled materials have been evaluated as sustainable alternatives for vertical drains, this has not been frequent; therefore, further research using physical and numerical modelling is required.

Fig. 2.9 Gravel and tyre chips (Bahadori *et al.*, 2018).

2.5 Settlement of shallow foundations

Mitigation of structural damage, in terms of settlement reduction is the principal objective of using countermeasure techniques. Therefore, existing research concerning the settlement response of shallow foundations due to liquefaction needed to be summarised.

The approach utilised for settlement estimation involves the use of empirical charts to obtain volumetric strains in saturated sand. Ishihara and Yoshimine (1992) developed curves to obtain settlement after performing laboratory tests. The relationship between volumetric strains in the soil during the reconsolidation stage, soil density and the liquefaction factor of safety was established. Previously, Tokimatsu and Seed (1987) proposed an estimation of volumetric strains based on the stress ratio and SPT values. In both cases, an undrained behaviour of the soil was considered, including volumetric strains during the reconsolidation stage.

The foundation width was recognised as a relevant parameter for the settlement response in the field data collected by Yoshimi and Tokimatsu (1977) from the 1964 Niigata earthquake. In the work performed by Liu and Dobry (1997), wherein the structures' widths were normalised with the liquefiable layer thickness, the results obtained from the centrifuge tests showed agreement with this field information (Fig. 2.10), validating the relevance of the width parameter and the direct relationship between the settlement (S) and foundation width (B). In addition, the depth of the liquefiable soil (D_L) was considered to be another important factor in the settlement response; nevertheless, centrifuge tests performed by Dashti *et al.* (2010b) revealed that considering the liquefiable layer thickness, as a parameter of normalisation, is inaccurate as the results obtained for shallow layers were out of the margins from the field data (Fig. 2.11). This was also verified by Bertalot *et al.* (2013) using field data from Maule earthquake (Chile). Furthermore, dynamic centrifuge tests were carried out by Adamidis and Madabhushi (2018) to evaluate the response of shallow foundations over liquefiable soil with different thicknesses. The structural settlement responses obtained in the different tests were plotted in the graph developed by Liu and Dobry (1997). For B/D_L ratios equal to 1, the settlement responses were in the range proposed by Liu and Dobry (1997). However, in cases of higher ratios, in which the liquefiable layer was thin, results were out of the range, suggesting that the empirical graphs were inaccurate.

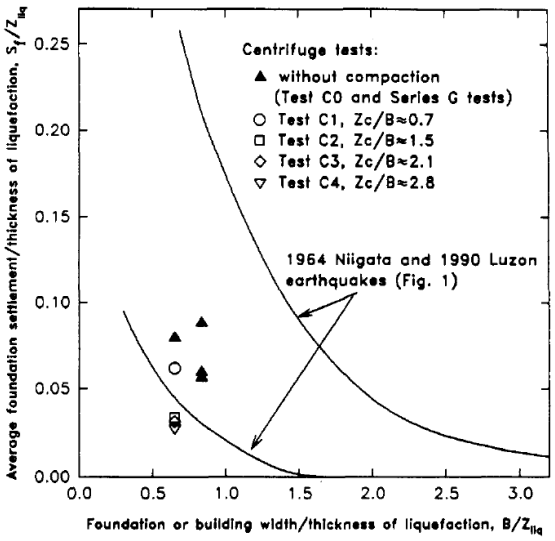

Fig. 2.10 Foundation settlement versus foundation width, normalised with the liquefaction depth, from centrifuge tests and the 1964 Niigata and 1990 Luzon Earthquakes (Liu and Dobry, 1997).

The bearing pressure influence in the settlement response was examined by Dashti *et al.* (2010b), performing a series of centrifuge tests. In addition, this parameter was also evaluated by Bertalot *et al.* (2013) after collecting field data from the Maule earthquake (Chile). Both analyses revealed that the increment of bearing pressure in the soil enabled a decrease in soil softening and lower strains below the foundation, due to the low level of excess pore pressure generation. The field data was utilised by Bertalot *et al.* (2013) to elaborate the contours of S/D_L, in which the relation between the building width and the bearing pressure was established (Fig. 2.12). This trend was then verified with experimental tests carried out by Bertalot and Brennan (2015), validating the relevance of the bearing pressure parameter in the settlement response.

The mechanisms responsible for the settlement of shallow foundations due to earthquake-induced liquefaction required further evaluation for an improved understanding of the structural response. Therefore, Dashti *et al.* (2010b) evaluated the deformation mechanisms for shallow foundations, classifying them into two groups as follows:

- Volumetric-induced mechanisms: localised strains during partially drained cyclic loading, sedimentation, consolidation and expansion.
- Deviatoric-induced mechanisms: partial bearing capacity failure and SSI-induced cyclic loading.

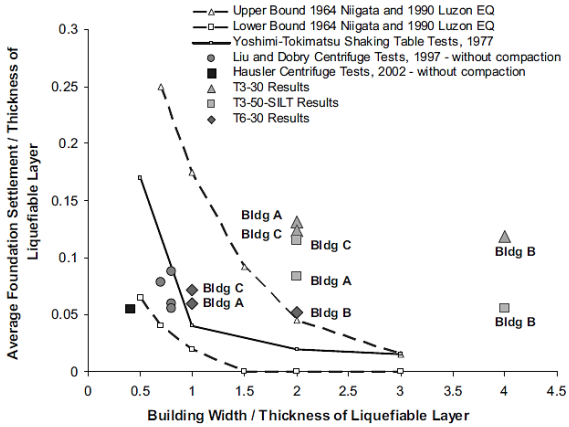

Fig. 2.11 Normalised foundation settlements measured in centrifuge tests compared with historical cases and prior physical tests (Dashti *et al.*, 2010b).

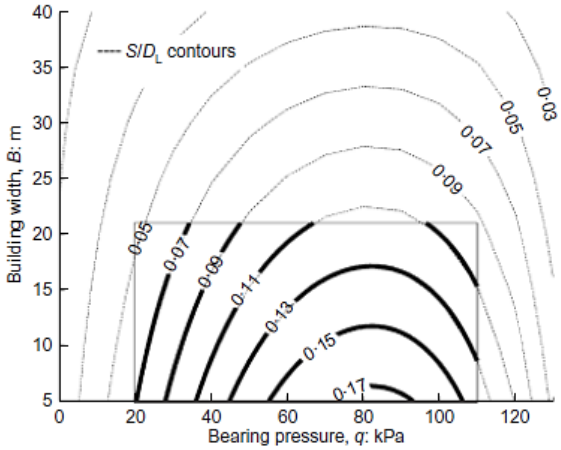

Fig. 2.12 Contour plot of maximum S/D_L (Bertalot *et al.*, 2013)**.**

The empirical approach, utilised to predict settlement of shallow foundations, involves a miscalculation of the liquefaction effects, as deviatoric strains due to bearing pressure are not considered in the settlement mechanism, leading to an inaccurate prediction of the structural response. In addition, the selection of mitigation techniques for liquefiable areas, cannot rely on these methods as an underestimation of the settlement could be considered for the technique design.

The settlement of structures, located in improved soil with a drainage technique, becomes more complex to predict as volumetric and deviatoric deformations are likely to be influenced by the presence of the gravel columns or vertical drains in the soil. Therefore, further analysis of the settlement mechanisms that influence the foundation response when considering drainage mitigation techniques is required.

2.6 Summary

The literature review concerning earthquake-induced liquefaction was presented in the first section. Liquefaction definition and particle behaviour were summarised including the framework related to the steady-state and phase transformation. In addition, the simplified procedure utilised for liquefaction potential estimation was outlined, remarking the limitations of the empirical method when considering structures.

A general overview of the countermeasure techniques used in the free field and below structures was presented, including historical cases in which their effectiveness was verified. Experimental work focused on the performance of mitigation techniques with regard to the presence of buildings, using centrifuge modelling and shaking table tests, was explained, highlighting the relevance of analysing the structural performance in improved soil.

The theory behind vertical drains was detailed, explaining initial theoretical procedures for the design of drains arrangement, stating the limitations of this method for structural mitigation. The installation of vertical drains and their effective action in field were presented. In addition, physical modelling of different vertical drains, granular columns and PVD configurations for the free field and below structures was summarised, emphasising the relevance of evaluating the countereffects on the structure in response to the enhanced soil containing drainage technique. Research work related to the performance of vertical drains using numerical modelling and work developed on recycled vertical drains were also indicated. The insufficient research centred on the use of recycled materials inside drains drew attention to the need of further work related to this issue.

In the last section, research regarding settlement prediction, considering empirical methods and the mechanisms of deformation, has been presented. Further, the need for detailed research regarding the settlement mechanisms for shallow foundations considering unmitigated and mitigated soil has been recognised.

Chapter 3
Methodology

3.1 Introduction

The evaluation of soil behaviour during an earthquake, using full scale models, implies a high cost and results unpredictable in terms of time. Accordingly, physical modelling techniques that accurately simulate soil structure interactions with small scale models in a laboratory, are necessary. In particular, centrifuge modelling is an optimal option, as the stress and strains of the soil prototype could be accurately reproduced in a scaled model by raising the acceleration and hence the body forces within the soil.

Although centrifuge modelling presents a number of advantages, limitations also exist; for instance, a limited number of models could be developed. For this reason, numerical modelling has been extensively utilised by practitioners over the years to evaluate soil and structural responses. This methodology could be more beneficial compared to the experimental techniques, especially in terms of time; nevertheless, existing software continue to be ineffective in providing consistent solutions, particularly for liquefaction simulations. For instance, the effectiveness of numerical simulations has been analysed by the VELACS (Verification of Liquefaction Analysis by Centrifuge Studies) project, where the soil behaviour observed in centrifuge tests was contrasted with numerical models. The limitations of the numerical tools in liquefaction modelling were corroborated, as they were not successful in replicating the physical behaviour (Arulanandan and Scott, 1993). The continuous development of accurate techniques for simulating soil behaviour during and after earthquake-induced liquefaction using numerical modelling is required. More recently, NSF funded LEAP project has renewed the process of developing well curated database for liquefaction problems (Kutter *et al.*, 2018).

Dynamic centrifuge modelling was utilised in this work to evaluate the performance of drain arrangements below new and existing building. Numerical modelling was also used to establish a finite element (FE) simplified technique, that can accurately model the excess pore pressure dissipation in presence of drains, under buildings. This procedure was developed using ABAQUS software and then validated with the results obtained from physical modelling. The proposed technique offers practitioners a useful and uncomplicated method for selecting adequate drain material permeability so as to reduce structural damage in case of earthquake-induced liquefaction. The details of both methodologies, including the particulars of the FE simplified technique, are presented in this chapter.

3.2 Dynamic Centrifuge Modelling

3.2.1 Principles and scaling laws

The scaled model evaluated using centrifuge modelling corresponds to 1/N of the prototype; it is tested to a centrifugal acceleration equivalent to N times gravity. The scaled model demonstrates similar behaviour to the protype, as stresses and strains match at homologous points when incrementing the centrifugal acceleration. Scaling laws are required in centrifuge modelling, to relate the behaviour of the scale model and the prototype performance. These scaling laws are summarised in Table 3.1 (Madabhushi, 2014).

Table 3.1 Centrifuge modelling scaling laws

Parameter	Dimension	Model (N·g)/Prototype
Length	L	$1/N$
Mass	M	$1/N^3$
Force	MLT^{-2}	$1/N^2$
Stress	$ML^{-1}T^{-2}$	1
Strain	1	1
Velocity	LT^{-1}	1
Time (dynamic)	T	$1/N$
Acceleration	LT^{-2}	N
Frequency	T^{-1}	N
Time (seepage)	T	$1/N^2$
Velocity (seepage)	LT^{-1}	N

3.2.2 Cambridge geotechnical centrifuge

The Philip Turner Beam at the Schofield Centre of the University of Cambridge has been utilised to perform the dynamic centrifuge tests. Specifications of the Turner Beam are presented in Schofield (1980).

3.2.3 Servo-shaker actuator

The actuators utilised in centrifuge modelling must achieve the objective of applying sufficient energy in a short period of time. The earthquakes in this work were generated using the servo-shaker actuator (Madabhushi *et al.*, 2012). Realistic seismic shaking was simulated, considering specific amplitude and frequency. A detailed explanation of the actuator operating system is presented in Madabhushi (2014).

3.2.4 Model construction

Model container: Laminar box

The laminar box designed by Brennan *et al.* (2006) was used for all tests, as it represents a suitable option for liquefaction modelling. The box is composed of aluminium frames sliding on roller connections that allow each lamina to move independently, thereby reducing boundary effects as the laminae move with the soil. It has a cross-section of 500 × 250 mm and a depth of 300 mm. In addition, the box has a latex bag covering the inside area to maintain the fluid in the soil following saturation.

Sand pouring and installation of drains

The first centrifuge tests carried out in this work, involved evaluating the performance of vertical drain arrangements below new buildings. For the model construction, a layer of loose Hostun sand was poured inside the laminar box, using the automatic sand pouring machine at the Schofield Centre (Madabhushi *et al.*, 2006). After this, paper tubes with a specific diameter were stood at the base of the box, forming equilateral triangles spaced according to a specific *a/b* ratio (Fig. 3.1a,b). The tubes were filled with fraction B sand and carefully tamped to obtain uniformity (Fig. 3.1c). Later, these tubes were sealed with aluminium tape at the top to impede fine particles from entering (Fig. 3.1d). The sand pouring was continued, and the machine was stopped at specific depths for instrument placement, until the required soil height was reached. Finally, the tubes were removed gently following a vertical direction, to avoid disturbing the soil (Fig. 3.1e,f). The effectiveness of this construction process was validated after the test, as the lower part of the drains (far from

the foundation influence) conserved uniformity. Details of the model construction in each centrifuge test are presented in Section 3.2.9.

(a)

(b)

(c)

(d)

(e)

(f)

Fig. 3.1 Model construction procedure

A similar construction procedure was used for the arrangements of encased vertical drains (SG5) and single column (SG9) below new buildings, with small variations in the equipment used depending on the configuration. In the first case, perforated aluminium encasements (Fig. 3.2) with a radius of 10 mm and height of 42 mm were placed externally around the tubes, at the top part (Fig. 3.3), prior to their installation in the sand. After the sand pouring was finished, the tubes were withdrawn and the encasements were left in the model. For the single column arrangement, an aluminium square frame with a cross-section of 60 x 60 mm and a height of 142 mm was utilised instead of tubes (Fig. 3.4).

In the model construction of inclined perimeter drains below existing buildings (SG6, SG7), inclined paper tubes were carefully pushed into the sand, approximately 15 mm deep, using an angle of 28° to the vertical axis (Fig. 3.6a). Steel stay wires were utilised, which were inserted at the top of the tubes, to ensure that the drains maintained correct positioning during sand pouring for the shallow layers (Fig. 3.6b,c). In this case, the distance from the drains to the vertical axis below the foundation varied along the stratum.

Saturation

After finishing the sand pouring, the laminar box was sealed from the bottom to start the saturation process. At this stage, the model was subjected to a vacuum of -85 kPa for roughly 30 minutes to remove the air from inside the sand. In addition, CO_2 was utilised to flush the model to ensure a high level of saturation. This procedure was performed two times. After applying the last vacuum of -85 kPa, fluid was injected from the bottom of the soil at a rate of 0.3 kg/h to avoid disturbance of particles. This was conducted using the CAM-Sat system, wherein the model and tank pressures were regulated by the computer. Details of the CAM-Sat system could be found in Stringer and Madabhushi (2009).

The model saturation was conducted utilising a concentration of hydroxypropyl methylcellulose (HPMC) mixed with water, as an increment of the fluid viscosity was desired to obtain a match between the scaling laws of the rate of generation and dissipation (reconsolidation) of excess pore pressures.

Solutions with different concentrations of HPMC were measured at T=20° (laboratory temperature) by Adamidis and Madabhushi (2015), who proposed equation 3.1 to calculate the concentration percentage (c) required for a specific viscosity at this temperature. In addition, the relation between the fluid viscosity at T=20° and different temperatures was also established, after the evaluation of the temperature variation in the solution viscosity was developed (equation 3.2). Both equations were utilised to obtain the mass concentration required for a particular viscosity in the model at a specific temperature in the centrifuge room. Fluid viscosity at $20°C$ in the models were in a range between 33-42 cSt.

$$\mu(mPa \cdot s) = (0.268 \cdot c(\%) + 1.094)^8 \tag{3.1}$$

$$\frac{\mu_{T°C}}{\mu_{20°C}} = 2.44e^{-0.045 \cdot T°(C)} \tag{3.2}$$

The foundations were made of brass alloy (CZ121), with a cross-section of 60×60 mm and a height of either 11.7 (50 kPa) or 35.1 mm (150 kPa) depending on the required bearing pressure (Fig. 3.7). After the model saturation, and after the model was placed in the centrifuge beam, the foundation was placed on the sand surface to avoid previous soil densification (Fig. 3.8).

The bearing pressure of 50 kPa was considered in the analysis as this represents a reasonable bearing pressure below foundations of single or two storied residential buildings. This is also considered a standard value utilised by researchers when evaluating liquefaction cases using centrifuge modelling. On the other hand, the foundation of 150 kPa was selected to represent much taller buildings. Also the main aim of this research was to obtain a significant variation in the response of the soil and the structure compared to that of the lighter structure. Moreover, this represents a high value of pressure that is not regularly analysed by many researchers when using physical modelling, with the exception of Ghosh (2003); therefore, considerable data is required in terms of foundation and soil response.

Fig. 3.2 Aluminium encasement

Fig. 3.3 SG5 construction procedure

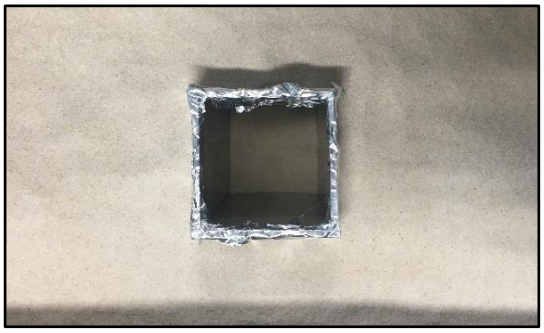

Fig. 3.4 Aluminium square frame

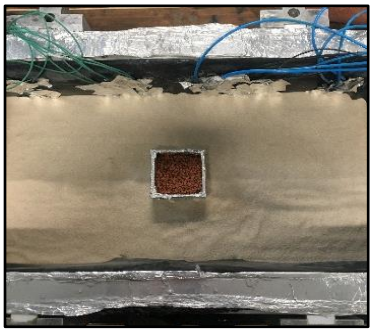

Fig. 3.5 SG9 construction procedure

(a)

(b)

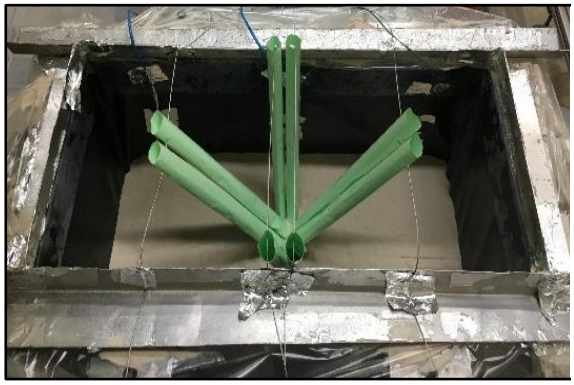

(c)

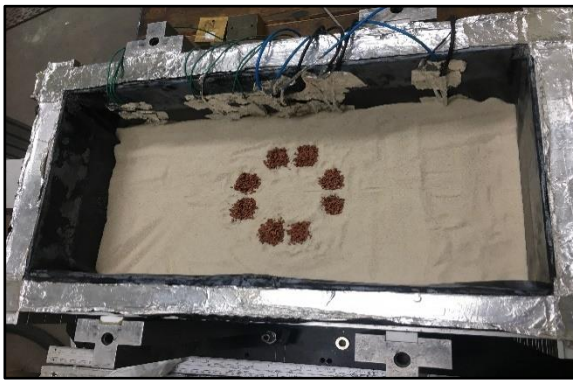

(d)

Fig. 3.6 Construction procedure of the inclined perimeter drain arrangement

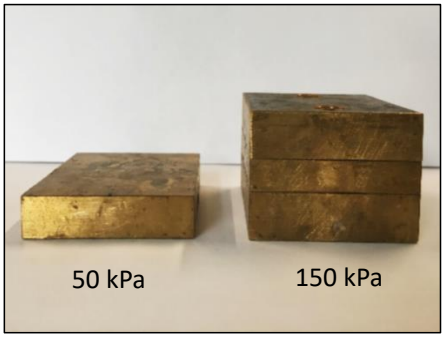

Fig. 3.7 Foundations

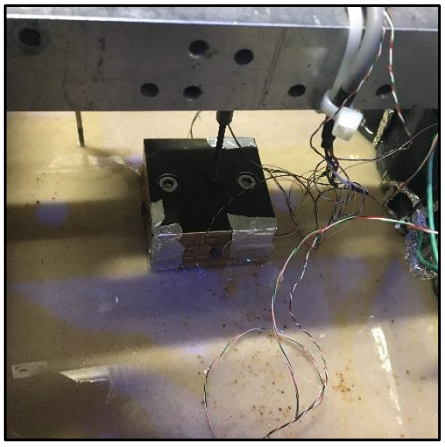

Fig. 3.8 Foundation placed at the soil surface

3.2.5 Instrumentation

Four different instruments were utilised in the centrifuge model to measure the soil and foundation response. The calibration of instruments was performed prior to and after the tests. The output voltage was processed using MATLAB. Data filtering of frequencies over 400 Hz was conducted utilising the filter of low-pass Butterworth in order to clean the response. The specifications of the instruments mentioned in this section are presented in Madabhushi (2014).

Pore pressure transducers

Pore pressure transducers (PPTs) were used in the model, which were located at strategic locations in the soil. These PPTs, produced by Druck Ltd, has a porous bronze stone at the top, with a diameter of 6.4 mm as well as a steel casing capable to produce a voltage output. De-aired water pressure was utilised for instrument calibration. In this procedure, following a load and unload sequence, the pore pressure was varied from 0 to approximately 7 bar, The voltage output was recorded for each pore pressure value.

Linear variable displacement transducers

The settlement of the foundation was measured using linear variable displacement transducers (LVDTs), which were placed at the top of the structure together with an aluminium circular piece to improve attachment to the foundation. Moreover, LVDT extensions were required for all tests as a significant settlement response was expected. The calibration factor was calculated from the displacement and voltage graph, which presented a linear trend.

Piezo-electric accelerometers

Piezoelectric accelerometers were used to measure the acceleration in the soil. The accelerometers, fabricated by D.J.Birchall Ltd, are made with a piezocrystal that received a specific stress which is then transformed into an electric response. The instrument calibration was performed employing the Brüel & Kjær's calibrator, which applied acceleration to the instrument. Waterproof piezo accelerometers were required for the saturated models. A layer of wax was laid around the instruments before they were placed in the sand. The location of the piezo accelerometers in the model followed the direction of shaking.

Microelectromechanical system accelerometers

Microelectromechanical system accelerometers (MEMS) were bonded to the foundation, to obtain the structural acceleration at specific locations. The instruments register the acceleration response based on a mechanism containing a spring and a mass. The calibration factor was obtained from the rotation angle and voltage output graph. Horizontal and vertical MEMs were utilised for the foundations.

3.2.6 Earthquakes

The dynamic centrifuge tests were carried on at 50 g. Four different earthquakes were fired for each centrifuge test (Table 3.2). The earthquakes were intended to have the same characteristics for each test; however, due to issues related to instrumentation, input motions were not consistently similar. The data was recorded using DASYLab, with a sampling frequency of 6000 Hz for the earthquake duration and 100 Hz for the swing up and down.

The first earthquake (EQ1) was not considered for analysis as excess pore pressures were not significantly generated during the shaking; moreover, negligible settlement response of the foundation was registered. In contrast, significant increment of excess pore pressures was observed during the second earthquake (EQ2), as well as a more realistic structural response. The model subjected to additional earthquakes after EQ2, implies a significant variation in the initial soil state, as the soil liquefaction resistance rises (Mitrani, 2006). Therefore, the third and fourth earthquakes do not represent ideal options for analysis. The second earthquake was selected for evaluation and comparison between centrifuge tests. The details of the selected earthquake are presented in Section 3.2.9 for each test.

Table 3.2 Earthquakes programme (prototype scale)

Earthquake	Duration (s)	Peak acceleration (g)	Frequency (Hz)
EQ 1	10	0.04	1
EQ 2	10	0.2	1
EQ 3	10	0.3	1
EQ 4	60	0.1	2

3.2.7 Material characterisation

Three different soil materials were used in this work. Hostun sand was used as the host fine soil, while Fraction-B LB and rubble brick were utilised as drain coarse material. The required relative density for the soil materials was approximately 40% (see Section 3.2.9).

The grading curves for the soils, developed using the sieving method, are presented in figure 3.9. Particular attention was given to the material characterisation of the rubble brick. This material was acquired by crushing masonry red bricks with a hammer, until average, small-size particles were obtained (Fig. 3.10). The standard method ASTM D4254 (ASTM, 2016) was used to attain the e_{max} value, and the e_{min} was acquired by the compaction method BS 1377-4 (BSI, 1990). In addition, the standard method of water pycnometer ASTM D854 (ASTM, 2014) was performed to obtain the specific gravity (G_s) of the soils.

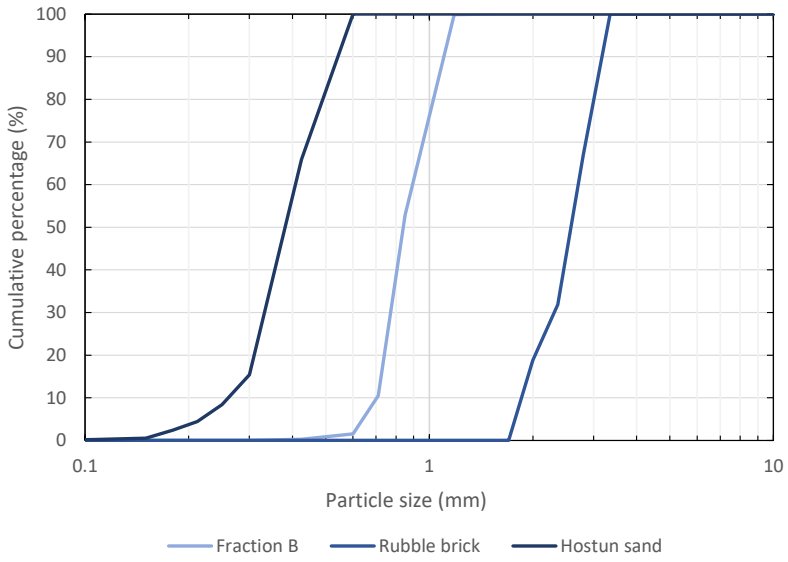

Fig. 3.9 Grading curves for the soils

Properties of the materials are presented in Table 3.3, including the properties for Hostun sand and Fraction B obtained by Haigh *et al.* (2012) and Garala *et al.* (2020) respectively, together with the values attained for the rubble brick material.

Permeability

Soil permeability is a critically relevant factor in this research, as vertical drains must contain highly permeable material to achieve optimal behaviour. Permeability tests were developed for the three materials using the constant head method and considering relative

densities close to that of the model. A permeability value of 1×10^{-3} m/s was obtained for the Hostun sand, which is similar to the magnitude obtained by Haigh *et al.* (2012). Fraction B permeability reached a value of 2×10^{-3} m/s, comparable to the magnitude attained by Vickers (2001), using the same method. Finally, the rubble brick has a permeability of 5×10^{-3} m/s. Although the latter differs from the estimation of permeability obtained using the Hazen equation (1892), this result, obtained experimentally, was utilised as it represents a trustworthy value. Permeability values are detailed in Table 3.3.

Fig. 3.10 Rubble brick

Clogging

The effect of clogging represents an issue in drainage countermeasure techniques, as high-permeable drains contains large particle sizes. The grain size range selected for Fraction B and rubble brick, followed the anti-clogging criteria proposed by the Japanese Large Dam Conference (JLDC), which was recommended by Orense *et al.* (2003) for crushed stones (equation 3.3). Indeed, the non- interference of fine particles inside the drains, particularly at the top of the columns, cannot be guaranteed as the foundation bearing pressure could present considerable influence over the drain.

$$\frac{D_{15\,(drain)}}{D_{85\,(soil)}} < 5 \tag{3.3}$$

Table 3.3 Properties of soil

Property	Hostun sand	Fraction B	Rubble brick
Maximum void ratio, e_{max}	0.648[a]	0.767[b]	1.45
Minimum void ratio, e_{min}	1.041 [a]	0.49 [b]	0.87
Specific gravity, G_s	2.65 [a]	2.65 [b]	2.50
Average particle size, D_{50}: *mm*	0.39	0.82	2.5
Relative density, *Dr:%*	44	43	46
Permeability, *k:mm/s*	1	2	5

[a.] Haigh *et al.* (2012)
[b.] Garala *et al*, (2020)

Direct shear tests

The soil materials were subjected to direct shear tests, with a vertical stress of 100 kPa. A relative density similar to the soil in the centrifuge test was intended to achieve for the samples. Figure 3.11 presents the results for Hostun sand, Fraction B and rubble brick.

The angle of friction of the Hostun sand reached a value of 35°, which is close to the critical friction angle (φ_{crit}) obtained by Heron (2013) from a drained triaxial test (35.4°). The obtained angle is slightly higher compared to the φ_{crit} value of 33° proposed by Mitrani (2006) for Hostun sand. For the purpose of liquefaction simulation using numerical modelling, 33° was assumed for this material. In addition, the friction angle of Fraction B reached 37°, which is also close to the critical friction angle obtained by Garala *et al.* (2020) for the same material (37.7°), in a drained triaxial test. In the case of rubble brick, a friction angle of 46.5° was obtained, a larger value compared with the previous materials, as expected.

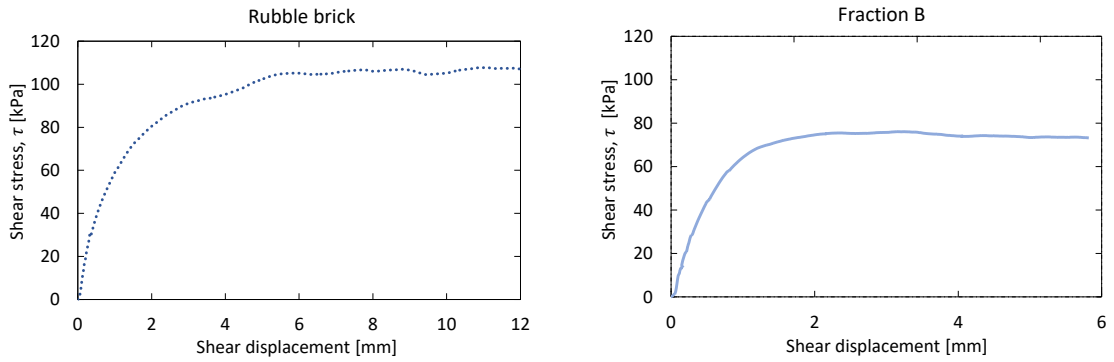

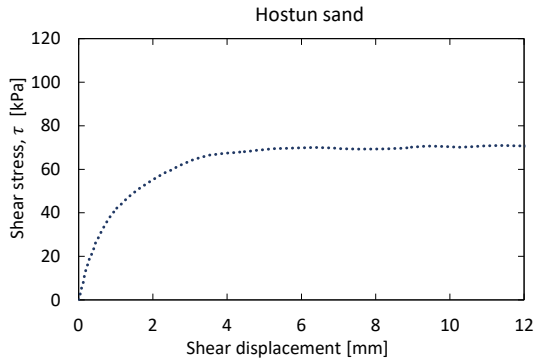

Fig. 3.11 Direct shear test for soil materials

3.2.8 Data processing: Excess pore pressure contours

PPTs were placed at relevant locations in the soil, as a reduced number of pore pressure transducers were suitable to be used in the model, limiting the quantity of data. Due to the symmetry of the drain arrangements, extra data points with a pore pressure similar to the real data point were established. These are denominated as “image points”. According to Brennan (2004), if the real point is denoted as z = x + iy (referred from the centre of the arrangement) the “image points” would be -z, z* and -z*. Figure 3.12 shows a plan view of the symmetry axes presented in the evaluated arrangements, illustrating the location of real and image data points at the top layer. Various symmetry axes could be presented per arrangement, depending on the drain configuration. In addition, the symmetry axis could differ for each drain ring. For instance, only four symmetry axes were presented in SG2 due to the simple rectangular drain pattern (Fig. 3.12a). Alternatively, due to the number of drains in SG4, located particularly inside the configuration (Fig. 3.12b), the number of symmetry axis varied per drain ring. Four symmetry axes were presented for the internal ring, while six and four were presented for the sub-perimeter and perimeter ring, respectively. In this way, it was possible to obtain the soil behaviour in terms of pore pressure over the entire layer. Horizontal layouts of the soil showing the symmetry axes of the arrangement may be found in the Appendix A for the other tests. In addition, horizontal and vertical pore pressure contours were generated using the griddata function from MATLAB. By using this function, a cubic interpolation of the excess pore pressure magnitudes was developed, which considered the real and image data points of the soil layer.

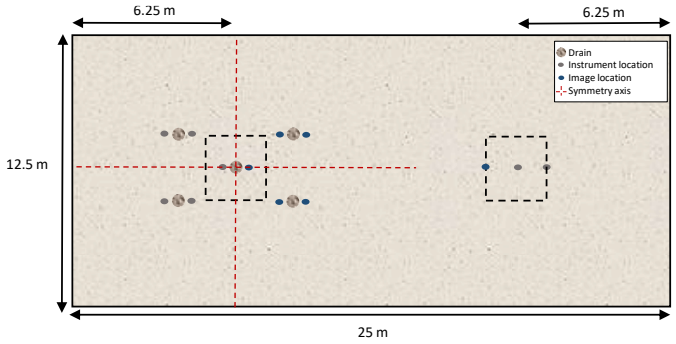

(a) Test SG1 and SG2

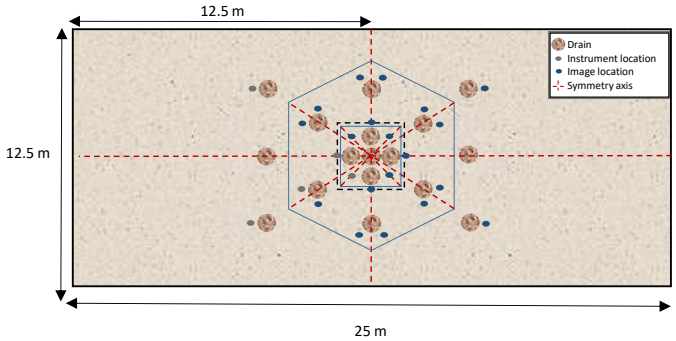

(b) Test SG4 and SG5

Fig. 3.12 Symmetry axes of the arrangement

3.2.9 Centrifuge test plan

Layouts corresponding to the nine centrifuge models are presented in this section (Fig. 3.14-3.21). Details related with the drain arrangement and the foundation are presented, together with specifications of the earthquake selected for analysis. In some models, a coarse sand layer placed below the foundation keeps drainage in this area and allows a connection between drains at the surface. This may have an effect on drainage rates below the building and hence on performance. Horizontal layouts of the soil top layer are provided, including a 3D vertical perspective of the inclined drain arrangement for an improved visualization. Dimensions are presented in prototype scale. Similarly, data in the following chapters is presented in prototype scale, unless otherwise indicated.

SG1

- Arrangement: five vertical drains below new buildings
- Bearing pressure: 50 kPa
- Drain material: Fraction B
- Drain radius: 0.3 m
- a/b ratio: 0.2
- Relative density (Fraction B): 42%
- Relative density (Hostun sand): 44%
- Selected earthquake for analysis: 1 Hz, Peak acceleration: 0.31 g, 10 s.

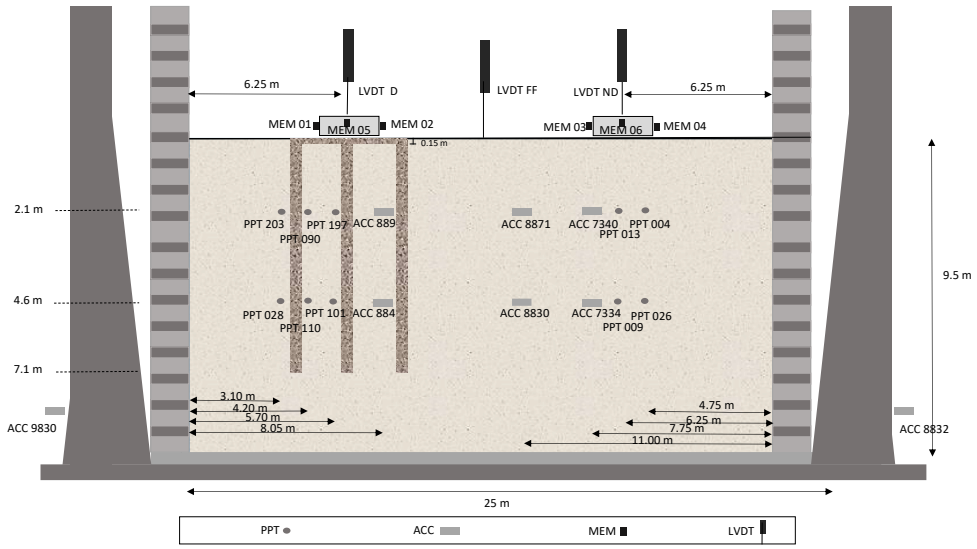

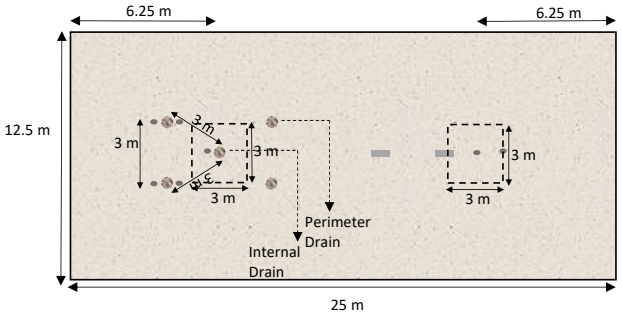

Fig. 3.13 Test SG1

SG2

Left side

- Arrangement: five vertical drains below new buildings
- Bearing pressure: 150 kPa
- Drain material: Fraction B
- Drain radius: 0.3 m
- a/b ratio: 0.2
- Relative density (Fraction B): 44%

Relative density (Hostun sand): 43%

Right side

- Unimproved soil
- Bearing pressure: 150 kPa

- Selected earthquake for analysis: 1 Hz, Peak acceleration: 0.3 g, 10 s.

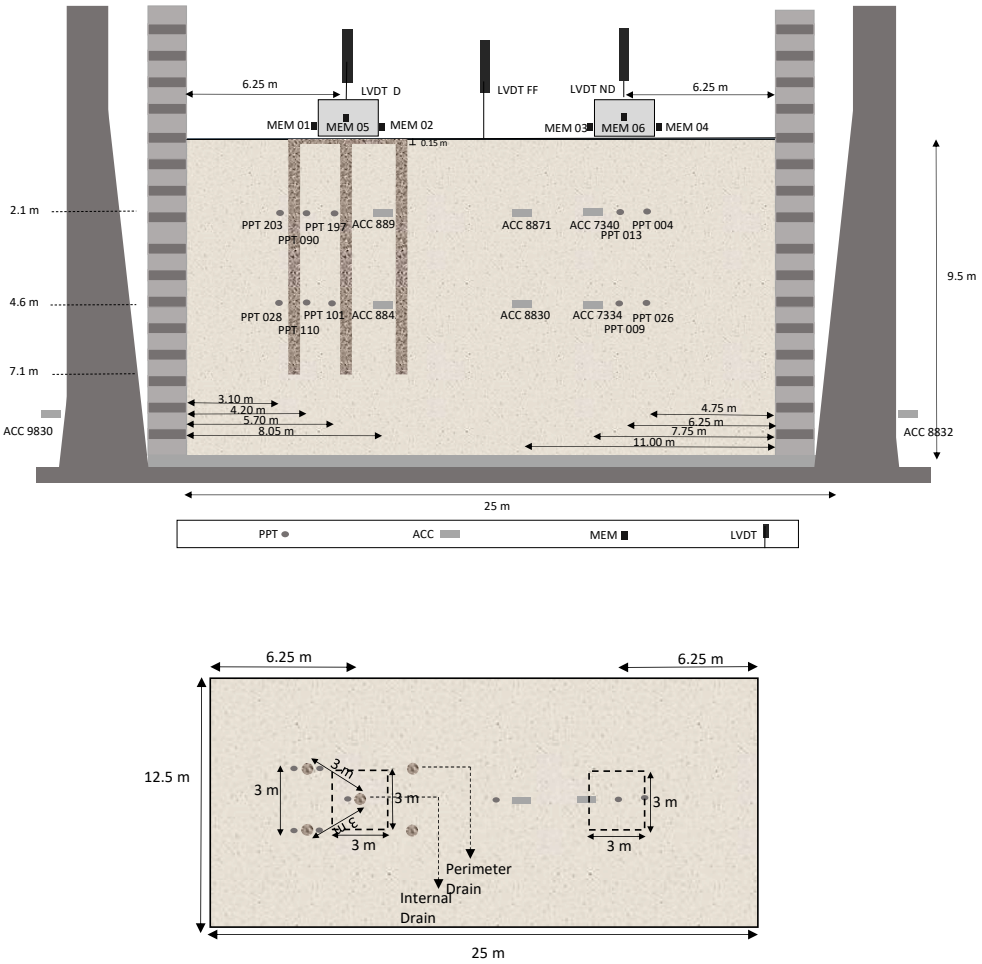

Fig. 3.14 Test SG2

SG3

- Arrangement: 13 vertical drains below new buildings
- Bearing pressure: 150 kPa
- Drain material: Rubble brick
- Drain radius: 0.4 m
- a/b ratio: 0.27
- Relative density (Fraction B): 41%
- Relative density (Hostun sand): 43%
- Selected earthquake for analysis: 1 Hz, Peak acceleration: 0.19 g, 10 s.

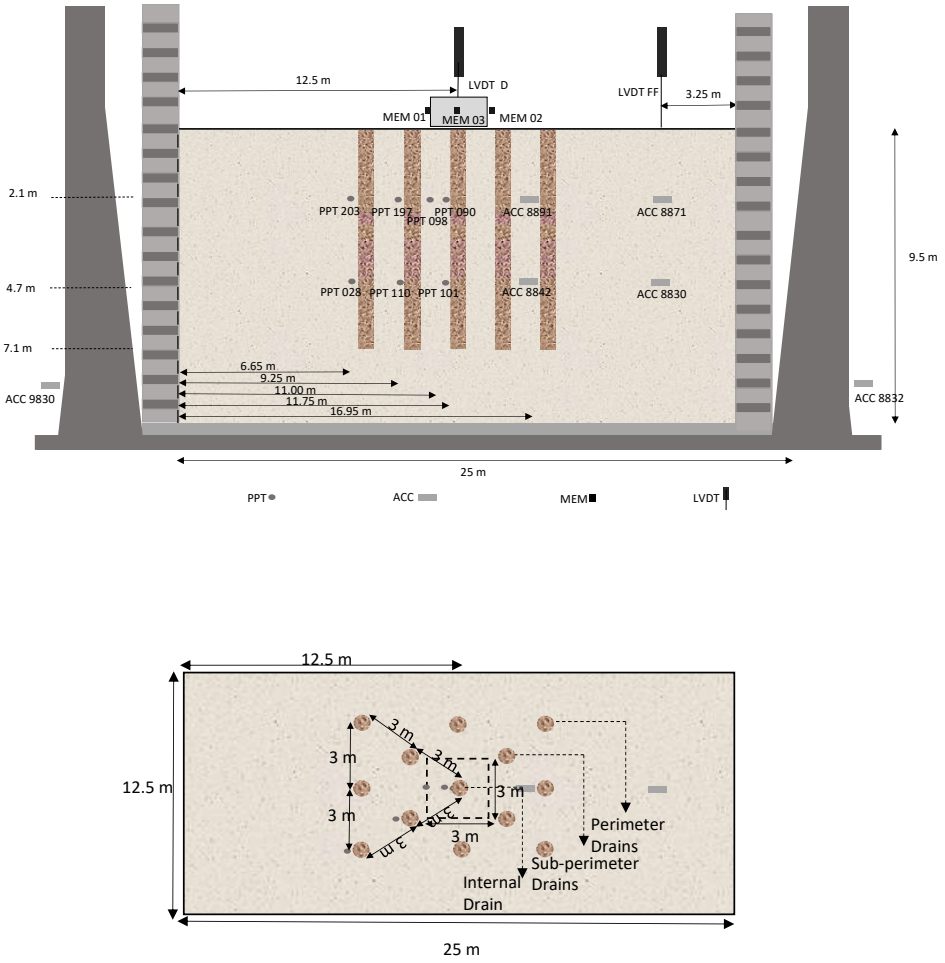

Fig. 3.15 Test SG3

SG4

- Arrangement: 17 vertical drains below new buildings
- Bearing pressure: 150 kPa
- Drain material: Rubble brick
- Drain radius: 0.4 m
- a/b ratio: 0.27
- Relative density (Fraction B): 40%
- Relative density (Hostun sand): 43%
- Selected earthquake for analysis: 1 Hz, Peak acceleration: 0.2 g, 10 s.

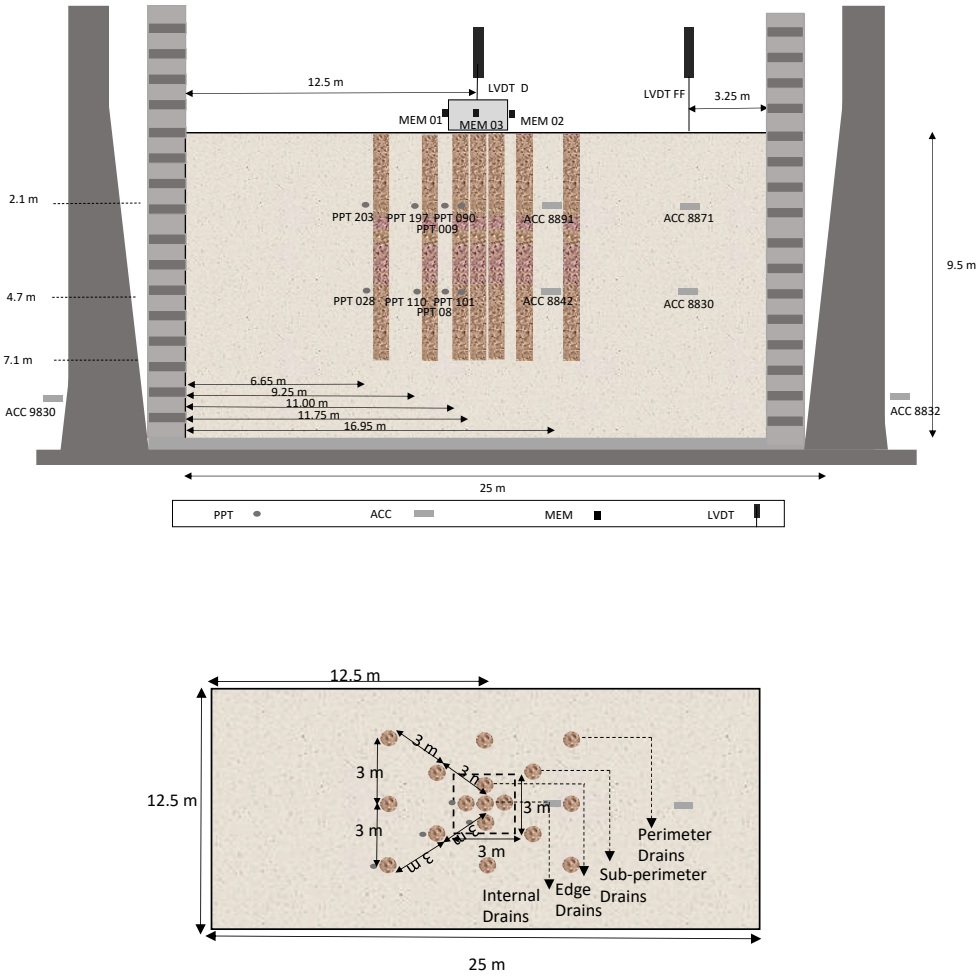

Fig. 3.16 Test SG4

SG5

- Arrangement: 17 encased vertical drains below new buildings
- Bearing pressure: 150 kPa
- Drain material: Rubble brick
- Drain radius: 0.4 m
- a/b ratio: 0.27
- Relative density (Fraction B): 39%
- Relative density (Hostun sand): 44%
- Selected earthquake for analysis: 1 Hz, Peak acceleration: 0.21 g, 10 s.

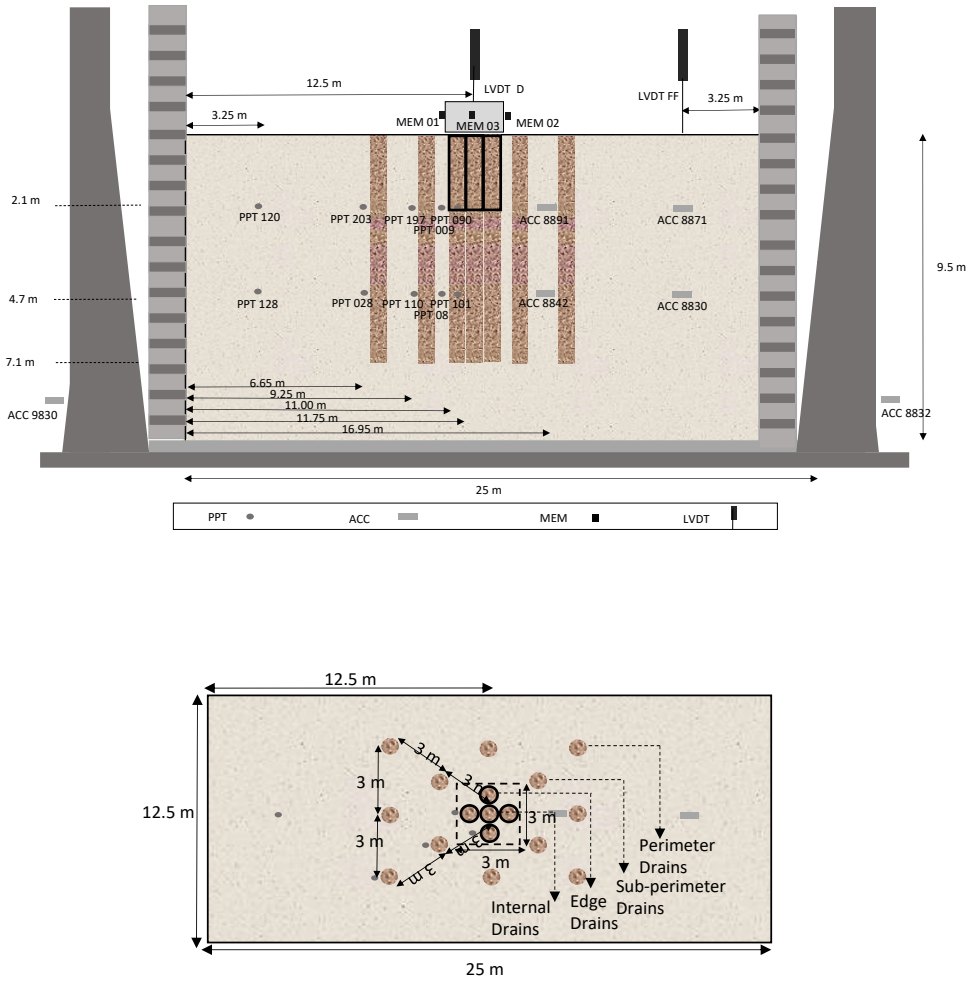

Fig. 3.17 Test SG5

SG6

- Arrangement: Inclined perimeter drains below existing buildings
- Bearing pressure: 150 kPa
- Drain material: Rubble brick
- Drain radius: 0.5 m
- a/b ratio: 0.45
- Relative density (Fraction B): 41%
- Relative density (Hostun sand): 43%
- Selected earthquake for analysis: 1 Hz, Peak acceleration: 0.21 g, 10 s.

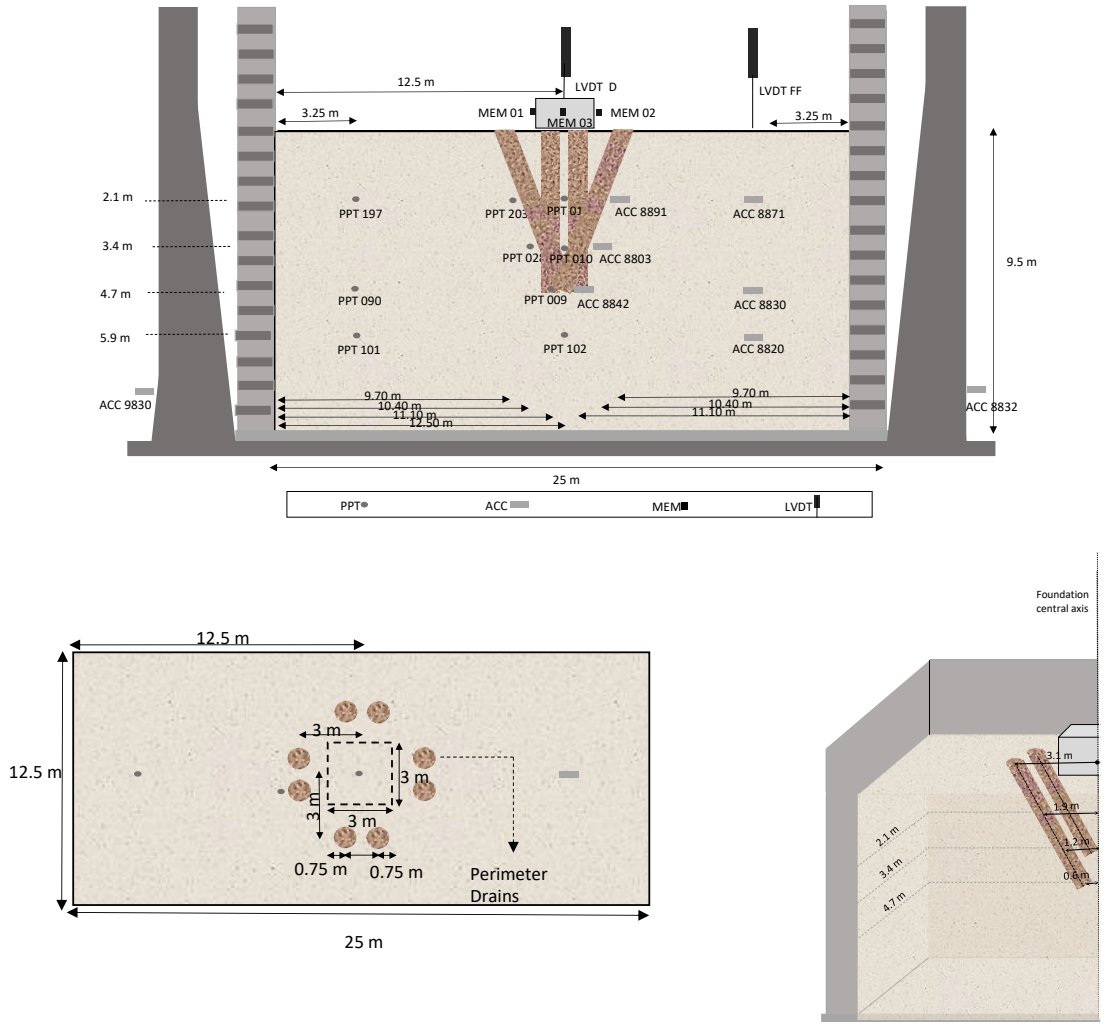

3D view of soil with inclined drains

Fig. 3.18 Test SG6

SG7

- Arrangement: Inclined perimeter drains below existing buildings
- Bearing pressure: 50 kPa
- Drain material: Rubble brick
- Drain radius: 0.5 m
- a/b ratio: 0.45
- Relative density (Fraction B): 39%
- Relative density (Hostun sand): 45%
- Selected earthquake for analysis: 1 Hz, Peak acceleration: 0.2 g, 10 s.

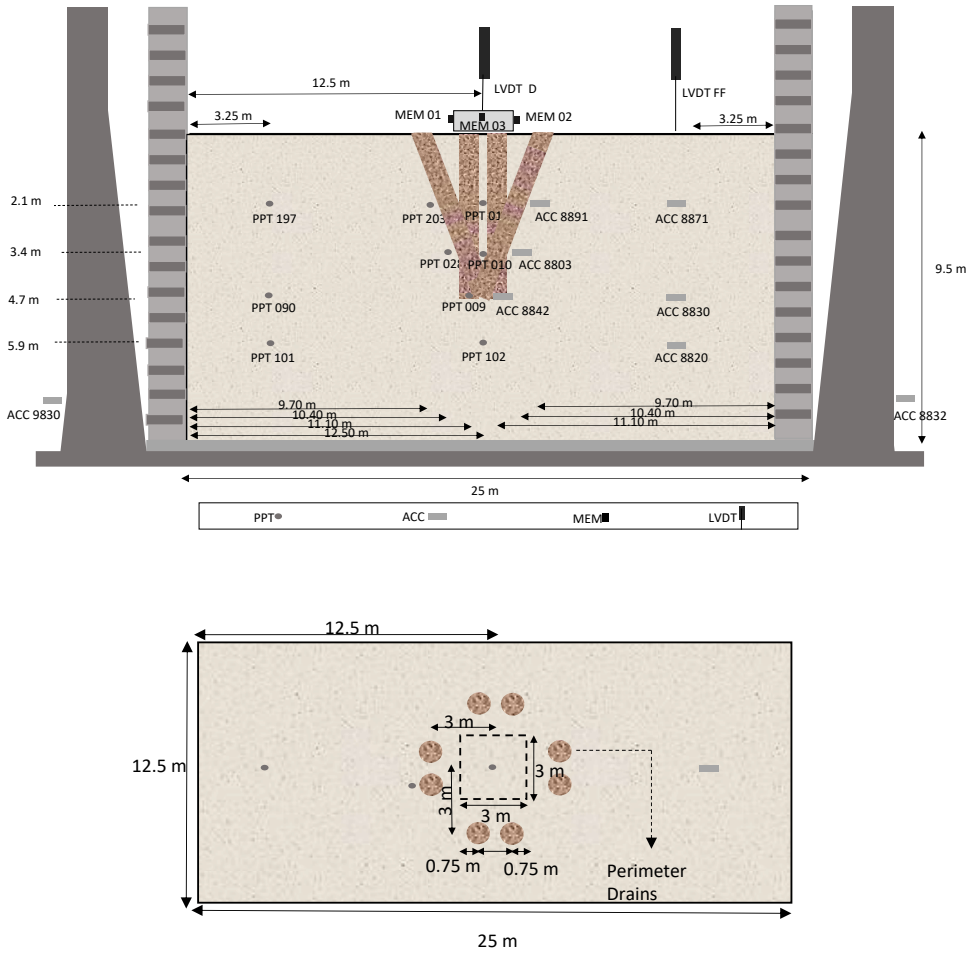

Fig. 3.19 Test SG7

SG8

- Arrangement: Vertical perimeter drains below existing buildings
- Bearing pressure: 50 kPa
- Drain material: Rubble brick
- Drain radius: 0.5 m
- a/b ratio: 0.45
- Relative density (Fraction B): 38%
- Relative density (Hostun sand): 44%
- Selected earthquake for analysis: 1 Hz, Peak acceleration: 0.2 g, 10 s.

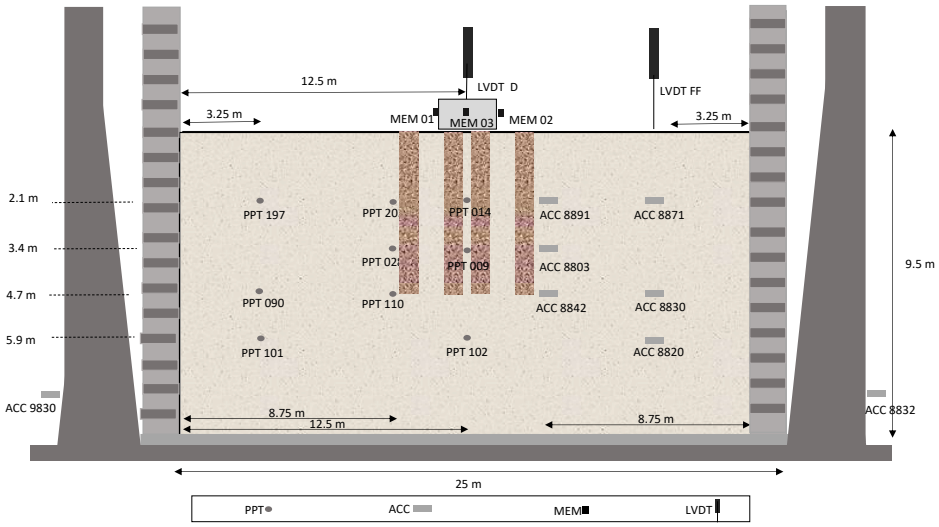

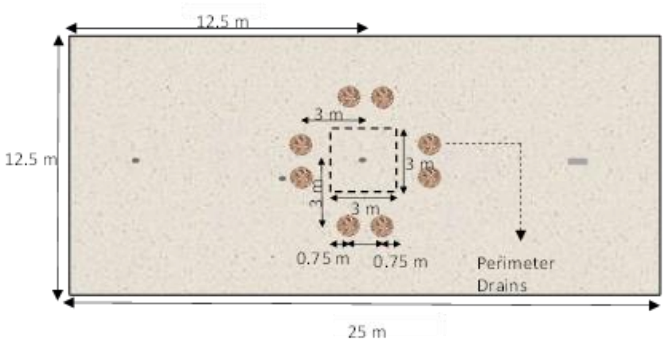

Fig. 3.20 Test SG8

SG9

- Arrangement: Single column below new buildings
- Bearing pressure: 150 kPa
- Drain material: Rubble brick
- Column cross-section area: 3 m × 3m
- Relative density (Fraction B): 39%
- Relative density (Hostun sand): 40%
- Selected earthquake for analysis: 1 Hz, Peak acceleration: 0.2 g, 10 s.

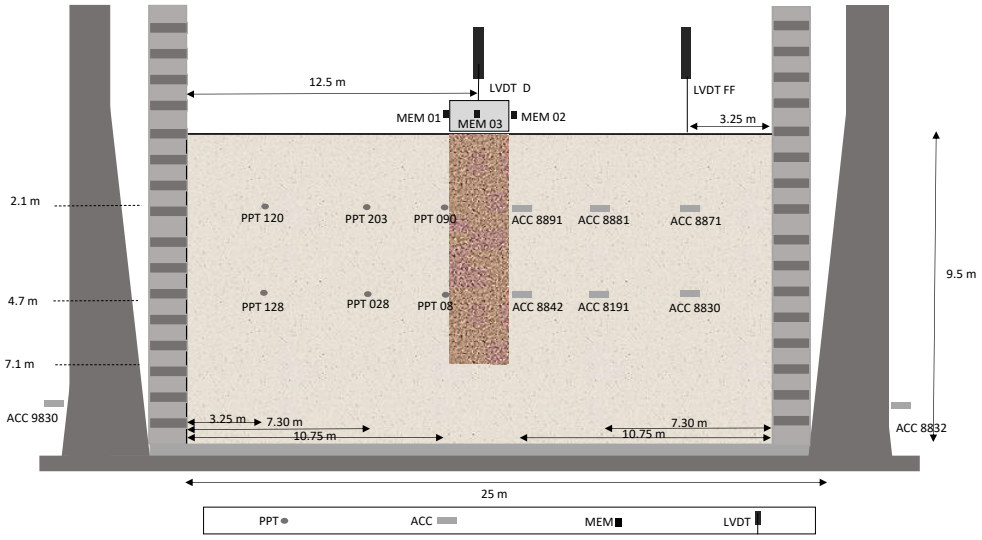

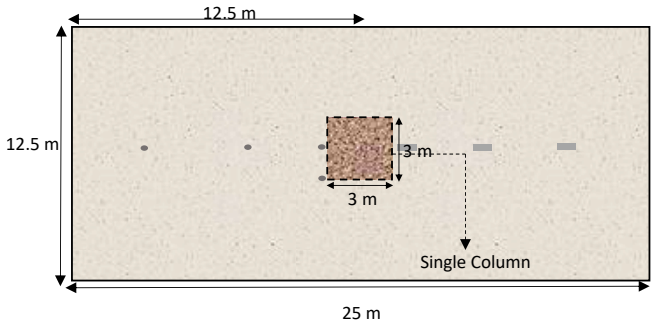

Fig. 3.21Test SG9

3.3 Numerical modelling

A simplified FE technique was developed for the effective simulation of excess pore pressure dissipation of the soil containing a specific drain arrangement, below new and existing buildings. The methodology behind the technique is described in this section.

The software utilised for this analysis was ABAQUS (6.14), which is widely used by researchers for 3D geotechnical proposes due to its capacity of using soil characteristics that are necessary to represent an approximation of the real prototype.

The software is able to perform a series of procedures to evaluate soil-structure interaction, considering static and dynamic analysis in the process; nevertheless, coupled pore fluid and dynamic analysis could not be developed, suggesting the impossibility of simulating earthquake-induced liquefaction. For this reason, the simplified procedure developed in this work considers, the excess pore pressure replication as a load boundary condition in the stratum. In doing so, soil liquefaction behaviour was simulated in the coupled pore fluid diffusion and stress analysis.

3.3.1 Model elaboration in ABAQUS/ CAE

The steps followed for the FE technique are described in this section. Relevant details required for the model construction are presented.

3.3.1.1 Parts

The soil, drain arrangement and foundation were modelled as solid bodies in 3D with dimensions in prototype scale. The cross-sectional area of the soil has dimensional variations across different models, with the aim to obtain more accurate results. These modifications will be explained in detail in Chapter 7, where the simplified technique is applied and validated.

3.3.1.2 Constitutive model and properties

Soil

The constitutive model defines the relation between stress and strains in the soil, becoming highly relevant in the analysis as the suitability of the material behaviour is related with the precision of the results. This relation is denoted by the constitutive equation (3.4), in which *D* corresponds to the constitutive matrix (Franzius, 2003).

$$\sigma = D\varepsilon \tag{3.4}$$

In this work, the *Mohr-Coulomb* constitutive model was utilised for the behaviour of fine and coarse soil. This criterion was selected because the main aim of the assessment involves the performance of vertical drains in terms of excess pore pressure dissipation. In addition, the dynamic simulation was omitted in the analysis, therefore the shear strength provided by the drains will not be considered in these analyses. Moreover, linear elastic model criteria were effectively employed by previous researchers for the behaviour of drains in clay consolidation using the same software, based on the principal drainage function of vertical drains (Ye *et al.*, 2013; Liu and Rowe, 2015).

The soil stiffness (*E)* was approximated using equation 3.5. The shear modulus (G), at initial conditions was calculated with equation 3.6, provided by Hardin and Drnevich (1972) for the G_{max}value (shear modulus considering small strains in the soil), where *e* is the void ratio, p' the mean effective stress, and ν is Poisson's ratio. The increase of soil stiffness along the stratum depth was expected for cohesionless sands; for this reason, the stratum was divided into one-metre deep parts to assign various Young's modulus values for fine sand (Table 3.4). An average *E* constant value was assumed for the drain coarse materials, corresponding to the column mid-depth stiffness, for model simplification. Poisson's ratio for the soils was assumed to be 0.3, which was based on conventional values of loose sand (Gunaratne, 2006).

$$E = 2(1 + \nu)G \tag{3.5}$$

$$G_{max} = 100\frac{(3 - e)^2}{1 + e}(p')^{0.5} \tag{3.6}$$

The friction angle parameter for the Fraction B and rubble brick materials were obtained from the direct shear tests, previously indicated. For the Hostun sand, the critical friction angle of 33° proposed by Mitrani (2006) was considered. The dilation angle is frequently considered to be low for loose sand (Vermeer and Borst, 1984; Haji, 2017); therefore, a

magnitude of 3° was considered for the different soils in the analysis. A parametric evaluation contemplating the variation of the dilation angle was developed, showing no effect on the results.

Table 3.4 Young's modulus values for Hostun sand along the stratum depth

Depth (m)	Young's modulus *E* (MPa)
1.0	52.49
2.0	74.23
3.0	90.92
4.0	104.98
5.0	117.37
6.0	128.57
7.0	138.88
8.0	148.47
9.0	157.47
9.5	161.79

Although a zero-cohesion condition should be considered for sands, a small value of 0.25 kPa was utilised in the model due to convergence problems. Finally, the permeability obtained from the constant head permeability test for the Hostun sand and coarse materials was considered.

The indicated properties of the fine and coarse soil, utilised for the numerical model, are summarised in Tables 3.5 and 3.6. Calibrating certain properties was required to accurately simulate the soil liquefaction behaviour during the generation and dissipation of excess pore pressures. Although the simulation of the soil behaviour during shaking is not the aim of the technique, it is required because it corresponds to the initial comportment of the soil during the reconsolidation stage. This calibration is detailed in Chapter 7.

Table 3.5 Hostun sand properties

Material	Density	Permeability	Void ratio	Poisson's ratio	Friction angle	Dilation angle	Cohesion
	ρ (kg/m^3)	k (m/s)	e	ν	φ (°)	ψ (°)	c (kPa)
Hostun sand	1417	1×10^{-3}	0.87	0.3	33	3	0.25

Table 3.6 Drain material properties

Material	Density	Young's modulus	Permeability	Void ratio	Poisson's ratio	Friction angle	Dilation angle	Cohesion
	ρ (kg/m^3)	E (MPa)	k (m/s)	e	ν	φ (°)	ψ (°)	c' (kPa)
Fraction B	1600	158.9	2×10^{-3}	0.64	0.3	37	3	0.25
Rubble brick	1135	48.1	5×10^{-3}	1.20	0.3	46	3	0.25

Foundation

The foundation of 150 kPa was modelled with a linear elastic behaviour. The material properties (brass alloy CZ121) are presented in Table 3.7.

Table 3.7 Foundation properties

Material	Density	Young's modulus	Poisson's ratio
	ρ (kg/m^3)	E (MPa)	ν
Foundation (brass alloy)	8553	1×10^5	0.31

3.3.1.3 Assembly

The stratum containing the vertical drain arrangement, together with the foundation, were assembled and merged into a single geometry retaining intersecting part boundaries, which denotes a tie constraint interaction between the parts (SIMULIA, 2014) (Fig. 3.22). The surfaces of the parts inside the soil were strongly attached during the analysis and no separation or movement between the drains and the soil was expected. Moreover, due to the foundation high stiffness and non-dynamic response, separation from the soil surface was not likely to occur. Although the total geometry considered the entire soil and the foundation, for the evaluation of the soil behaviour during the first steps (in which only the soil stratum was analysed) the foundation presence was deactivated.

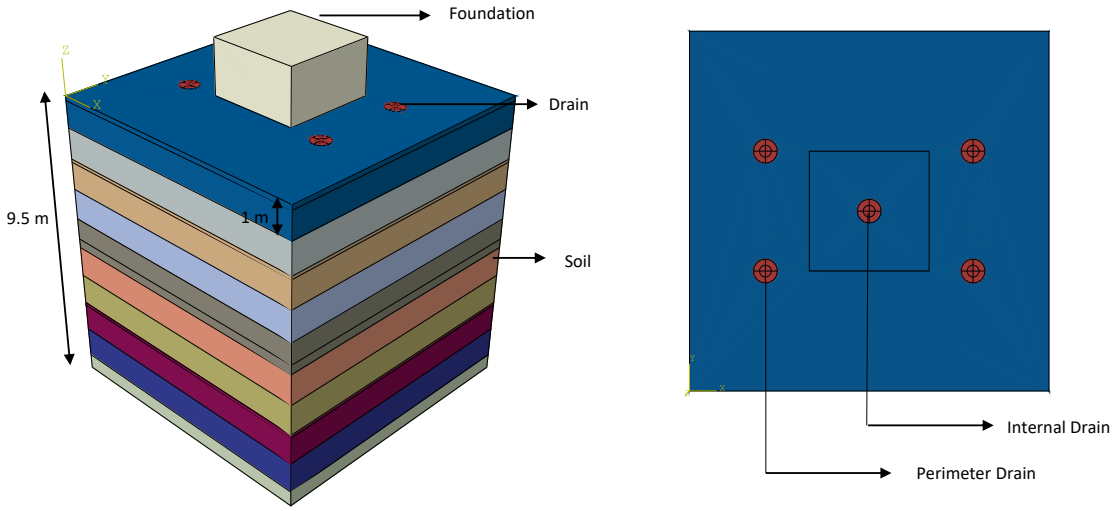

(a) Parts assembly (3D view) **(b) Soil cross-section (x-y view) (without foundation)**

Fig. 3.22 Model assembly

3.3.1.4 Mesh

The model mesh was generated after the different parts were assembled. The seed technique was utilised to provide a specific element size to the edges, approximately one metre wide. In addition, the element types and shapes were determined. Pore fluid/stress elements (C3D8P: 8-node trilinear displacement and pore pressure) were considered to replicate the soil behaviour (Ye *et al.*, 2013), while 3D stress elements (C3D8R: 8-node linear brick) were utilised for the foundation. The 3D model mesh for the simplified arrangement of SG2 is presented in figure 3.23.

3.3.1.5 Initial boundary conditions

At the stratum boundaries, node displacement was enabled in the perpendicular direction, including rotation in their same axis and in the depth direction. All degrees of freedom were constrained at the base of the model. In addition, zero excess pore pressure was set at the soil surface, enabling a drainage behaviour of the soil. Complete saturation of the model was considered as initial predefined field (Fig. 3.24a).

3.3.1.6 Analysis steps and application of loads

A sequence of five steps were followed to model the performance of drains below new and existing buildings. The steps are described in detail in Table 3.8.

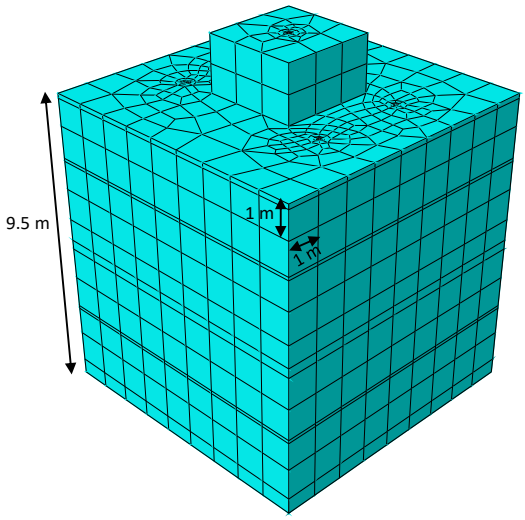

Fig. 3.23 Model mesh

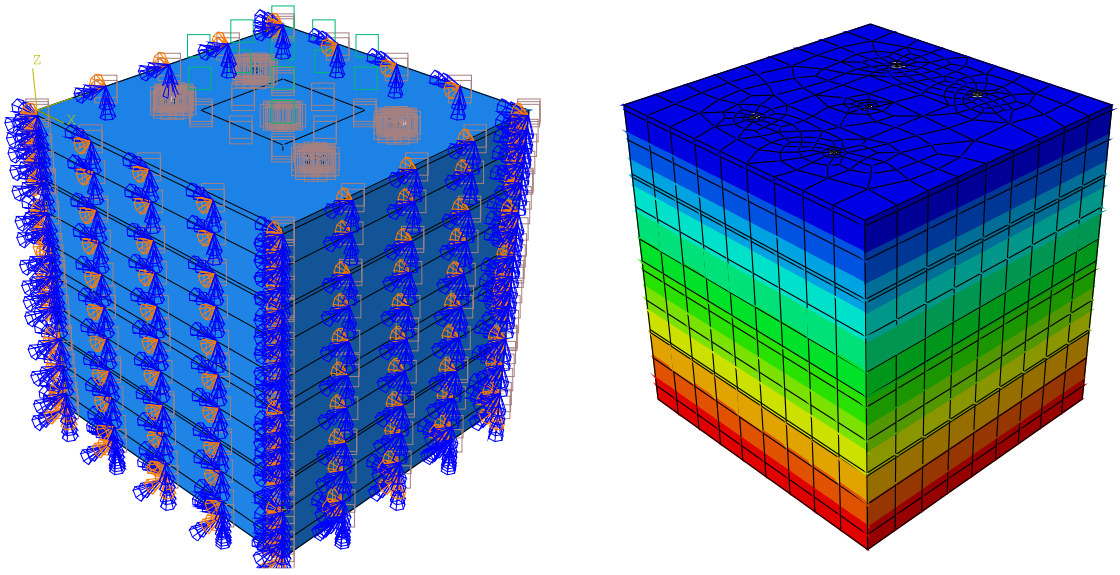

(a)Boundary conditions and predefined fields **(b) Hydrostatic pore pressure in the soil**

Fig. 3.24 Initial and Geostatic step (Step 1)

Table 3.8 Steps followed to develop the FE simplified technique in ABAQUS

Step	Description
	Initial Default step created by the software, in which the initial boundary conditions and predefined loads were applied.
1	***Geostatic*** The equilibrium of the soil was verified. The hydrostatic pore pressure condition of the soil was corroborated (Fig. 3.24b).
2	***Soil Transient Consolidation*** The foundation of 150 kPa was placed over the soil (Fig. 3.25).
3	***Soil Transient Consolidation*** The excess pore pressure was applied in the soil as an external load boundary condition per one-metre deep increments for a period of one second (Fig. 3.26). Load ramp behaviour was considered. The peak magnitude of excess pore pressures achieved in the soil, represented the free field complete liquefaction behaviour ($\sigma'_{vo} = \bar{u}$). The time step designated in the transient consolidation step becomes relevant when the dissipation stage is analysed, as an adequate time for the fluid to flow along the element should be considered. The evaluation of the excess pore pressure behaviour in the soil was considered from this step.
4	***Soil Transient Consolidation*** The excess pore pressures applied in the previous step were maintained at their peak values over a period of nine seconds to simulate the total shaking time. A condition of propagated load during this time, was requested in the software load module.
5	***Soil Transient Consolidation*** The dissipation of excess pore pressures in the soil was enabled considering a period of 135 seconds to match the total dissipation time presented in the physical model. The excess pore pressure condition was deactivated following a "smooth" load step behaviour and reaching the hydrostatic pore pressure as a final amplitude (load module).

After the model was developed (pre-processing stage), the data was deferred to the software code in which matrix systems are created and algebraic equations resolved (Roylance, 2001). After the job was executed by the program, the output of specific nodes was recorded for comparison with the physical model (Fig. 3.27).

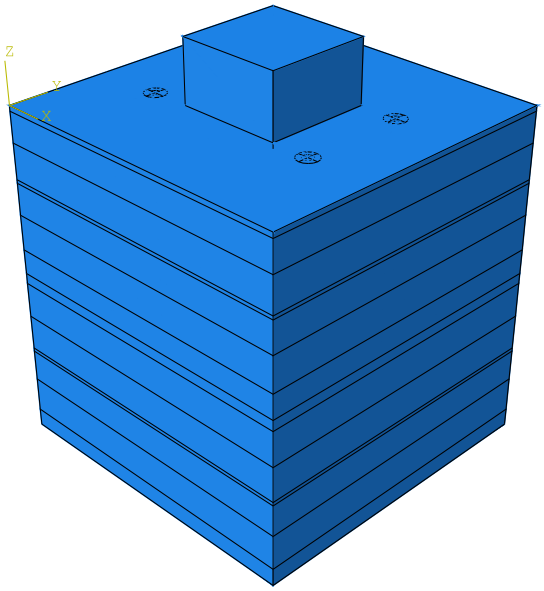

Fig. 3.25 Foundation placed over the stratum surface (Step 2)

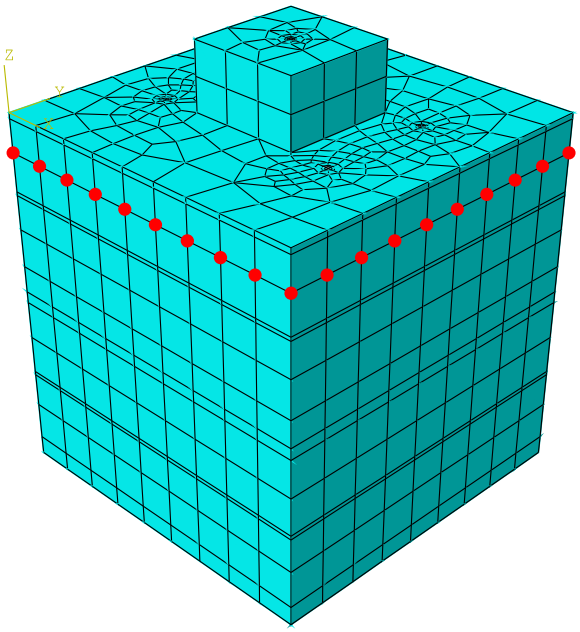

Fig. 3.26 Excess pore pressure applied as an external load boundary condition (Step 3)

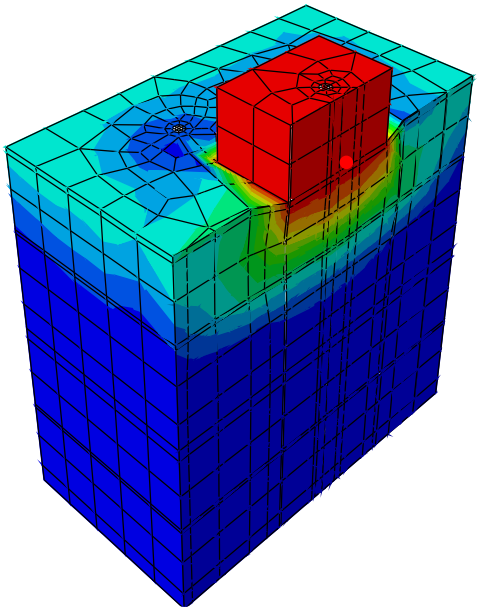

Fig. 3.27 Selection of specific nodes (for settlement response)

3.4 Summary

Centrifuge modelling is considered to be an efficient technique for geotechnical analysis as stresses and strains in the protype soil model can be accurately reproduced in the scaled model. In this chapter, dynamic centrifuge modelling was utilised for the evaluation of the performance of different drain arrangements under buildings. Definition of the methodology, the model construction process and material characterisation (mainly of the sustainable coarse material) are presented in this chapter.

The use of centrifuge modelling could be highly beneficial; however only a reduced number of tests could be performed, becoming a limitation of the technique. Therefore, numerical modelling has been extensively utilised by practitioners to solve geotechnical problems. Although this method is advantageous in terms of time and the quantity of analysed models, current software is not sufficiently effective particularly for soil liquefaction analysis. In this work, a 3D FE simplified technique is proposed, using ABAQUS for the simulation of soil and structure behaviour during the reconsolidation stage of soil improved with drains. This technique was developed using ABAQUS software, which is frequently utilised by engineers in the evaluation of soil-structure interaction; however, earthquake-induced liquefaction is not possible to model, as coupled pore fluid and dynamic analysis cannot be carried out. A detailed explanation of the steps followed in order to develop the technique is presented. The 3D numerical model elaboration, including the soil constitutive model and material properties utilised in the software, are presented.

Chapter 4

New buildings: Vertical drains performance in liquefaction mitigation

4.1 Introduction

Countermeasure techniques against liquefaction damage are designed to achieve a building's optimal functionality during liquefaction. Vertical drains effectiveness relies on the rapid dissipation of high excess pore pressures generated during an earthquake to reduce structural loss. Due to this advantage, drains can be used in a variety of applications, such as new buildings (during the preconstruction phase), existing buildings (as perimeter drains), or the free field (for temporary work camps or similar).

Vertical drains design is commonly based on the conceptual procedures of free field conditions that do not represent a regular context. In addition, despite the multiple options available in the use of vertical drains, studies on their performance under seismic activity have focused mainly on perimeter drains for existing buildings. It is relevant to investigate the behaviour of vertical drains under a range of conditions to take full advantage of this technique. Therefore, further research is required for the evaluation of the performance of vertical drains installed during the preconstruction phase,before new buildings are built.

In this chapter, the performance of a simplified vertical drain arrangement below a new shallow foundation is evaluated as a mitigation technique used to avoid liquefaction damage. The analysis considers the generation of excess pore pressures during an earthquake and its following dissipation in the presence of vertical drains, along with the foundation's settlement and dynamic response. The effectiveness of the arrangement is evaluated by

comparing it with a similar foundation over unimproved soil. Moreover, the drain's performance is analysed when subjected to vertical stress variation as a result of different bearing pressures. This chapter is a base case study for the evaluation of upcoming scenarios related to inclined drains, which will be discussed in chapter 6.

4.2 Vertical drains performance under new buildings

The performance of a simplified drain arrangement below a foundation of 150 kPa (SG2) (Fig. 3.14) is analysed in this section. The evaluation considers a comparison with an unimproved region subjected to the same foundation bearing pressure for the analysis of the arrangement's effectiveness.

4.2.1 Soil response

4.2.1.1 Excess pore pressure generation

Excess pore pressure generation in the improved soil was analysed to understand the influence of the foundation confining pressure over the vertical drain's performance prior to the dissipation stage. Excess pore pressure ratios are presented in figure 4.1 for the improved and the unimproved soil at depths of 2.1 m and 4.6 m. The increase of vertical stresses in the soil below the foundation for the calculation of excess pore pressure ratios was determined using Boussinesq's approximation (1883). The Boussinessq solution is based on the notion that soil presents an elastic, homogenous and isotropic behaviour. The distribution of stress follows a bulb shape. The vertical stress increment in the soil due to a rectangular loading was determined based on the following Boussinessq solution (equation 4.1). Circles and dashed lines in the figures represent times for dissipation initiation and end of the shaking.

$$\Delta\sigma = \int_{y=0}^{B}\int_{x=0}^{L} \frac{3qz^3(d_x d_y)}{2\pi(x^2+y^2+z^2)^{5/2}} = qI_2 \qquad (4.1)$$

$\Delta\sigma$: vertical stress increase

q: load per unit area

z: depth

B: width of the rectangular loading

L: length of the rectangular loading

I_2: f (m,n)

m: B/z

n: L/z

In the improved region, excess pore pressure ratios (r_u) below the foundation (close to the internal drain) reached a peak value of 0.25 at the top layer, while larger values of 0.5 and 0.65 in the soil inside and outside the perimeter drains were observed (Fig. 4.1a). The high confining pressure below the foundation provided a large resistance to high excess pore pressure generation, and more importantly resulted in greater r_u values at the perimeter ring. At this depth, the free field presented a complete liquefaction behaviour (r_u =1) as a result of the lack of drainage improvement in the area and a significant fluid flow from bottom layers. At a depth of 4.6 m, a larger generation of excess pore pressures was reached outside and inside the perimeter drains reaching peak r_u values of 0.9 and 0.75, while the soil close to the internal drain reached a value of 0.55 (Fig. 4.1c). Complete liquefaction in the free field was also observed at this depth.

The foundation response in the unimproved soil presented r_u values of 0.25 and 0.3 below the foundation central axis and at the foundation's edge at the top layer (Fig. 4.1b). This behaviour was consistent with the proposal of Liu and Dobry (1997), who attributed the low pressures under the foundation central axis to the primary driving shear that causes the dilative behaviour within the soil. At a depth of 4.6 m, the generation of excess pore pressures below the foundation and at the edge presented similar trends over time, reaching a peak r_u of 0.6 (Fig. 4.1d).

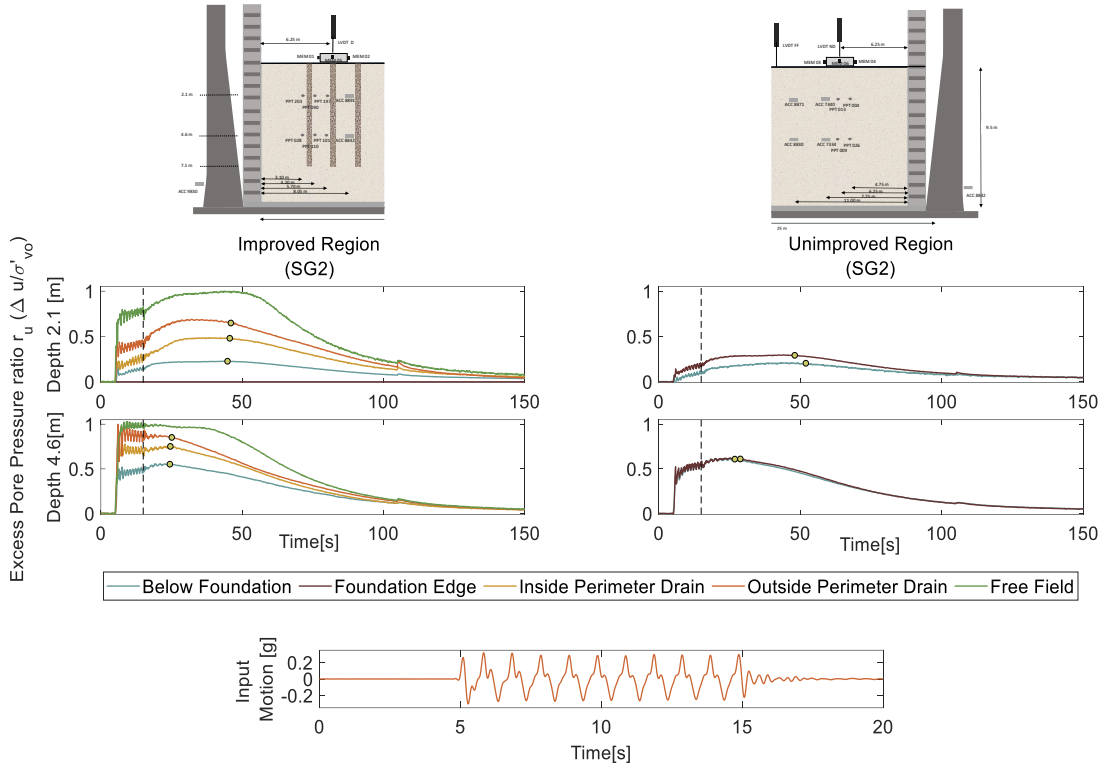

Fig. 4.1 Excess pore pressure ratio (r_u) time-histories for the improved and unimproved region

Similar peak r_u values registered at the top layer and middle layer below the foundation in the improved and unimproved cases, suggested the weak behaviour of the internal drain in controlling excess pore pressures generation under the foundation and the deficient performance of the arrangement during the shaking stage.

The foundation bearing pressure is highly relevant in the generation of excess pore pressures for mitigated and unmitigated soil. Limited excess pore pressures were generated in the soil close to the internal drain due to the significant additional confinement stress applied by the foundation, while the area located near the perimeter ring attained higher excess pore pressure values in presence of a lower confining pressure. Moreover, the structure's influence over liquefiable soil represent a positive factor with regard to soil softening, reducing the risk of complete liquefaction (r_u =1) under the foundation. The design of drains arrangements considering a free field context could represent an overestimated cost of the technique, as larger soil softening and high risk of liquefaction occurrence is considered.

4.2.1.2 Spatial variation of excess pore pressure dissipation

The analysis of flowfront arrival times for the vertical drains subjected to the influence of confining pressure exerted by the foundation, is required for the evaluation of the drain's optimal performance as it is related with the rapid dissipation of excess pore pressures.

Horizontal contours of excess pore pressure ratios for the improved region are presented in Figure 4.2 for times corresponding to the end of the shaking, flowfront arrival for the internal and perimeter drains and for sixty seconds after the shaking (t=75 s).

At the end of the shaking, r_u of 0.2 and 0.4 below the foundation and outside the perimeter drains were observed due to the high bearing pressure presented in the central zone (Fig. 4.2a). Between t=15 s and t=44.8 s, the generation of high excess pore pressures across the layer was presented due to the radial and upward flow from lower depths towards the drains after shaking, incrementing the ratio in 0.1 below the foundation and 0.2 outside the perimeter drains.

The first flowfront at the top layer arrived at the internal drain at t=44.8 s (Fig. 4.2b) suggesting a "unit cell" behaviour of the drain, influenced by the high confining pressure exerted by the foundation and with restricted fluid to dissipate. In the unimproved soil, dissipation started below the foundation seven seconds later (see Fig. 4.1b) indicating the efficient work of the internal drain in accelerating dissipation process under the foundation. At t=47.5 s, the flowfront arrived close to the perimeter drains, a slight reduction in the excess pore pressure in the central area was observed, while a maximum ru of 0.65 was reached at the perimeter drains. The delay in the dissipation initiation observed outside the perimeter drains verified the ring's "infinite cell" behaviour, receiving constant fluid flow from farther locations and acting as a barrier for the internal zone during the dissipation stage. The dissipation pattern that began on the internal drain and continued with the perimeter drain ring emphasises in the presence of the foundation's high confining pressure. At t=75 s, dissipation across the layer was observed including the free field, showing r_u of 0.15 below the foundation central axis and 0.4 at the perimeter drains (Fig. 4.2d).

4.2.1.3 Vertical dissipation path in the presence of drains

Figure 4.3 shows vertical contours for excess pore pressure ratios for the improved soil at different times during the dissipation stage. Profile contours provide the fluid flow's behaviour along the stratum depth in the presence of the vertical drains after the end of shaking. The contours do not present the exact excess pore pressure magnitudes for the soil inside the drains, as it was not possible to place instruments in this zone following the model construction procedure.

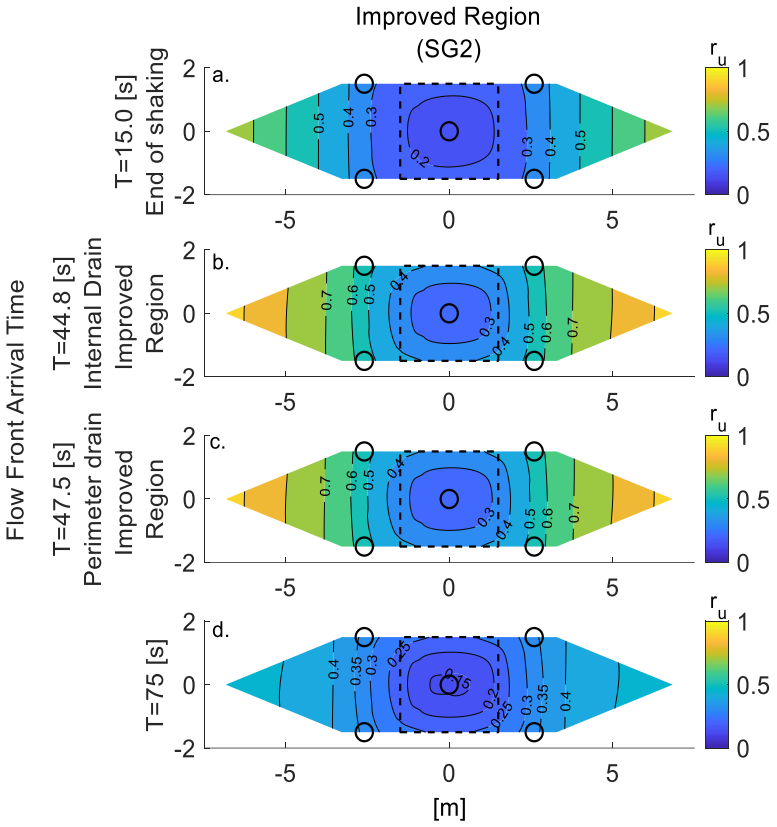

Fig. 4.2 Horizontal contours of excess pore pressure ratios (r_u) for the improved region

At the end of the shaking, excess pore pressure ratios in the improved soil reached low r_u values below the foundation in which large confining pressure was exerted. On the contrary, a larger generation of pore pressures outside the foundation footprint was observed, with peak values of r_u =0.8 close to the border drains at depth of 4.6 m (Fig. 4.3a). At t=30 s, a volume of soil with low pressure below the foundation was presented, suggesting a better controlled flow along the internal drain depth compared to those on the perimeter (Fig. 4.3b). At t=45 s, the dissipation of the volume of low pressures was managed by the internal drain and the confining pressure exerted by the foundation. The perimeter drains were in charge of the fluid flow from outside the arrangement, showing r_u values of 0.55 and 0.65 inside and outside them (Fig. 4.3c). Although the vertical contours were not illustrated for the unimproved case due to the lack of instrumentation, at t=45 s, the excess pore pressure ratios below the foundation at depths of 2.1 m and 4.6 m were 0.2 and 0.5, respectively (see Fig. 4.1b,d) verifying the slower dissipation in this zone compared to the improved region. At t=75 s, r_u of 0.15 was observed below the foundation while r_u values of 0.3 and 0.4 at the top and lower layers were registered outside the perimeter drains, showing a faster dissipation from the bottom layers of the stratum (Fig. 4.3d).

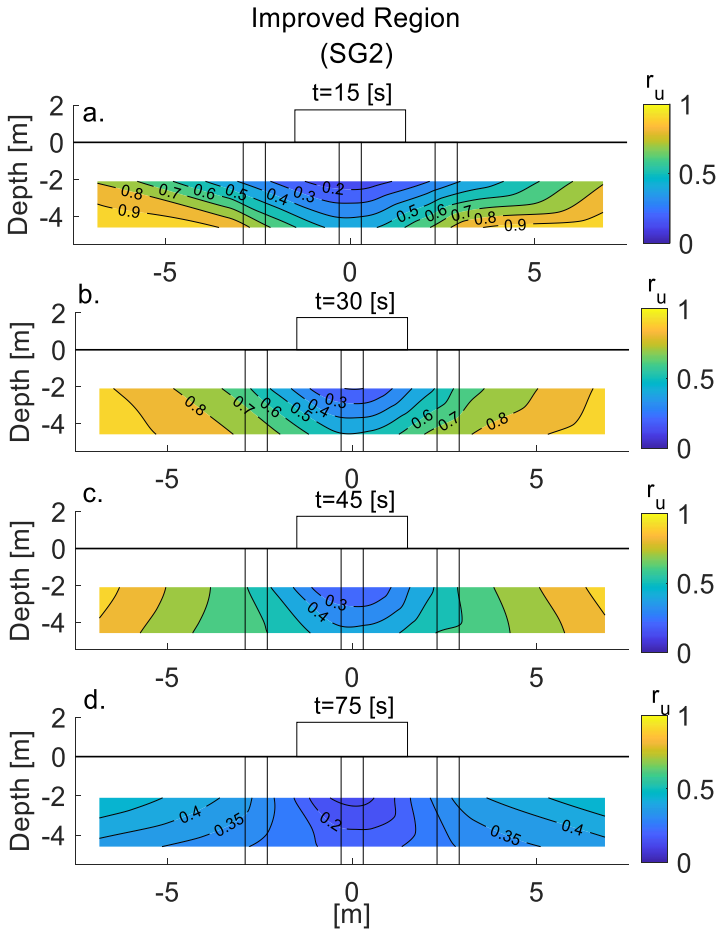

Fig. 4.3 Vertical contours of excess pore pressure ratios (r_u) for the improved region

The arrangement of drains, particularly the internal drain permitted the rapid dissipation of the volume of fluid resulting in low pore pressures ratios below the foundation, verifying the effectiveness of the arrangement during the dissipation stage. In previous tests in which vertical perimeter drains were installed around structures as countermeasure technique, fluid flowed rapidly from the area enclosed by the drains towards the perimeter ring, leading to a quick dissipation of excess pore pressures below the structure (Paramasivam *et al.*, 2018). In this context, an enhanced performance in terms of dissipation is expected under the foundation considering the addition of an internal drain ring, as the internal drain's area of influence involves the foundation footprint. The installation of internal drains below foundations is an impractical option in case of existing buildings; nevertheless, the use of drain rings with significant proximity to the foundation, such as inclined drains, could be a more feasible alternative. The effectiveness of inclined drains as a variation of the conventional vertical arrangement is analysed for existing buildings in Chapter 6.

4.2.1.4 Soil acceleration

Figure 4.4 shows acceleration time histories for the free field, soil close to the perimeter drain and outside the foundation footprint in the unimproved region at depths of 2.1 m and 4.6 m. Complete acceleration decoupling took place at both depths in the free field after the first cycle of the shaking due to the large softening in the soil and the earthquake's significant magnitude. In the improved region, significant reduction of the input motion was presented close to the perimeter drains as a result of the large softening in the soil, particularly at a depth of 4.6 m. In the unimproved region, a large acceleration deamplification, with a similar trend to the free field response was observed in the soil outside the foundation footprint for both depths, suggesting large soil softening in the absence of drainage enhancement and additional confining stress.

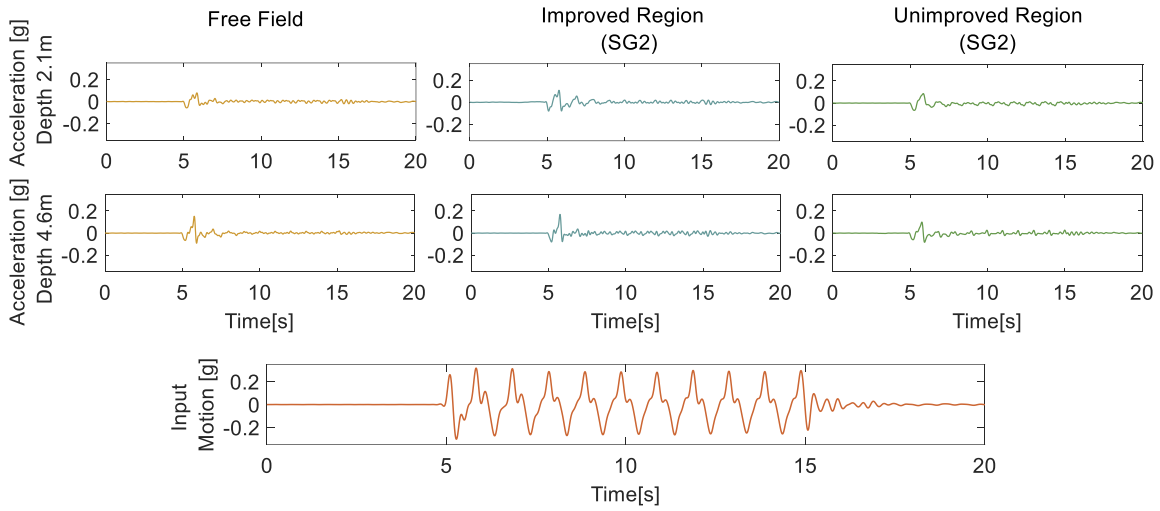

Fig. 4.4 Soil acceleration time-histories for the free field, improved and unimproved region

The soil acceleration response is highly influenced by the presence of vertical drains and the level of soil softening. In this work, the contribution of drains in terms of shear reinforcement is unclear as the soil acceleration response was also influenced by the drainage enhancement; nevertheless, the relevant differences between both materials properties justify an analysis in terms of shear strength.

Table 4.1 presents the percentage of additional shear reinforcement (τ_{A_r}) provided by the drains together with replacement ratios (A_r) at a depth of 2.1 m. The area replacement ratio (A_r) is the ratio between the area of the drains and the total treatment area, commonly used for the design of gravel columns (Baez and Martin, 1993; Badanagki et al., 2018). The additional shear resistance supplied by the drains was calculated as a ratio of the drains' shear strength to the shear strength of the total treatment area. Calculation of the shear

strength was performed using Mohr Coulomb-failure criterion (equation 4.1) for both materials, considering the effective stress in the soil at different depths and assuming zero cohesion (c'). The shear strength calculated for the coarse material was then multiplied by the total area of drains presented in the soil layer, while the shear strength calculated for the fine soil was multiplied by the entire treatment area. In this way, magnitudes of shear strength were possible to obtain, and consequently the additional shear resistance provided by the drains. In the case of vertical drains, the treatment area refers to the drain's area of influence. A larger presence of drains or a higher percentage of A_r, involves a greater shear reinforcement supplied by the columns in the soil (Badanagki et al., 2018). Although this is a simplified calculation, it will lead us to understand the improved performance of the foundation in terms of reduced settlement due to the additional shear reinforcement.

Table 4.1 Additional shear reinforcement in the soil layer

Depth (m)	**Vertical Drains**	
	A_r (%)	τ_{A_r} (%)
2.1	3	3

A_r: Area replacement ratio
τ_{A_r}: Additional drains shear reinforcement

$$\tau = \sigma' tan(\phi') + c' \tag{4.1}$$

σ': soil effective stress
ϕ': angle of internal friction
c': cohesion

In the free field, no shear reinforcement was provided by the drains, reflecting a complete acceleration decoupling at both depths of the stratum. In addition, the significant acceleration reduction in the treated soil close to the perimeter drains was managed by the soil softening reached at the top and middle layers as well as the minimal additional shear reinforcement of 3% provided by the vertical drains.

Besides the weak performance of the drains in terms of drainage enhancement, the drains containing fraction B as coarse material were unable to provide sufficient shear reinforcement to the soil. Although the main role of vertical drains is the rapid dissipation

of excess pore pressures generated due to the earthquake, sufficient shear reinforcement must be provided for an improved performance of the technique.

4.2.2 Foundation response

4.2.2.1 Foundation settlement

The effectiveness of vertical drains as a mitigation technique depends on the settlement reduction of the foundation. Figure 4.5 shows the free field and foundation settlement in the improved and unimproved soil. The free field settled 50% of its total amount during the shaking as a result of volumetric strains generated due to partial drainage in the soil (Madabhushi and Haigh, 2012), while the other 50% occurred as a result of considerable reconsolidation volumetric deformation in the absence of drainage improvement. The significant difference between the free field and foundations settlement response was explained by the additional deviatoric strains generated in presence of the significant load (Dashti *et al.*, 2010a).

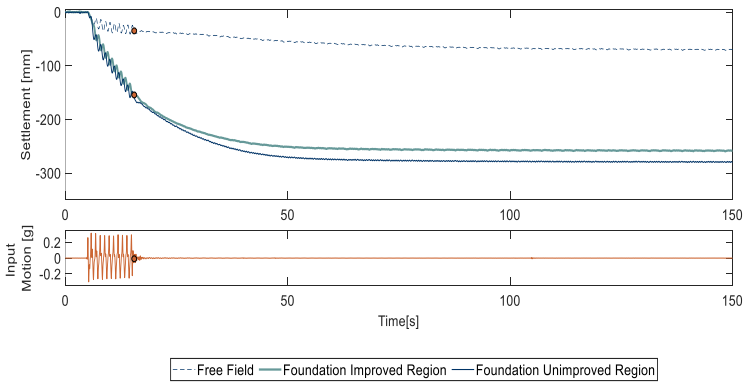

Fig. 4.5 Settlement time-histories for the free field and foundations over the improved and unimproved region

The foundation over the improved region reached a total settlement of 280 mm, with 60% generated during the shaking because of deviatoric strains due to strength loss in the soil as well as significant reconsolidation volumetric deformations. During the dissipation stage, a lower settlement percentage was obtained compared to the shaking stage due to drainage improvement. Vertical drains allowed a rapid dissipation of excess pore pressures, particularly below the foundation, reducing the time for volumetric strains and deviatoric deformations due to the rapid recovering of strength in the soil. However, the foundation over the unimproved soil presented more settlement compared to the improved case, particularly during the post-shaking stage. The lack of drainage enhancement below and surrounding the foundation allowed a longer time for soil deformation. An improvement of

10% in the foundation settlement response was obtained by installing the proposed arrangement of drains, verifying its effectiveness in reducing structural damage.

Although the effectiveness of the five drain arrangement below the foundation has been validated by the reduction of the settlement response; the weak performance of the drains, mainly during the shaking stage was observed. The similar settlement response obtained for both cases during the shaking proved the ineffective control of excess pore pressures in presence of the internal drain under the foundation. Therefore, in addition to the effective performance of the technique during the dissipation stage, adequate limitation of soil softening below the structure must be guaranteed. Moreover, the small settlement reduction during the post-shaking stage was obtained as a result of the insufficient drainage capacity of the arrangement. This could be explained by the low permeability difference between Fraction B and Hostun sand, as a larger order of magnitude is frequently required for drainage improvement (Port and Harbour Research Institute, 1997; Orense *et al.*, 2003). Furthermore, the lack of sub-perimeter drains in the arrangement delayed the dissipation of excess pore pressures, affecting the drainage's effective behaviour.

The foundation of 150 kPa located over the non-remediated soil presented a minor difference in terms of settlement response compared to that of the improved soil. This represents an inconsistent response of the structure with respect to the trend previously observed by different authors using centrifuge modelling, for settlement of foundations in liquefiable soils (Dashti et. al, 2010b; Bertalot and Brennan, 2015). This inconsistency was probably obtained due to experimental issues in the model such as the proximity of the structure to the remediated zone, presenting some influence of the perimeter drains.

The settlement response presents an incremental linear trend proportional to the foundation bearing pressure, when considering bearing pressures lower than 100 kPa. This trend was verified using physical models and field data (Dashti et. al, 2010b; Bertalot et. al, 2013). In cases of structures with higher bearing pressures, lower settlement compared to that of 100 kPa should be expected due to the large shear and confinement stresses in the soil induced by the significant bearing pressure exerted by the heavier structure. Limited excess pore pressures are generated, and consequently a lower settlement response is obtained compared to the light foundation.

Centrifuge tests developed by Adamidis (2016) considering a structure of 100 kPa over non-improved, loose, Hostun sand, showed a foundation settlement response of 770 mm. The trend established by Bertalot and Brennan (2013), who performed centrifuge tests using foundations of 90 kPa and 130 kPa, presents an approximate reduction of 12% in the settlement response when increasing the bearing pressure from 100 kPa and 150kPa. Considering this declining behaviour and the response obtained by Adamidis for a structure of 100kPa, a settlement value of 680 mm should be expected for a structure of 150 kPa in

unimproved soil. This reflects a reasonable base case of structural response in unmitigated soil, including a satisfactory improvement when comparing treated and untreated soil, emphasizing the effectiveness of the drainage technique.

The effectiveness of vertical drains in terms of settlement reduction has been confirmed by previous studies, wherein significant reductions between 40% and 34% were obtained for structures of 80 kPa and 187 kPa, considering an arrangement of perimeter drains (Olarte *et al.*, 2017; Paramasivam *et al.*, 2018). Although only perimeter rings were utilised on those cases, the significant number of prefabricated vertical drains around the structure and the high permeable material used inside the drains (345 times larger compared to the permeability of the host sand) led to a considerable improvement in terms of settlement. Hence, a variation of the proposed arrangement in this work, in terms of coarse material and number of drains was required for the following tests, in which the performance of different arrangements below new buildings were analysed.

4.2.2.2 Foundation horizontal acceleration

The use of drainage enhancement techniques in the soil required the evaluation of the foundation dynamic response, as the amplification of the seismic demand and greater possibility of structural tilting are expected. The foundation's horizontal acceleration for the improved region is presented in figure 4.6 together with the input motion (Fig. 4.6a). In the case of the unimproved soil, the instrument stopped working after the initial few seconds of the shaking (Fig. 4.6b). Low transference of the input motion was observed for the foundation in the improved soil, as a result of soil softening and lack of shear reinforcement below the foundation, showing a mean acceleration value of 0.07g during the shaking. Moreover, in the case of the unimproved soil, a similar horizontal acceleration should be expected for the foundation due to their close magnitudes in soil softening and the absence of shear reinforcement below the foundation.

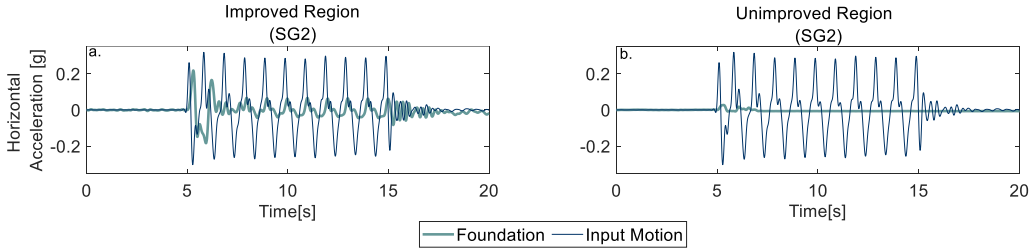

Fig. 4.6 Foundation horizontal acceleration for a) improved and b) unimproved region

Considerable shear reinforcement is usually provided by vertical drains due to the large shear strength of the coarse material inside them. However, in this case, the insufficient shear

reinforcement imparted by the arrangement was verified by the significant reduction of the foundation's horizontal acceleration and the minor settlement improvement.

4.3 Bearing pressure variation over vertical drains

Different mechanisms of earthquake-induced settlement in liquefiable soil have been evaluated on the basis of inaccurate predictions obtained from methodologies and empirical graphs commonly utilised in practice (Yoshimi and Tokimatsu, 1977; Tokimatsu and Seed, 1987; Ishihara and Yoshimine, 1992; Liu and Dobry, 1997). The variable of bearing pressure has been considered in recent years, verifying its significance in the mechanism of settlement response (Dashti *et al.*, 2010b; Bertalot *et al.*, 2013; Bertalot and Brennan, 2015; Adamidis, 2017). Limited generation of excess pore pressures below the foundation was observed in cases of significant bearing pressure, due to the increase in soil cycle resistance in presence of great shear and confining stresses (Liu and Dobry, 1997; Kawasaki *et al.*, 1998; Ghosh, 2003). The influence of the bearing pressure in mitigated soil as a mechanism in the structural response, is presented in the following section. The drains arrangement analysed in section 4.1 is evaluated under a foundation of 50 kPa and compared with results obtained in SG2 (q=150 kPa).

4.3.1 Soil response

4.3.1.1 Excess pore pressure generation

Excess pore pressure ratios for the soil close to the internal drain, inside and outside the perimeter drains at depths of 2.1 m and 4.6 m are presented in figure 4.7 for SG2 and SG1. In SG1, r_u values of 0.75 and 0.9 were observed close to the perimeter drains at the top layer while a value of 0.45 was reached in the internal drain (Fig. 4.7b). Larger r_u values were registered in the soil surrounding the perimeter drains compared to the internal drain, due to the lower confining stress and the smaller resistance of the soil leading to the generation of higher excess pore pressures outside the foundation of 50 kPa. Higher excess pore pressure ratios at the three locations were reached compared to the soil below the foundation of 150 kPa, that showed peak values of 0.7 and 0.5 for the soil inside and outside the perimeter drains and of 0.2 around the internal drain. In addition, the excess pore pressures required a larger time to reach peak values in SG2, while in SG1, elevated magnitudes were reached during the initial seconds of the shaking, verifying the ease of generating significant excess pore pressures under low confining stresses.

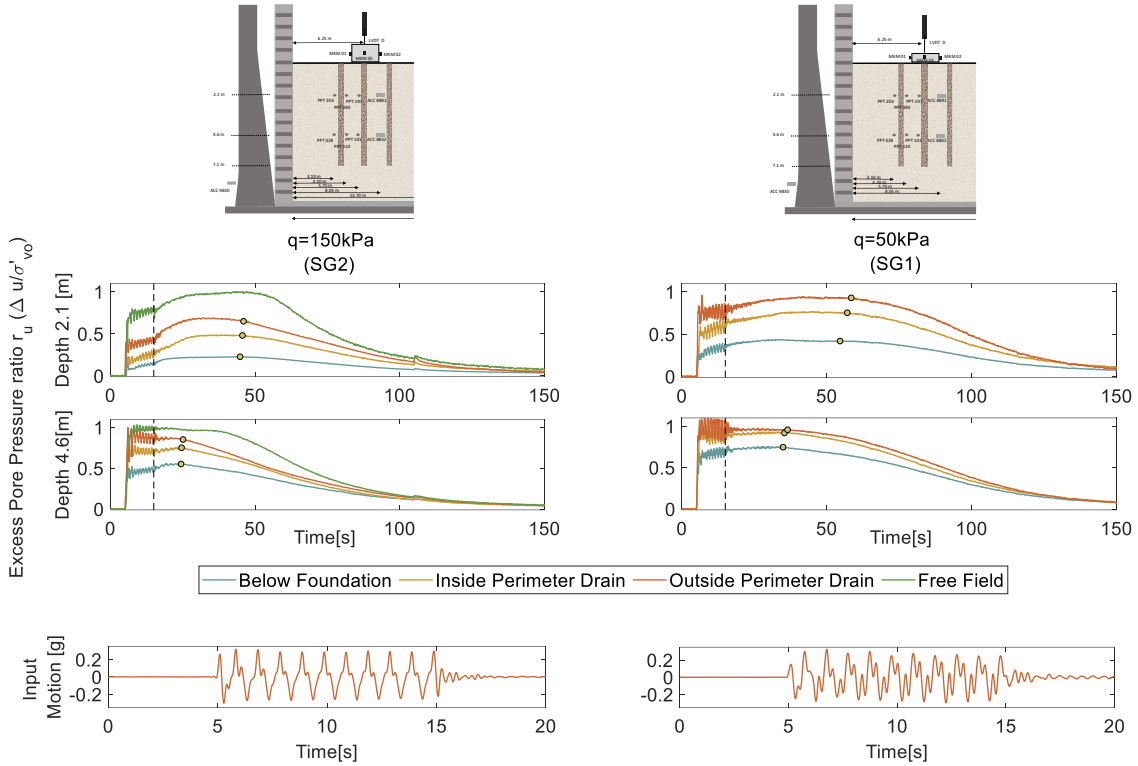

Fig. 4.7 Excess pore pressure ratio (r_u) time-histories for SG2 and SG1

Higher peak values were obtained at a depth of 4.6 m compared to the top layer below the foundation central axis due to lower confining pressure, reaching an r_u of 0.75 in SG1 (Fig. 4.7d). A value of 0.95, close to complete liquefaction was observed after the first cycle of shaking outside the perimeter drains, due to their poor performance in controlling a large generation of excess pore pressures in the zone in which the low confining pressure was exerted. Greater reduction of excess pore pressures was observed in the case of the foundation of high bearing pressure compared to SG1, for the soil close to the internal and perimeter drains (Fig. 4.7c), suggesting the relevance of high confining stresses in the mitigated soil during the shaking.

4.3.1.2 Excess pore pressure dissipation: Bearing pressure influence

Figure 4.8 presents horizontal contours of the excess pore pressure ratios for SG2 and SG1 considering the flowfront arrival times at the internal and perimeter drains in SG1. The flowfront arrival time comparison allowed the evaluation of the drain ring's performance under varied confining pressure. The contours for SG1 do not extend to the free field due to the lack of instrumentation in that zone.

At the end of the shaking, r_u of 0.4 and 0.8, close to the internal drain and outside the perimeter drains, were reached in SG1, showing an intermediate value of 0.65 in the area

enclosed by the perimeter drains. Greater values across the layer in SG1 were registered compared to the soil below the foundation of 150 kPa, particularly at the perimeter drains outside the foundation's influence (Fig. 4.8b).

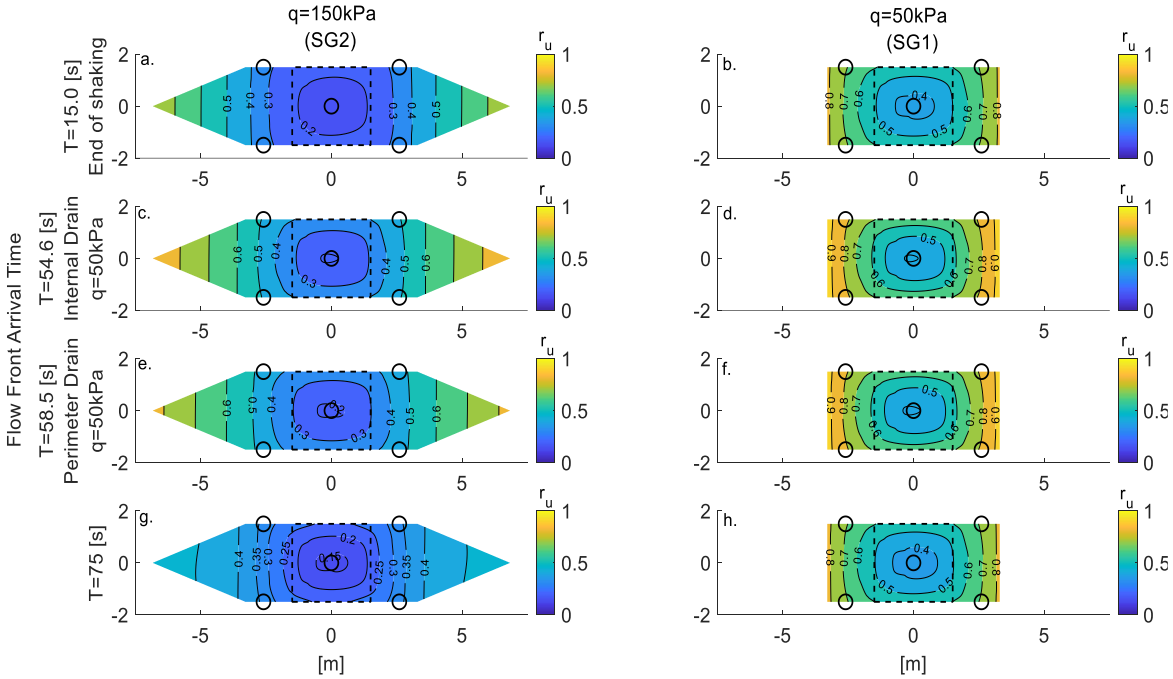

Fig. 4.8 Horizontal contours of excess pore pressure ratios (r_u) for SG2 and SG1

At t=54.6 s, the flowfront arrived at the internal drain below the foundation of 50 kPa showing a peak r_u of 0.45 and 0.95 close to the perimeter drains due to the upward and radial flow from bottom layers (Fig. 4.8d). At this time, excess pore pressures continued to dissipate in SG2 showing lower r_u values compared to the other case, especially outside the perimeter drains (Fig. 4.8c). The significant resistance of the soil to generate excess pore pressures in presence of a great bearing pressure denotes a large resistance of the soil to maintain these peak values under the structure. The high bearing pressure induced a faster reconsolidation of soil particles compared to the foundation of low confining stress. Four seconds later, the flowfront arrived at the perimeter drains in SG1 verifying an "infinite cell" behaviour of the drains due to radial and vertical constant fluid flow from far field, showing peak values of 0.95 (Fig. 4.8f). On the other hand, an excess pore pressure ratio of 0.55 was registered close to the perimeter drains in SG2 at this time (Fig. 4.8e). The difference between the flowfront arrival times at the internal and perimeter drains considering both cases was ten and eleven seconds respectively, verifying an improvement on the arrangement's performance during the dissipation stage in the presence of the high confining pressure. At t=75 s, dissipation in SG1 was observed in the central zone and around the perimeter drains presenting excess pore pressure ratios of 0.4 and 0.8 respectively (Fig.

4.8h). However, a larger reduction of high excess pores in the region below the foundation of 150 kPa was registered, including the free field. The rapid reconsolidation generated in the soil enclosed by the perimeter drains when subjected to high confining stresses, allowed the faster flowfront arrival near the internal and perimeter vertical drains, verifying the relevance of the bearing pressure on the effective performance of the arrangement during the dissipation stage.

4.3.1.3 Foundation influence on the vertical dissipation path

Vertical contours for SG2 and SG1 considering similar timesteps from section 4.1 are presented in Figure 4.9. At the end of the shaking, an area of low pore pressures ratios was observed below the foundation of 50 kPa, with r_u of 0.45 and 0.7 close to the internal drain at depths of 2.1 m and 4.6 m, respectively (Fig 4.9b). Fifteen seconds later, the excess pore pressures increased close to the drains, showing significant generation close to the perimeter drains (Fig 4.9d). On the other hand, at this time the soil in SG2 presented lower r_u values at the perimeter drains and below the foundation due to higher foundation confining pressure (Fig 4.9c).

At t=45 s, while the volume of low pressures in SG2 started to dissipate (Fig 4.9e) excess pore pressures continued to increase in SG1, reaching r_u values of 0.4 and 0.7 at depths of 2.1 m and 4.6 m close to the internal drain. Thirty seconds later, the internal drain in SG1 allowed a rapid dissipation along the foundation central axis under the influence of the confining pressure. A higher value of 0.9 at the surface close to the perimeter drain was observed due to the drain's lack of effectiveness in dissipating the excess pore pressures in the presence of minimal additional confining stress, allowing a delay in the start of dissipation in this zone (Fig 4.9h). On the other hand, at this time, a significant reduction in high excess pore pressures under the foundation of 150 kPa footprint was observed (Fig 4.9g) reaching half the r_u value present below the foundation of 50 kPa. In addition to the "unit cell" behaviour of the drain, the significant bearing pressure allowed an efficient performance of the internal drain, managing a more rapidly dissipation of the zone under the foundation footprint, compared to the case of low bearing pressure.

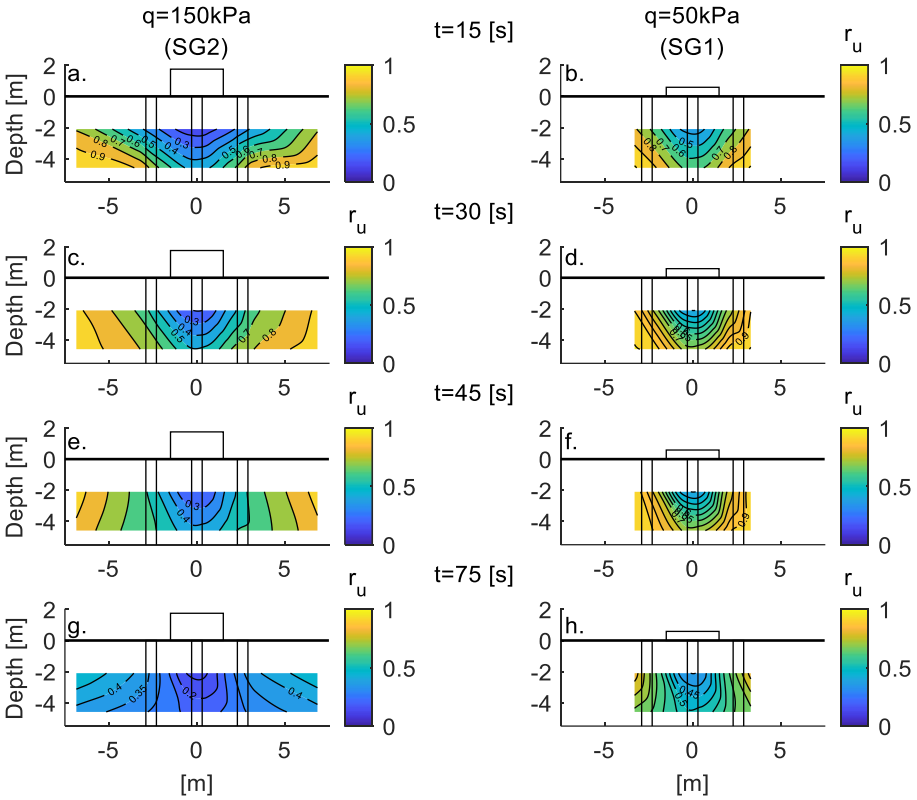

Fig. 4.9 Vertical contours of excess pore pressure ratios (r_u) for SG2 and SG1

In addition, vertical contours of excess pore pressures are presented in Fig 4.10, in order to have an improved visualization of the fluid's behaviour in the soil with drains below a structure. Similar timesteps as in Fig 4.9 were considered for the plots.

In SG2, significant amount of fluid were observed near the perimeter drains due to the "infinite cell" behaviour and weak performance of the drains in controlling significant fluid flow. An excess pore pressure magnitude of 11.7 kPa was registered outside the drains, while the magnitude reached below the foundation, around the internal drain was 11 kPa at the top layer. Moreover, restricted fluid flow was observed near the internal drain in response to the greater resistance of excess pore pressure generation (Fig 4.10a). At t=30 s, the fluid flowed from lower layers and increased excess pore pressure magnitudes, particularly outside the perimeter drains, showing a value of 19.5 kPa at the top level (Fig 4.10c). After some seconds, the fluid flowed fast from the area below the foundation towards the internal drain, while permanent fluid was registered surrounding the external drains. The greater bearing pressure exerted by the foundation in the soil around the internal drain enabled a faster reconsolidation below the foundation compared to the area surrounding the perimeter drains (Fig 4.10e,g).

A similar behaviour of the fluid flow in the soil was observed in the case of SG1. The internal drain presented a low level of fluid during the generation stage near the internal

drain, while higher excess pore pressures were registered near the perimeter drains (Fig 4.10b). Nevertheless, compared to SG1, a greater magnitude of excess pore pressure was observed in the soil surrounding the drains in response to the lower confining pressure. The fluid flows with difficulty towards the area below the foundation of high confining pressure. During the dissipation stage, the fluid first flowed towards the internal drain below the heavy foundation showing a 15kPa at the top layer (Fig 4.10e), while at the same time, a larger magnitude of 20 kPa was registered in SG1 for the same location (Fig 4.10f). At t=75 s, the total drains received the fluid, showing significant dissipation in SG2 and SG1. Nevertheless, the greater bearing pressure of 150 kPa in SG2 enabled a faster fluid flow, compared to that below the foundation of 50 kPa (Fig 4.10g,h).

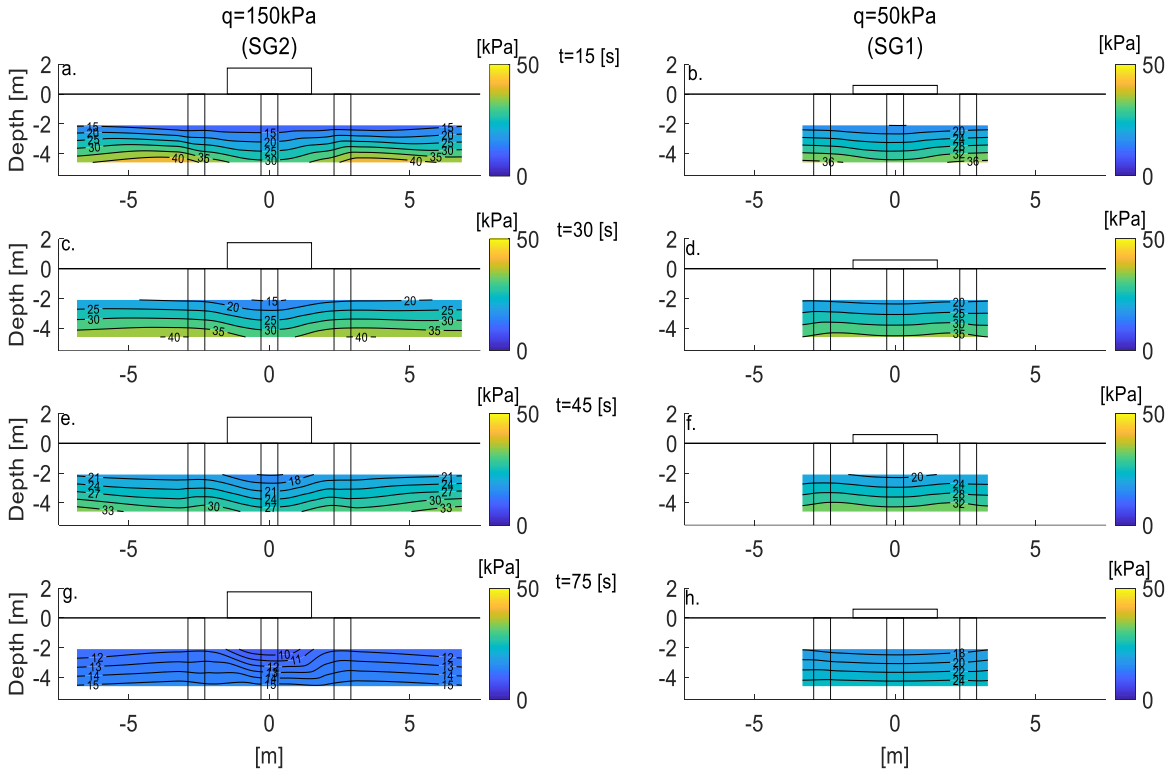

Fig. 4.10 Vertical contours of excess pore pressure for SG2 and SG1

4.3.1.4 Soil Acceleration

Soil acceleration time-histories for the free field and the soil close to the perimeter drains, together with the input motion are presented in Figure 4.11 for SG2 and SG1. Complete acceleration decoupling was observed in SG1 after the first cycle of shaking, verifying complete liquefaction due to large soil softening in the free field, as in SG2.

A significant reduction of the input motion was presented in the soil close to the perimeter drains below the foundation of 50 kPa at the top depth. This was after the first cycle of the shaking, as a result of the considerable soil softening close to the perimeter

drains, showing a similar acceleration behaviour to the free field. At this depth, slightly larger acceleration in SG2 during the first seconds of the motion was presented compared to SG1, due to the softening limitation in the soil close to the perimeter drains during this period in SG2. In contrast to the top layer in SG1, a larger acceleration decoupling at the lower layer was observed due to the further softening in the soil generated at this depth, similar acceleration response as that of SG2. Negligible shear reinforcement was provided by the drain arrangement in both cases for the free field and the soil close to the perimeter drains as previously seen (See Table 4.1).

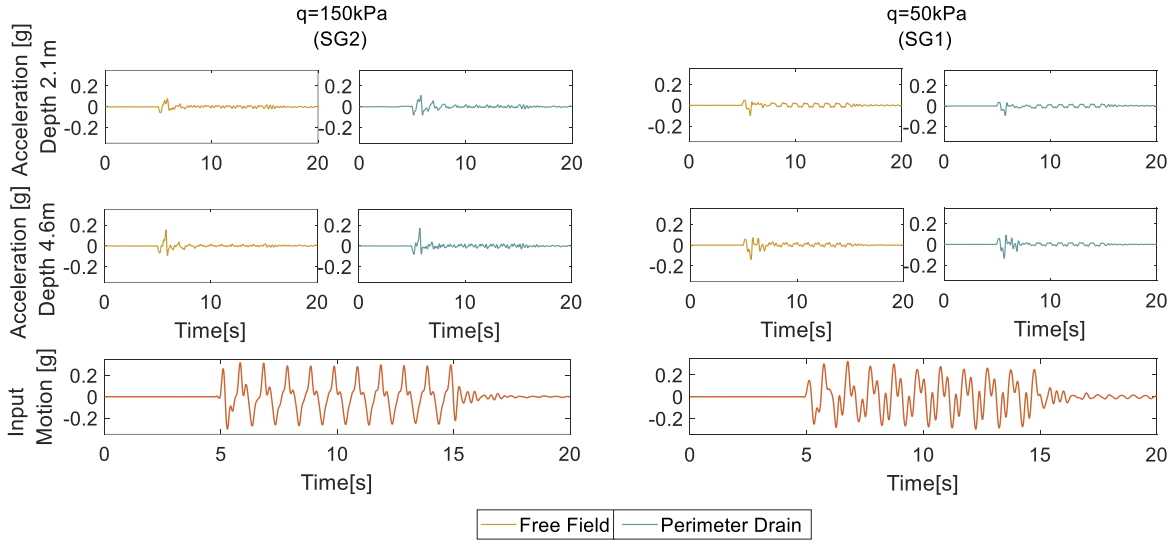

Fig. 4.11 Soil acceleration time-histories at the free field and close to the perimeter drains for SG2 and SG1

4.3.2 Foundation response

4.3.2.1 Foundation settlement

Figure 4.12 shows the foundation's settlement and input motions for SG2 and SG1. Settlement of the foundation of 50 kPa during the shaking stage was controlled by the significant soil softening that allows large deviatoric strains and volumetric deformations in the soil. During this stage, a larger settlement response was obtained in SG1 compared to the foundation of 150 kPa, due to the greater soil softening presented below the foundation.

The foundation's settlement response in SG1 during the post-shaking stage, reached a lower amount than that obtained during the shaking. The presence of the vertical drains allowed a reduction of reconsolidation volumetric deformation due to the rapid dissipation of excess pore pressures under the foundation and a decrease in deviatoric strains because of the faster regained of strength in the soil. Nevertheless, the differences in SG2 and SG1,

in terms of settlement response over time, suggested a better performance of the drains arrangement below the heavy foundation. The settlement of the foundation of 150 kPa stopped sixty seconds after the earthquake as a result of the quick dissipation and rapid regaining of stiffness in the soil, reducing the time for soil deformation. On the other hand, the foundation of 50 kPa required more than one hundred seconds, after the end of the shaking to stop settlement. The moderate dissipation in SG1 caused a longer time for reconsolidation volumetric strains and deviatoric deformation in the soil, producing a slightly larger settlement response compared to the foundation three times heavier.

The settlement response obtained for both foundations follows a similar behaviour previously observed by researchers in data field and experimental tests (Dashti et al., 2010b; Bertalot et al., 2013). In these cases, the great bearing pressure induced large shear and confinement stresses in the soil allowing a limited generation of excess pore pressures under the structure and enabling a close settlement response to that of a lighter foundation. An improved response in terms of foundation settlement was obtained for the case of 150 kPa. This performance was managed by the significant influence of the bearing pressure in the soil during the generation stage, allowing limited soil softening and the reduction of volumetric and shear deformations in the soil. Moreover, the effective dissipation of excess pore pressures allowed by the drains arrangement, influenced by the high confining pressure, let to a rapid regained of stiffness in the soil and consequent improved performance of the arrangement in terms of settlement during the post-shaking stage. The vertical drains' performance depends significantly on the foundation bearing pressure, suggesting the relevance of considering this parameter in the design of the arrangement.

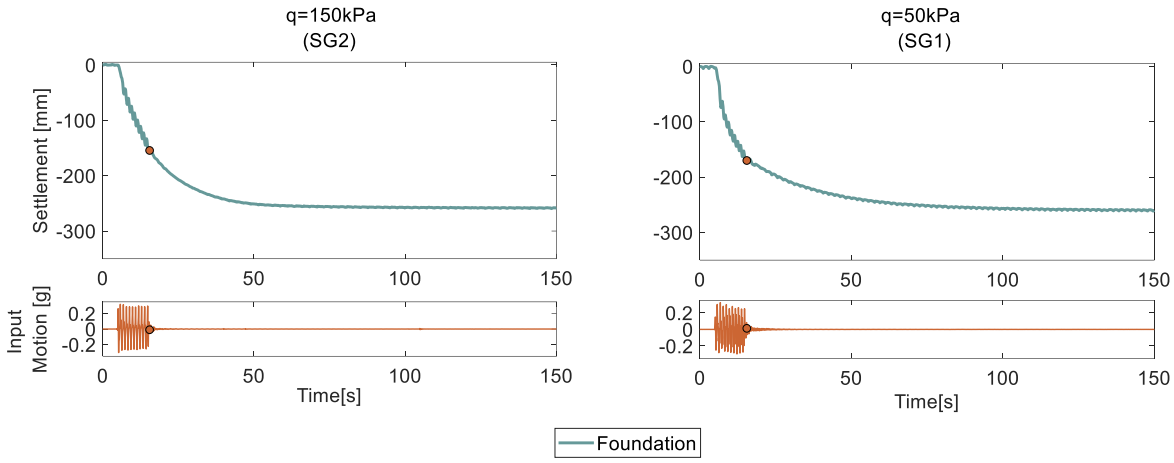

Fig. 4.12 Settlement time-histories for foundations in SG2 and SG1

4.3.2.2 Dynamic response of the foundation

The transference of the input motion to the foundation and the consequent rotational response is analysed in this section for SG2 and SG1. Figure 4.13 shows horizontal accelerations for both foundations including input motions for each case. Reduction of the input motion was observed in both cases as a consequence of the soil softening and negligible shear reinforcement provided by the drains under the foundations. However, a lower transference of the horizontal acceleration was observed in SG1 due to the larger soil softening below the foundation, presenting a reduction of 90% of the input motion after the third cycle of shaking (Fig. 4.13b).

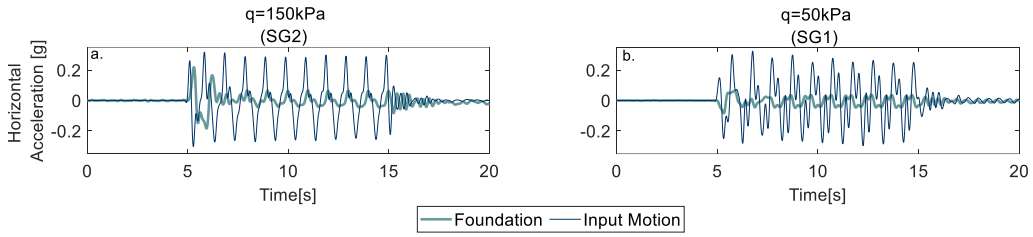

Fig. 4.13 Foundation horizontal acceleration for a) SG2 and b) SG1

Figure 4.14 shows the rotation time-histories (Fig. 4.14a) and settlement vs rotation for SG1 (Fig. 4.14b). The foundation of 50 kPa presented a minor rotational response with a peak value of 7×10^{-3} rad during the first few seconds of the shaking as a result of the lower transference of the input motion to the foundation. Settlement rates after the earthquake are substantial, while rotation rates are slow. The rotation, however, continues to accrue after settlement has ceased. The foundation reached a permanent rotation of 2×10^{-3} rad. Although the foundation rotational response in SG2 was not possible to record due to the

malfunctioning of the instrumentation, a larger rotational response was expected due to the lower softening that was reached compared to SG1, evoking a larger acceleration transference and rotational stiffness. The insufficient drainage enhancement provided by the arrangement was emphasised in the case of light foundations.

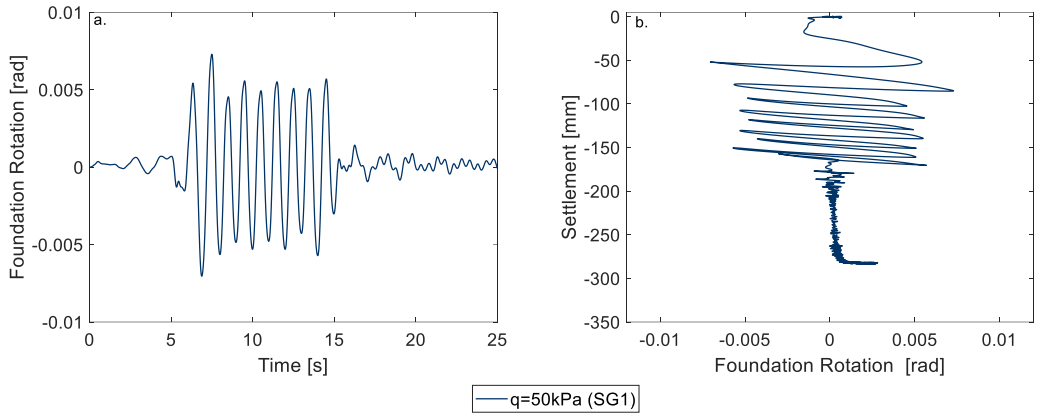

Fig. 4.14 a) Foundation rotational response and b) foundation rotation vs settlement for SG1

4.4 Conclusions

In this chapter, the performance of a simplified arrangement of vertical drains below new buildings has been evaluated as a base case study. In such a scenario, vertical drains can be incorporated in the ground prior to the construction of the building. The evaluation considers a comparison between a foundation over improved and unimproved soil and the bearing pressure variation in relation to the drain's performance.

Greater resistance to high excess pore pressure generation in the soil was observed below the foundation, allowing less soil softening around the internal drain compared to the area surrounded by the perimeter drains. A volume of soil with low pressures was generated below the foundation for the improved and unimproved cases as a result of the foundation's high confining pressure. During the dissipation stage, the arrangement of vertical drains allowed a faster dissipation of excess pressure in the soil compared to that of the unimproved case. Moreover, the arrangement presented "unit cell" and "infinite cell" dissipation pattern for the internal and perimeter drains, respectively; this behaviour was emphasised by the foundation's larger influence over the internal drain. Drainage enhancement in the soil caused a reduction in the foundation's settlement response, indicating the drain arrangement's effectiveness. Nevertheless, the simplified arrangement was unable to control

high excess pore pressures around the internal and perimeter drains and provide enough shear reinforcement to the soil. The insufficient enhancement in the soil was verified by the small settlement reduction and the decrease of the seismic demand on the foundation.

The evaluation of the bearing pressure variation over the improved soil verifies the relevance of this parameter on the effective performance of the drains during the shaking and post-shaking stages. Lower excess pore pressures were reached under the foundation of significant bearing pressure due to the greater shear and confining stresses generated in the soil. In addition, during the dissipation stage, the arrangement's effectiveness was highly influenced by the foundation's confining stress. A better settlement response was observed in the case of the heavier foundation as a consequence of the faster dissipation in the soil induced by the great confining pressure, resulting in a lower permanent settlement as that of the light foundation. Moreover, great softening in the soil generated below the light foundation and minimal shear reinforcement provided by the drains let to a significant reduction of the input motion in the soil and consequent lower rotational response.

Although it is expected an improved performance of the arrangement when installed and compacted in field due to the locked effect in the horizontal stresses around the drains, further improvement in terms of drainage enhancement and shear reinforcement is required to avoid considerable damage in the structure. The permeability of the coarse material inside the drains and the addition of internal drain rings in the soil are factors that should be considered in the design variation.

Chapter 5

New buildings: Improved arrangement alternatives using sustainable materials as vertical drains

5.1 Introduction

Vertical drain arrangements designed for free field are frequently considered as a practical solution against liquefaction damage prior to the construction of new buildings. However, in addition to the absence of overburden pressure in these designs, the shortcomings of these type of arrangements include the use of theoretical parameters (e.g. optimal spacing between drains) that result in a weak mitigation of the critical area below the foundation. Therefore, improved designs of vertical drain arrangements that focus on an adequate mitigation of the soil under the foundation are required if an optimal foundation performance in terms of settlement and dynamic response is to be achieved.

In addition, the use of rubble brick as coarse material inside the vertical drains is proposed as a sustainable economical alternative in this chapter. Reusing construction material from building demolition, or from debris generated after earthquakes in geotechnical solutions, produces attractive results for the environmental field as this enables challenges related to waste management to be met. In addition to the benefits of using rubble brick in terms of sustainability, an improved mechanism of the technique is expected as higher permeability and shear strength is provided by the rubble brick columns. The greater size particles naturally result in a greater permeability. In addition, due to the angular shape of the particles, the coarse material will have a greater friction angle compared to the finer

material (Tatsuoka *et al.*, 2013). Moreover, a higher nominal cohesion is expected in the case of the coarser material because of the improved interlocking behaviour between the coarse particles (Bhuiyan *et al.*, 2015). Previous work focusing on the use of crushed stones inside the drains has been performed using shaking table tests. An improved response of the structure as a result of the highly permeable material inside the drains has been verified (Orense *et al.*, 2003); however, further studies on the performance of drainage mitigation techniques using highly permeable recycled material are necessary.

In the previous chapter, the performance of a simplified vertical drain arrangement below the foundation, used as liquefaction countermeasure technique for new buildings, was evaluated as a base case that considered a variation in the foundation bearing pressure. In this chapter, enhanced arrangement using rubble brick drains centred on a proper mitigation of the area below future constructions are evaluated with the aim of reducing structural damage in terms of settlement. The utilisation of additional vertical drains below the foundation is analysed in the first section by comparing the performance of 13- and 17-drain arrangements. In section 5.2, the 17-drain arrangement containing aluminium encased drains below the foundation is evaluated and compared to a similar arrangement with no encasement in the drains. Finally, a single column covering the entire base area of the foundation is analysed as a simplified alternative for liquefaction damage reduction. The analysis considers the performance of these arrangements in terms of excess pore pressure generation and dissipation, influenced by the significant bearing pressure of the foundation. The effectiveness of each alternative in terms of settlement response is analysed together with the foundation dynamic response. Some of the results obtained from this analysis were presented in García-Torres and Madabhushi, (2019).

5.2 Additional vertical drains in the arrangement configuration

The utilization of additional edge drains below the foundation in order to improve the foundation structural response is analysed in this section; here, performance of 13-(SG3) and 17- (SG4) vertical drain arrangements is considered.

5.2.1 Soil Response

5.2.1.1 Excess pore pressure generation

Excess pore pressure ratios time-histories for soil containing an arrangement of 13 and 17 vertical drains below a foundation of 150 kPa are presented in Figure 5.1, considering

the soil near the internal, edge, sub-perimeter and perimeter drains at depths of 2.1 m and 4.7 m.

At the top layer in SG3, limited generation of excess pore pressures was observed close to the internal drain below the foundation when compared to the soil adjacent to the sub-perimeter and perimeter drains (Fig. 5.1a). The high confining pressure exerted by the foundation of 150 kPa over the central area allowed significant resistance of the soil to great pore pressure generation around the internal drain. The soil near the sub-perimeter drains reached a value of 0.63 at the end of the shaking, while the perimeter drains were unable to avoid complete liquefaction (r_u=1) in the nearby soil, suggesting a weak performance of the rubble brick drains in free field conditions (no overburden pressure). The excess pore pressure ratio higher than 1 obtained in the soil surrounding the perimeter drains was assumed to be a consequence of the upward fluid flow and the movement of the instrument in the soil. At the middle layer (depth 4.7 m), excess pore pressure ratios near the internal and sub-perimeter drains exhibited peak values of 0.4 and 0.65, respectively (Fig. 5.1c). A larger degree of generation was observed at this level compared to the top layer due to the lower additional confining stress in the soil at lower depths. By contrast, the soil close to the perimeter drains presented lower excess pore pressures ratios at this level as a result of the greater soil effective stress and the negligible influence of the foundation at the top layer.

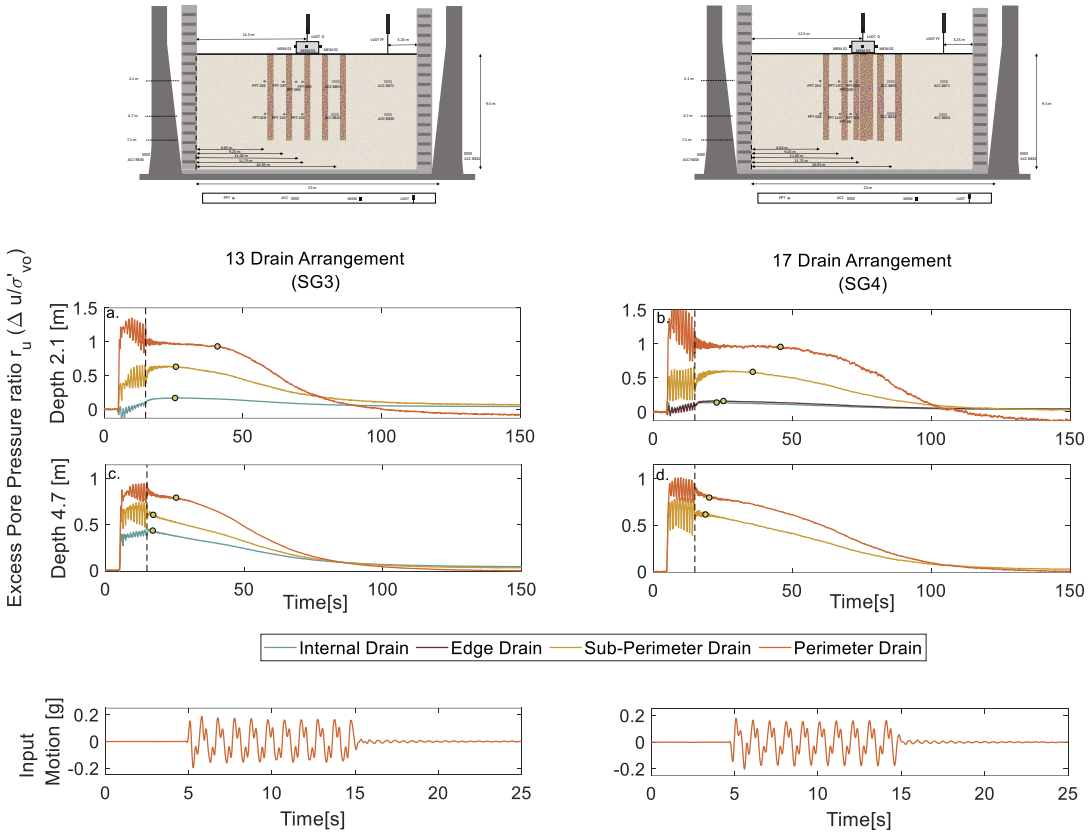

Fig. 5.1 Excess pore pressure ratios (r_u) time-histories for SG3 and SG4

In SG4, large excess pore pressures ratios close to the perimeter drains were reached at both stratum depths, while small values were registered around the drains located closer to the foundation. At the top layer, ratios of 0.15 and 0.17 were recorded near the internal and edge drains; by contrast, the soil adjacent to the sub-perimeter and perimeter drains presented greater r_u values of 0.6 and 1 (Fig. 5.1b). At the middle depth, the soil near the sub-perimeter and perimeter drains reached peak ratios of 0.66 and 0.85 (Fig. 5.1d). Similar to SG3, the perimeter drains were unable to prevent liquefaction in the adjacent soil at the top layer of the stratum.

A lower ratio of excess pore pressure was observed at the internal drain in test SG4 compared to test SG3, suggesting an effective control of excess pore pressure generation below the foundation, managed by the additional drains. The area of influence of the edge drains involved a limited zone, generating a negligible effect around the sub-perimeter and perimeter drains during the generation stage, as verified by the similar peak ratios reached at both locations in tests SG4 and SG3. The addition of the edge drains in the 13-vertical drain configuration enabled a more effective control of excess pore pressures in the soil, suggesting that it is relevant to consider a large number of drains and large area replacement

ratio (A_r) below the foundation for effective performance during the excess pore pressure generation phase.

5.2.1.2 Dissipation of excess pore pressures: Influence of edge drains in the arrangement performance

The effect of additional edge drains around the internal drain in the 17 vertical drain arrangement during the dissipation stage is analysed in this section. Figure 5.2 presents the horizontal contours of excess pore pressure ratios (r_u) for SG3 and SG4 at a depth of 2.1 m, considering the time at which shaking ends, flowfront arrival times at the internal, sub-perimeter and perimeter drains in SG4, and t=75 s. Contours were plotted using a similar procedure as in the previous chapter.

At the end of the shaking, the soil around the internal drain in SG3 exhibited a low r_u value, as the foundation exerted significant influence over this area. A peak value of 0.15 was reached in the soil surrounding the internal drain, while comparatively large values of 0.5 and 1 were observed close to the sub-perimeter and perimeter drains at this time (Fig. 5.2a). On the other hand, in SG4, excess pore pressure ratios reached a value of 0.1 at the soil adjacent to the internal and edge drains. Higher values of 0.4 and 1 were observed close to the sub-perimeter and perimeter drains, respectively; these were influenced by the low bearing pressure of the foundation (Fig. 5.2b).

After the end of shaking, an increase of excess pore pressures was observed over the entire top layer in SG4 until the flowfront arrived near the internal drain at t=22.8 s (Fig. 5.2d). The soil around the internal and edge drains showed r_u values of 0.1 and 0.2, while a greater ratio of 0.6 was observed in the soil adjacent to the sub-perimeter drains. The faster dissipation observed near the internal drain compared to that near the edge and outer drains occurred due to the "unit cell" behaviour of the internal drain, together with the significant confining stress exerted by the foundation. On the other hand, excess pore pressures were generated below the foundation in SG3 at this time, as there was only one drain in charge of controlling and dissipating the fluid. A high r_u value of 0.7 and complete liquefaction (r_u =1) were observed at the sub-perimeter and perimeter drains, due to the fluid flow from the bottom layers (Fig. 5.2c). The edge drains below the foundation, surrounding the central drain in SG4, allowed a fast flowfront arrival near the internal drain, accelerating the excess pore pressure dissipation under the foundation.

The flowfront arrived at t=25.3 s near the edge drains in SG4 (see Fig. 5.1b), showing a peak ratio of 0.17. The soil at the sub-perimeter drains began to dissipate ten seconds later (t=35 s). The edge drains allowed a faster flowfront arrival in the adjacent soil due to their higher "unit cell" behaviour, while the sub-perimeter drains presented a reduced "unit cell" behaviour and a lower influence of the foundation, delaying the flowfront arrival and the

rapid action of the outer drains (Fig. 5.2f). The sub-perimeter drains presented lower "unit cell" performance, as they were in charge of additional fluid that was not able to be collected by the perimeter drains due to their infinite supply (Brennan, 2004). Meanwhile, in SG3, the soil near the sub-perimeter drains showed a faster dissipation initiation compared to SG4 in the absence of the edge drains ring, verifying the delay of the flowfront arrival at the outer drains when additional internal drain rings are located in the soil.

The soil near to the perimeter drains began to dissipate at t=45.8 s in SG4. The r_u values at the internal drain were smaller under the foundation compared to SG3 at this time; nevertheless, soil near the sub-perimeter and perimeter drains showed greater ratios (Fig. 5.2h). The edge and internal drains in SG4 led to a faster dissipation of excess pore pressures below the foundation; however, similar to the soil behaviour near the sub-perimeter drain, the rapid action of the perimeter drains was altered by the additional drain ring. At t=75 s, dissipation throughout the entire layer of SG4 was observed, mainly under the foundation presenting r_u values of 0.08 and 0.1 close to the internal and edge drains (Fig. 5.2j). On the other hand, a more uniform dissipation was observed in SG3, showing a ratio of 0.16 under the foundation edge and 0.21 and 0.26 at the sub-perimeter and perimeter drains (Fig 5.2i).

The performance of a 13- and 17-vertical drain arrangement containing Fraction B as coarse material have been previously evaluated by Brennan (2004), albeit without considering overburden pressure over the soil. In this case, the additional four drains were located in the perimeter ring of the 17 drain configuration. Complete liquefaction was reached near the perimeter drains in both arrangements, while lower r_u values between 0.95 and 0.90 were registered close to the internal drain rings in the absence of bearing pressure and drains able to control high excess pore pressures. Compared to the present work, a longer time was required for the internal drain to initiate dissipation in the 13-drain arrangement, which can be explained by the lower permeability of the drain's material and the absence of significant confining pressure in the soil. Similarly, an improved performance of the 17-drain configuration with additional edge drains below the foundation was observed in terms of dissipation, particularly around the internal drain, verifying the improved performance of the technique of placing the additional drain ring in the configuration within the internal zone.

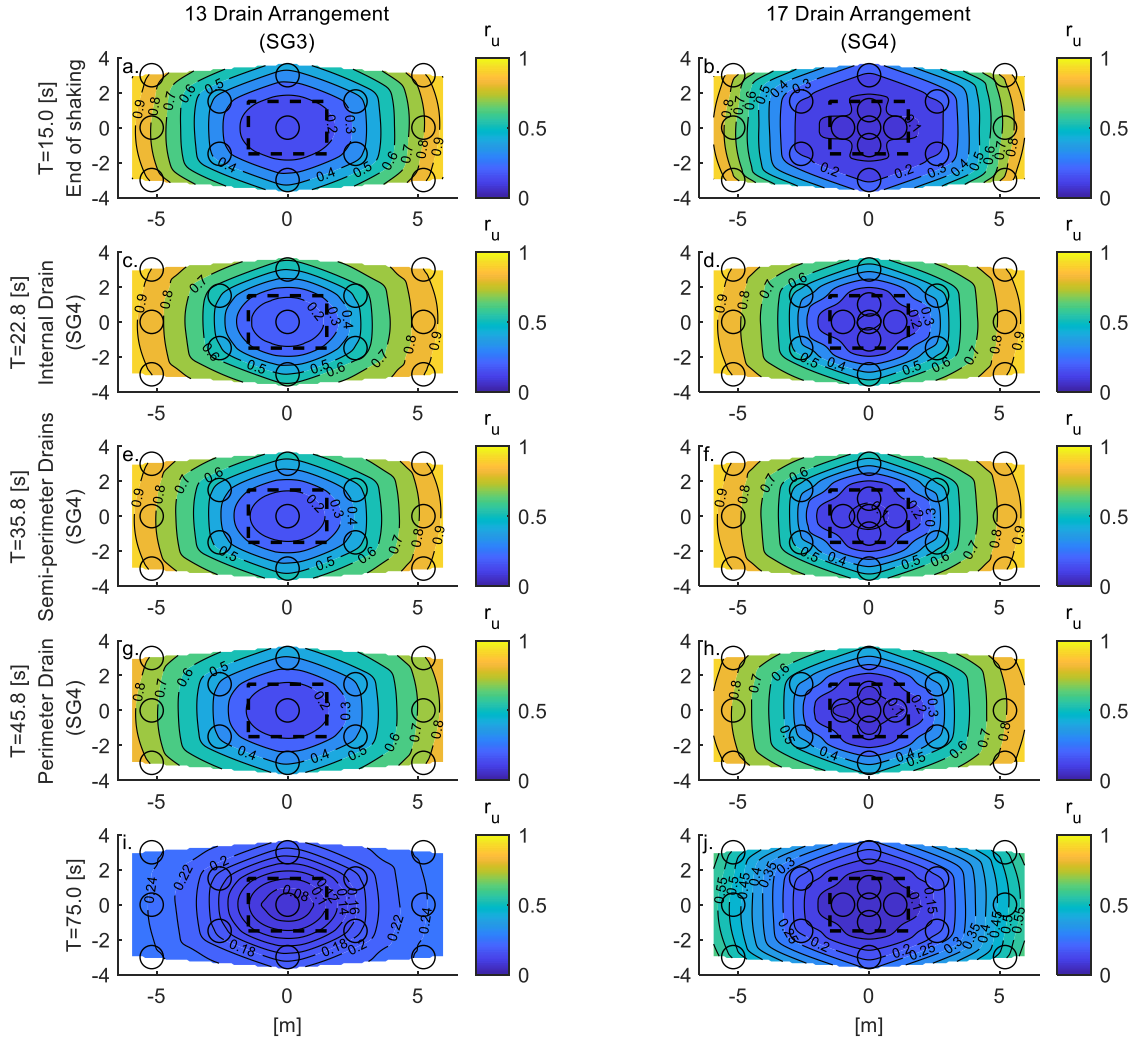

Fig. 5.2 Horizontal contours of excess pore pressure ratios (r_u) for SG3 and SG4 at depth of 2.1 m

In addition, Badanagki *et al.* (2019) analysed the performance of granular columns arrangements with an area replacement ratio (A_r) of 10% and 20% in liquefiable soil and without structures over the surface. Greater excess pore pressures were reached close to the internal drains in the presence of a lower number of columns (A_r =10%), while limited generation was presented at a similar location in the soil containing a higher area replacement ratio (20%). Moreover, the large number of granular columns allowed for a faster dissipation of excess pore pressures compared to the other case, verifying the significant influence of additional drains and large area replacement ratio for enhanced control and effective dissipation.

5.2.1.3 Vertical dissipation of excess pore pressures

Vertical dissipation of excess pore pressures ratios in the soil containing a 13 and 17 drain arrangement is evaluated in this section (Fig. 5.3). A comparative analysis between both cases is presented; however, vertical contours were plotted only for the 13 drain configuration due to technical problems arising with the instrument located near the internal drain, at the middle layer of SG4.

At t=15 s, a low r_u value in the soil around the internal drain in SG3 was observed at the top layer, while high excess pore pressures showing complete liquefaction were registered near the perimeter drain (Fig. 5.3a). After the end of shaking, excess pore pressures continued to increase particularly in the soil located far from the foundation, until t=22.8 s, at which point the soil at the internal drain started to dissipate from the top layer (see Fig 5.1a). A volume of soil with low pressures enclosed by the sub-perimeter drains was generated up until this time due to the significant confining stress exerted by the foundation and the presence of the internal drain. After five seconds, (t=30 s) the soil under the foundation showed significant dissipation, presenting small r_u values of 0.16 and 0.35 at the top and bottom layers (Fig. 5.3b). Meanwhile, the soil close to the sub-perimeter and perimeter drains began to dissipate from the bottom layers. A volume of lower pressures surrounding the internal and edge drains was expected in SG4 compared to the 13-drain configuration, influenced by an improved control of excess pore pressures below the foundation managed by the additional edge drains.

At t=45 s, excess pore pressures near the sub-perimeter and perimeter drains in SG3 were dissipating at the top layer, reaching r_u values of 0.5 and 0.9 (Fig 5.3c). Moreover, greater values of 0.55 and 1 were reached at similar locations in SG4 (see Fig 5.1b), suggesting a slower dissipation in this area compared to SG3. Significant reduction of excess pore pressures in the stratum was observed at t=75 s in SG3, presenting a small ratio of 0.1 under the foundation at the top layer (Fig 5.3d). As previously analysed, rapid dissipation below the foundation was registered in SG4 at this time, due to the presence of the internal and edge drains in this area, while a slow dissipation behaviour was observed in the soil close to the sub-perimeter and perimeter drains due to the delay on flowfront arrivals. The volume of low pressures generated around the internal drain below the foundation was influenced by the additional edge drains that controlled the high excess pore pressure generation around it. Moreover, this additional drain ring facilitated the rapid dissipation observed in this zone. Although the edge drains allowed for effective performance below the foundation, a longer time was required for the soil near the sub-perimeter and perimeter drains to start dissipation along the stratum depth.

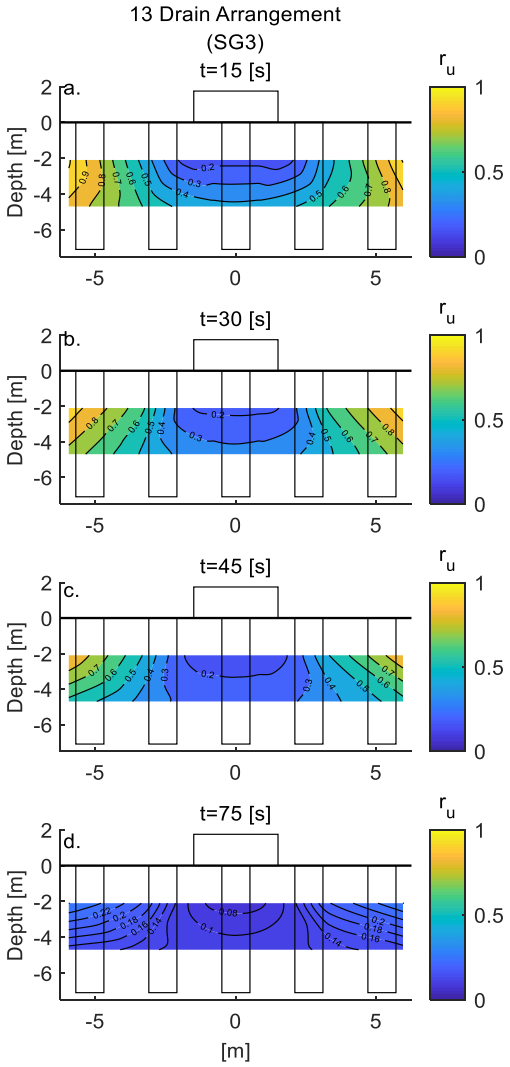

Fig. 5.3 Vertical contours of excess pore pressure ratios (r_u) for SG3

5.2.1.4 Soil Acceleration

Acceleration of the soil near the perimeter drains and the free field at the top and middle layers is presented for SG3 and SG4 in Figure 5.4. In the free field, complete acceleration decoupling was observed for both cases after the first cycle of the shaking at the top and middle layers, due to complete liquefaction (r_u=1) having occurred in the absence of vertical drains. Significant acceleration reduction was observed in the soil near the perimeter drains at the top layer in SG3 and SG4 as a response to the considerable soil softening reached at 2.1 m. Greater soil acceleration close to the perimeter drains at the middle layer was observed compared to the top level in both cases, due to the lower softening in the soil observed at the bottom layers.

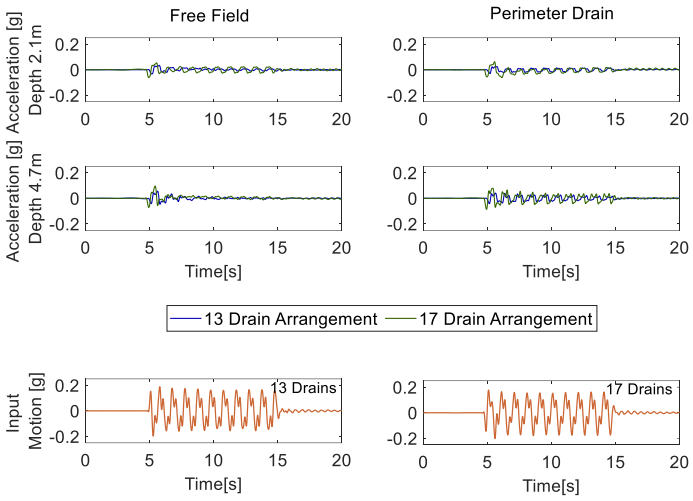

Fig. 5.4 Acceleration time-histories for soil near the perimeter drains and the free field in SG3 and SG4

As previously stated, the influence of the drains arrangement in terms of shear reinforcement remains uncertain in this research as the soil response was also influenced by the drainage enhancement. In this section, the similar procedure performed in previous chapter has been developed to estimate the drains behaviour with regard to shear strength, considering rubble brick as coarse material inside the drains.

The additional shear reinforcement provided by the vertical drains in the treated area is presented in Table 5.1 for SG3 and SG4, at depth of 2.1m. Although similar level of excess pore pressure were generated in the free field and near the perimeter drains, lower deamplification was observed in the soil adjacent to the perimeter drains at both layers in SG3 and SG4; this can be explained by the additional shear reinforcement of 6.7% and 8.7% provided by the drains (Table 5.1). Moreover, the soil softening reached similar magnitudes near the perimeter drains in SG3 and SG4 at the top and middle layers. Nevertheless, a slightly larger acceleration was observed in SG4 due to the greater shear strength provided by the addition of edge drains in the 17-drain arrangement (A_r=7.1%).

5.2.2 Foundation response

5.2.2.1 Foundation settlement

The effectiveness of the 17 vertical drain arrangement containing edge drains below the foundation is evaluated in this section in terms of settlement, considering a comparison with the settlement response of the foundation in SG3. Figure 5.5 illustrates the foundation settlement for SG3 and SG4 along with the input motions.

Table 5.1 Additional shear reinforcement in the soil layer for SG3 and SG4 (depth of 2.1 m)

Depth (m)	SG3		SG4	
	Vertical Drains		Vertical Drains	
	A_r (%)	τ_{A_r} (%)	A_r (%)	τ_{A_r} (%)
2.1	5.4	6.7	7.1	8.7

In SG3, 89% of the total foundation settlement occurred during the shaking, while only 10% was generated during the dissipation stage. The soil softening generated around the internal drain led to large reconsolidation volumetric deformations and deviatoric strains during the shaking. Subsequently, limited settlement was expected in the presence of drains that enabled a rapid dissipation below the foundation, reducing the time in which high excess pore pressures were retained and diminishing reconsolidation volumetric deformations (Fig. 5.5a). On the other hand, the foundation in SG4 reached 310 mm of settlement during the shaking, a value that represents 89% of the total (Fig 5.5b). The effective control of excess pore pressures below the foundation in presence of the internal and edge drains allowed limited soil softening under the foundation compared to SG3, decreasing the volumetric and deviatoric deformations in the soil during the shaking. During the dissipation stage, excess pore pressures were quickly dissipated in SG4. The edge drains facilitated significant drainage enhancement below the foundation, reducing volumetric and deviatoric strains in the soil and allowing soil stiffness to be regained more rapidly.

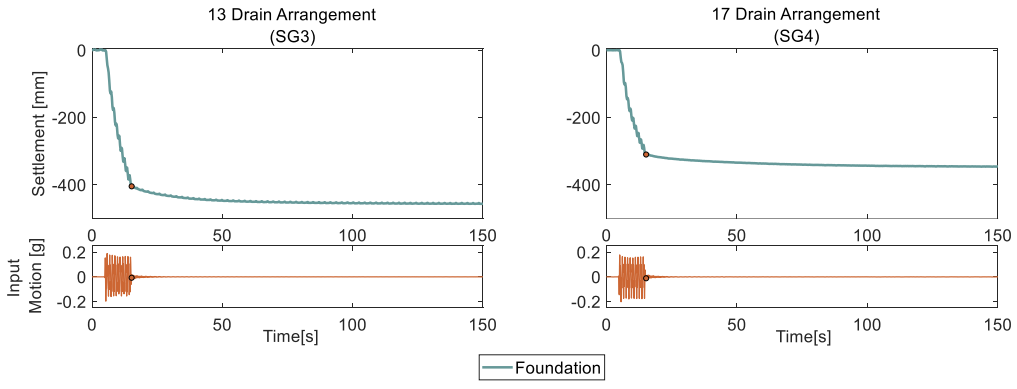

Fig. 5.5 Settlement time-histories of foundations for SG3 and SG4

Badanagki *et al.* (2019) evaluated a structure of 80 kPa over mitigated soil containing an arrangement of granular columns, with 24% of the area under the foundation footprint covered by the pillars. Although the lower bearing pressure resulted in increased soil softening below the foundation, the 80 kPa structure reached a lower settlement during the shaking compared to the 17-drains arrangement evaluated in this work. This response may have been due to the major shear reinforcement provided by the granular columns below the foundation in Badanagki's study. Nevertheless, the vertical drain arrangement resulted in more effective performance in terms of settlement reduction during the dissipation stage. Even though more permeable material and greater shear strength of the granular columns was provided in Badanagki's work; the larger area covered by the drains below the foundation footprint in the drain configuration (28%) and the significant bearing pressure of 150 kPa enabled faster dissipation in the soil and a consequently greater reduction of the foundation settlement.

Although a reduction of 25% was obtained in the foundation settlement response by using the 17-vertical drain alternative due to the effective performance of the additional edge drains during and after the shaking, a larger settlement reduction was expected considering that a significant area below the foundation was mitigated by drains. Photos taken during the soil excavation in SG4 (Fig. 5.6) reveal a difference between the width of the edge drains at the top and bottom depths, suggesting the existence of bulging at the top of the columns. The significant bearing pressure allowed great deformation to occur in the vertical drain due to the absence of lateral confinement from the surrounding liquefied soil. This behaviour resulted in a decrease in the drain's bearing capacity, causing a larger foundation settlement. Bulging in the vertical drains and the complete reduction thereof are evaluated in the following section, resulting in an improved performance of the arrangement.

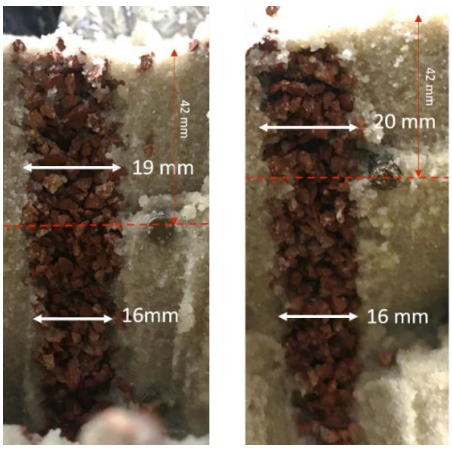

Fig. 5.6 Photos of vertical drains below the foundation taken after the test (dimensions in model scale)

5.2.2.2 Dynamic response of the foundation

The foundation horizontal acceleration and it's rotational response are analysed in this section. Figure 5.7 illustrates the foundation acceleration together with the input motion for SG3 and SG4. The greater soil softening generated below the foundation in SG3 resulted in a lower transference of the input motion to the foundation, reaching a peak acceleration of 0.05g at the initiation of the shaking (Fig. 5.7a). Slightly greater horizontal acceleration was observed for the foundation in SG4, managed by the reduced soil softening in the presence of the edge and internal drains below the foundation, attaining a peak acceleration of 0.1g at the second cycle of the shaking (Fig. 5.7b). Minor transference of the input motion to the foundations was observed in both cases, corroborating the weak shear reinforcement provided by the rubble brick vertical drains in the soil.

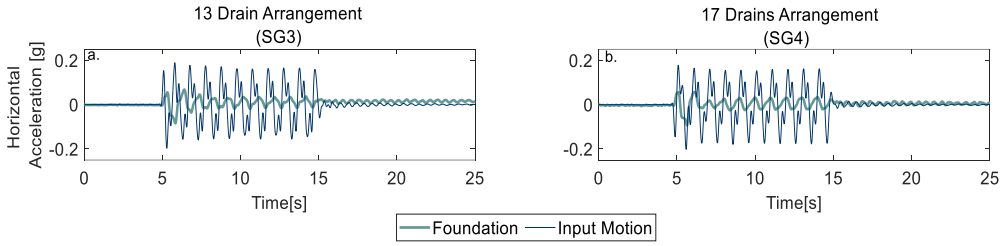

Fig. 5.7 Foundation horizontal acceleration for a) SG3 and b) SG4

Figure 5.8 presents the foundation rotational response for SG3 and SG4. The foundation in SG3 reached a maximum rotation of 2×10^{-3} radians at the second cycle of the shaking as a response to the low transference of the seismic demand to the foundation (Fig. 5.8a). In SG4, a slightly larger rotation was reached, with a peak rotation of 3×10^{-3} rad at t=7 s, in response to the slightly larger foundation horizontal acceleration. In addition, figure 5.8b shows the foundation rotation vs settlement for SG3 and SG4. Larger rotation of the foundation was observed during the first 100 mm of the settlement in SG4. Rotation and settlement of the foundation stopped at the same time,reaching a permanent value of 4×10^{-4} rad. In SG3, greater rotation also occurred during the initiation of the settlement response when higher horizontal acceleration was presented. In addition, the foundation ceased settling and reached a negligible permanent rotation of 1×10^{-4} rad.

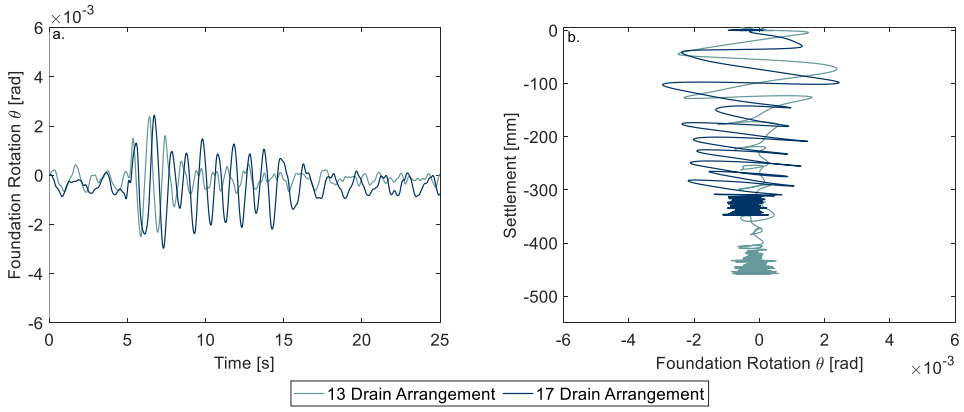

Fig. 5.8 a) Foundation rotational response and b) Foundation rotation vs settlement for SG3 and SG4

5.3 Influence of encased vertical drains in the arrangement performance

The use of gravel columns as a countermeasure technique against liquefaction is highly effective in the reduction of structural damage; nevertheless, limitations arise when these columns are located in soft soil. Bearing pressure over the soil induces vertical and lateral deformation in the columns, meaning that the column's load capacity depends on the lateral confinement offered by the nearby soil (Castro and Sagaseta, 2011). In soft soils, this lateral confining support is negligible, generating bulging in the columns and consequent reduction of their bearing capacity to support the overburden load. For this reason, the encasement of gravel columns emerges as an optimal alternative that improves the technique's ability to reduce liquefaction damage, as the bulging can be completely avoided in this way. The casing shell provides stiffness and strength to the column influenced by the significant lateral confinement (Murugesan and Rajagopal, 2010).

In the previous analysis, additional vertical drains located below the foundation presented an effective performance by controlling large soil softening during the shaking; however, this was insufficient to obtain considerable settlement reduction. This limited reduction can be attributed to the bulging effect observed at the top of the drains in the absence of lateral confinement. Therefore, the use of aluminium encased vertical drains replacing the edge and internal drains in the 17-drain configuration is evaluated in this section. A comparative analysis between the arrangement of 17 vertical drains, considering drains with (SG5) and without encasement (SG4) under the foundation, is presented below.

5.3.1 Soil Response

5.3.1.1 Excess pore pressure generation

The generation of excess pore pressure in the soil containing a 17-vertical drain arrangement with encased drains below the foundation (SG5) and in the original arrangement with no encasement in the drains (SG4) is presented in Figure 5.9, considering the soil adjacent to the internal, edge, sub-perimeter and perimeter drains, including the free field.

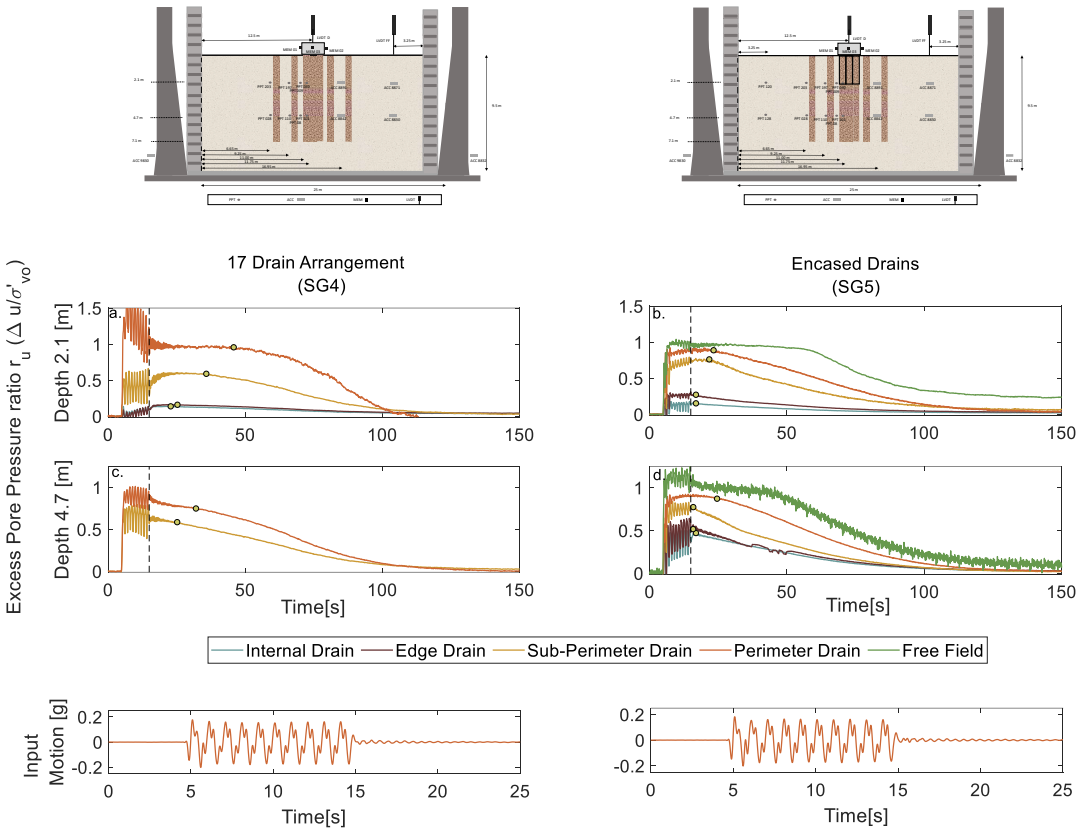

Fig. 5.9 Excess pore pressure ratios (r_u) time-histories for SG4 and SG5

In SG5, the generation of excess pore pressure in the soil near the internal drain at the top layer, reached a peak r_u value of 0.17 at the end of the earthquake; this was due to the additional confining stress exerted by the foundation and the effective action of the surrounding encased edge drains at controlling great excess pore pressure generation. A higher ratio of 0.3 was reached in the soil near the encased edge drains in response to the low influence of the foundation at this location. Moreover, increased generation was observed close to the sub-perimeter and perimeter drains, presenting peak values of 0.75 and 0.9 due to the limited influence of the foundation confining stress. The free field exhibited

a complete liquefaction behaviour at this depth due to the lack of drainage improvement (Fig. 5.9b).

In the middle layer, larger excess pore pressure ratios were reached under the foundation near the internal and the edge drains compared to the top layer due to the reduced influence of the foundation at this level, with r_u values of 0.45 and 0.55 respectively. Higher excess pore pressure ratio was registered near the sub-perimeter drain at this depth, while the soil adjacent to the perimeter drain presented a slightly lower r_u ratio compared to the top layer, which was influenced by the large effective stress of the soil at this depth. Complete liquefaction behaviour was also observed at this level in the free field (Fig 5.9d).

Greater r_u values were recorded in the soil close to the internal and edge encased drains in SG5 compared to SG4 at the top layer. During the first seconds of the shaking, a rapid generation of excess pore pressure was observed near the internal and edge encased drains below the foundation, reaching peak values instantaneously (Fig 5.9b). By contrast, excess pore pressures near the internal and edge drains in SG4 were generated gradually, taking a longer time to reach peak values during the shaking (Fig 5.9a). This suggests a more effective control of excess pore pressures in the absence of the encased material as the fluid is able to flow easily towards the uncased drains during the motion. The aluminium encased drains in SG5 led to a deficient management of high excess pore pressures, affecting the soil near the sub-perimeter drains, which thus showed a higher ratio compared to SG4.

5.3.1.2 Dissipation of excess pore pressures: Effect of reducing bulging in vertical drains

The performance of the encased drains in the 17-vertical drain configuration during dissipation is evaluated in this section, considering a comparison with the same arrangement without encased drains. Figure 5.10 presents excess pore pressure contours in the horizontal plane for SG4 and SG5, considering flowfront arrival times in the soil near the drain rings in SG5.

At the end of the shaking, a peak value of 0.1 was reached close to the central drain in SG5, while greater r_u values of 0.3 were observed near the edge drains. Greater excess pore pressure generation was reached close to the sub-perimeter and perimeter drains due to the lower additional confining stress applied by the foundation at this area, reaching values of 0.8 and 0.9 (Fig. 5.10b). At this time in SG4, lower r_u values were reached below the foundation, near the internal drain and between the edge and the sub-perimeter drains (Fig. 5.10a), indicating improved control of excess pore pressure generation in the absence of the aluminium encasement.

An increment of excess pore pressures was observed near the internal and outer drains in SG5, until the soil near the internal drain reached a peak value of 0.17 two seconds after the shaking (t=16.9 s). Moreover, the flowfront arrived at the edge drains at the same time, enabling dissipation under the entire foundation footprint (see Fig. 5.9b); this suggests that the internal drain worked together with the edge drains to create an entire block that exhibited a "unit cell" behaviour during the dissipation stage. While this was occurring, r_u values at the sub-perimeter and perimeter drains were still high. At this time in SG4, an increment of excess pore pressure was observed in the entire layer (Fig 5.10c). The faster dissipation near the encased drains following the shaking responds to the absence of the bulging effect in the drains. The complete reduction of the bulging at the top of the columns due to lateral confinement enabled the drains to exhibit improved drainage behaviour, as the risk of clogging and misplacement of coarse material from inside the drains was reduced. Furthermore, in addition to the closeness between the internal encased drains, the covering also provided stability to the columns; this allowed the five drains to perform as an entire block below the foundation, with great potential to perform rapid dissipation in the soil.

The flowfront arrived at the sub-perimeter drain at t=21.7s in SG5, showing significant dissipation in the soil below the foundation, with r_u values of 0.14 and 0.24 near the encased internal and edge drains (Fig. 5.10f). Meanwhile, no dissipation near the perimeter drains was observed due to their "infinite cell" behaviour. The flowfront arrived at the perimeter drain at t= 23.3 s, showing a reduction of excess pore pressures close to the sub-perimeter ring and significant dissipation near the internal and edge encased drains below the foundation (Fig. 5.10h). At this time in SG4, dissipation close to the internal drain was observed, and no flowfront arrived at the edge and sub-perimeter drains (Fig 5.10g). The rapid dissipation initiation close to the encased internal and edge drains, along with their performance as a block in SG5, led to a faster dissipation initiation in the soil adjacent to the sub-perimeter and perimeter drains when compared to SG4. More than fifty seconds after the flowfront arrival near the perimeter drain in SG5 (t=75 s), complete dissipation of the internal zone below the foundation was observed along with considerable reduction of excess pore pressures at the sub-perimeter and perimeter drains (Fig. 5.10j). Furthermore, larger r_u values around the internal and edge drains were recorded in SG4 at this time, including greater excess pore pressure magnitudes near the outer drain rings (Fig. 5.10i).

The complete reduction of the bulging in the drains improved the performance of the arrangement during the dissipation stage, as the drains were consequently able to maintain their original drainage capacity. Moreover, the enhanced stability of the columns due to the lateral confinement pressure, enabled a block performance of the internal and edge drains below the foundation inducing rapid dissipation in the entire layer.

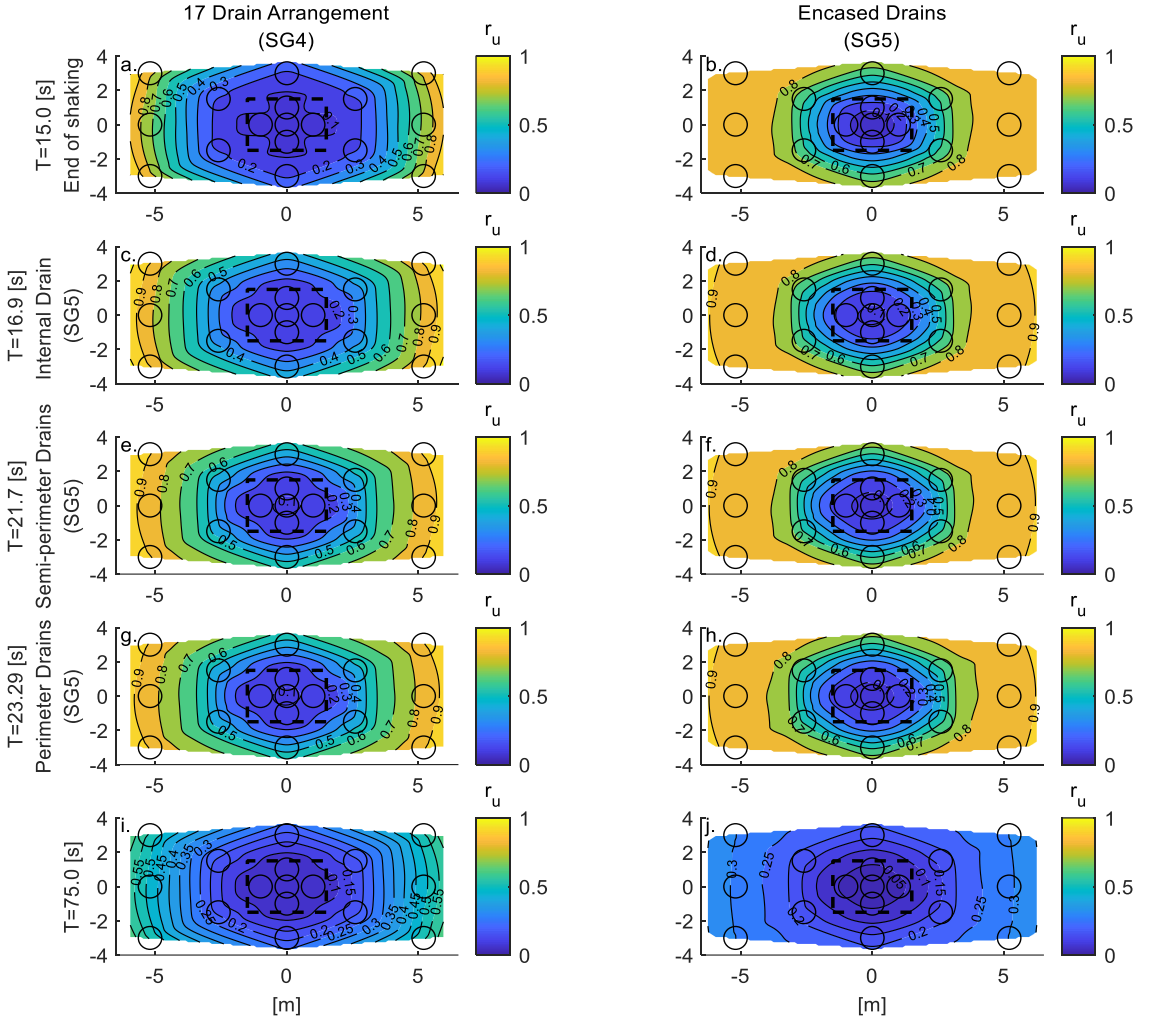

Fig. 5.10 Horizontal contours of excess pore pressure ratios (r_u) for SG4 and SG5 at depth of 2.1m

Previous studies focusing on the performance of encased gravel columns as liquefaction mitigation technique have not been comprehensively evaluated using physical modelling. Nevertheless, finite element analysis has been used to evaluate the behaviour of encased drains in mildly sloping soil, as a liquefaction countermeasure method. Tang *et al.* (2015) and Geng *et al.* (2017) performed numerical modelling analysis to evaluate the performance of granular columns with and without encasement, with the aim of reducing lateral deformation in liquefiable sand. Similar to this work, significant improvement in the soil containing encased columns were observed during the dissipation stage rather than during the shaking, as the pillars were unable to prevent significant excess pore pressure generation. On the other hand, positive results were observed during the dissipation stage through the use of encased granular columns, suggesting the relevance of eliminating the bulging at the top of the columns to maintain the initial permeability of the drains.

Although a number of different geosynthetic materials, such as geotextiles and geogrids have been used for gravel columns, the principal aim of the aluminium encasement in this work was to provide sufficient lateral confinement in the drains. Improved performance of the drains is expected to result from the use of a geotextile encasement, as this material offers additional filters that avoid the entrance of fine material inside the drains entirely, leading to better performance of the drains during the generation and dissipation stages.

5.3.1.3 Vertical dissipation path in the soil with encased vertical drains under the foundation

The contours of excess pore pressures ratios in the vertical profile for SG5 are presented in Figure 5.11 to facilitate an analysis of the behaviour of the fluid along the stratum depth during the dissipation stage, considering encased drains below the foundation. Dissipation initiation times of 15, 30, 45 and 75 s were considered for the plots.

At the end of the shaking, a volume of soil with low pressures was concentrated below the foundation, around the internal and edge encased drains, showing r_u values of 0.3 and 0.5 at the top and bottom layers (Fig 5.11a). This soil behaviour was generated due to the large influence of the foundation bearing pressure, as well as the effectiveness of the encased edge drains in controlling high excess pore pressures. At this time, excess pore pressure ratios close to the sub-perimeter and perimeter drains presented greater r_u values at the top and lower layers. On the other hand, the volume of low pressures below the foundation in SG4 was expected to show lower ratios than the top layer compared to SG5, as a more effective control of excess pore pressures below the foundation and between the edge and sub-perimeter drains was observed considering drains with no coating.

After the shaking, excess pore pressures continued to be generated due to the fluid from bottom layers flowing upwards in all the stratum, particularly at the outer rings. After reaching a peak value of 0.3 at the top layer, the volume of low pressures enclosed by the internal and the perimeter drains began to dissipate at t=16.9 s. The performance of the five encased drains acting as a block all together, along with the significant influence of the foundation over the soil, enabled a rapid dissipation below the foundation. At t=30 s, significant dissipation below the foundation was observed, while the soil near the outer drains started dissipation from bottom layers (Fig. 5.11b). The volume of low pressures around the internal and edge drains in SG4 were also dissipating from the top layer at this time (see Fig. 5.9a); however, this represented a delayed dissipation compared to SG5.

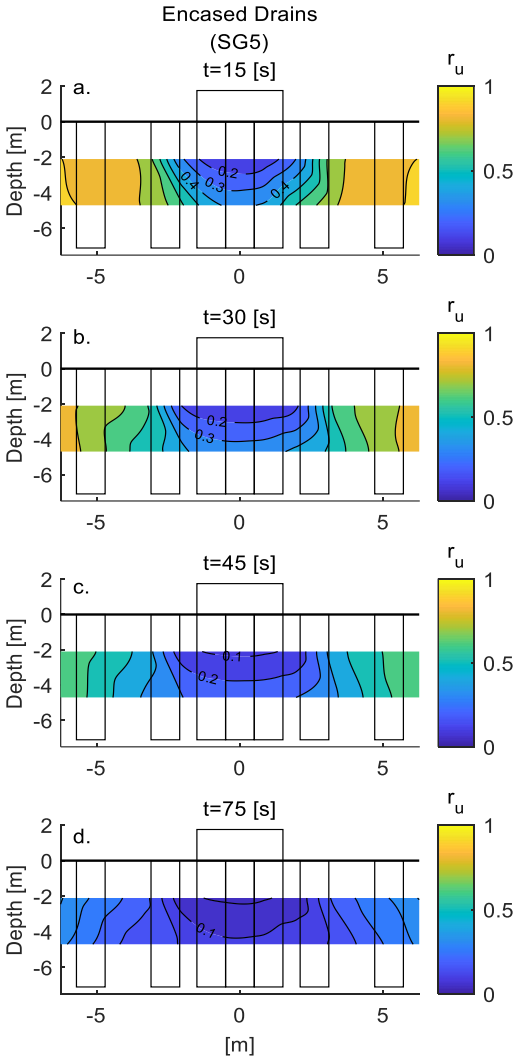

Fig. 5.11 Vertical contours of excess pore pressure ratios (r_u) for SG5

At t=45 s, the soil near the sub-perimeter and perimeter drains was dissipating at the top layer, showing r_u values of 0.45 and 0.65 (Fig. 5.11c). After thirty seconds, the soil below the foundation and between the edge and sub-perimeter drains in SG5 reached low excess pore pressure ratios, showing a negligible r_u value of 0.04 at the top layer near the encased internal drain (Fig. 5.11d). The volume of low pressures below the foundation quickly dissipated in the presence of the encased internal and edge drains in addition to the strong influence of the foundation. Larger r_u values near all drain rings at the top and middle layers were present at this time in SG4 (see Fig. 5.9a, Fig.5.9c) compared to SG5, indicating a weak performance of the drains without encasement below the foundation during the dissipation stage.

5.3.1.4 Soil Acceleration

Soil acceleration and input motions for SG5 and SG4 are observed in Figure 5.12, considering the soil near to the perimeter drains, the free field and close to the internal drain in the case of SG5. The free field showed a complete reduction of acceleration at the top and middle layer in SG5, after the first and third cycle of the shaking due to the complete liquefaction reached in the soil, similar to the free field behaviour in SG4.

In SG5, the soil softening generated near the perimeter drains at the top layer caused a significant reduction of the input motion, with an average value of 0.07g. At the middle layer, a greater acceleration response was observed, due to the lower soil softening reached at this level, presenting a maximum value of 0.17 g. Moreover, a great acceleration response was presented near the internal drain below the foundation in SG5 compared to the soil around the perimeter drains due to the lower soil softening presented at both depths.

The acceleration in the soil adjacent to the perimeter drains in SG5 was greater compared to SG4 as a response of the slightly lower soil softening presented. In addition, although acceleration in the soil near the internal drain is not presented for SG4 in Fig. 5.12, the minimum transference of the input motion to the foundation previously observed in Section 5.2 suggests limited soil acceleration below the foundation compared to SG5. The encased vertical drains prevented bulging at the top of the drains, maintaining the shear strength attributes of the column.

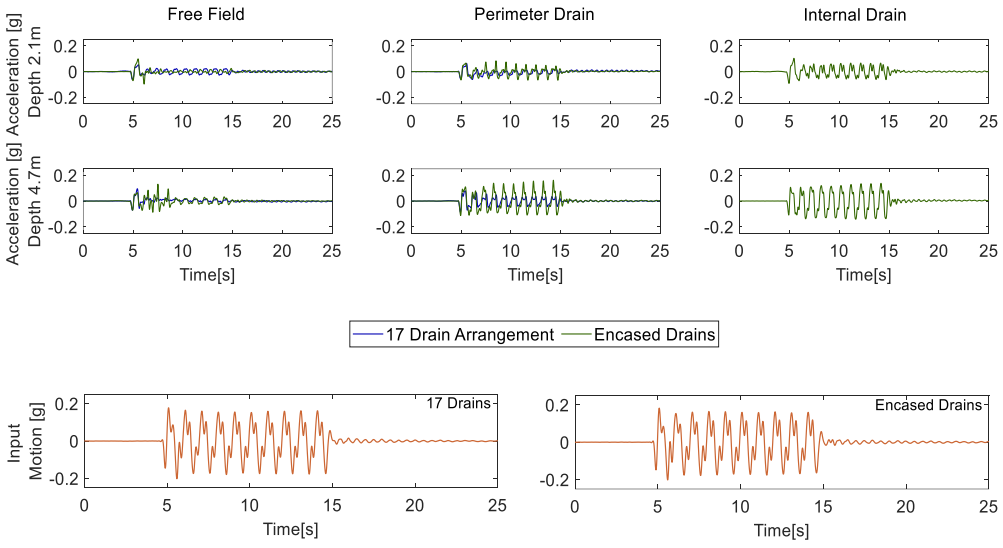

Fig. 5.12 Acceleration time-histories for the soil in SG4 and SG5

5.3.2 Foundation response

5.3.2.1 Foundation settlement

The settlement response of the foundation in SG4 and SG5 is presented in this section to evaluate the effectiveness of using encased drains below the structure. Figure 5.13 shows the foundation settlement for both cases, together with the input motions.

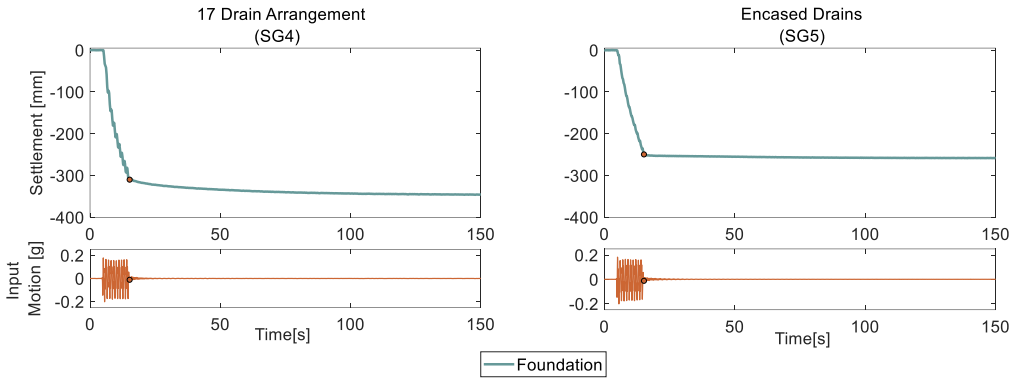

Fig. 5.13 Settlement time-histories of foundations for SG4 and SG5

The foundation in SG5 reached 96% of its total settlement during the generation stage, as a result of the soil softening generated below the foundation that allowed reconsolidation volumetric strains and deviatoric deformations. Although an increased soil softening below the foundation was presented compared to SG4, the foundation settlement response in SG5 exhibited a reduction of 20% during the shaking stage due to the use of encased vertical drains below the foundation. The complete reduction of the bulging effect in the drains, which occurred as a result of the significant lateral confinement provided by the aluminium encasement in the drains, improved the columns bearing capacity. In addition, although considerable soil softening was observed around the columns, the deformation in the soil was mainly controlled by the columns' stabilisation; similar behaviour was observed in Geng *et al.* (2017). During the dissipation stage, the foundation settlement in SG5 reached a small value of 10 mm; this is an improvement compared to the foundation in SG4, which settled 36 mm during this stage. The effective action of the encased drains in response to the bulging withdrawal in the columns, along with the conservation of the original properties in the drains, accelerated dissipation in the entire stratum, particularly below the foundation. Consequently, the rapid regaining of strength in the soil enabled limited deviatoric deformations and reconsolidation of volumetric strains during the dissipation stage.

5.3.2.2 Dynamic response of the foundation

Figure 5.14 presents the foundation horizontal acceleration for SG4 and SG5 together with the input motions. Significant transference of the input motion was observed in SG5, particularly at the start of the shaking, showing a uniform acceleration of 0.14g after the second cycle of the earthquake (Fig 5.14b). The encased vertical drains below the foundation prevented the loss of shear strength in the columns in the absence of bulging at the top, as the original characteristics of the granular material were conserved. Although less soil softening was observed below the foundation in SG4, the deficient performance of the drains with no encasement led to a minor transference of the input motion to the foundation. Positive results in terms of settlement reduction were obtained by using this alternative; however, the great transference of the input motion to the foundation placed over the encased drains represents a countereffect in terms of tilting and damage in the superstructure.

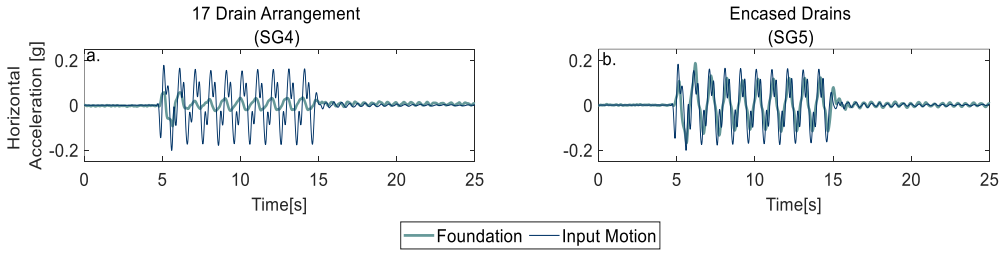

Fig. 5.14 Foundation horizontal acceleration for a) SG4 and b) SG5

Figure 5.15 shows the foundation rotation time-histories and the settlement vs rotational response for SG4 and SG5. The rotational response of the foundation over encased drains reached a peak value of 6×10^{-3} rad at the third cycle of the shaking, followed by a uniform rotation behaviour until the end of the shaking, as a response of the significant transference of the horizontal acceleration to the foundation (Fig. 5.15a). This value was two times greater compared to the peak rotation in SG4, in which the input motion transference was limited. The foundation rotational response in SG5 along the settlement of the foundation during the shaking was significant. A minimal rotation was observed during the dissipation stage, which ended at the same time as the foundation settlement. In addition, the foundation over the encased drains reached a negligible permanent rotation of 1×10^{-4} rad (Fig 5.15b).

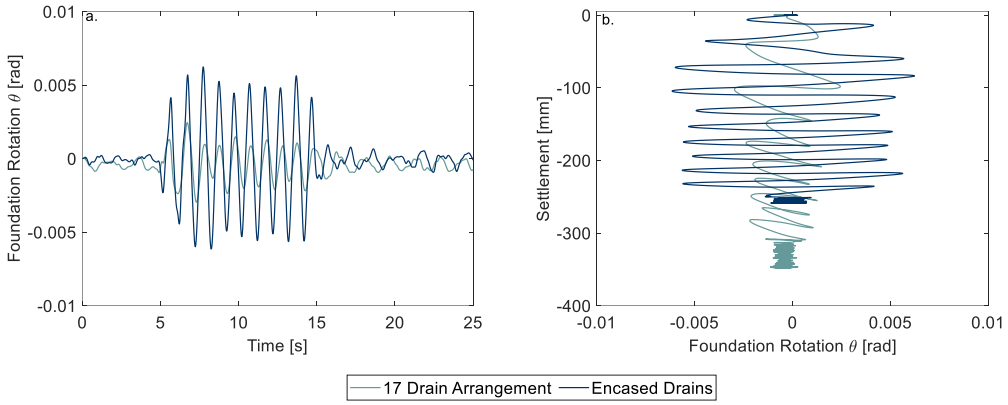

Fig. 5.15 a) Foundation rotational response and b) Foundation rotation vs settlement for SG4 and SG5

5.4 Rubble brick single column as a simplified alternative

The performance of a rubble brick column as a simplified option for mitigating damage below a new building is evaluated in this section. This represents the upper bound case in terms of treated area below the foundation. The effectiveness of this alternative is analysed in comparison with the 17-vertical drain configuration, which presents a great area of the foundation footprint covered by drains.

5.4.1 Soil Response

5.4.1.1 Excess pore pressure generation

Figure 5.16 presents the excess pore pressure ratios time-histories for SG9, considering the soil at 1.75 m and 5.25 m from the column central axis, along with the free field at different depths of the stratum.

At the top layer, the excess pore pressure in the soil at 1.75 m from the column reached a smaller peak value of 0.25 at the end of the earthquake, while a higher ratio (r_u=1) was presented in the soil at 5.2 m. The high bearing pressure and the proximity of the soil to the column allowed limited excess pore pressures generation in the soil at close distances. In addition, the free field presented a complete liquefaction behaviour during the initiation of the shaking due to the lack of influence of the column in this area (Fig. 5.16a).

At the middle layer, a larger degree of excess pore pressures was generated at 1.75 m from the column influenced by the lower confining stress at this level compared to the top layer and exhibiting a peak ratio of 0.4. The soil at a greater distance (5.2 m) presented a

complete liquefaction behaviour, similar to the free field. In addition to the negligible confining pressure, the gravel column was unable to control significant generation of excess pore pressures from a distance of 5.2 m (Fig. 5.16b). The precise extent of the column's influence at different locations in the soil, in terms of excess pore pressure control, becomes unclear as the foundation confining pressure also plays some role in the generation stage.

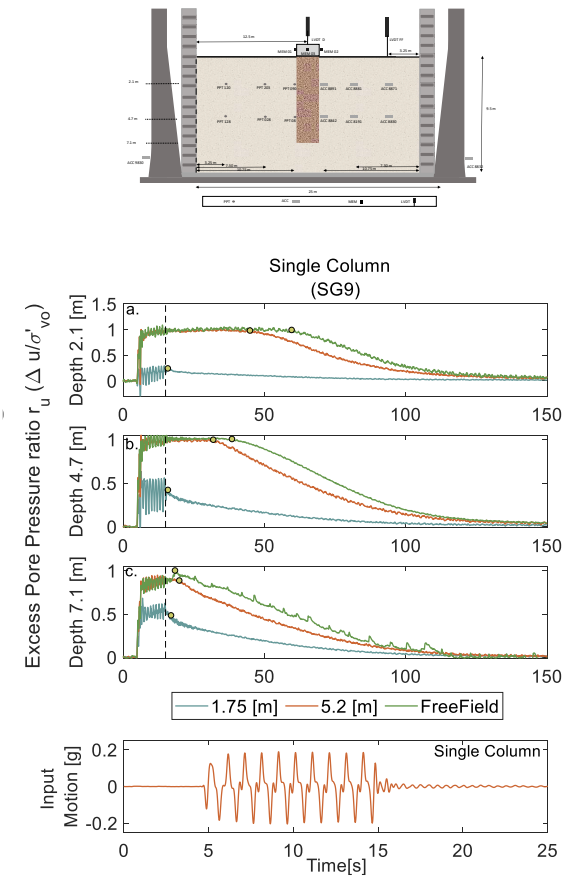

Fig. 5.16 Excess pore pressure ratios (r_u) time-histories for SG9

At a depth of 7.1 m, the soil near the column reached a peak value of 0.5 after the shaking. This was a greater ratio compared to the top and middle layer, as no significant additional confining pressure was exerted by the foundation at this level. On the other hand, the soil at 5.2 m did not present complete liquefaction at this depth; this was mainly due to the greater soil effective stress, as a negligible influence of the granular column in limiting excess pore pressure generation was observed at this distance (Fig 5.16c).

5.4.1.2 Spatial variation of excess pore pressures dissipation

Excess pore pressure dissipation in the soil containing a single column of rubble brick material below the foundation is analysed in this section. The contours of excess pore pressure ratios in the horizontal plane were plotted at a depth of 2.1 m. Square marks in the plots represent the soil location at 1.75 m and 5.2 m from the column central axis. Contours were plotted for different times, including the end of shaking, the initiation of dissipation for the soil at 1.75 m and 5.2 m from the column central axis, the start of dissipation in the free field and at t=75 s. Contours below the foundation do not necessarily represent the exact behaviour of excess pore pressures inside the column, as no instrumentation was placed in this location.

At the end of the shaking, the excess pore pressure ratio at 1.75 m from the column reached a low value of 0.25 due to its proximity to the foundation and the rubble brick column, enabling a great resistance to the generation of significant excess pore pressures and allowing effective control of high r_u values. The soil located at 5.2 from the column showed a great ratio of 0.98 at this time, while the free field presented complete liquefaction behaviour (Fig 5.17a). After the shaking, excess pore pressures continued to increase in the soil. At t=15.8 s, the flowfront arrived at 1.75 m, revealing a rapid dissipation of the fluid towards the column. This behaviour was greatly influenced by the soil's proximity to the rubble brick column and the high confining stress over this zone. The soil located at a longer distance from the column (5.2 m) and the free field maintained elevated r_u values of 1 at this time (Fig 5.17b).

After 20 seconds, the flowfront arrived at 5.2 m, while the soil between 1.75 m and 5.2 m presented a gradual dissipation showing a minor value of 0.1 near the column (Fig 5.17c). The time of flowfront arrival in the soil, when considering a single column with "infinite cell" behaviour, depends on its closeness to the column and the bearing pressure exerted by the foundation. The free field presented complete liquefaction and began to dissipate at t=59.6 s. At this time, reduction of excess pore pressures in the entire soil layer was observed, reaching values of 0.08 and 0.75 at 1.75 m and 5.2 m from the column central axis (Fig. 5.17d). Finally, significant dissipation in the entire layer including the free field, was presented at t=75 s, showing low ratios primarily near the column (Fig. 5.17e). Although the soil at 5.2 m reached high r_u values during the generation stage, the influence of the column during dissipation extended over a longer distance.

The performance of a single gravel column was evaluated by Badanagki *et al.* (2018) without considering a structure in the soil. The high-permeable column was unable to prevent liquefaction for a radial distance greater or equal to 2.5 m from the column central axis, due to the column's infinite spacing and the absence of bearing pressure. Nevertheless, the action of the column during the dissipation stage involved a radial distance longer than

2.5 m (i.e. between 2.5 m and 8.5 m), which can be explained by an increase of the dissipation rate after the end of the shaking; a similar trend has been observed in this research.

Although the infinite spacing of the rubble brick column represent a negative effect during the excess pore pressure generation, the influence of the foundation enhanced the behaviour of the soil and the single column as a larger radius of limited excess pore pressure ratios can be more easily controlled and dissipated. This could be translated into a reduction of the number of columns required to mitigate damage in a certain area prior to the construction of buildings.

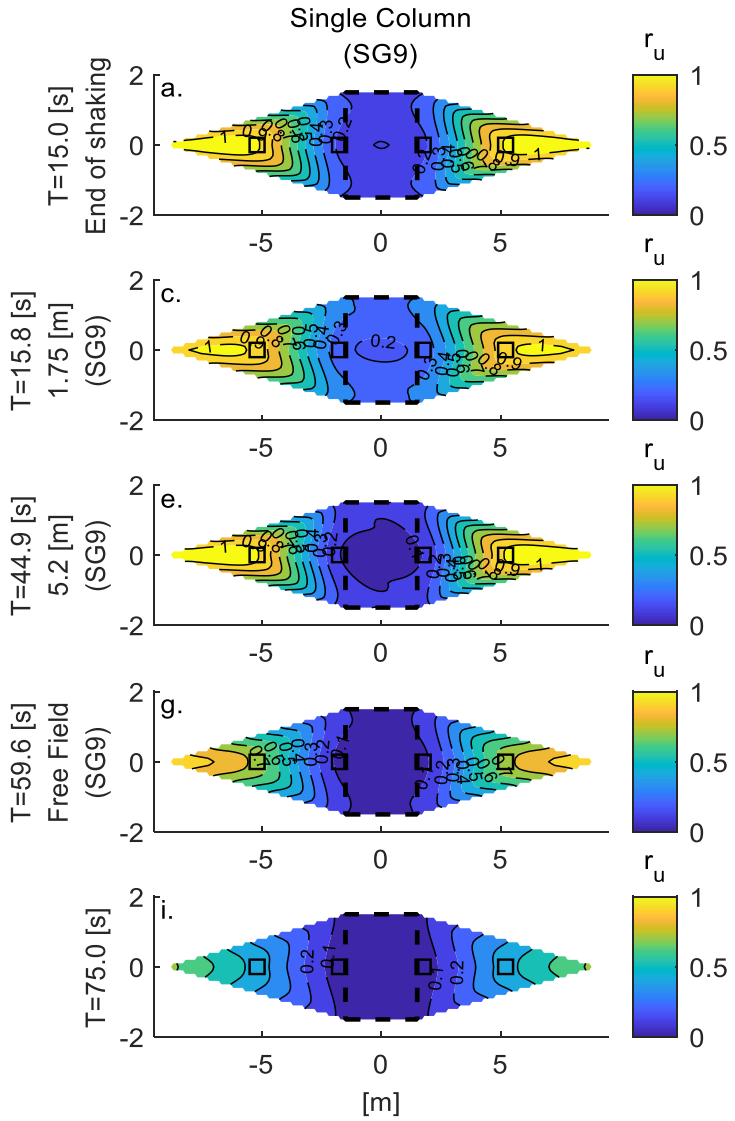

Fig. 5.17 Horizontal contours of excess pore pressure ratios (r_u) for SG9 at depth of 2.1 m

5.4.1.3 Vertical dissipation path

Vertical dissipation of excess pore pressure ratios in SG9 is presented in Figure 5.18. Contours in the vertical profile were plotted considering dissipation times of 15 s, 30 s, 45 s and 75 s. Moreover, Figure 5.19 presents contours of excess pore pressures to observe the fluid's behaviour in the soil containing a single column below the foundation of 150 kPa.

At the end of the shaking, the soil at 1.75 m from the rubble brick column presented small r_u values along the entire depth of the stratum compared to the soil at more distant locations, which presented ratios of 0.25 and 0.5 at the top and bottom layers. At this time, at a distance of 5.2 m, higher r_u ratios of 1 were observed at the top and middle layers, while a lower ratio of 0.9 was registered at the bottom of the stratum, similar to the free field behaviour (Fig. 5.18a). Limited amounts of fluid were observed in the soil surrounding the

column along the soil depth, reaching excess pore pressures of 10 kPa at the top layer. Similar excess pore pressures magnitudes were observed in the free field and at distance of 5.2 m from the column in response to the deficient performance of the column in controlling significant fluid flow at further distances (Fig 7.19a).

The soil at 1.75 m from the column started to dissipate immediately after the earthquake at the top and the lower depths, while complete liquefaction was still observed at 5.2 m from the column and in the free field. This was particularly true of the top layer, as dissipation starts from the bottom in the absence of additional confining stresses.

At t=30 s, dissipation continued in the soil surrounding the column, showing lower ratios compared to the soil at further distances (Fig. 5.18b). The foundation and the column allowed the generation of low excess pore pressures in the soil surrounding the column, which were later quickly dissipated due to the presence of the rubble brick pillar. The fluid flowed rapidly from the soil surrounding the foundation along the soil depth. On the other hand, excess pore pressures reached higher values of 16 kPa at 5.2 m from the column and in the free field at the top layer (Fig 5.19b).

At t=45 s, dissipation at 5.2 m was observed along the stratum depth, influenced by the column that enabled radial and vertical fluid flow in the soil. At this time, the area near the column, mainly at the top layer, showed a significant reduction of excess pore pressures, with a r_u value of 0.1. The free field still presented liquefaction at the top layer as fluid flowed in the vertical direction only (Fig. 5.18c).

Thirty seconds later (t=75 s), the total stratum, including the free field, showed dissipation, presenting small ratios of 0.09 and 0.2 at a distance of 1.75 m and 5.2 m from the column at the bottom layer (Fig. 5.18d). The fluid in the area surrounding the column flowed rapidly, while the free field presented a faster dissipation from bottom layers (Fig 5.19d).

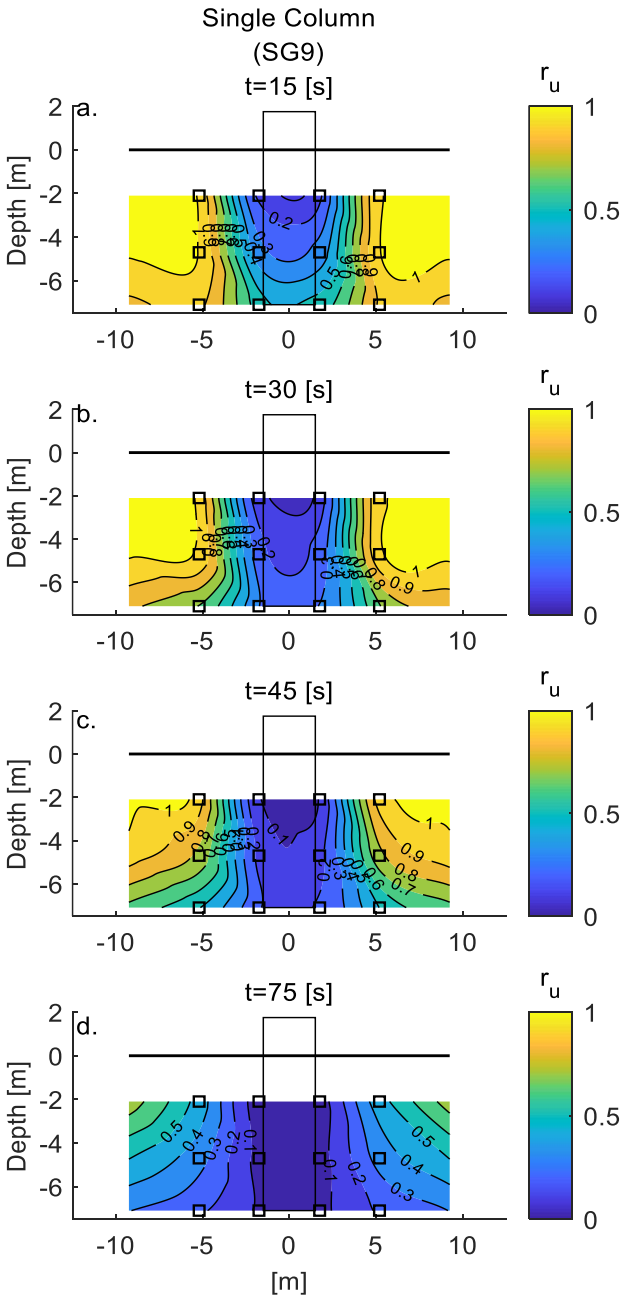

Fig. 5.18 Vertical contours of excess pore pressure ratios (r_u) for SG9

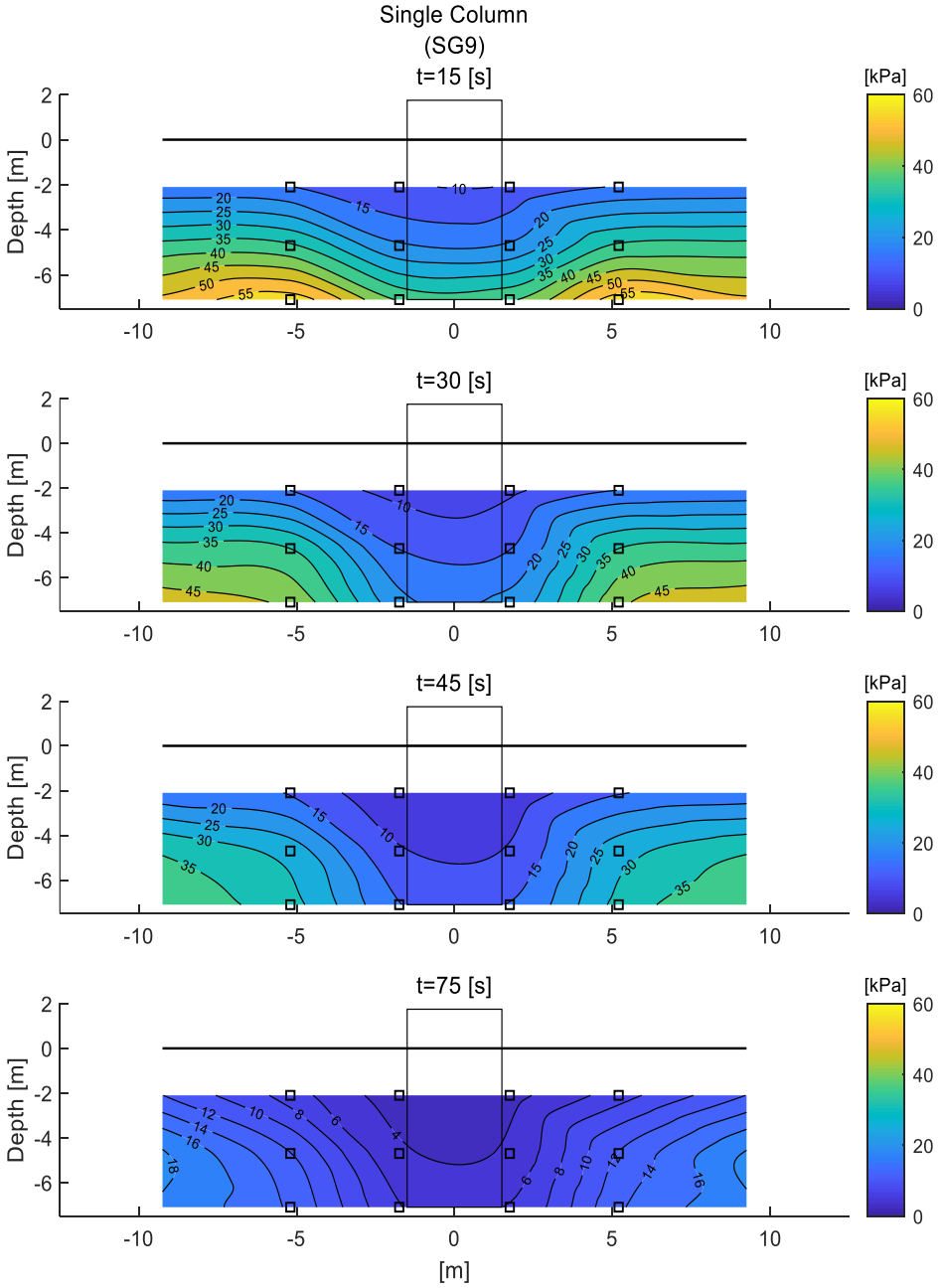

Fig. 5.19 Vertical contours of excess pore pressure for SG9

5.4.1.4 Comparison between the single column and a 17 vertical drain arrangement

A comparative analysis between this simplified alternative and the arrangement of 17 vertical drains below the foundation is performed in this section in order to evaluate the influence of mitigating the entire foundation footprint without considering additional external drains. The horizontal contours of excess pore pressure ratios were plotted for SG9

and SG4, considering the end of the shaking, flowfront arrival times near the drain rings in SG4, and t=75 s (Fig. 5.20).

At the end of the shaking, a greater excess pore pressure ratio was observed at 1.75 m from the column central axis in SG9 compared to the soil at the same location (near the edge drains) in SG4 (Fig 5.20a). The soil around the single column presented a greater ratio due to the infinite drain spacing in place, while the excess pore pressure generation in the soil between the edge and the sub-perimeter drains was effectively controlled by both drain rings in SG4,resulting in limited ratios. This verifies the weak performance of a single column during the generation stage compared to a configuration that includes a series of drain rings.

Dissipation started at 1.75 m from the column at t=15.9 s in SG9, reaching a peak value of 0.25, while excess pore pressure generation was observed in the entire layer of SG4, exhibiting a ratio of 0.15 close to the edge drains (see Fig 5.1b). At t=25.3 s, dissipation started near the edge drains in SG4 (Fig. 5.20c) after the flowfront arrived close to the internal drain. At this time, the soil close to the single column (1.75 m) had already begun to dissipate, reaching a ratio of 0.15, while higher values were observed at further distances (Fig 5.20d). The rubble brick column allowed a faster dissipation in the adjacent soil compared to the soil at same location in SG4; this was due to the significant influence of the column, which covered 100% of the foundation footprint.

At the time at which the flowfront arrived near the sub-perimeter drains in SG4 (t=35.8 s), the soil adjacent to the internal and edge drains presented moderate dissipation, while higher r_u values were observed near the perimeter drains (Fig 5.20e). On the other hand, at this time, the area around the single column presented a significant decrease in dissipation (Fig. 5.20f). The flowfront arrived close to the perimeter drains in SG4, starting dissipation at t=45.8s (Fig. 5.20g); meanwhile, a faster dissipation initiation was observed for the soil at the same location in SG9 (5.2 m). Finally, significant dissipation was observed in the entire layer of SG9 at t=75 s, showing a low ratio of 0.05 in the soil adjacent to the column (Fig 20j). The delay in the dissipation initiation near the drain rings in SG4 was concluded to be the result of the weak dissipation performance of the vertical drains below the foundation footprint.

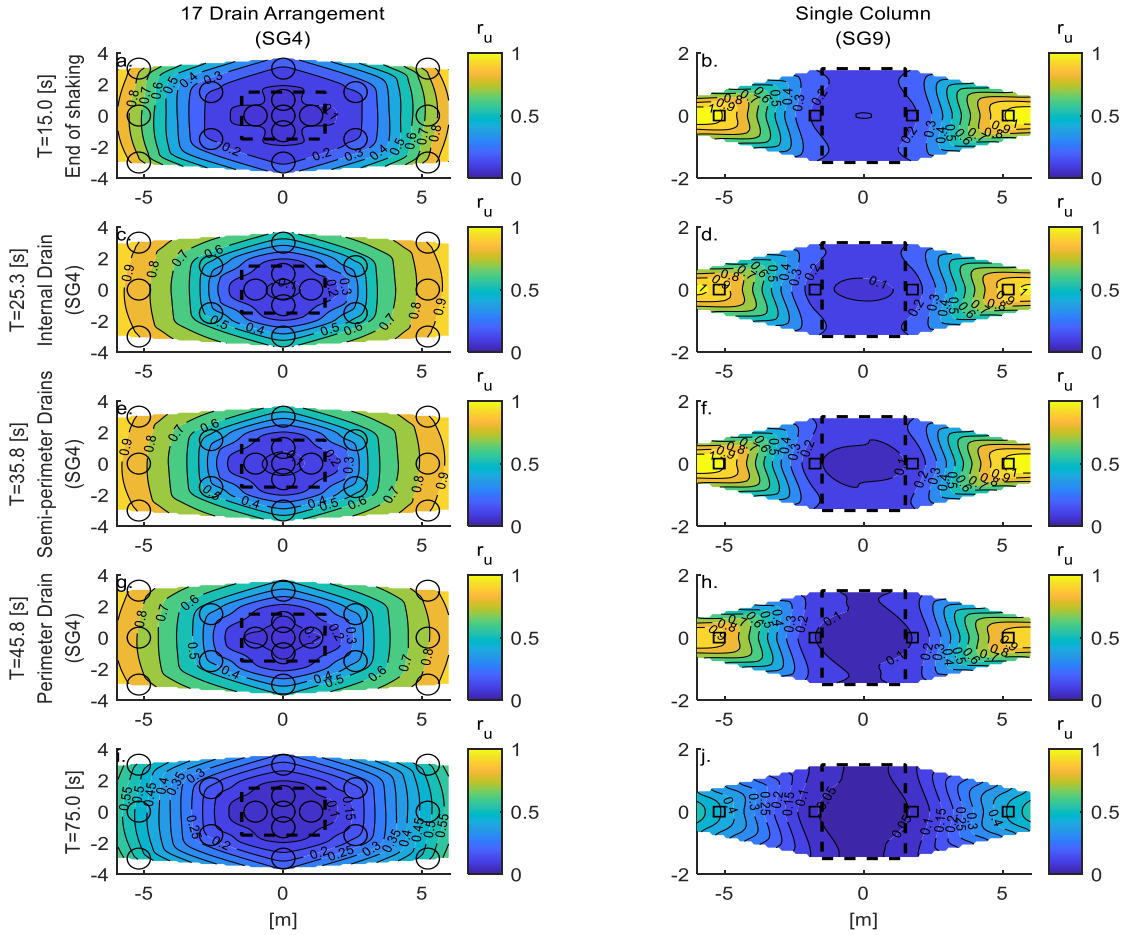

Fig. 5.20 Horizontal contours of excess pore pressure ratios (r_u) for SG4 and SG9 at depth of 2.1m

The single column mitigating the entire base of the foundation reached a significant radius of influence and allowed for more rapid dissipation in the soil compared to an arrangement of drains that covered 28% of the foundation footprint; this suggests the relevance of a significant mitigation below the foundation footprint. In addition, the presence of the outer drains was beneficial during the generation stage, as this allowed for better control of excess pore pressures in the soil surrounding the drainage column and the foundation; nevertheless, the effects of the external drain rings were impractical in terms of rapid dissipation when considering the complete mitigation of the foundation footprint.

5.4.1.5 Soil Acceleration

Figure 5.21 illustrates the soil acceleration at 1.75 m and 5.2 m from the gravel column central axis in SG9 and near the perimeter drains in SG4 at the top and middle layers of the stratum. Free field acceleration response is also presented for both cases.

Significant acceleration reduction was observed in the free field of SG9 at both depths of the stratum due to the complete liquefaction behaviour at both layers. Increased soil acceleration was presented at 1.75 m from the column, compared to the soil at 5.2 m in the top layer; this was due to the limited soil softening reached near the column. Similar behaviour (i.e. a greater acceleration response) at 1.75 m was present at the middle layer, reaching a uniform acceleration of 0.13g. The proximity of the soil to the column facilitated this greater acceleration response.

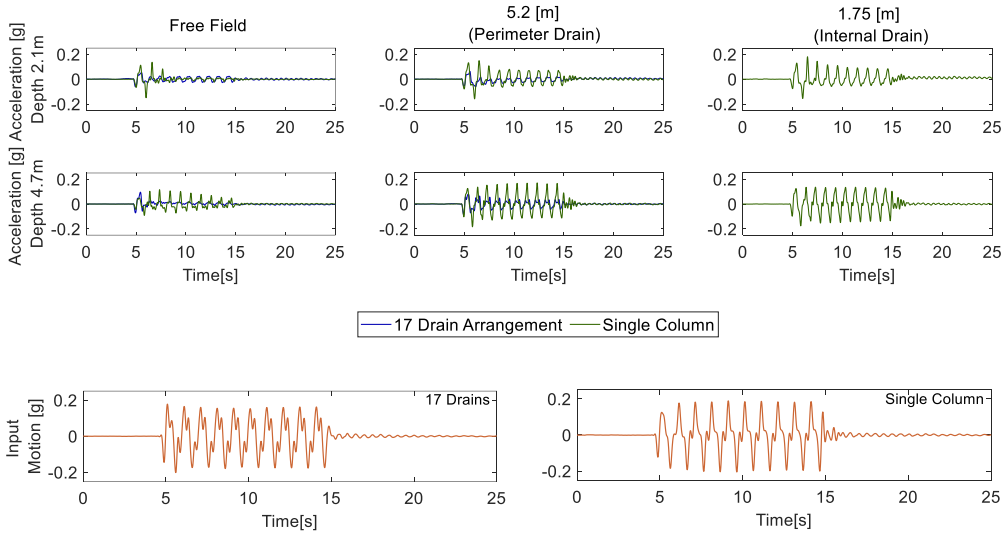

Fig. 5.21 Acceleration time-histories for the soil in SG4 and SG9

Table 5.2 presents the additional shear reinforcement provided by the single column and the vertical drains in the treated soil. Although complete softening was observed in the soil located 5.2 m from the column at both depths of the stratum, the acceleration response was not completely reduced at this location as it occurred in the free field, particularly at the middle layer. A great influence of the column in terms of shear reinforcement to a distance of at least 5.2 m was verified. The difference in the acceleration response between the top and middle layers near the column (1.75 m) could be explained by a loss of shear strength at the top of the column due to bulging. In addition, even though lower soil softening was reached close to the perimeter drains at the top and middle layers in SG4 when compared to the soil at the same location in SG9, greater acceleration reduction was observed in SG4 due to the lower shear reinforcement of 8.7% provided by the arrangement with A_r of 7.1%.

Table 5.2 Additional shear reinforcement in the soil layer for SG4 and SG9 (depth of 2.1m)

Depth (m)	SG4		SG9	
	Vertical Drains		Vertical Drains	
	A_r (%)	τ_{A_r} (%)	A_r (%)	τ_{A_r} (%)
2.1	7.1	8.7	7.5	9.2

A_r: Area replacement ratio

τ_{A_r}: Additional drains shear reinforcement

5.4.2 Foundation response

5.4.2.1 Foundation settlement

Next, the effectiveness of using a single column as a simplified alternative for liquefaction mitigation was evaluated in terms of settlement. Figure 5.22 shows the foundation and free field settlement for SG9 and SG4 together with the input motions for a comparative analysis.

The settlement of the foundation during the shaking in SG9 represents 96% of the total amount. The soil softening generated around the rubble brick column resulted in the generation of volumetric and deviatoric deformations in the soil and affected the stability of the column, particularly at the edges. This behaviour led to a loss of the foundation bearing capacity, enabling significant settlement during the shaking (Fig. 5.22b). The level of soil softening generated around the foundation in SG9 was twice the magnitude of that presented in SG4; therefore, a lower settlement was observed by using the 17-drain arrangement during the generation stage (Fig. 5.22a). A minimal percentage of 4% was obtained for the foundation over the single column after the shaking due to the effective dissipation in the adjacent soil that allowed a rapid recovery of stiffness and decreased reconsolidation volumetric deformations and deviatoric strains. On the other hand, a greater settlement was observed for the foundation in SG4 during this stage as a result of the slower dissipation managed by the edge and internal drain, meaning that high excess pore pressures were retained for a longer time.

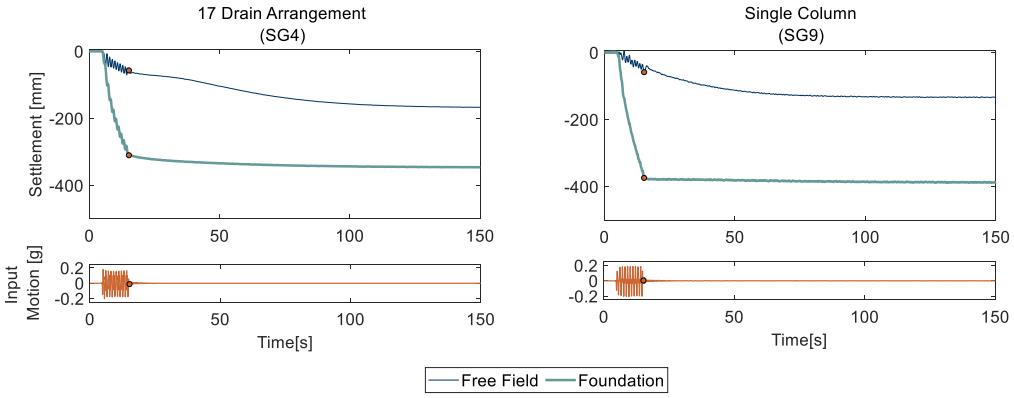

Fig. 5.22 Settlement time-histories of foundations for SG4 and SG9

Although significant settlement improvement was obtained during the dissipation stage through the use of the single column below the foundation, a greater permanent settlement was presented compared to the arrangement of 17-vertical drains. During the shaking, the external drain rings played a significant role in the soil surrounding the foundation; this indicates the relevance of proper mitigation not only in the soil below, but also outside the foundation, if an improved settlement response is to be obtained.

5.4.2.2 Dynamic response of the foundation

The significant soil acceleration near the rubble brick column previously observed as a response of great shear reinforcement, implies a significant transference of the input motion to the foundation and rotational response. Figure 5.23 presents the foundation horizontal acceleration for SG9 and SG4 along with the input motions. In SG9, the input acceleration was significantly transferred to the foundation in response to the great shear strength provided by the rubble brick column, reaching a mean value of 0.13g during the entire motion (Fig. 5.23b). On the other hand, although the internal and edge vertical drains enabled soil softening around the foundation in SG4, these drains were incapable of providing sufficient shear reinforcement in the soil, as verified by the small transference of the input motion to the foundation (Fig. 5.23a). Even though drainage enhancement was provided by using this simplified alternative, a negative effect was presented in terms of the great seismic demand on the foundation, which increased the risk of damage to the structure.

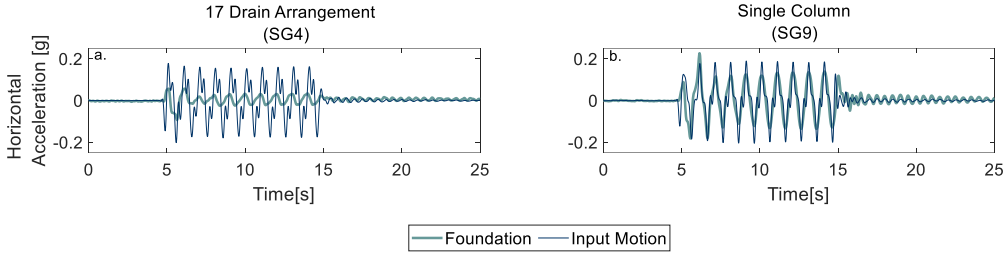

Fig. 5.23 Foundation horizontal acceleration for a) SG4 and b) SG9

The analysis of the foundation rotational response in SG9 required evaluation in response of the significant acceleration transference to the foundation. Figure 5.24a shows the rotation time histories for the foundation in SG9 and SG4. Significant horizontal acceleration in the foundation resulted in a larger rotation in SG9, reaching a peak value of 9×10^{-3} rad at the eighth cycle of the shaking. This value was higher compared to the foundation rotational response in SG4, which showed a peak magnitude of 3×10^{-3} rad during the initiation of the shaking. Figure 5.24b presents the settlement vs rotation response for the foundation in both arrangements. The foundation in SG9 exhibited a great rotation during the shaking before reaching a settlement of 380 mm; subsequently, lower rotation was observed. This foundation reached a permanent negligible rotation of 4×10^{-4} rad. On the other hand, the lower transference of the input motion to the foundation in SG4, led to a smaller rotational response of the foundation that stopped at the same time as the settlement, reaching a similar negligible permanent rotation to the value obtained in SG9. In addition to the larger settlement, the significant dynamic response of the foundation obtained using the single column implies that the 17-vertical drain arrangement continues to be more effective in terms of structural damage reduction.

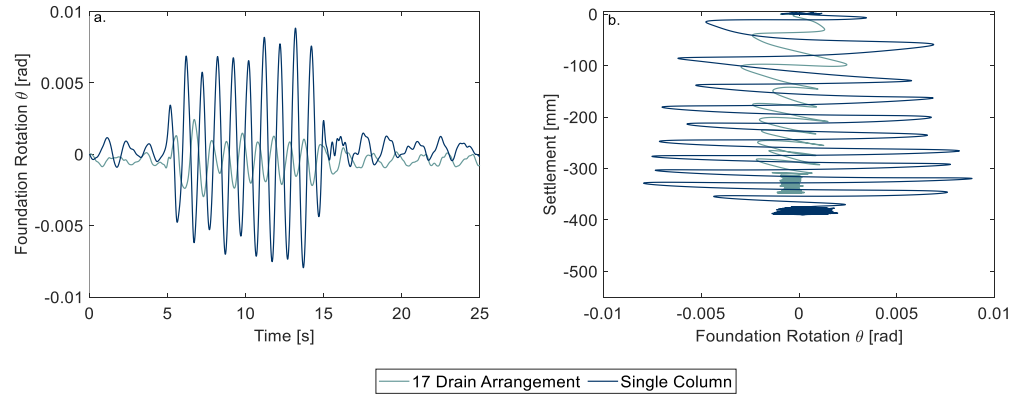

Fig. 5.24 a) Foundation rotational response and b) Foundation rotation vs settlement for SG4 and SG9

5.5 Conclusions

In this chapter, different rubble brick drain arrangements that consider significant mitigation in the soil below the foundation have been evaluated to assess their suitability as liquefaction countermeasure techniques for new buildings.

The addition of edge drains under the foundation as a variation of the 13-vertical drain configuration was evaluated in the first section. These additional drains allowed for the effective control of high excess pore pressures below the foundation of 150 kPa, verifying their superior performance in the soil in the presence of a greater area replacement ratio (Ar%). In addition, significant drainage enhancement and rapid dissipation of excess pore pressures under the foundation was accomplished by the internal and edge drains. Although the additional drain ring yielded positive results in terms of the limited generation of excess pore pressures and the fast fluid dissipation, primarily below the foundation, a counter-effect arising from the use of this alternative also presented during dissipation. The delay of the flowfront arrivals in the outer drain rings resulted in the deficient performance of the external drains.

The effectiveness of the 17-drain arrangement containing edge drains below the foundation was verified in terms of settlement reduction. The limited soil softening and the fast dissipation of excess pore pressures below the foundation led to a reduction of volumetric and deviatoric deformations and enabled a faster regaining of stiffness in the soil below the foundation. In both arrangements, insufficient shear reinforcement was provided by the rubble brick columns; however, slightly greater acceleration response and rotational stiffness were observed in the foundation placed over the internal and edge drains. Moreover, adding a ring of drains below the foundation resulted in a reduction of only 25% of the structural settlement, this limited reduction can be explained by the bulging effect generated at the top of the drains located under the foundation, which caused a reduction of the drain's carrying capacity.

The performance of the aluminium encased drains below the foundation was evaluated in section 5.2 to determine whether this technique could reduce the foundation settlement response. The encased drains achieved further improvement in the soil after the shaking. During the generation stage, the aluminium encasement in the drains impeded the proper control of high excess pore pressures; nevertheless, the complete reduction of the bulging in the columns resulted in an enhanced performance of the drains during dissipation, as the drain's permeability had been conserved. Moreover, the drains' stability allowed the internal and edge drains to act as a block, accelerating the dissipation in the complete stratum. The effectiveness of the 17-drain arrangement considering encased vertical drains below the foundation was validated achieving a settlement reduction of 25% compared to the

configuration with no encased drains. This improvement in the foundation settlement response was principally managed by the prevention of bulging in the drains, resulting in the initial bearing capacity of the drains being maintained during and after the shaking. Although an enhanced response concerning the foundation settlement was obtained, counter-effects for the foundation also emerged in terms of seismic demand due to the significant shear strength capacity of the columns in response to the bulging reduction.

A single column of rubble brick material covering the entire base area of the foundation was evaluated in the last section as a simplified alternative to mitigate liquefaction damage. The generation and dissipation of excess pore pressures in the soil surrounding the rubble brick column were influenced by the proximity to the gravel column and the foundation bearing pressure over the soil. In addition, even though a deficient performance of the single column was observed due to the infinite drain spacing during generation, the foundation exerted a positive influence in the soil and the single column in terms of the generation and dissipation of excess pore pressures. The performance of this alternative was compared with the 17-drain configuration during the generation and dissipation stages. The edge and sub-perimeter drains below the foundation in the 17-drain arrangement, achieved improved performance in controlling high excess pore pressures in the area between both drain rings compared to the influence of the single column at the same location. After the shaking, a faster dissipation under the foundation facilitated by the single rubble brick column was observed compared to the other configuration that presented 45% of the foundation footprint covered by vertical drains. Although the presence of the sub-perimeter and perimeter drains were relevant in the arrangement of drains during the shaking, they were useless during the dissipation stage in the presence of a single column mitigating the entire foundation footprint.

Although effective performance was observed during the dissipation stage when a single column below the foundation footprint was used, great settlement response compared to the 17-drain arrangement was obtained. The role of the external drain rings during the generation stage became relevant in limiting soil softening around the foundation and preventing the loss of stability in the drains that enabled settlement of the foundation. Therefore, the use of drains outside the foundation in order to reduce the “infinite cell” behaviour of the column should be considered. In addition to the large settlement, a significant acceleration and rotational response was observed for the foundation due to the large shear reinforcement provided by the rubble brick column. Although it could be logical to assume a significant settlement reduction by using this alternative, as the entire foundation footprint is mitigated, it also presents adverse effects in terms of settlement and rotation compared to a conventional arrangement of 17 vertical drains.

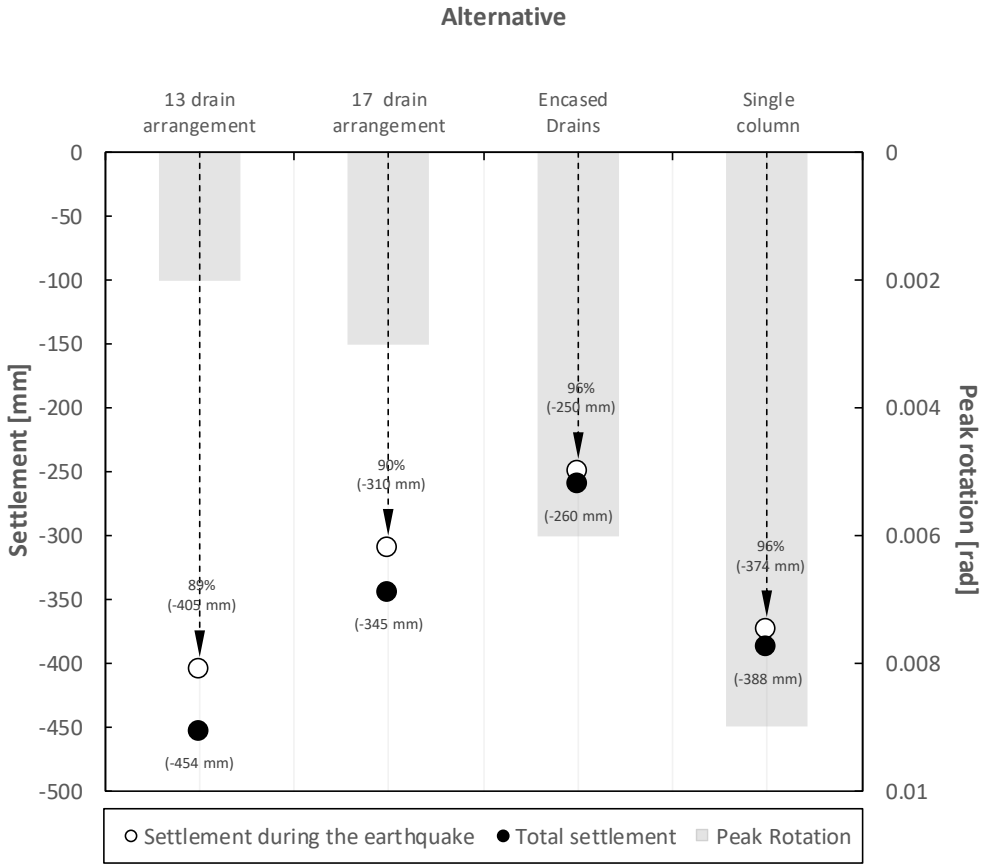

Fig. 5.25 Settlement and rotational response of the foundation per alternative

Finally, a chart comparing the different alternatives of drain arrangement evaluated in this chapter, subjected to an input motion of approximately 0.19g, was elaborated in terms of settlement and rotational response of the foundation (see figure 5.25). The significant difference between the settlement obtained during and after the shaking indicates the relevance of an optimum configuration design based on the drains' effective performance during an earthquake. The 17-vertical drain arrangement with encased drains below the foundation becomes the best alternative in terms of settlement, although high rotational response of the foundation is expected. The arrangement of 13 vertical drains and the single column represent the weakest alternatives. The latter presented a slightly lower settlement response particularly during the dissipation stage; nevertheless, this is clearly the most unfavourable option, as significant rotational response is likely to occur, thereby increasing the risk of damage in the superstructure. Although a selection of the most adequate alternatives can be arrived at using only these two parameters, further studies such as a cost-benefit analysis are desirable in order to involve stakeholders in the development of a mitigation program. This analysis should include the response of the building above the foundation through a soil-structure interaction evaluation that could led to a better definition of different damage state.

Chapter 6

Existing Buildings: Performance of inclined perimeter drains as liquefaction mitigation technique

6.1 Introduction

The use of conventional arrangements of vertical drains, mostly designed as a countermeasure technique in free field, is not practical for the case of already existing buildings. Installation of drains in such cases frequently implies extensive structural modifications or even the demolition of existing constructions. In order to avoid invasive structural interventions, techniques such as chemical grouting have been proposed recently, although this measure could represent an added cost (Rasouli *et al.*, 2018).

The performance of vertical perimeter drains as an alternative to the regular arrangement has been evaluated in recent years in order to reduce damage to existing buildings. Vertical perimeter drains have the principal objective of accelerating dissipation of high excess pore pressures generated during liquefaction events in the soil around a building. The effectiveness of this technique has been verified by performing shaking table and dynamic centrifuge tests, which revealed satisfactory results in terms of reduced settlement and tilt of structures, however at the cost of increased seismic demand due to the amplification of acceleration (Rasouli *et al.*, 2016; Olarte *et al.*, 2017; Paramasivam *et al.*, 2018). Furthermore, the advantages of this arrangement involve the factors such as low-cost and easy installation in the field.

The installation of vertical drains around existing buildings is a convenient solution against structural damage caused by liquefaction phenomenon. Nevertheless, the drain's radial proximity to the area below the foundation is not attained, increasing the risk of further damage to the structure. This is particularly true for buildings with large plan area. For this reason, the use of inclined perimeter drains becomes a suitable option as a variation of the conventional vertical perimeter arrangement and could be suitably installed in the field due to the developments in current geotechnical construction procedures, such as directional drilling.

In previous chapters, the effectiveness of various vertical drain arrangements using two different types of coarse material for drainage enhancement in soil under new constructions has been evaluated. This chapter focuses on the evaluation of the performance of an inclined perimeter drain arrangement as a variation of the traditional vertical arrangement installed around buildings for damage mitigation against liquefaction. The evaluation focuses on excess pore pressure redistribution in the presence of inclined drains, influenced by the increase of vertical stresses in the soil along their depth. The dynamic and settlement responses of foundations are also evaluated. Parts of these results have been presented in García-Torres and Madabhushi (2020).

6.2 Inclined drain arrangement effectiveness

In this section, a detailed comparison between inclined (SG6) and vertical (SG8) perimeter drain arrangements is presented in order to evaluate the effectiveness of inclined perimeter drains below a foundation of 150 kPa.

6.2.1 Soil Response

6.2.1.1 Excess Pore Pressure Generation

Excess pore pressure ratios (r_u) time-histories for EQ2 are presented in figure 6.1 for SG6 and SG8, considering soil under the foundation central axis, close to the perimeter drains and free field at four different depths of the stratum.

Free field excess pore pressure ratios reached complete liquefaction (r_u=1) along the entire stratum depth in SG6 and SG8, suggesting significant softening in the soil due to the lack of any increase in drainage and significant fluid flow from the bottom layers during the first few seconds of the earthquake.

In SG6, the excess pore pressure ratio was higher in the soil close to the perimeter drain compared to the area under the foundation at the top layer, showing a value of 0.5 (Fig.

6.1a). The same trend of larger r_u close to the perimeter drains was observed in SG8. A peak r_u of 0.8 was reached close to the vertical drains, four times larger than the r_u observed for the inclined drains (Fig. 6.1b). During the generation stage, the high confining stress exerted by the foundation over the soil enclosed by the inclined drains generated further resistance to the generation of high excess pore pressures in this zone.

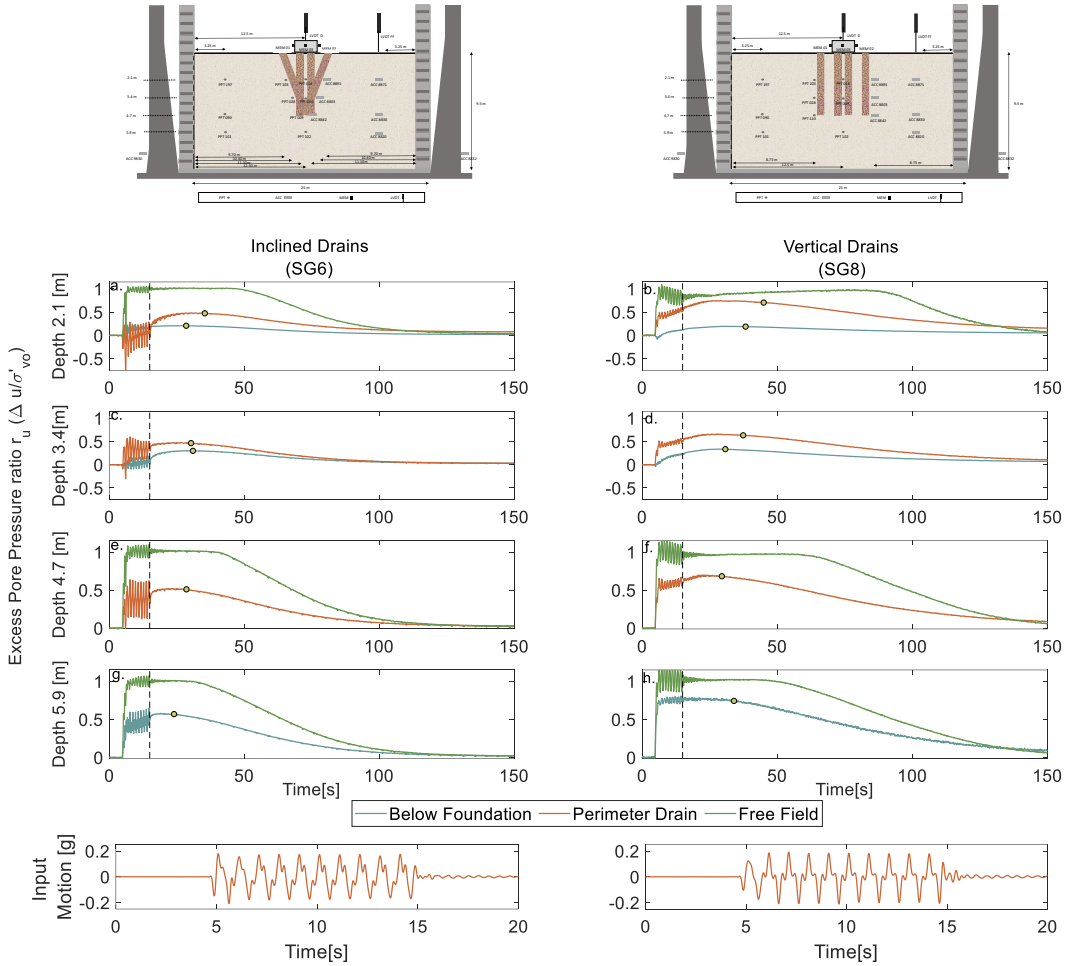

Fig. 6.1 Excess pore pressure ratios (r_u) time-histories for the soil under the foundation central axis, close to the perimeter drains and free field in SG6 and SG8

At a depth of 3.4 m, generation of excess pore pressures in SG6 for soil close to the inclined perimeter drains and under the foundation reached r_u values of 0.5 and 0.3 (Fig. 6.1c). The smaller confinement stress present at this depth due to the stress distribution compared to the top layer allowed a greater generation of excess pore pressures below the foundation central axis, while the perimeter drain presented a reduction of r_u due to the nearness of the drains to the foundation central axis in SG6, limiting high excess pore pressure ratios. Moreover, a lower r_u value was reached below the foundation in SG6

compared to SG8, suggesting the better control of excess pore pressure generation in presence of inclined drains due to their significant proximity to the foundation at this depth (Fig. 6.1d).

Inclined drains show a lower value of r_u at a depth of 4.7 m (base of drain) compared to the vertical ring, due to the influence of the drain's overlapped zone under large confining pressure (Fig. 6.1e). Moreover, effective control of excess pore pressure generation in SG6 at a depth of 5.9 m was observed, while in SG8 the independent behaviour of the vertical drains allowed a peak r_u of 0.8 (Fig. 6.1h). The excess pore pressure ratio increased below the foundation and reduced close to the perimeter drains at greater depths during the generation stage, especially in the case of inclined drains, as they are subjected to high foundation confining stress along their depth.

The effective role of vertical perimeter drains in controlling large excess pore pressures under structures due to their proximity to the foundation was previously observed by Olarte *et al.* (2017) for a bearing pressure of 80 kPa. Lower excess pore pressures were generated in the area enclosed by the vertical drains below the foundation compared to the magnitude generated under a similar foundation in unmitigated soil. This behaviour was attributed to the efficient performance of the vertical drains in limiting high excess pore pressure below the structure as they were located near to the foundation's edge in addition to the large confining stress exerted by the structure. Based on this, an improved performance should be expected in the case of inclined drains during the generation stage, due to the drain's greater proximity to the foundation along the soil depth, allowing lower excess pore pressure ratios below the foundation compared to the vertical drains case. In addition to the influence of the confining pressure exerted by the soil, the excess pore pressure generation is controlled by the drains, which are higher effective in case of inclined drains arrangements.

6.2.1.2 Dissipation of excess pore pressures: Influence of the radial proximity of the drain to the foundation

In this section, the performance of inclined and vertical perimeter drains during the post-seismic dissipation stage is presented considering the radial proximity from the drain's centres to the foundations. Flowfront arrival times close to the perimeter drains were analysed as a relevant parameter for the effectiveness of the arrangement. Contours were plotted using the geometrical symmetry provided by the arrangement, previously explained in section 3.1. Horizontal contours at different times including the end of the shaking, flowfront arrival times for inclined and vertical perimeter drains, and the start time of free field dissipation in SG8 are presented in figures 6.2 and 6.3.

Figure 6.2 shows contours of excess pore pressure ratios at a depth of 2.1 m for SG6 and SG8. The radial distance between the inclined perimeter drain centre and the foundation

central axis is 1.9 m at this depth, while a constant value of 3.1 m is presented along the vertical perimeter drains depth (see figure 3.5).

At the end of the shaking, (t=15 s) a uniform generation of excess pore pressures was observed at the central area below the foundation and outside the inclined perimeter drains, showing r_u values of 0.2 (Fig. 6.2a). In the case of the vertical drains, higher excess pore pressure ratios were reached under the foundation and close to the drains compared to SG6, suggesting insufficient control of high excess pore pressures in this area (Fig. 6.2b).

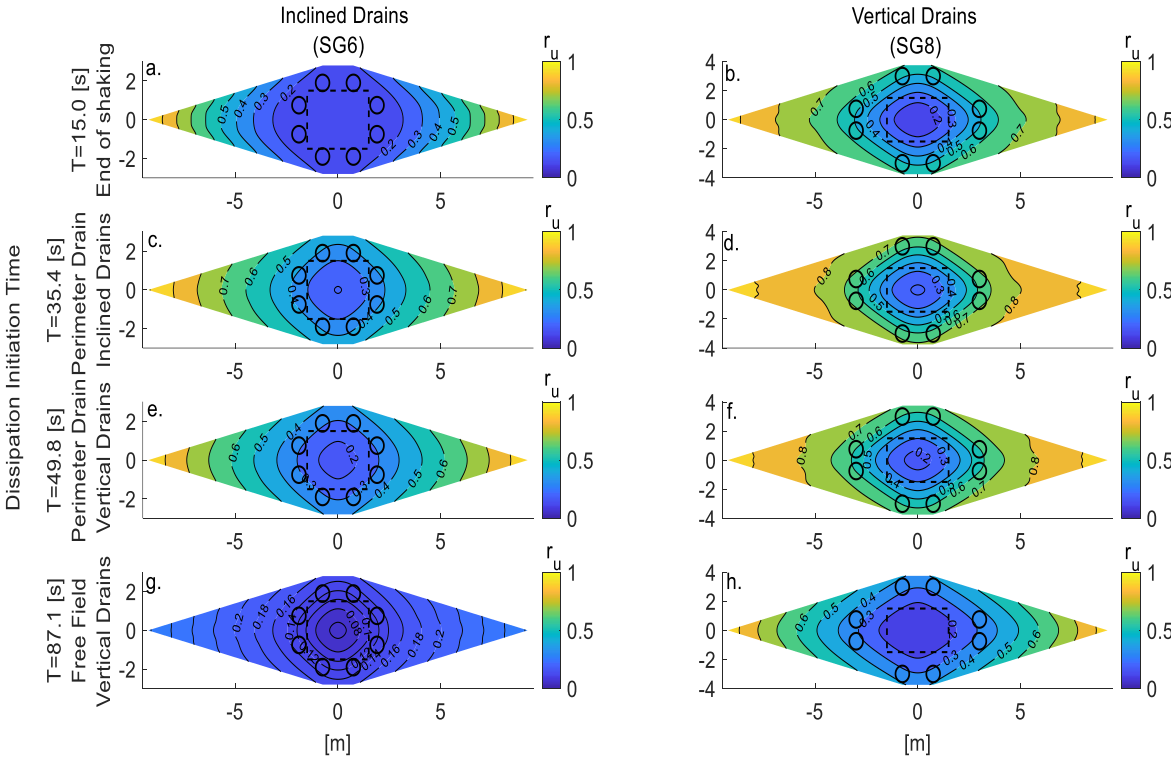

Fig. 6.2 Horizontal contours of excess pore pressure ratios (r_u) for SG6 and SG8 at depth of 2.1m

The flowfront arrived at the soil close to the inclined perimeter drains at t=35.4 s (Fig. 6.2c). The soil under the foundation started to dissipate six seconds before this, generating radial fluid flow from the central area towards the drains and increasing the excess pore pressure to r_u=0.4 outside the inclined drains. However, the generation of excess pore pressure continued in SG8 and show higher r_u values when compared to SG6, particularly close to the drains (Fig. 6.2d). The inclined drain's radial proximity to the foundation and the greater influence of the foundation around the drains allow a rapid dissipation of the central area when compared to the vertical perimeter drains.

At t=49.8 s, the flowfront arrived at the soil close to the vertical perimeter drains (Fig. 6.2e). At this time, a decrease in excess pore pressure ratios in the soil under the entire

foundation footprint and close to the inclined perimeter drains was observed. In SG8, the soil under the foundation show lower values in the central zone and higher values at the edges due to the faster dissipation below the foundation at t=38.3s (Fig. 6.2f). Complete dissipation was observed below the foundation at t=87.1 s, showing small r_u values close to the inclined drains (Fig. 6.2g). In SG8, the free field started to dissipate in the presence of the vertical drains at this time, showing r_u values of 0.2 under the foundation and of 0.4 around the vertical drains (Fig. 6.2h).

The reduction of the radial distance of 40% allows a reduction of 30% on the initiation of dissipation times for the soil below the foundation and close to the perimeter drains, which represents a relevant improvement to the drainage performance.

The radial distance from the inclined drains to the foundation central axis is 1.2 m at a depth of 3.4 m. Flowfront arrival times for the perimeter drains at this depth are shown in figure 6.3. A difference of 0.15 between excess pore pressure ratios close to the drains and under the foundation was observed in SG6 at t=15 s (Fig. 6.3a). On the other hand, excess pore pressure ratios reached higher values close to the drains and under the foundation in SG8 (Fig. 6.3b). Although the foundation applied the same bearing pressure under the foundation central axis in both cases, vertical drains could not restrict the generation of high r_u values in this zone due to the further distance.

Flowfront arrived at t=30.3 s close to the inclined perimeter drains. At this time, r_u of 0.3 was reached under the foundation while an increment of 0.06 was observed at the perimeter drains (Fig. 6.3c). Both zones started dissipation at very close times (see Fig 6.1) as drains were located under the foundation's edges at this depth. In SG8, r_u of 0.35 under the foundation and 0.6 close to the perimeter drains were observed as flow continued to raise radially and upwards from bottom layers (Fig. 6.3d). Lower foundation confining stress was applied over the soil at this depth when compared to the top layer, however the radial proximity from the inclined drains allowed a larger influence of the foundation and the faster flowfront arrival close to the inclined drains when compared to the top layer. At 37.2 s, the flowfront close to the vertical drains arrived, reaching r_u of 0.6 and 0.35 close to the drains and below the foundation (Fig. 6.3f). In SG6 the entire zone under the foundation showed a rapid dissipation at this time, with the inclined perimeter drains receiving fluid from the free field.

The excess pore pressures behaviour in presence of vertical perimeter drains was analysed considering a structure of 80 kPa (Olarte *et al.*, 2017; Paramasivam *et al.*, 2018). A faster dissipation below the foundation was observed compared to a similar structure over unimproved soil, due to the closeness of vertical drains to the foundation. The fluid flow easily from the area below the structure towards the drains, verifying the efficacy of placing them near the foundation. In the case of inclined drains arrangement, the radial proximity

and the larger influence of the bearing pressure over the arrangement, led to a more rapidly dissipation of excess pore pressures below the foundation and close to the drains compared to the vertical arrangement case.

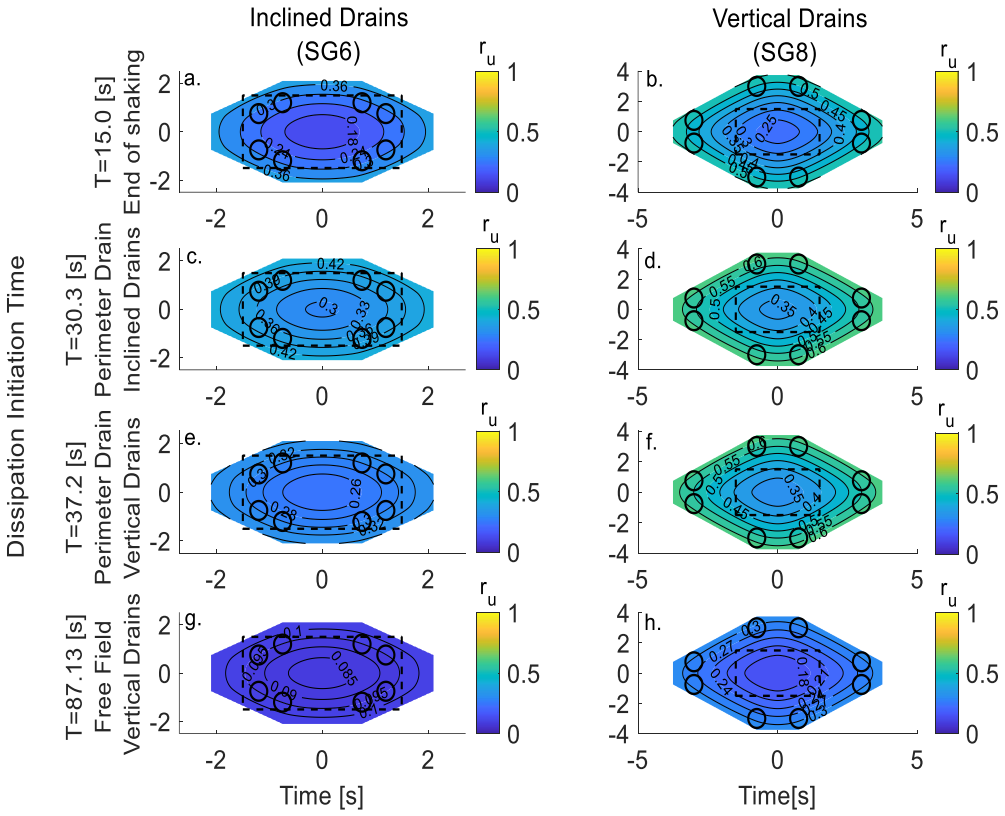

Fig. 6.3 Horizontal contours of excess pore pressure ratios (r_u) for SG6 and SG8 at depth of 3.4m

6.2.1.3 Vertical dissipation path in the presence of drains

Vertical contours at regular time intervals provide a clear visualisation of the drain's behaviour along the depth of the stratum considering the fluid flow course during the dissipation of excess pore pressures. Figure 6.4 shows vertical contours of excess pore pressure ratios at different dissipation times for SG6 and SG8.

At the end of the shaking (t=15 s), the zone enclosed by the inclined drains in SG6 shows an effective control of excess pore pressure generation under the foundation at the top layers, while higher r_u values outside the perimeter drains were observed as a result of the radial and upward fluid flow from the bottom layers and free field towards the perimeter drains. At this time, the free field presented complete liquefaction (r_u=1) due to the wide distance from the inclined drains and the lack of extra confining stress in the soil (Fig. 6.4a). In SG8,

excess pore pressure ratios (r_u) of 0.7 close to the vertical drains and of 0.2 below the foundation were observed (Fig. 6.4b).

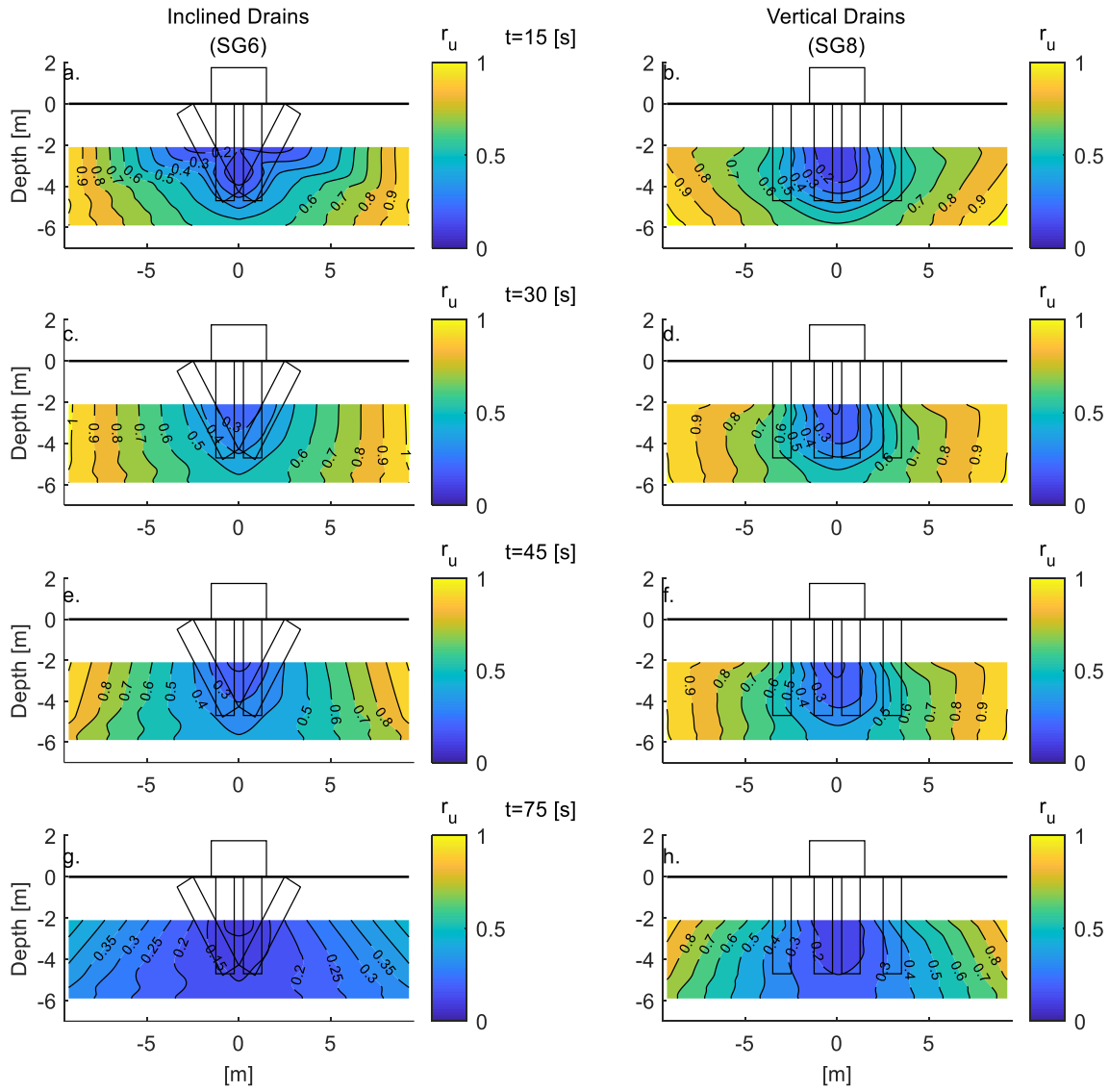

Fig. 6.4 Vertical contours of excess pore pressure ratios (r_u) for SG6 and SG8

Between the end of the shaking and time t=30 s, a bulb of low pressures that reached the bottom layer was generated in the soil enclosed by the inclined drains suggesting the relevance of the radial proximity from the drains to the foundation during the generation stage (Fig. 6.4c). At this time, excess pore pressures continued to increase in SG8, showing an elevated r_u of 0.7 close to the vertical drains.

At t=45 s, excess pore pressure in the soil under the foundation and close to the inclined drains was already dissipating from the top layer (Fig. 6.4e). The bulb of low r_u values

enclosed by the inclined drains was the first to start dissipation at t= 28.5 s, followed by the inclined perimeter drains at t=35.4 s. Inclined drains were able to create a shielded zone of low pressure that was rapidly dissipated by the inclined drains in the presence of high bearing pressure. In SG8, the area under the foundation started to dissipate ten seconds later, due to the infinite cell behaviour of the vertical drains with minimal influence of the foundation, resulting in a greater time for the dissipation initiation.

Thirty seconds later (t=75 s), a significant reduction in the r_u below the foundation in SG6 and close to the perimeter drains was observed as a result of the fast dissipation in the presence of the inclined drains (Fig. 6.4g). Lower r_u values at the bottom layers below the central axis were presented in contrast to the slower dissipation produced at the top layers, especially at the free field due to the upward flow still dissipating. In SG8, the r_u reached a value of 0.2 under the foundation while excess pore pressures in the free field did not start to dissipate at this point (Fig. 6.4h).Within a period of 60 seconds, significant dissipation occurred in the bulb zone and soil surrounding the inclined drains, while a longer time was required for the soil around vertical drains to reach this point.

In previous work performed by Rasouli *et al.*, (2016), the performance of inclined and vertical prefabricated drains around a structure of 27 kPa (prototype scale) was evaluated using shaking table test. In this research, vertical and inclined drains arrangements were unable to limit high excess pore pressures below the foundation and to generate a shielded zone under the structure, allowing complete liquefaction at the top layers of the stratum. This behaviour could be explained by the low confining pressure exerted by the foundation in the soil, which permits significant generation of excess pore pressures at the surface together with a weak performance of the drains arrangement. Although liquefaction could not be avoided at the top layers, the excess pore pressure generation was limited at the bottom of the stratum, where the radial proximity of the drains to the foundation was minimum. This behaviour verifies the relevance of decreasing radial distances between the drains and the structure for an effective performance of the technique. The installation of inclined drains considering a design in which the soil below the foundation is significantly mitigated, allow an adequate control of excess pore pressures during the shaking and quick dissipation in the reconsolidation stage.

6.2.1.4 Soil acceleration

Acceleration time-histories for the free field, soil close to the perimeter drains and below the foundation together with the input motions are presented in figure 6.5 for SG6 and SG8 considering depths of 2.1 m and 4.7 m. The free field presented complete acceleration decoupling in both cases due to the high excess pore pressure ratios that induced significant

softening in the soil and consequently complete liquefaction. Greater de-amplification was observed at top layers of the stratum.

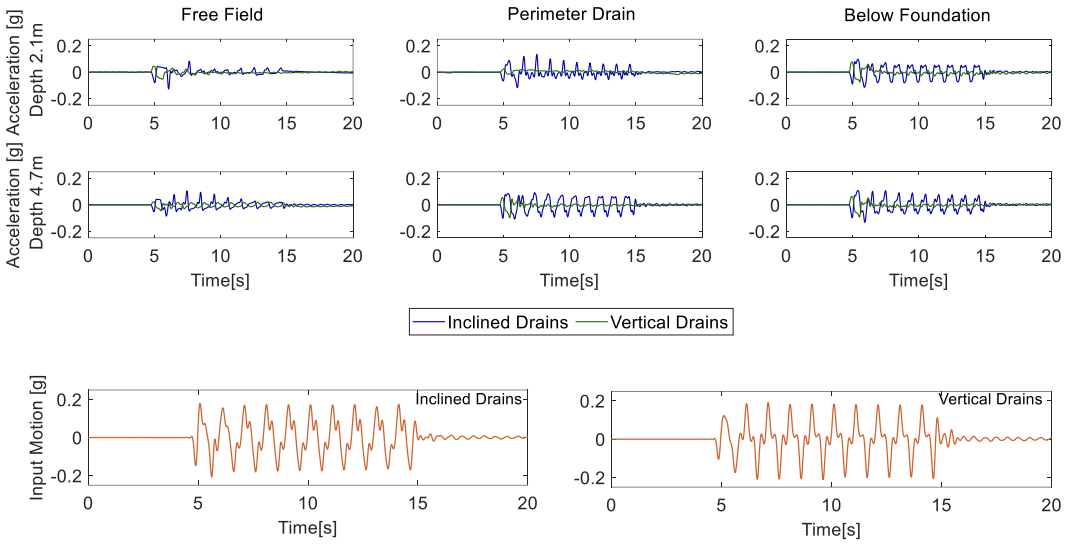

Fig. 6.5 Acceleration time-histories for soil below the foundation, close to the perimeter drains and free field in SG6 and SG8

Acceleration in the soil close to the perimeter drains and below the foundation shows a similar trend in case of SG6, demonstrating moderate de-amplification of the input motion as a result of soil softening. Lower attenuation of the input motion was presented under the foundation in the soil enclosed by the inclined drains due to the drains' effective performance during the shaking and the large influence of the foundation bearing pressure at this depth, avoiding large amounts of softening in the soil. Larger acceleration decoupling was observed below the foundation at a depth of 4.7 m compared to the top layer as a result of less foundation confining stress and consequent greater soil softening. Complete acceleration decoupling in the soil was observed for soil close to the vertical perimeter drains at both depths as a result of the considerable generation of excess pore pressures during the shaking and subsequent loss of shear strength in the soil.

The procedure previously performed for the estimation of shear strength provided by the drains, has been utilised in this section for the vertical and inclined drains cases. Table 6.1 presents the percentage of additional shear reinforcement (τ_{A_r}) provided by the drains together with replacement ratios (A_r) for free field, inclined and vertical drains cases at depths of 2.1 m and 4.7 m. The treatment area refers to the drain's area of influence and varies in the case of inclined drains along the stratum depth. In addition, elliptical cross-section was considered for the inclined drains.

In addition to the lack of drainage enhancement, the absence of shear reinforcement in the free field allowed a complete softening in the soil and a significant acceleration reduction. In the case of inclined drains, a shear reinforcement of 24% was supplied by the drains considering an A_r of 19% at the top layer. This value was larger compared to the shear reinforcement from vertical drains with an A_r of 10% at the same depth. In addition to the effective control of softening in the soil enclosed by the inclined drains, the drains' shear reinforcement might have contributed to a lower deamplification of the input motion compared to the vertical drains case. Furthermore, similar peak excess pore pressures were reached in the soil close to the inclined drains at both depths of the soil (see Fig 6.1). This suggests that, in addition to the drainage enhancement given by the drains, the slightly larger acceleration observed at a depth of 4.7 m occurred as a response of the great shear reinforcement provided by the drains.

Table 6.1 Additional shear reinforcement in the soil layer

Depth (m)	Inclined Drains		Vertical Drains	
	A_r (%)	τ_{A_r} (%)	A_r (%)	τ_{A_r} (%)
2.1	19	24	10	12
4.7	63	77	10	12

A_r: Area replacement ratio
τ_{A_r}: Additional drains shear reinforcement

Sufficient shear reinforcement should be provided by the drains in addition to drainage enhancement, in order to achieve an effective performance of the technique. The simplified calculation used to analyse the drain's contribution of shear reinforcement in section 6.5 provides an overview of the drains' influence in the soil acceleration response; however the accurate assessment of the drain's performance in terms of shear reinforcement during the shaking, require an experimental evaluation in which the drain's drainage capacity should be restricted (e.g. the use of membranes around the drains to avoid fluid flow inside).

6.2.2 Foundation response

6.2.2.1 Foundation settlement

The foundation settlement is a relevant parameter to determine the effectiveness of the mitigation technique. Figure 6.6 shows the settlement of the foundation and free field for SG6 and SG8 together with the input motions.

The free field in SG6 reached a total settlement of 160 mm with 58% generated during the shaking stage as a result of the partial drainage condition in the soil and consequent volumetric deformations (Dashti *et al.*, 2010a; Madabhushi and Haigh, 2012). During the post-shaking stage, the free field settled 68 mm in a period of 70 seconds. In SG8 the free field reached a larger total settlement compared to SG6, with further differences during the dissipation stage. Although vertical drains were closer to the free field when compared to the inclined drains, the slower dissipation in the central zone delayed the dissipation of high excess pore pressures in the free field allowing a longer time for reconsolidation, leading to volumetric strains.

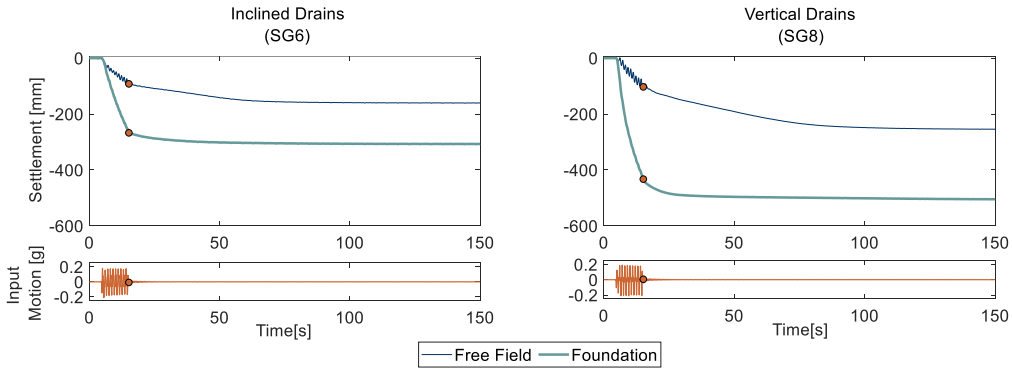

Fig. 6.6 Settlement time-histories of foundations and free field for SG6 and SG8

Settlement of the foundation in SG6 reached 87% of the total settlement during the shaking stage as a result of drainage volumetric strains due to reconsolidation and deviatoric deformation as a consequence of the strength loss in the soil under a heavy foundation. The percentage of settlement during the post-shaking stage was smaller compared to the shaking stage. The limitation of excess pore pressure generation during the shaking stage and the fast dissipation of peak values in the presence of inclined drains subjected to high confining pressure along their depth allowed a reduction in the time during which high excess pore pressures were maintained. Therefore, a decrease of reconsolidation volumetric strains due to the rapid regaining of stiffness in the soil, especially below the foundation was observed.

Although the same trend of majority of the settlement during the shaking and relatively smaller settlement after the motion was observed in SG8, verifying an effective performance of the drains during the dissipation stage; the foundations over vertical perimeter drains settled 505 mm, which represents a value 67% larger than the total permanent settlement obtained in SG6. During the dissipation stage, the greater softening in the soil generated as a result of the insufficient drainage improvement in the presence of vertical drains caused significant foundation settlement due to the expanded presence of volumetric deformation.

Previous tests have corroborated a significant improvement in terms of settlement when using perimeter drains as a countermeasure technique under structures. Improved soil containing high permeable vertical drains has been evaluated considering structures of 80 kPa and 187 kPa (Olarte *et al.*, 2017; Paramasivam *et al.*, 2018). Settlement reductions of 40% and 34% were obtained for both cases, compared to similar structures over unimproved soil. This response was attributed to the effective control and faster dissipation of excess pore pressures, particularly in the zone enclosed by the vertical drains. Moreover, larger settlement response of the foundation was observed during the shaking compared to the post-shaking stage, for both structures. A similar response was obtained in this work for the foundation over inclined and vertical arrangements, suggesting the importance of an adequate performance of the drains during the shaking stage rather than just the dissipation phase. Although the performance of inclined drains was not evaluated in the studies mentioned above, a greater settlement reduction should be expected by using the inclined arrangement. Inclined perimeter drains allow a further effective control and rapid dissipation of excess pore pressures in the enclosed area below the foundation, reducing reconsolidation volumetric strains and deviatoric deformations in the soil and providing an improved performance in terms of settlement compared to the vertical drains case.

6.2.2.2 Dynamic response of the foundation

Settlement and tilt of foundations are two of the most damaging effects of the liquefaction phenomenon as previously indicated. Rotational response of the foundation is directly related to the foundation's horizontal acceleration. Figure 6.7 shows the foundation's transverse acceleration for SG6 and SG8 together with the input motion in order to provide a clear comparison. A reduction of 0.1g of the input motion was observed in SG6 due to the soil softening below the foundation (Fig. 6.7a) which allowed low transference of the input motion to the foundation over the inclined perimeter drains. On the other hand, in SG8 an almost complete reduction of horizontal acceleration was achieved for the foundation after the first cycle of shaking, as a result of the high level of softening generated in the soil generating a negligible transference of the input motion (Fig. 6.7b).

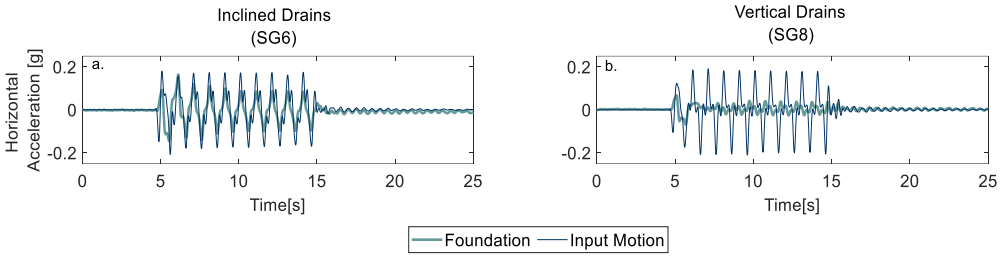

Fig. 6.7 Foundation horizontal acceleration for a) SG6 and b) SG8

Although de-amplification of the horizontal acceleration in the foundations was observed, rotation of foundations requires a proper evaluation as relevant acceleration transference to the foundation over inclined drains was observed. Foundation rotation time-histories and settlement versus foundation response for SG6 and SG8 are presented in figures 6.8 a and b. Foundation rotation in SG6 reached a maximum value of 5.5×10^{-3} rad during the first cycles of shaking at the same time as the foundation horizontal peak acceleration. Lower peak rotation of 2×10^{-3} rad was reached in the case of the foundation over vertical drains as a consequence of the minor foundation acceleration (Fig. 6.8a). At the time when the foundation stops to settle, rotations of 2×10^{-3} and 1×10^{-3} rad were observed for SG6 and SG8, respectively (Fig. 6.8b).

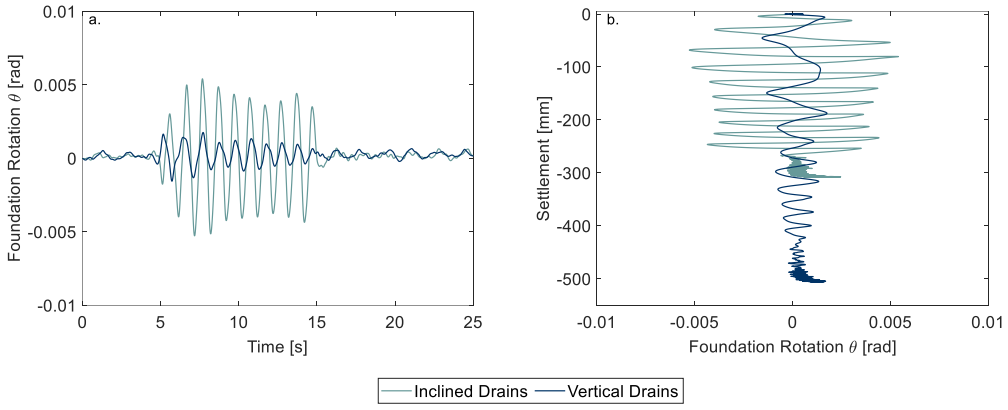

Fig. 6.8 a) Foundation rotational response and b) Foundation rotation vs settlement for SG6 and SG8

Amplification of horizontal acceleration is frequently expected in the case of soil drainage enhancement as soil softening is largely controlled and shear reinforcement is usually provided by the columns, allowing a larger transference of the input motion. However, in this analysis the high levels of excess pore pressures and the drain's inability to provide sufficient shear reinforcement to the soil caused de-amplification of the horizontal acceleration in the foundations.

6.3 Bearing pressure influence over inclined drains

Empirical methods used to predict settlement of structures due to earthquake-induced liquefaction (Yoshimi and Tokimatsu, 1977; Ishihara and Yoshimine, 1992; Liu and Dobry, 1997) have been examined by researchers in the last few decades. The variable of the depth of liquefable layer (D_L) has been evaluated together with other mechanisms related to liquefaction-induced settlement; concluding that certain parameters were omitted in the proposed methodology; such as relative density of the soil, characteristics of the input motion or bearing pressure of the foundation (Dashti *et al.*, 2010b). Within these mechanisms, the latter has been discussed in recent years (Bertalot and Brennan, 2015; Adamidis and Madabhushi, 2018).

Soil settlement occurred as a result of particles reconsolidation during the dissipation stage. Considering this, a structure with significant bearing pressure is expected to have a greater influence during the reconsolidation of the soil compared to a structure of low bearing pressure (Bertalot *et al.*, 2013); nevertheless, this behaviour has been refuted by researchers in the last years (Liu and Dobry, 1997; Ghosh, 2003; Dashti *et al.*, 2010b; Bertalot and Brennan, 2015). The lower settlement response for a foundation of high bearing pressure was attributed to the raise in soil cycle resistance when subjected to large confining and shear stresses, allowing generation of smaller excess pore pressures and limited soil softening in the soil.

The analysis of the performance of an inclined drain arrangement, taking into consideration the variation of bearing pressure as a mechanism of the foundation settlement is presented in this section. The results of SG6 (q=150 kPa) as previously analysed are summarised and presented in this section for a direct comparison with SG7 (q=50 kPa).

6.3.1 Soil Response

6.3.1.1 Excess Pore Pressure Generation

Fig. 6.9 shows excess pore pressure ratios for SG6 and SG7 at different depths, considering the soil under the foundation central axis, close to the inclined drains and free field. Complete liquefaction was observed in the free field, along the soil depth in SG7, a similar response obtained for SG6 due to the absence of drainage influence. At the top layer in SG7, larger excess pore pressure ratios below the foundation and close to the perimeter drains were observed reaching values of 0.3 and 0.7 respectively (Fig. 6.9b), compared to the soil in SG6 that presented r_u values of 0.2 and 0.5 for both locations (Fig. 6.9a). The foundation of 150 kPa exerted larger confinement stress in the soil compared to the

foundation in SG7, providing additional resistance to the generation of high excess pore pressures in the soil.

At a depth of 3.4 m, a peak r_u of 0.5 was generated below the foundation of 50 kPa (Fig. 6.9d). A larger generation of excess pore pressure at this depth compared to the top layers was observed due to the lower foundation confining pressure at lower depths. Furthermore, soil close to the perimeter drains in SG7 showed an excess pore pressure ratio of 0.7, while a value of 0.5 was observed in SG6 at a depth of 4.7 m (Fig. 6.9e). Although the radial proximity from the drain centres to the soil under the foundations was similar in both cases, r_u values exceeded the design requirement of r_u=0.6 (Seed and Booker,1977) under the foundation central axis in SG7. This demonstrates the relevance of the foundation bearing pressure in the inclined drains' performance during the generation stage. The r_u reached at the bottom layer (depth of 5.9 m), in SG7 was close to complete liquefaction with a value of 0.9 below the foundation of 50 kPa (Fig. 6.9h). Even though both cases had the influence of the drains' overlapped zone at a depth of 4.7 m, the r_u generated below the foundation of q=150 kPa reached a value of 0.55 (Fig. 6.9g), suggesting a larger influence of the foundation at this zone compared to SG7.

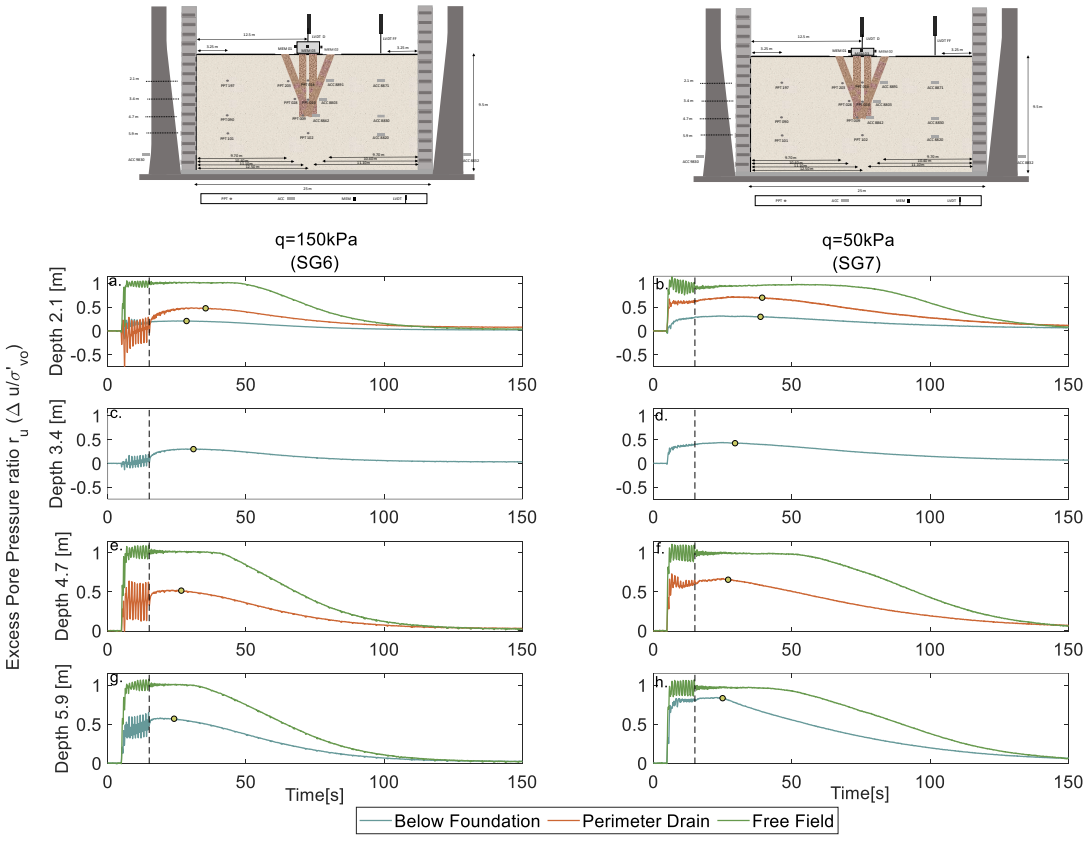

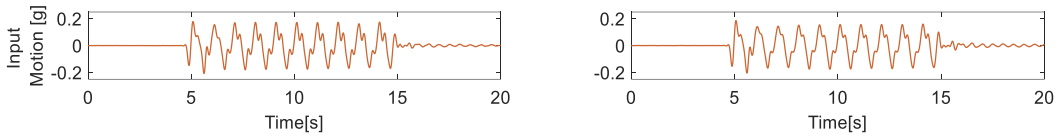

Fig. 6.9 Excess pore pressure ratios (r_u) for the soil under the foundation central axis, close to the inclined perimeter drains and free field for SG6 and SG7

The foundation bearing pressure is an important variable in the generation of excess pore pressures. The increase of confining pressure and shear stresses let to a greater cycle resistance in the soil. This allows a lower generation of excess pore pressures below the foundation and limited softening in the soil during the shaking. The relevant influence of the bearing pressure considering a mitigated soil containing perimeter vertical drains, was also verified by Paramasivam *et al.* (2018) for structures of 80 kPa and 187 kPa. A lower generation of excess pore pressures was observed in case of the structure of 187 kPa compared to the light foundation, as a result of the great resistance to excess pore pressure generation. Regardless of the arrangement of drains utilised and the proximity of the drains to the structure, the bearing pressure exerted by the foundation is a predominant factor in the generation of excess pore pressures.

6.3.1.2 Excess pore pressure dissipation: Bearing pressure influence

Horizontal contours of excess pore pressure ratios (r_u) are presented in Fig. 6.10 for the analysis of excess pore pressure dissipation in the soil with inclined perimeter drains under different bearing pressures at a depth of 2.1 m. Different times were plotted, considering the end of the shaking and dissipation initiation times under the foundation, close to the inclined drains and the free field in SG6. At this depth, the radial distance between the drains and the foundation central axes was 1.9 m in both cases. The analysis is centred on a comparison of the dissipation behaviour of soil with inclined perimeter drains considering bearing pressures of q=150 kPa and q=50 kPa.

In SG6, a homogeneous behaviour was observed at t=15s in the soil under the heavy foundation and outside the perimeter drains reaching peak values of r_u =0.4, until they started to dissipate at t=28.5 s. While excess pore pressures were observed to be dissipating in SG6 (Fig. 6.10c), under the edges of the foundation of q=50 kPa and in the soil surrounding the inclined drains in SG7, the r_u reached 0.4 and 0.7 values. The high bearing pressure of q=150 kPa allowed a faster dissipation of peak r_u values and the soil below the foundation rapidly regained of stiffness when compared to SG7 (Fig. 6.10d). The significant resistance of the soil to generating excess pore pressures below a foundation of high confining stress, implies at the same time, a great resistance of the soil to maintain these pore pressure magnitudes for a long time after the shaking. The reconsolidation of soil particles will attempt to occur

more rapidly in the presence of a significant load force exerted by a foundation with high bearing pressure.

Seven seconds later, the flowfront arrived at the inclined perimeter drain in SG6. At this time, r_u values under the foundation in SG7 presented a slight reduction while the perimeter drains showed an increment of excess pore pressure ratios (Fig. 6.10e). The flowfront arrived at the inclined perimeter drains four seconds later in SG7 (see Fig 6.9). The lower confinement stress in the soil allowed a delay in the flowfront arrival time for perimeter drains in SG7, maintaining peak excess pore pressures for a longer time (Fig. 6.10f). In the case of the absence of internal and sub-perimeter drain rings, the flowfront arrival time depends on the confining stress exerted by the foundation.

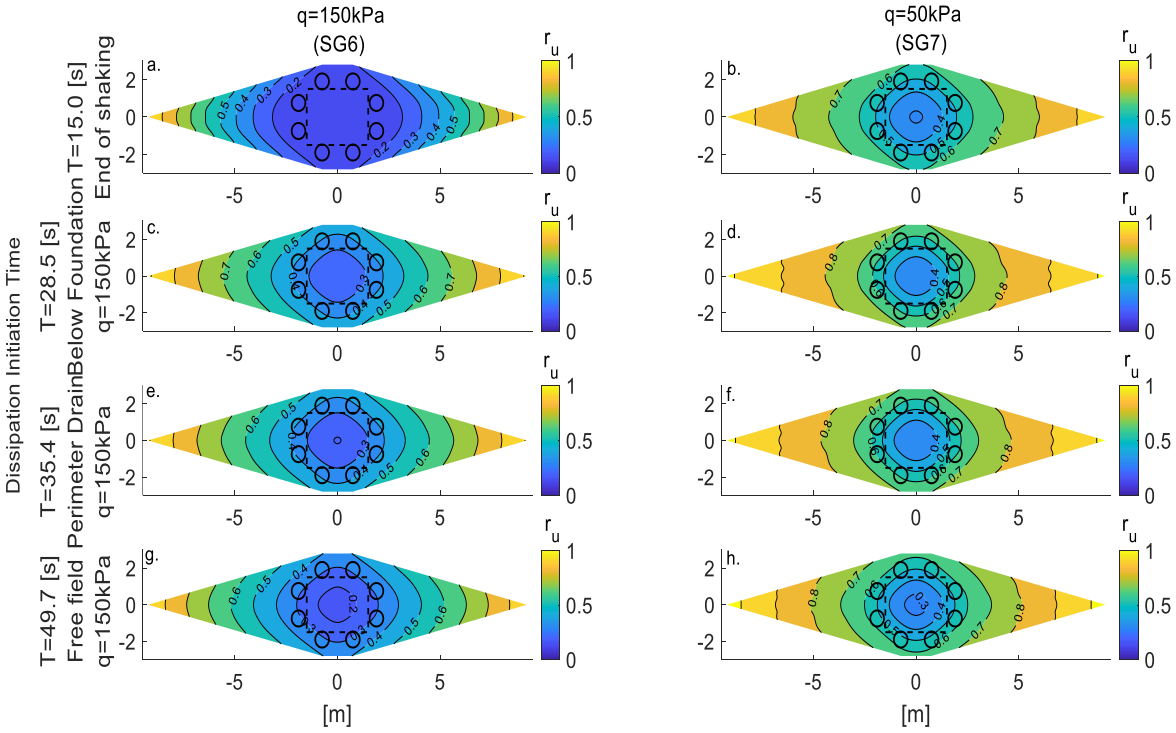

Fig. 6.10 Horizontal contours of excess pore pressure ratios (r_u) for SG6 and SG7 at depth of 2.1m

Finally, at t=49.7 s the free field started to dissipate showing a continuous reduction of 0.1 in the soil below the foundation and close to the perimeter drains in SG6. However, the central area and the soil close to the perimeter drains in SG7 presented dissipation of excess pore pressures with only a negligible influence of the drains in the free field (Fig. 6.10h).

A great confinement stress in the soil below the foundation allows a rapid dissipation of excess pore pressures in the area enclosed by the drains due to its tendency to a faster reconsolidation. Excess pore pressures generated in the case of low confining stress require a longer time to dissipate, suggesting a significant dependence between the foundation bearing pressure and the dissipation stage.

6.3.1.3 Foundation influence on the vertical dissipation path

Vertical contours of excess pore pressure ratios for SG6 and SG7 are shown in figure 6.11, considering the dissipation times presented in figure 6.4. In SG7, trends of a higher r_u value close to the perimeter drains and in the free field, and a lower value below the foundation when subjected to high effective stress were observed at t=15 s (Fig. 6.11b). The "infinite cell" behaviour of the inclined perimeter drains in SG7 allowed for a large generation of excess pore pressures outside the inclined perimeter drains with a vertical flow pattern more than the radial in the free field.

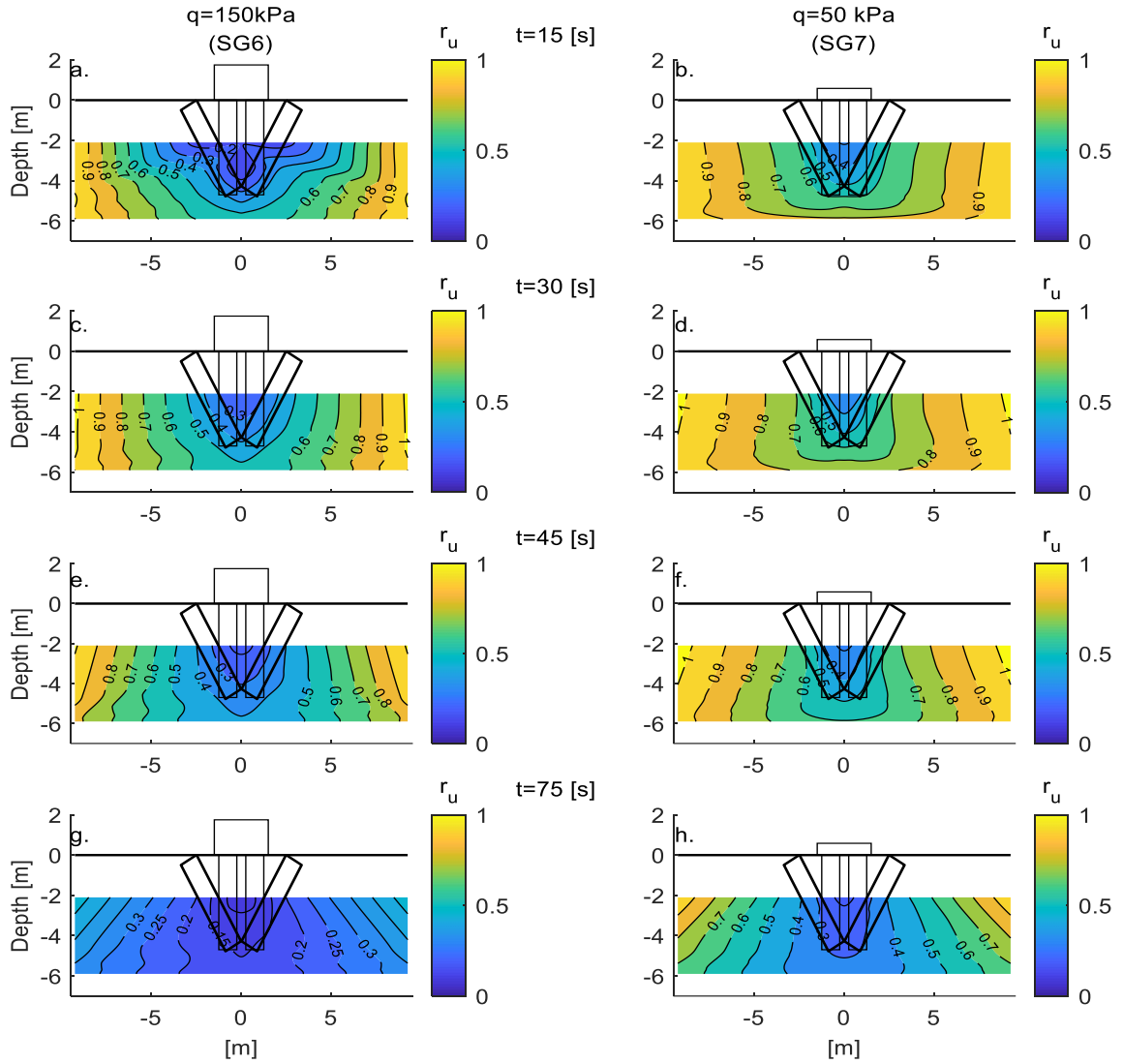

Fig. 6.11 Vertical contours of excess pore pressure ratios (r_u) for SG6 and SG7

Dissipation of the bulb of low pressures enclosed by the inclined drains in SG6 occurred at t=28.5 s from the top layer after reaching peak values of 0.3 as previously seen (section 6.1). At t=30 s, the bulb in SG6 continued to dissipate while the soil under the foundation of 50 kPa generated a peak excess pore pressure ratio of 0.4 below the foundation and of 0.7 at the perimeter drains. A bulb of low pressures was also generated under the lighter foundation; however, the bulb did not reach the bottom layer due to the lack of confining pressure (Fig. 6.11d). At t=45 s, the insufficient action of the overlapped zone at the base of the drains allowed a passive dissipation of the bulb in SG7 while the free field at this depth still presented high excess pore pressure ratios (Fig. 6.11f). Finally, 60 seconds after the end of the shaking, the soil around the drains at the bottom layers reached r_u=0.4 in SG7, two times larger than the value observed for the same zone in SG6.

Vertical contours of excess pore pressures for SG6 and SG7 are presented in Figure 6.12, considering similar dissipation times as in Figure 6.11 for the plots.

In SG6, the fluid flows easily towards the perimeter drains rather than to the zone below the foundation, due to the infinite cell behaviour of the drains and the difficulty with which the soil generates excess pore pressures (Fig 6.12a). After the shaking, the fluid flowed from the bottom to the top layer, raising the fluid level and showing higher excess pore pressures of 11 kPa and 15 kPa below the foundation and surrounding the drains respectively (Fig 6.12c). Meanwhile, the free field presented significant amounts of fluid, indicating a value of 51 kPa at the lower layer. The fluid started to dissipate, flowing effortlessly from below the foundation to the inclined drains, enabling significant dissipation in the zone surrounded by the columns (Fig 6.12e,g).

A similar behaviour of excess pore pressures dissipation was observed in SG7, showing significant fluid, particularly outside the drains at the end and after the shaking, with improved control of the fluid below the foundation (Fig 6.12b,d). However, a larger increase of excess pore pressures was observed compared to the soil below the heavy foundation in SG6. Excess pore pressures were more easily generated below the foundation of light bearing pressure compared to the heavy foundation.

Thirty seconds after the shaking, higher excess pore pressure magnitudes were registered below the foundation of 50 kPa compared to that of 150 kPa (Fig 6.12f). Although the fluid flowed easily from the area enclosed by the inclined drains and from the bottom layer in SG7, a faster dissipation was observed below the foundation of 150 kPa. The entire layer showed significant dissipation in both cases at t=75s, particularly below the foundation due to the confining pressure. A minor value of 7 kPa was registered at the top layer in SG6, while 9 kPa was recorded in SG7.

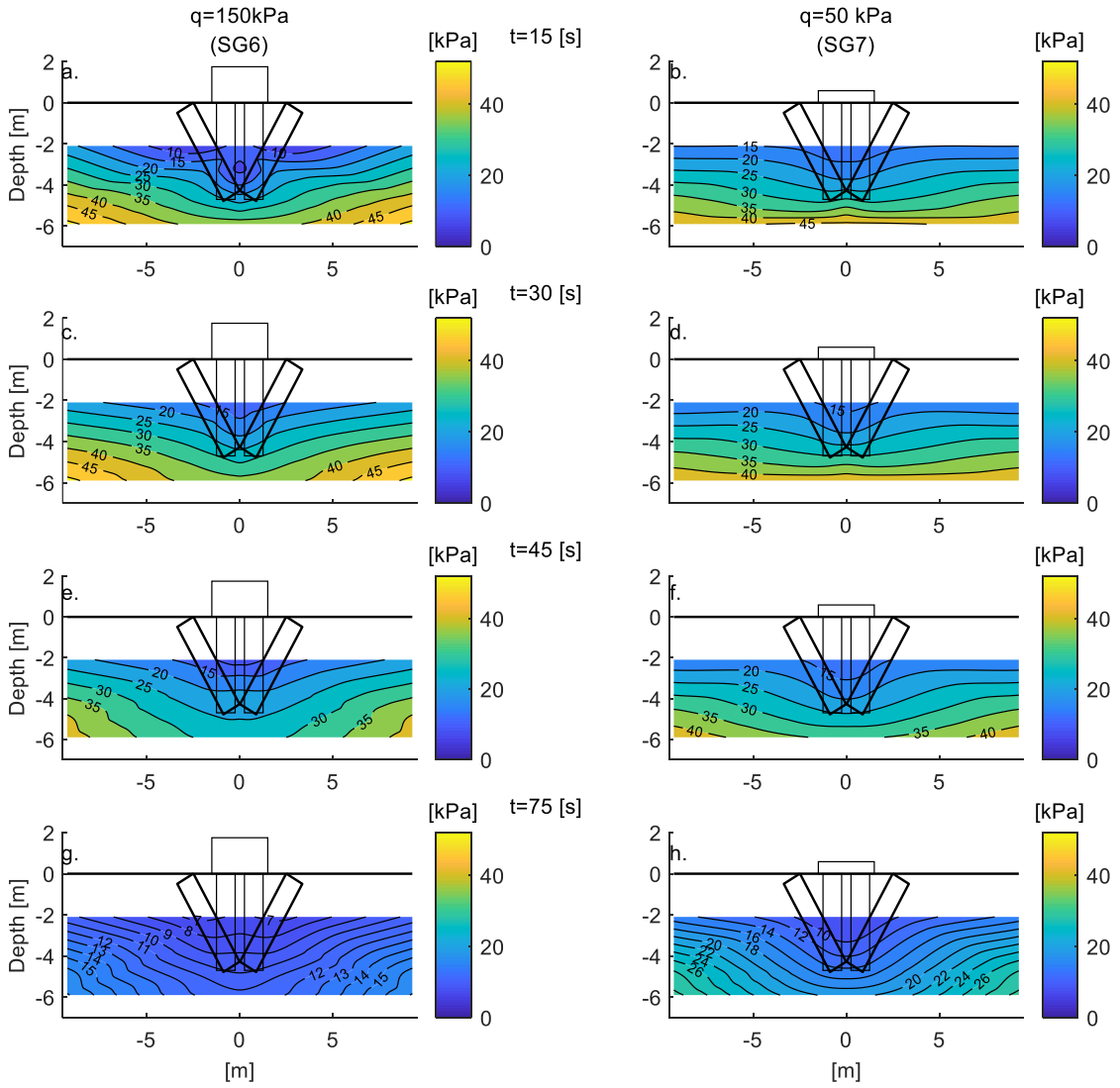

Fig. 6.12 Vertical contours of excess pore pressure for SG6 and SG7

6.3.1.4 Soil acceleration

Acceleration time-histories for the free field, close to the perimeter drains and below the foundations, together with the input motions are presented in figure 6.13 for SG6 and SG7 at different depths. Complete acceleration decoupling was observed in the free field for SG7 along the depth of the stratum as a result of complete softening in the soil generated by high excess pore pressure ratios (r_u) and the minimal additional shear reinforcement provided by the drains (see Table 6.1). Differences in the acceleration response for SG6 and SG7 were managed by the drainage enhancement, as similar additional shear reinforcement was provided by the drains for both cases along the stratum depth (see Table 6.1). In SG7, greater softening in the soil close to the perimeter drains and below the foundation was observed

when compared to SG6 due to the high levels of excess pore pressures reached in presence of the low bearing pressure, resulting in significant acceleration de-amplification. The soil acceleration is higher below the foundation of 50 kPa at the top layer compared to the soil response at a depth of 4.7 m. The significant softening in the soil generated at a depth of 4.7 m allowed complete acceleration decoupling after the second cycle of shaking, outside the perimeter drains and below the foundation of 50 kPa, suggesting the minimal influence of the foundation in the soil at this depth.

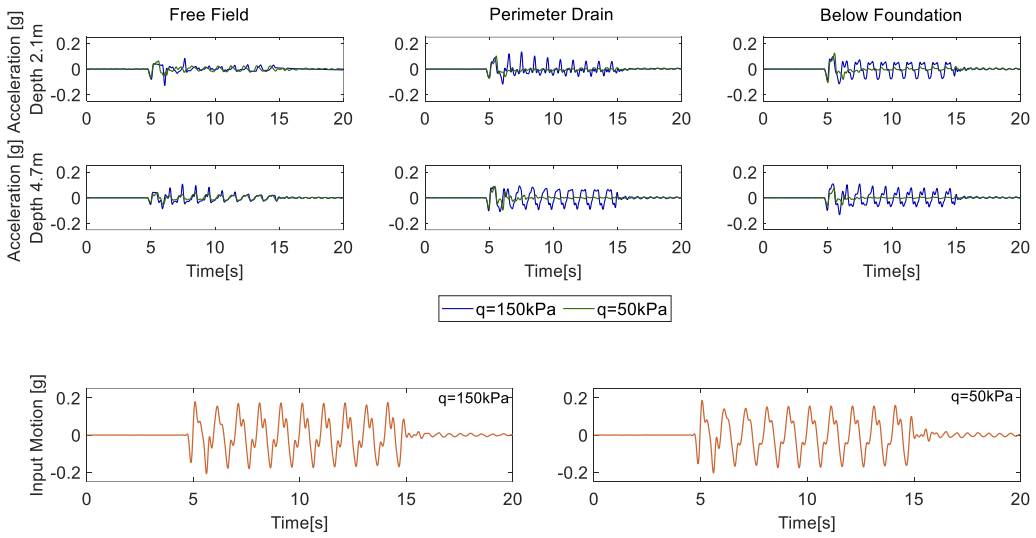

Fig. 6.13 Acceleration time-histories for soil below the foundation, close to the perimeter drains and free field in SG6 and SG7

6.3.2 Foundation Response

6.3.2.1 Foundation settlement

The foundation settlement time-histories are presented in figure 6.14 for SG6 and SG7, together with the free field settlement and input motions in each case. Free field settlement in SG7 reached a value of 115 mm and 106 mm during the shaking and post-shaking stages respectively. Both values were larger when compared to the free field settlement in SG6 as a result of the lower performance of the inclined drains below low bearing pressure during the dissipation stage, allowing larger time for reconsolidation volumetric strains in the free field.

The settlement below the foundation of 50 kPa reached 87% of the total permanent value during the shaking stage. Larger volumetric and deviatoric strains during the shaking compared to the post-earthquake stage, verify the efficient work of inclined drains during dissipation. However, this settlement was slightly larger when compared to the settlement

in SG6, as larger soil softening was generated below the foundation of 50 kPa during the shaking stage generating deformation due to strength loss in the soil in addition to drainage volumetric strains. During the dissipation stage, settlement of the foundation of 50 kPa was only 1% larger than the foundation settlement in SG6. The rapid dissipation of excess pore pressures in the presence of high bearing pressures, permits the reduction of reconsolidation volumetric strains and an important decrease of deviatoric strains in response to soil rapidly regaining stiffness, particularly the soil enclosed by the drains. A similar settlement response between a foundation of 50 kPa and another one, three times heavier, suggests the relevance of the foundation bearing pressure in the effective performance of inclined perimeter drains.

Larger settlement was generated in the case of low bearing pressures during the shaking stage due to the considerable level of excess pressures reached under the foundation, allowing significant reconsolidation volumetric strains and deviatoric deformations in the soil. In addition, the delayed dissipation presented below the foundation, led to a longer time in which high excess pore pressures were maintained. This caused an increase of deviatoric and volumetric strains below the foundation of low bearing pressure. In a previous evaluation of the performance of perimeter vertical drains under structures, similar permanent settlement was obtained for structures of 187 kPa and 80 kPa, in spite of the significant difference between bearing pressures (Paramasivam *et al.*, 2018). This response was explained by the limited soil softening reached in the area enclosed by the vertical drains below the heavy foundation. Although the dissipation stage was not analysed, results showed a faster dissipation of excess pore pressures in presence of the large bearing pressure verifying the behaviour of faster reconsolidation under high confining stresses.

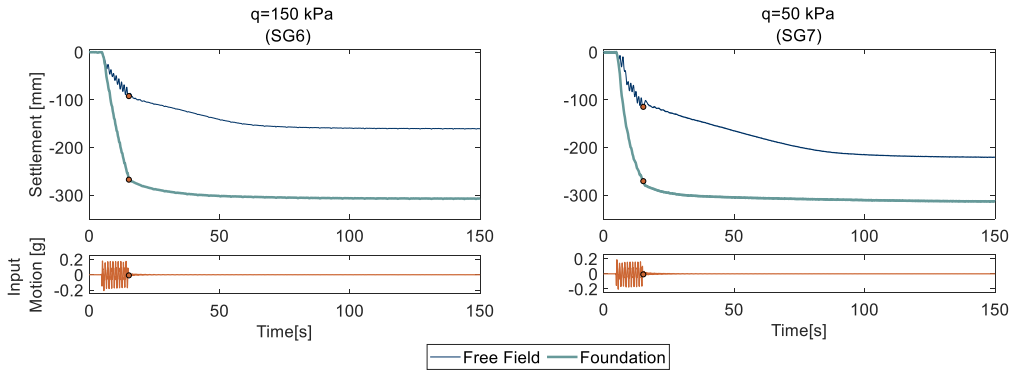

Fig. 6.14 Settlement time-histories of foundations over perimeter drains and free field for SG6 and SG7

The bearing pressure of a structure is a relevant parameter in the settlement mechanism during the generation and dissipation stages. The improved settlement response obtained in the case of a foundation with larger bearing pressure, suggests that the effectiveness of the

drains arrangement relies on the magnitude of the confining pressure exerted by the structure; therefore, it is crucial to consider this parameter in the design of the mitigation technique.

6.3.2.2 Foundation dynamic response

Foundation horizontal accelerations together with input motions are presented in figure 6.15 for SG6 and SG7. A larger de-amplification of acceleration was observed in the foundation of 50 kPa after the first cycle of shaking as a result of the greater softening in the soil that impeded a large transference of the input motion (Fig. 6.15b). The lower r_u values in the case of a high bearing pressure on the foundation of 150 kPa allowed a larger acceleration transference in SG6, showing a de-amplification of 0.05g in the horizontal acceleration, while a maximum de-amplification of 0.18g was observed for the lighter foundation.

The rotation magnitude of foundations over drain arrangements requires detailed analysis as it is directly related to the damage on the superstructure. Figure 6.16a shows rotation time-histories for the foundations of 150 kPa and 50 kPa. Maximum rotation of 2.5×10^{-3} rad was observed in SG7 during the first cycles of shaking, while a larger rotation of 5.5×10^{-3} rad was obtained for the heavy foundation (Fig. 6.16a). The lower rotational acceleration of the light foundation was managed by the softening in the soil and the lower input motion transference to the foundation. However, the effective performance of the inclined drains under heavy foundations allowed for rapid drainage and eased a larger input motion transference to the foundation as well as high rotational stiffness. Furthermore, a permanent tilt of 2×10^{-3} rad was reached by the heavy foundation, while a negligible value was attained by the lighter foundation during this earthquake (Fig. 6.16b). No amplification of the transverse acceleration in the foundations was expected, as the principal role of the drains was to enhance drainage.

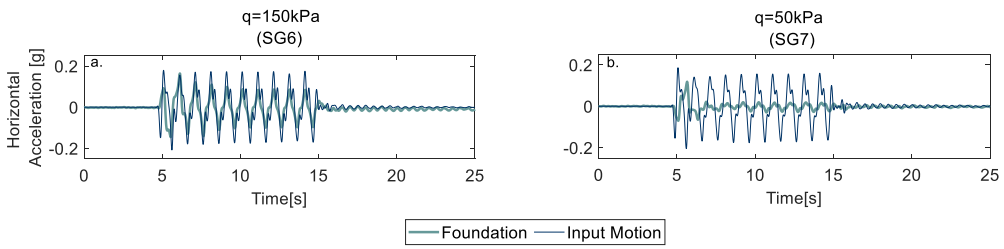

Fig. 6.15 Foundation horizontal acceleration for a) SG6 and b) SG7

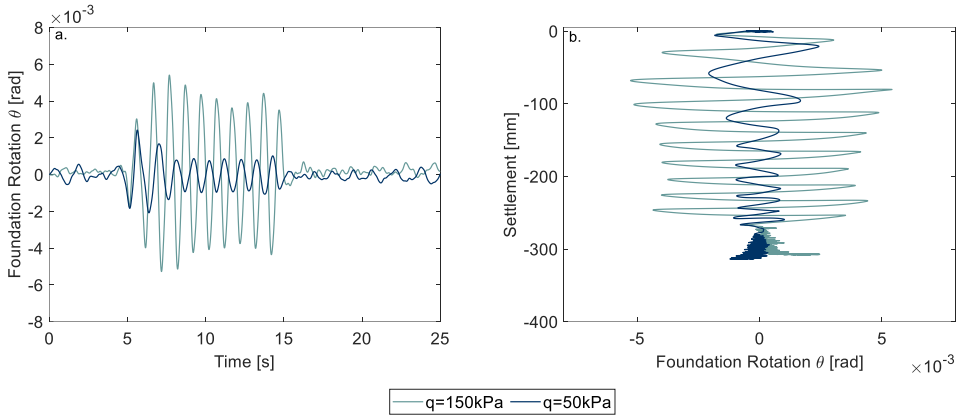

Fig. 6.16 a) Foundation rotational response and b) Foundation rotation vs settlement for SG6 and SG7

6.4 Conclusions

In this chapter, the performance of inclined perimeter drains under existing buildings has been evaluated taking into consideration the generation of excess pore pressures due to earthquakes and the following dissipation. The effectiveness of the inclined arrangement was analysed by setting a comparison with a vertical perimeter drain arrangement and considering variations of bearing pressures over soil. Furthermore, the foundation settlement and dynamic response were analysed.

The inclined perimeter drain arrangement was able to control high excess pore pressures during the generation stage below the foundation and close to the soil surrounding the drains. A bulb of relatively low pressures was generated in the volume of soil enclosed by the inclined drains and easily dissipated due to the radial proximity from the drains to the foundation's central axis. In addition, this region is subjected to significant influence of the foundation bearing pressure. Rapid dissipation allowed the reduction of reconsolidation volumetric strains and deviatoric deformation due to the rapid recovery of shear strength, resulting in a foundation total settlement of 307 mm. On the other hand, the constant radial distance of vertical drains to the foundation central axis led to a less effective drain performance during the generation and dissipation stages. The excess pore pressure peak values generated below the foundation were maintained for a longer time, permitting a greater time for reconsolidation volumetric and deviatoric strains in the soil and resulting in a foundation settlement of 505 mm. Furthermore, a lower transference of the input motion to the foundations over vertical drains was observed, causing minor rotation of the foundations when compared to the inclined drain arrangement.

A foundation settlement reduction of 40% was obtained by enhancing drainage in the soil using inclined perimeter drains, and therefore verifying the effectiveness of the proposed

simplified arrangement. Nevertheless, minimising the radial proximity of the drains to the foundation is not sufficient in the case of low bearing pressure, as the effective drainage performance of inclined perimeter drains is controlled by the high confining stress exerted by the foundation. The excess pore pressures were quickly dissipated in the presence of inclined drains under a bearing pressure of 150 kPa, allowing a rapid regained of stiffness in the soil. The reduction of reconsolidation volumetric strains and deviatoric deformation under a foundation of 150 kPa triggered a similar settlement response to that of a foundation of 50 kPa. To obtain optimal performance of inclined perimeter drains (below any bearing pressure) the variation of certain parameters must be considered in the design of the arrangement. Shallow inclined drains, additional rings of perimeter drains or higher permeable material can ensure a rapid dissipation of excess pore pressures, particularly below the foundation.

It is anticipated that the inclined drains would perform even better in the field conditions due to the locked in horizontal stresses created around the drains during installation and compaction of the drain material. This aspect could not be modelled in small scale centrifuge tests carried out in this research.

Chapter 7

Numerical modelling of drain arrangements below new and existing buildings

7.1 Introduction

The analysis of soil behaviour during the reconsolidation stage is highly relevant when it concerns drainage countermeasure techniques, as the principal aim of vertical drains is the reduction of structural damage due to rapid effective excess pore pressure dissipation. Although numerical modelling (NM) and physical modelling (PM) have been used over the years to evaluate the performance of drain arrangements during liquefaction, particularly through the reconsolidation stage; both these methodologies require extensive use of different resources, including time and cost, thus limiting the evaluation of a large number of models. In addition, different software utilised to simulate soil liquefaction, present complications for the structural settlement prediction**.** The drainage behaviour of the soil containing vertical drains requires a 3D analysis considering the complete mitigated area; nevertheless, this becomes unfeasible to perform, as excessive time and cost are needed. The drains performance has been widely analysed considering the drain unit cell behaviour in a 3D model, which provides an imprecise response of the soil (Howell *et al.*, 2015).

For this reason, the elaboration and validation of a 3D simplified finite element (FE) technique focused on an effective simulation of the excess pore pressure dissipation below new and existing building and also the settlement response of the foundation is of significant interest.

In this chapter, the simplified FE technique developed in ABAQUS, previously detailed in chapter 3, is utilised to evaluate a series of models with similar characteristics to the physical prototypes evaluated in previous chapters. This analysis involves the validation of the numerical modelling method, using results from the dynamic centrifuge tests and a discussion related to the different factors that influence the relationship between the numerical and physical models.

Moreover, a parametric study is presented in the last section that considers the validated FE model of a simplified drain arrangement below new buildings. The variation in the vertical drain's permeability is intended to provide an optimal permeability factor in terms of the settlement reduction.

7.2 Numerical model calibration

The proposed simplified technique involves the use of a boundary condition to simulate the excess pore pressure generation and liquefaction behaviour in the soil due to a dynamic loading. Because of this "shaking" simulation, limitations arise in terms of the soil properties, forcing the calibration of the numerical model for a prediction of an accurate liquefaction behaviour of the soil.

Considering that the soil rate of reconsolidation at low effective stresses depends on the soil stiffness (E_o) and its permeability (k) factors (Haigh *et al.*, 2012), the calibration of the FE model takes into account both these parameters for the replication of the soil behaviour during the excess pore pressure generation and dissipation.

The coefficient of consolidation (C_v) reaches a low value during liquefaction (Brennan and Madabhushi, 2011). This occurs in response to the significant decrease of stiffness in the soil at low effective stresses (Haigh *et al.*, 2012). Adamidis and Madabhushi (2016) evaluated the variation of the soil stiffness influenced by the soil effective stress using oedometer tests for Hostun sand. The soil at low effective stresses (less than 3 kPa) reached a maximum stiffness of 6 MPa. Based on this, a significant reduction of the soil stiffness for the fine and coarse material was considered in the FE model to simulate the soil behaviour during liquefaction.

In contrast to the soil stiffness, the permeability factor is expected to increase during soil liquefaction due to the significant disturbance of the soil particles and their separation owing to excess pore pressure generation while shaking, that enable hydraulic fissures in the stratum (Haigh *et al.*, 2012). Additionally, this increment in the soil permeability has previously been explained by Scott (1986), attributing this variation to the agitation effect in the stratum. Moreover, in the work undertaken by Haigh *et al.* (2012), a rapid increment

in permeability was verified for soil with an effective stress of under 0.1 kPa for different types of sands.

In numerical analysis, a high constant permeability factor is usually considered to model the soil during liquefaction (Shahir *et al.*, 2012). In the work carried out by Arulanandan and Sybico (1992), an increment in the original permeability value was used for an accurate simulation of the centrifuge tests in terms of settlement. Similarly, Balakrishnan (2000) performed a numerical analysis using a permeability value ten times higher compared with the original factor to obtain similar results to those attained in the physical model tests. This variation led to a good match in the settlement response.

Therefore, in addition to the low ratio of soil stiffness, a significant increment in the original permeability was considered for the fine and coarse material in the numerical analysis. The permeability for the fine sand was assumed to be the centrifuge model value, while the in the in-drains case, the model permeability was significantly increased. This was assumed to simplify the numerical model because the aim was to evaluate principally the sensitivity and effectiveness of the drains.

7.3 Simplified drain arrangement below new buildings

FE analysis performed for the simplified arrangement of five vertical drains under new buildings (SG2) is detailed in this section. The soil behaviour, in the presence of this drain arrangement, is analysed and compared with the results obtained from the centrifuge test, for an input motion of 0.3g (prototype scale) (see Chapter 4). For this model, 8.5% of the soil stiffness (see Section 3.3.1.2) was utilised for the fine and coarse materials, to simulate liquefaction, while the permeability of Fraction B inside the drains showed an increment of 23 times that of the centrifuge model value.

Excess pore pressure generation

Figure 7.1 presents the excess pore pressures time-histories, obtained from the numerical and centrifuge modelling, for the soil near the internal and perimeter drains, including the free field at the top layer (depth of 2.1 m). The results from CM (centrifuge modelling) and NM (numerical modelling) are presented in colour and black dotted lines, respectively. In both cases, the dissipation initiation times are illustrated by yellow circles as in previous chapters.

Excess pore pressure generation in NM reached a maximum value of 0.15 near the internal drain after the “shaking”, as a result of the great bearing pressure in the soil and its “unit cell” behaviour (Fig. 7.1a). A greater ratio was observed close to the perimeter drains,

showing a peak value of 0.6 in response to the low influence of the bearing pressure (Fig. 7.1b). The free field presented a peak value of 1 in the presence of no bearing pressure and lack of drainage enhancement (Fig. 7.1c). Furthermore, this complete liquefaction behaviour in the free field was expected due to the excess pore pressure boundary condition of r_u=1.

Differences of 25% and 10% between the peak generation ratios were observed in the soil near the internal and perimeter drains in the numerical and physical modelling, respectively. Although the principal aim of the proposed FE technique is the simulation of the soil dissipation behaviour with consideration of the presence of vertical drains and the consequent settlement response, the excess pore pressure ratios obtained in NM suggests an accurate model of the soil behaviour during the generation stage as well. However, the cyclic variation in excess pore pressures can not be captured in these numerical models as only consolidation process is modelled. The model captures the transmission of the excess pore pressures applied at the boundary nodes to the soil, within the 3D FE model.

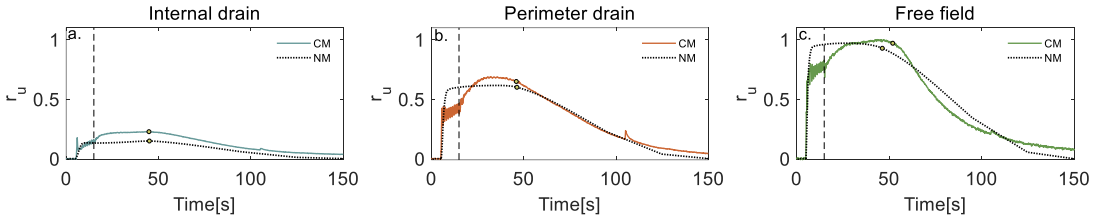

Fig. 7.1 Excess pore pressure ratios (r_u) time-histories for SG2 in NM and CM, at depth of 2.1m

Dissipation of excess pore pressures

The soil dissipation behaviour obtained from the FE analysis is presented in this section. The evaluation was performed using contours of excess pore pressures for the numerical and centrifuge modelling, considering dissipation initiation times in the soil near the drains in NM. The end of the shaking and t=75 s were also considered for the dissipation path analysis.

At the end of the shaking in NM, excess pore ratios reached a lower value of 0.13 near the internal drain compared with the perimeter drain and the free field in response to the significant bearing pressure of the foundation (Fig. 7.2a). On the other hand, low r_u values of 0.17 and 0.4 were registered below the foundation and at the external drain ring, respectively (Fig. 7.2b). Dissipation started near the internal drain at t= 45 s in the numerical model (Fig. 7.2c), suggesting a good match with the initiation time at the same location in CM (t=44.8 s). Excess pore pressures presented great values in the soil near the perimeter drains at this time, showing ratios of 0.6 and 0.7 in NM and CM.

At t=46.4 s, the flowfront arrived near the perimeter drain in NM after reaching a peak value of 0.6, while slight dissipation close to the internal drain was registered (Fig. 7.2e).

Meanwhile, dissipation also occurred near the internal drain in CM, while the soil at the perimeter drain began to dissipate one second later (Fig. 7.2f). The free field exhibited similar behaviour of complete liquefaction in NM and CM, starting to dissipate at t=48.5 s and t=51.5 s, respectively (see Fig 7.1).

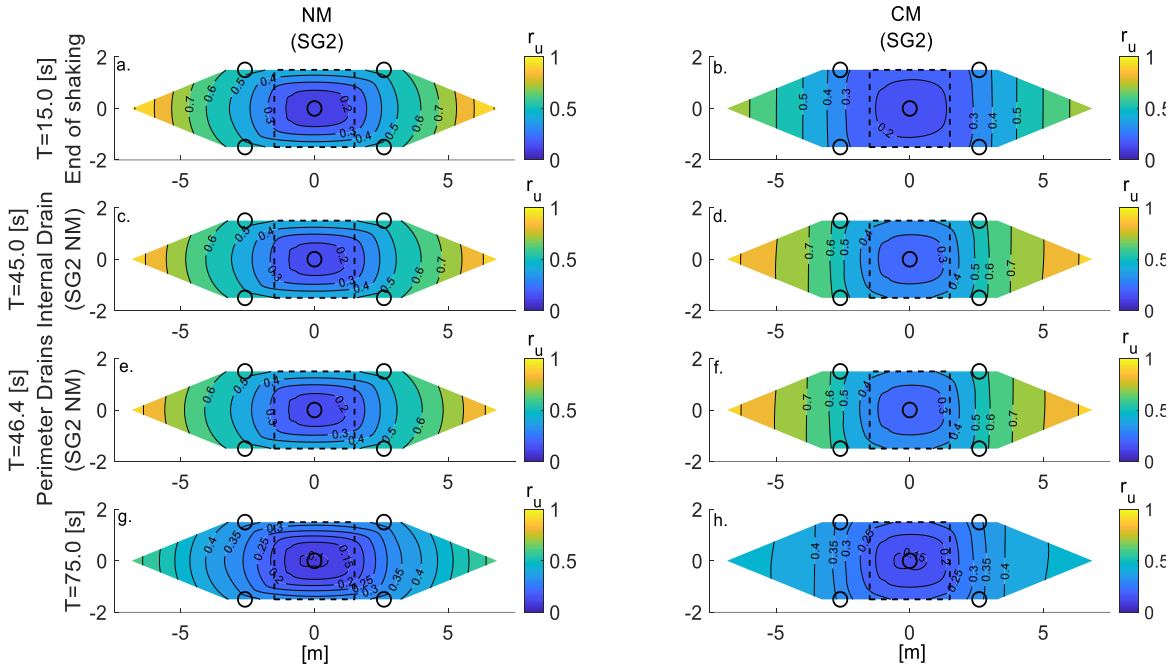

Fig. 7.2 Horizontal contours of excess pore pressure ratios (r_u) for SG2 in NM and CM at depth of 2.1m

Significant dissipation below the foundation and close to the perimeter drains was observed at t=75 s in NM and CM (Fig. 7.2g) ; nevertheless, the free field in NM showed higher excess pore pressure ratios compared with the CM at this time (Fig. 7.2h). Additionally, although similar flowfront arrivals were reached near the vertical drains, slightly faster rate of dissipation was observed in CM below the foundation. This behaviour occurred due to the increment of the coefficient of consolidation (C_v) along the reconsolidation stage, after the shaking (Brennan and Madabhushi, 2011; Haigh *et al.*, 2012).

At the start of reconsolidation, the C_v factor reached a significantly lower value compared with the magnitude registered at the end of the stage (Brennan and Madabhushi, 2011). The regaining of soil stiffness along the dissipation stage due to the increment of soil effective stresses and densification (Adamidis and Madabhushi, 2016), enabled a variation in the rate of reconsolidation. In the FE analysis, this varying behaviour cannot be accurately

modelled as the soil stiffness and permeability are considered constant parameters along the "shaking" and reconsolidation stage, becoming a limitation for the numerical model.

Foundation settlement

The foundation settlement response for SG2 NM is analysed in this section. Table 7.1 retraces the steps utilised for the FE model, previously detailed in the methodology chapter. The foundation response during the "shaking" stage consists of the settlement obtained in steps 2,3 and 4, wherein the foundation is placed in the soil of limited stiffness (simulating stiffness degradation during soil liquefaction) and simultaneously influenced by the additional excess pore pressure applied as a boundary condition over a period of ten seconds. The foundation settlement during the dissipation stage is obtained from step 5. It is relevant to emphasise that the principal objective of this technique is to model the dissipation behaviour of excess pore pressures in soil and the foundation settlement response during this stage.

Table 7.1 Steps for the FE simplified technique in ABAQUS (summarised version)

Step	Description
	Initial: Default step created by the software.
1	*Geostatic:* The equilibrium of the soil is verified.
2	*Soil Transient Consolidation:* The foundation of 150 kPa is placed over the soil.
3	*Soil Transient Consolidation:* The excess pore pressure is applied in the soil as an external load boundary condition for one second.
4	*Soil Transient Consolidation:* The applied excess pore pressures, are held at their peak values for nine seconds, to replicate the total time of shaking.
5	*Soil Transient Consolidation:* Excess pore pressure dissipation in the soil is enabled for a period of 135 seconds.

Figure 7.3 presents the foundation settlement for SG2 considering numerical and centrifuge modelling results. Settlement of the foundation in NM reached a value of 126 mm during the "shaking", representing 49% of the total settlement obtained (Fig. 7.3). This response was managed by the low level of soil stiffness and the additional excess pore pressure below the foundation, which enabled volumetric and deviatoric deformations in this area. On the other hand, a slightly greater settlement was observed for the foundation in CM during this stage. The slightly lower generation of excess pore pressures around the internal drain in NM allowed minor strains during the "shaking" stage. Additionally, considering that excess pore pressures were not generated due to a dynamic force, the deviatoric strains due to ratcheting or rotation were not considered in the foundation

response, representing another factor for the lower settlement in NM during this stage. Nevertheless, the overall match of the settlement from NM to that obtained in CM is acceptable.

The foundation settled 132 mm during the dissipation stage in NM due to the effective action of the vertical drains, thereby accelerating dissipation and reducing deviatoric and volumetric deformations in the soil. This value was 25% greater compared with the amount obtained in CM during dissipation. The slightly lower level of settlement in the physical modelling resulted as a consequence of the higher rate of dissipation and the faster regaining of stiffness below the foundation compared to the NM.

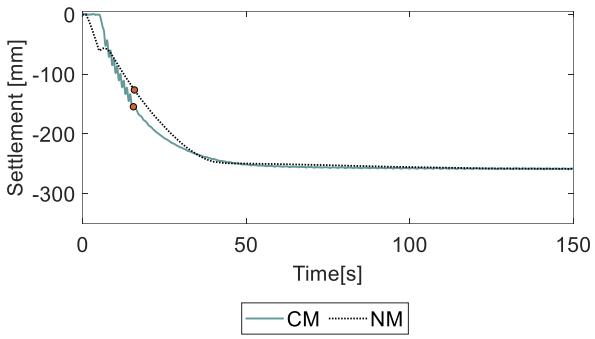

Fig. 7.3 Settlement time-histories of the foundation for SG2 in NM and CM

Settlement of the foundation in NM during the generation stage was managed by the low level of stiffness in the soil, as well as the excess pore pressure generation under the foundation. During the dissipation stage, the lower rate of dissipation enabled a slightly greater settlement response compared with the amount obtained in the physical modelling. In addition to the minor quantitative difference between the foundation settlement in NM and CM during the generation and dissipation stages, the total permanent settlement reached a value of 258 mm using both methodologies, suggesting a validation for the FE model and the soil parameters used.

7.4 Arrangements of rubble brick drains below new buildings

The arrangement of rubble brick drains (SG3, SG4) and a single column (SG9) below the foundation of 150 kPa were evaluated using the 3D FE analysis and compared with the drains' performance in the physical modelling considering EQ2 (see Chapter 5). In these

models, a permeability of 0.35 m/s was required for the rubble brick drains, representing an increment 70 times that of the model value.

A significant reduction in the soil stiffness was required depending on the evaluated model. The soil containing 13 vertical drains required a stiffness of 1.3%*E* for the fine and coarse material, while a magnitude of 2.1%*E* was utilised in the case of the 17-drain arrangement. For the soil containing a single column below the foundation, a low value of 1.1%*E* was used for the gravel column as this represented the main support of the foundation, while 19%*E* was used for the fine soil.

7.4.1 The 13-drain arrangement below the foundation (SG3)

Excess pore pressure generation

Figure 7.4 presents excess pore pressure time-histories for the arrangement of 13 rubble brick drains under new buildings (SG3) at depth of 2.1 m, considering results obtained from numerical and physical modelling analysis. The excess pore pressure ratio reached a lower value near the internal drain (Fig. 7.4a) compared with the soil close to the sub-perimeter and perimeter drains (Fig. 7.4b,c) in NM, due to the foundation influence and the drain "unit cell" behaviour. A similar trend was observed in CM; however, greater ratios were reached near the internal and the sub-perimeter drains compared to the NM. The addition of excess pore pressure as a boundary condition in a stratum of large dimensions involves a limitation in terms of excess pore pressure generation. This behaviour can be explained by the effect of the distance from where the pressure is applied. The soil located far from the application point presents a lower influence, enabling minor excess pore pressure generation.

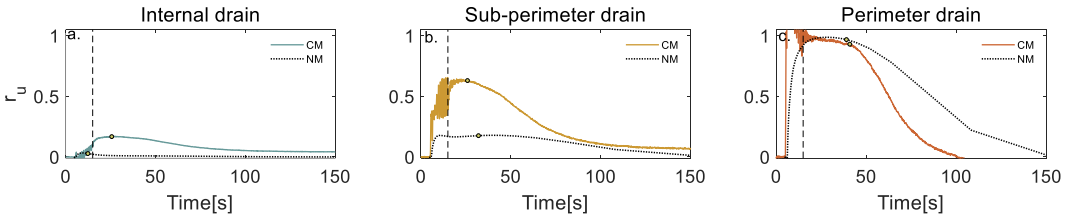

Fig. 7.4 Excess pore pressure ratios (r_u) time-histories for SG3 in NM and CM, at depth of 2.1m

This limited r_u ratios below the foundation in large soil volumes demanded the use of a lower value of soil stiffness compared with the previous case (SG2) to model an accurate settlement response, as no significant strains are expected to be generated under the

foundation. Therefore, lower stiffness magnitudes, previously mentioned were used for the model of the rubble brick drain arrangements.

Dissipation of excess pore pressures

Figure 7.5 presents excess pore pressure contours for SG3 considering dissipation initiation times for the soil near the external drain rings, at the end of shaking and at t=81.7 s in the FE analysis. The generation of excess pore pressures near the drain rings presented lower values at the end of the shaking compared with the CM, particularly near the internal drain (Fig. 7.5a). Dissipation started close to the internal drain at t=12 s in NM (see Fig. 7.4a). This early dissipation was principally influenced by the excess pore pressures hardly arriving at this location rather than the action of the internal drain. On the other hand, dissipation at this same location started eight seconds later (t=22.8 s) in CM, showing a slight increment of pore pressures close to the sub-perimeter drains and complete liquefaction near the perimetral ring (see Fig 7.4).

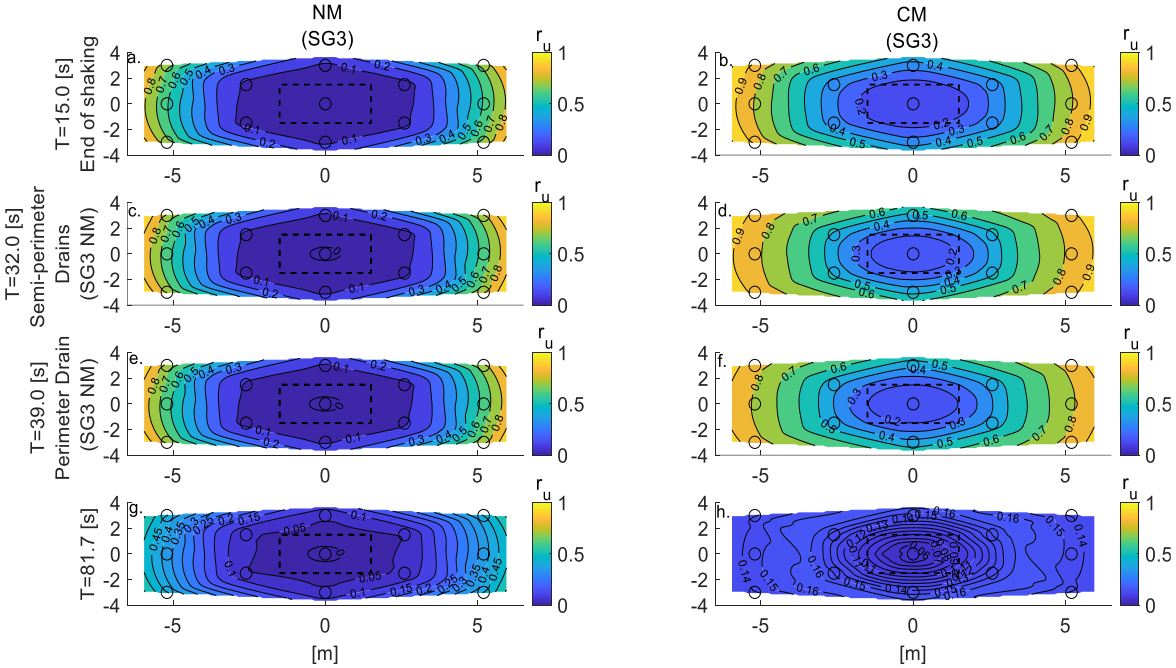

Fig. 7.5 Horizontal contours of excess pore pressure ratios (r_u) for SG3 in NM and CM at depth of 2.1m

At t=32 s, the flowfront arrived near the sub-perimeter drains in NM after reaching a peak magnitude of 0.18 (Fig. 7.5c). At this time, only a slight reduction of excess pore pressures was observed near the internal drain in NM, while a greater rate of dissipation was registered below the foundation in CM (Fig. 7.5d). The soil close to the sub-perimeter drains in CM presented a faster dissipation initiation (t=26 s). A greater rate of dissipation was registered below the foundation in CM compared with the NM due to the increase of C_v

during the reconsolidation stage. The soil close to the perimeter drains started to dissipate at very similar times in NM and CM, after reaching complete liquefaction. The flowfront arrived near the perimeter drains at t=39 s in NM (Fig. 7.5e), while dissipation began at t= 41 s in the physical model. The soil near the internal and the sub-perimeter drains presented an evident reduction of excess pore pressures in CM at this time, while no significant drop of r_u ratios was observed at both locations in NM (Fig. 7.5f). Thirty seconds later, the area below the foundation showed complete dissipation in NM, while the soil adjacent to the sub-perimeter drains was still dissipating (Fig. 7.5g). At the same time, the entire layer in CM showed low r_u values, including the soil surrounding the external drains. (Fig. 7.5h).

The soil in NM exhibited similar behaviour to that observed in CM, in which a faster flowfront arrival was observed for the internal drain compared with the zone at the outer rings; nevertheless, an early dissipation was registered for the soil near the internal drain, suggesting inaccurate modelling of the soil dissipation behaviour below the foundation. Furthermore, even though the 3D FE analysis presents a good match in terms of dissipation starting times for the external rings in NM and CM, the rate of reconsolidation varies as a response to the C_v factor variation in CM, reducing similarities in the dissipation simulation between both cases.

Foundation settlement

Figure 7.6 shows the foundation settlement in SG3 obtained from NM and CM analysis. Settlement of the foundation reached a value of 419 mm in NM during the "shaking". Although this amount was only 3% greater compared with the amount obtained in CM during this stage, this first one was generated principally by the degradation in soil stiffness that enabled significant deformation below the foundation rather than the excess pore pressure generation. Moreover, an upward behaviour of the foundation was observed during the addition of the excess pore pressure at the boundary nodes, as a response to the applied seepage force in a volume with low stiffness.

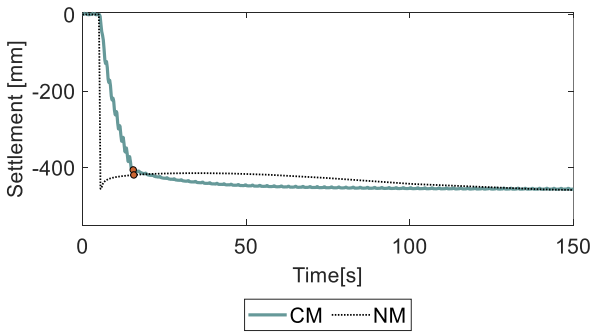

Fig. 7.6 Settlement time-histories of the foundation for SG3 in NM and CM

The foundation in NM reached 9% of the total permanent settlement during the dissipation stage, which represented a value of 40 mm. This amount signifies 82% of the settlement obtained in CM during dissipation, presenting a tolerable match of results between the numerical and physical models. The limited excess pore pressures generated below the foundation in NM were dissipated by the drains, allowing minor volumetric and deviatoric strains. Moreover, although lower excess pore pressure ratios were recorded below the foundation in NM compared with CM, a longer time was required for the foundation to cease settlement in NM. The time required for the structure to settle in the FE analysis differs by 20 seconds from the time required in CM, representing a limitation to be considered in the numerical model evaluation.

7.4.1.1 Alternative model SG3V

In the previous analysis, insignificant excess pore pressure generation and imprecise dissipation soil behaviour were observed below the foundation in the numerical model SG3 (SG3NM). Even though the foundation settlement response during the "shaking" is not the main objective, adequate modelling of excess pore pressure generation provides a more accurate dissipation behaviour of the soil and foundation settlement response during the reconsolidation stage.

Considering that one of the key difficulties observed in the numerical model was the stratum geometry and how far the soil boundaries were located from the foundation, a variation in the original model (SG3V) was required to model the accurate propagation of excess pore pressures below the foundation, while keeping the computation times reasonable.

The original model length and width dimensions were reduced by 47% and 44% (Fig 7.7), respectively, limiting the evaluation to the area involved by the sub-perimeter drains. The excess pore pressure (Δu) was applied as a boundary condition near the sub-perimeter drains considering the peak values obtained at the end of the shaking from the centrifuge test. In the physical model, Δu values were recorded at two different depths in the soil. To estimate Δu at different depths, an excess pore pressure profile was approximated by a polynomial function of order 3 (cubic). The approximate profile satisfied the condition of $\Delta u = 0$ at $z = 0$, and zero excess pore pressure gradient at the base of the liquefiable layer (Brennan, 2004). The relationship found between Δu and z, and the approximate excess pore pressure profile are shown in Fig. 7.8. In addition, the soil initial stiffness was slightly elevated to 1.45%E in this model, for an accurate settlement simulation.

Excess pore pressure generation and dissipation

Figure 7.9 shows excess pore pressure time-histories for the soil near the internal and sub-perimeter drains in SG3V and SG3CM. The r_u ratio near the internal drain reached a value of 0.05, which represented a quarter of the peak value obtained in CM (Fig. 7.9a). For the soil near the sub-perimeter drains, the excess pore pressure presented a closer result compared with the value obtained in CM due to the boundary condition, reaching a peak magnitude of 0.5 (Fig. 7.9b). Although the model dimensions were modified, the peak ratios obtained near the internal and sub-perimeter drains continued to be lower compared with CM. The high constant permeability magnitude, utilised since the start of "shaking" in NM, enabled a significant control of excess pore pressure generation in the soil compared with the CM. On the other hand, this modified model presented a significant increment in the excess pore pressure generation compared to the previous FE model (SG3NM).

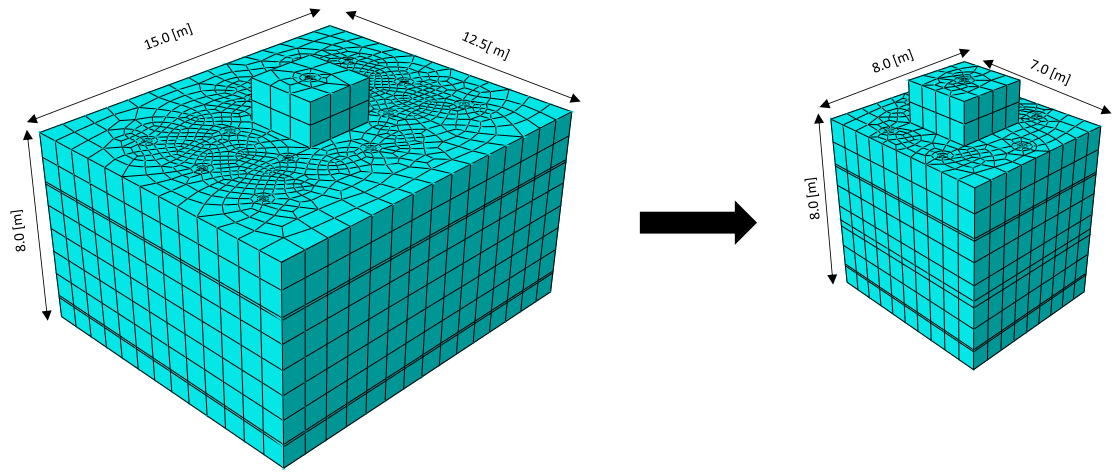

Fig. 7.7 Variation in SG3 original dimensions

Contours of excess pore pressure dissipation were plotted for SG3V and SG3CM with consideration of the flowfront arrival times for the drain rings in the modified FE model (SG3V). Dissipation started at t = 25.6 s below the foundation in SG3V (Fig. 7.10a); a similar starting time was obtained for the same location in SG3CM. Greater values were observed at this time near the sub-perimeter drains in the numerical and physical model, while lower ratios of 0.05 and 0.2 were registered close to the internal drain (Fig. 7.10b). Although excess pore pressure near the internal drain continued to be a lower value compared with CM, a significant improvement in the soil dissipation behaviour was obtained by varying the original FE model.

The soil surrounding the sub-perimeter drains started to dissipate at t=31.8 s, after reaching a peak ratio of 0.5 (Fig. 7.10c). At this time, slight dissipation was observed below the foundation in SG3V, while the soil near the perimeter drains in SG3CM was already dissipating as the flowfront arrived five seconds earlier (Fig. 7.10d). In addition to the faster flowfront arrival at the sub-perimeter drains, a greater rate of dissipation was observed in CM. Fifty seconds later, a significant reduction of excess pore pressures was observed in the entire layer of CM, presenting values of 0.08 and 0.15 near the internal and sub-perimeter drains (Fig. 7.10e), while a slower dissipation was registered in NM (Fig. 7.10f).

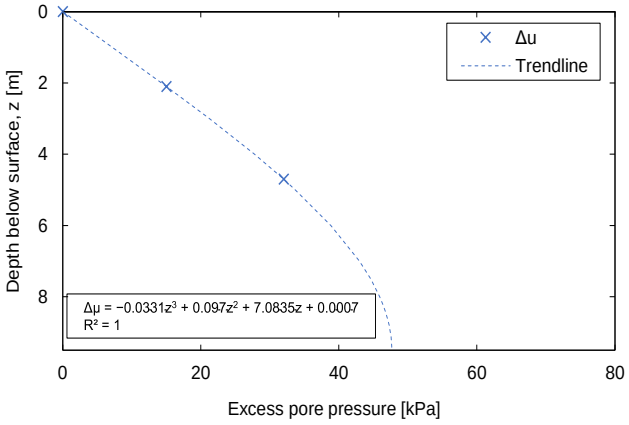

Fig. 7.8 Excess pore pressures profile for the soil adjacent to the sub-perimeter drains in centrifuge test SG3

Improved simulation of the soil behaviour during the dissipation stage, showing accurate flowfront arrivals for the soil around the drain rings, was attained by using the alternative SG3V model.

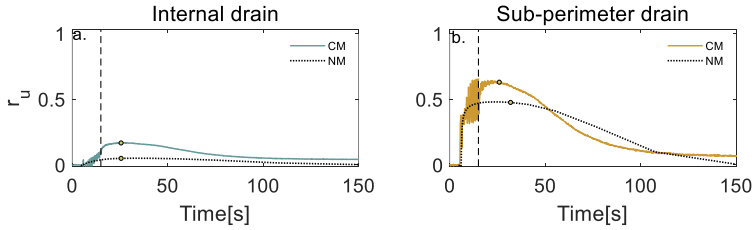

Fig. 7.9 Excess pore pressure ratios (r_u) time-histories for SG3V and SG3CM, at depth of 2.1m

Settlement of the foundation

Figure 7.11 presents the foundation settlement response for SG3V and SG3CM. Similar permanent settlement of 455 mm were obtained in the numerical and physical models,

showing significant settlement during the "shaking" stage in both cases. Similar to the case of the original finite element case (SG3NM), the foundation settlement in SG3V was mainly achieved by the low level of soil stiffness; however, an incremental settlement was observed before the end of the "shaking", explained by the raise in excess pore pressures below the foundation that enabled a more continuous settlement response.

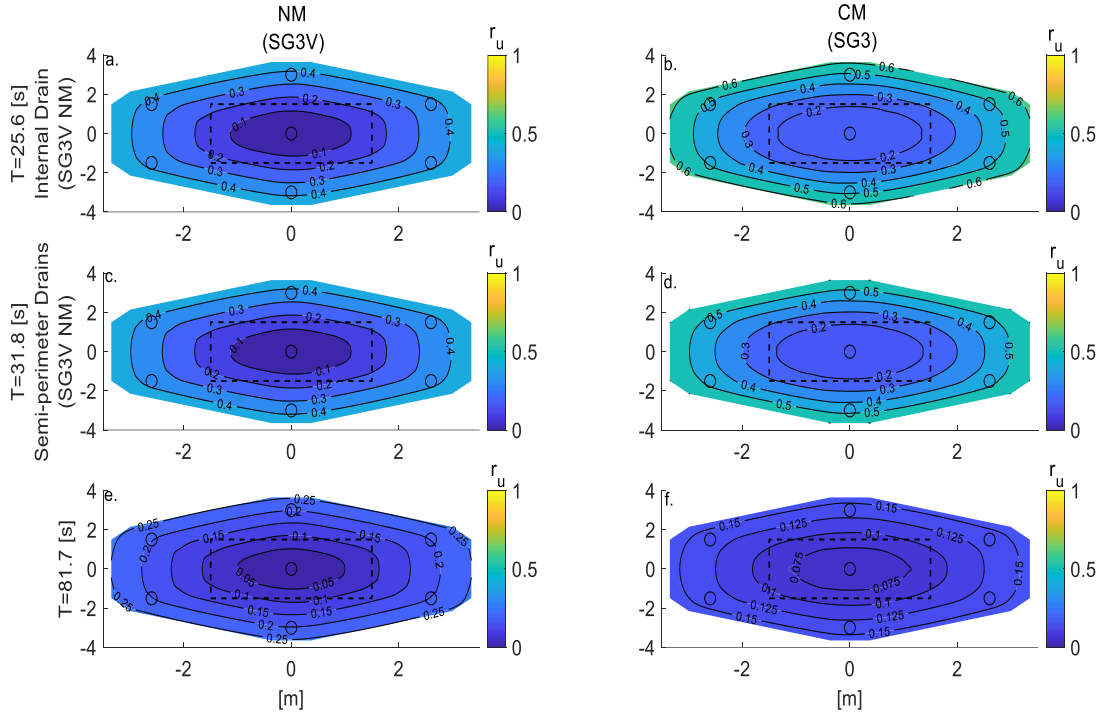

Fig. 7.10 Horizontal contours of excess pore pressure ratios (r_u) for SG3V and SG3CM at depth of 2.1 m.

The foundation settlement reached 54 mm during the dissipation stage in SG3V, a value close to the amount obtained in SG3CM (49 mm). The action of the internal drain led to a rapid dissipation in SG3V, limiting volumetric and deviatoric strains under the foundation. Although minor excess pore pressures were registered below the foundation, the slower rate of reconsolidation in SG3V allowed similar foundation settlement in the numerical and physical models.

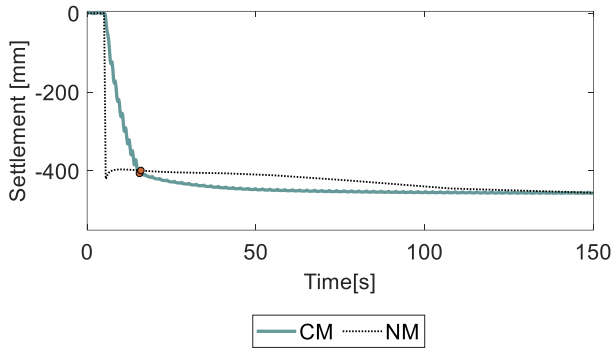

Fig. 7.11 Settlement time-histories of the foundation for SG3V and SG3CM

The increment of r_u ratios below the foundation enhanced the simulation of the settlement response during the "shaking" and dissipation stage, enabling a comparable response to that obtained in the centrifuge test.

7.4.2 The 17-drain arrangement below the foundation (SG4)

The performance of the 17-rubble brick drain arrangement below a foundation of 150 kPa (SG4) is evaluated using numerical modelling methodology. A comparative analysis considering the results from physical model SG4 is presented in this section.

Excess pore pressure generation

Figure 7.12 presents excess pore pressure time-histories for SG4, at the top layer, considering the soil close to the internal, edge, sub-perimeter and perimeter drain rings in NM and CM. Excess pore pressure ratios near the internal and edge drains in NM reached smaller values of 0.015 and 0.02 compared with the soil at the outer rings (Fig. 7.12a and b), as a consequence of the significant confining pressure exerted by the foundation. The edge drains enabled an enhanced performance of the soil below the foundation, in terms of limited excess pore pressure generation, verifying the relevance of a great area replacement ratio (A_r) under the structure. Although a slightly larger value was observed near the edge drains compared with the internal drain, these values did not accurately represent the excess pore pressure generation. Similar to the soil near the internal drain in SG3NM, r_u ratios under the foundation represented a minimal value compared with the ratios obtained in the centrifuge test. Moreover, the soil near the sub-perimeter drains reached a peak ratio of 0.24 after the "shaking", representing 40% of the maximum value registered for the same location in CM (Fig. 7.12c). The soil near the perimeter drains showed more similar r_u values in NM and CM as expected, in response to the soil boundary condition (Fig. 7.12d).

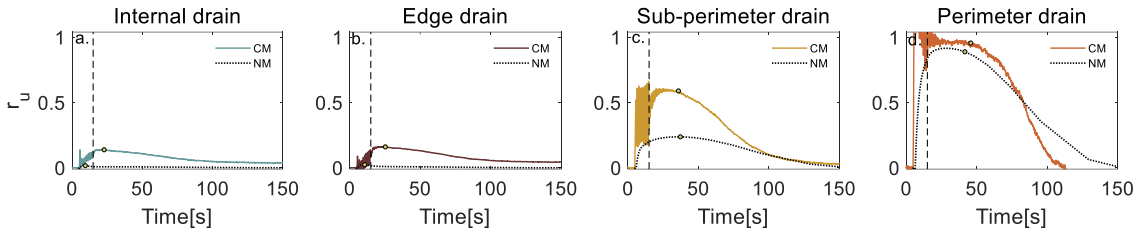

Fig. 7.12 Excess pore pressure ratios (r_u) time-histories for SG4 in NM and CM, at depth of 2.1m

Dissipation of excess pore pressures

Contours of excess pore pressure dissipation for SG4 are presented in Figure 7.13 considering the numerical and physical analyses. At the end of the shaking, the soil near the internal and edge drains exhibited negligible excess pore pressure generation in NM compared with the soil at the outer rings (Fig. 7.13a). Meanwhile, the soil near the internal and edge drains presented higher ratios of 0.14 and 0.16 in CM (Fig. 7.13b). Although a faster flowfront arrival was observed near the internal drain and then at the edge ring, dissipation at both locations was initiated before the end of the "shaking" with no significant difference in the dissipation starting times between them; this suggested a weak action and inaccurate performance of the edge drains in the numerical model (see Fig. 7.12a and b). Similar to SG3NM, this behaviour verifies the technique limitation in terms of excess pore pressure dissipation below the foundation.

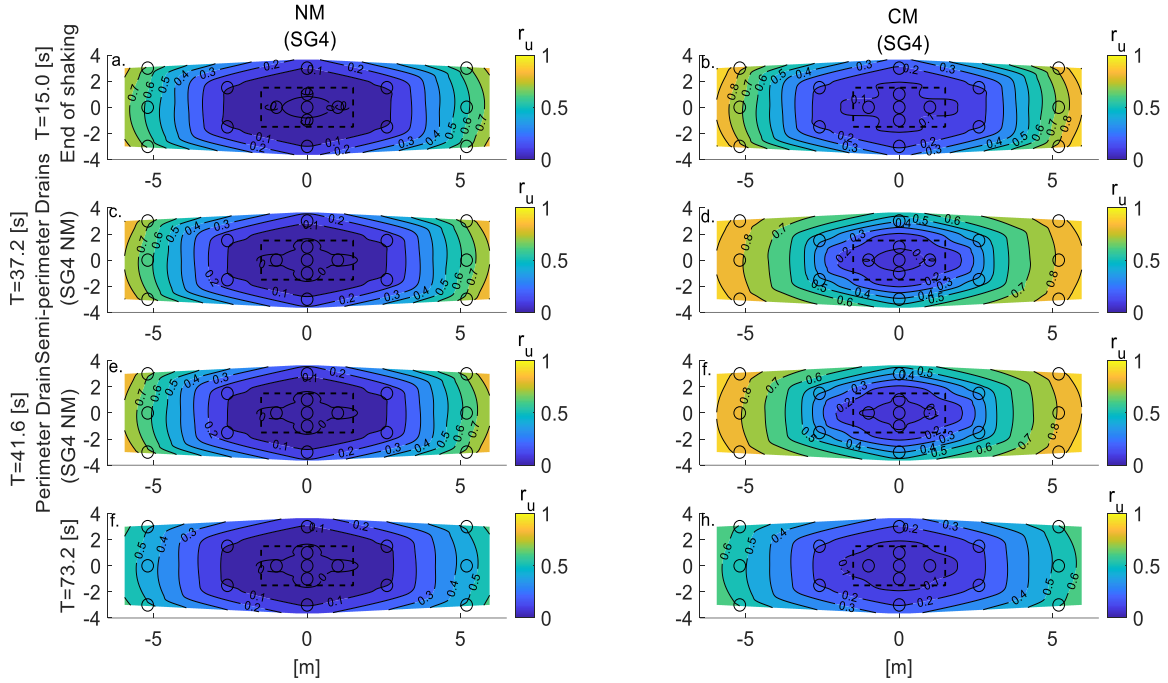

Fig. 7.13 Horizontal contours of excess pore pressure ratios (r_u) for SG4 in NM and CM at depth of 2.1m

Dissipation near the sub-perimeter drains started at t=37.2 s in NM, showing a peak value of 0.24 (Fig. 7.13c). At this time, slight dissipation was observed below the foundation, while the soil close to the perimeter drains still presented higher values. Dissipation close to the sub-perimeter drain in CM started at a very similar time (t=35.8s); however, the soil under the foundation presented a greater rate of dissipation compared with NM. The soil adjacent to the perimeter drains in NM and CM started to dissipate at t = 41.6 s and t=45.8 s respectively. Slight dissipation was observed near the internal, edge and sub-perimeter drain in NM at t=41.6 s (Fig. 7.13e), while a more significant drop in excess pore pressures ratios was observed in CM for the entire layer (Fig. 7.13f). Finally, excess pore pressure dissipation was observed in NM at t = 73.2 s, showing insignificant r_u ratios near the internal and edge drains, while the sub-perimeter and perimeter drains exhibited higher values (Fig. 7.13g). The soil below the foundation presented a high rate of dissipation in CM at this time, showing r_u magnitudes of 0.07 and 0.1 near the internal and edge drains (Fig. 7.13h).

The FE model did not present accurate results in terms of excess pore pressure generation due to limitations of the technique. The minimal excess pore pressures and the inaccurate dissipation behaviour, particularly below the foundation, impeded the verification of the effective performance of the additional edge drains in terms of accelerated dissipation close to the central drain.

Settlement of the foundation

The foundation settlement in SG4 reached a total value of 345 mm in NM and CM (Fig. 7.14). Settlement of the foundation in NM reached a value of 315 mm during the "shaking" stage, 2% greater than CM. Similar to the previous case, this response was significantly controlled by the minor soil stiffness as minimal generation of excess pore pressures was registered below the foundation. Moreover, a slight heave of the foundation was observed during the excess pore pressure insertion in the soil as part of the technique limitations.

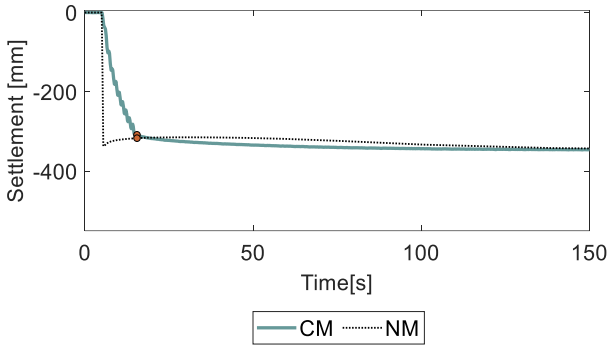

Fig. 7.14 Settlement time-histories of the foundation for SG4 in NM and CM

A small settlement of 30 mm was reached after the "shaking" in NM, a slightly lower value compared with the amount obtained in CM during the dissipation stage (35 mm). The low level of excess pore pressures was easily dissipated by the rubble brick drains, enabling a significant reduction in the deviatoric and volumetric strains below the foundation. The excess pore pressure near the internal and edge drains in NM required a longer time to complete dissipation compared with CM, resulting in a longer time being required for the foundation to stop settling.

Similar results, in terms of settlement response were obtained in the numerical and physical modelling for the generation and dissipation stages; nevertheless, a more accurate simulation of the soil dissipation behaviour and consequent foundation response was required.

7.4.2.1 Alternative model SG4V

Similar to SG3, a variation in the numerical model SG4 was recommended to provide the exact soil dissipation behaviour and an accurate settlement response. The stratum was modified taking into consideration the similar variation in the soil dimensions to SG3V (Fig. 7.15). The excess pore pressure magnitudes for the model boundary condition were obtained

from the cubic polynomial approximation presented in Figure 7.16. In this model (SG4V), soil stiffness of 1.9%E was utilised for the fine and coarse sand.

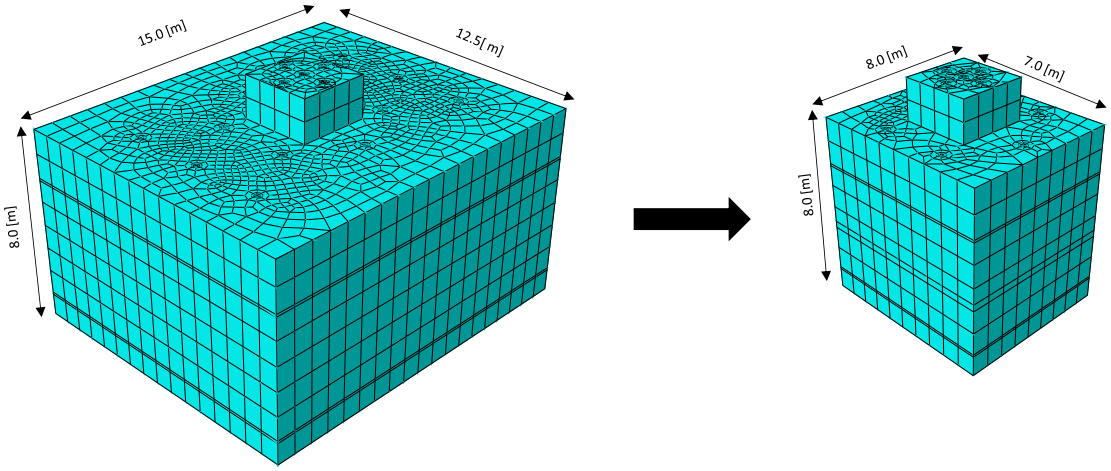

Fig. 7.15 Variation in SG4 original dimensions

Excess pore pressure generation and dissipation

Excess pore pressure time-histories for SG4V and SG4NM are presented in Figure 7.17. The excess pore pressure ratio near the internal drain reached a peak value of 0.03, representing 20% of the peak value obtained in CM (Fig. 7.17a). Similarly, in the soil close to the edge drains a maximum r_u of 0.05 was registered, which was also lower compared with the magnitude in the physical model (Fig. 7.17b). A considerable increment was obtained in the excess pore pressure generation near the internal and edge drains by shortening the FE model. The accurate performance of the edge drains, in terms of excess pore pressure control for the soil surrounding the internal drain was observed. The greater peak ratio near the sub-perimeter drain in SG4V was expected, due to the model boundary condition.

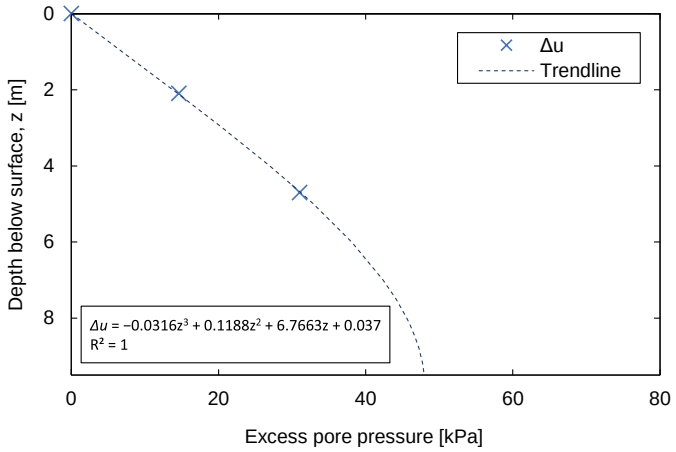

Fig. 7.16 Excess pore pressures profile for the soil adjacent to the sub-perimeter drains in centrifuge test SG4

The soil dissipation behaviour in SG4V and SG4CM is presented in Fig 7.18 considering dissipation initiation times for the soil near the internal, edge and sub-perimeter drains in the modified numerical model. Dissipation near the internal drain in SG4V began at t=22.5 s, after reaching a peak ratio of 0.03 (Fig. 7.18a). A similar flowfront arrival time was observed for the same location in CM. The area below the foundation continued to dissipate due to the action of the edge drains in NM and CM. The flowfront near the edge drains in NM arrived at t=26.6 s (Fig. 7.18c), showing a difference of one second to the dissipation initiation near the edge ring in CM. At this time, no dissipation was observed close to the sub-perimeter drains in both models. An excellent match was obtained for the flowfront arrival times for the drain rings below the foundation, verifying an accurate performance of the drains in the FE analysis; however, the slower rate of reconsolidation compared with CM, continued to be a limitation for the model.

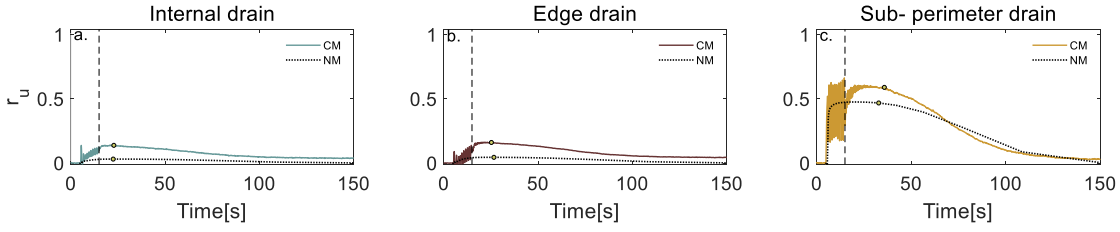

Fig. 7.17 Excess pore pressure ratios (r_u) time-histories for SG4V and SG4CM, at depth of 2.1m

Dissipation at the sub-perimeter drains started at t = 32.8 s, presenting low r_u ratios near the internal and edge drains (Fig. 7.18e). The flowfront arrived three seconds later for the same location in CM; nevertheless, more rapid dissipation of excess pore pressures was observed compared with NM (Fig. 7.18f). The limited "unit cell" behaviour of the sub-

perimeter drains and the delay in the flowfront arrivals near the outer rings due to the additional internal drains observed in the physical model, were verified in the FE analysis. At t = 73.1 s, a significant drop of r_u ratios below the foundation and close to the sub-perimeter drains was registered in CM (Fig. 7.18h), reaching similar ratios as NM for the entire layer.

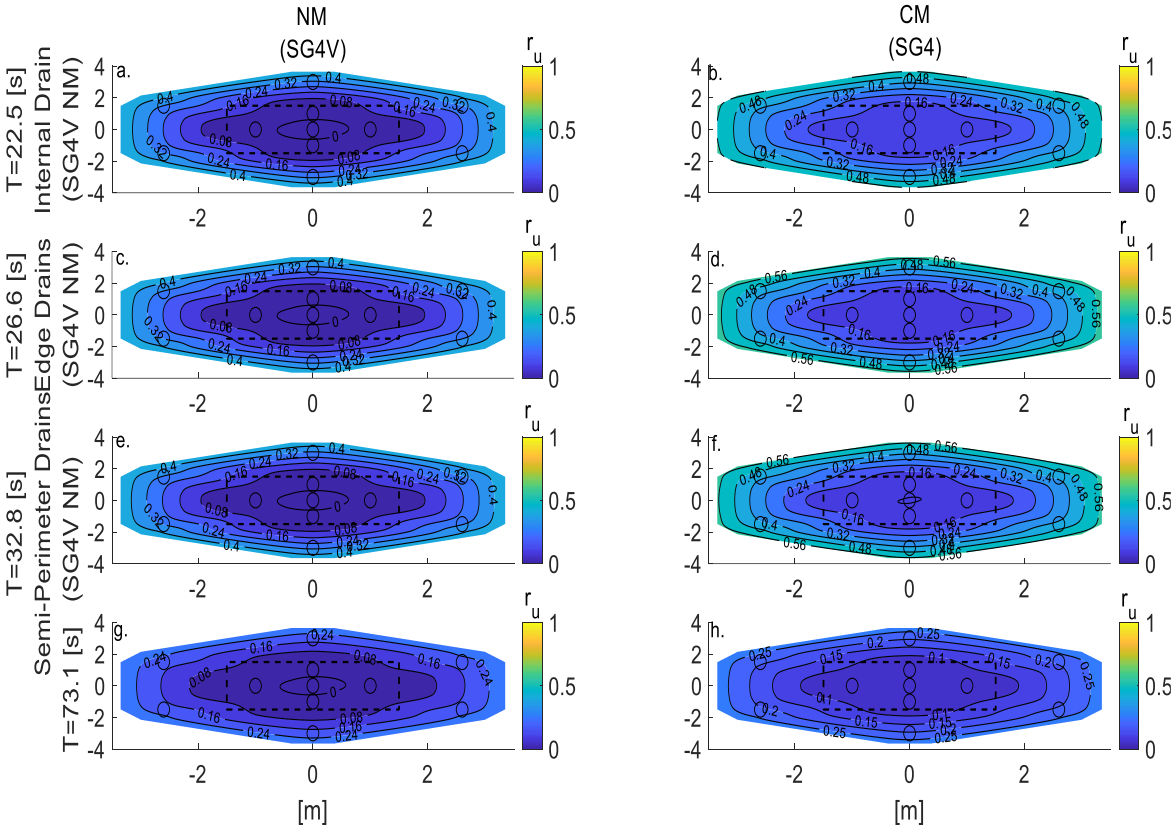

Fig. 7.18 Horizontal contours of excess pore pressure ratios (r_u) for SG4V and SG4CM at depth of 2.1m

Settlement of the foundation

Settlement of the foundation for SG4V and SG4CM is presented in Fig 7.19. The foundation reached a similar settlement of 305 mm during the "shaking" stage in the numerical and physical models. The low stiffness in the soil was the principal factor in the foundation response in SG4V; however, the greater excess pore pressure ratios below the foundation enabled a positive settlement response of the structure before the end of the "shaking".

The rapid dissipation of excess pore pressures near the internal, edge and sub-perimeter drains reduced the time during which the high excess pore pressures were maintained, limiting the foundation settlement to a value of 36 mm in NM, 2 mm lower compared with the foundation response in CM. In addition to the similar total settlement reached in both

the numerical and physical models, a significant improvement in the simulation of the soil behaviour during the generation and dissipation stages was observed by modifying the original stratum geometry.

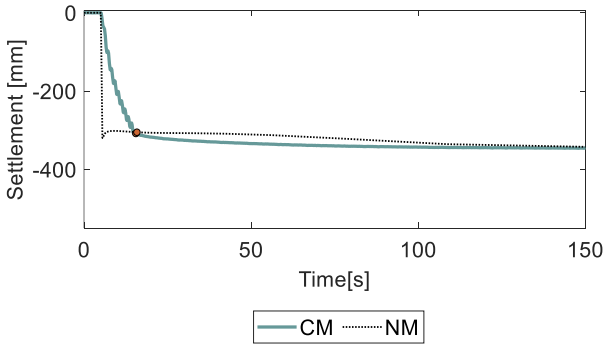

Fig. 7.19 Settlement time-histories of the foundation for SG4V and SG4CM

7.4.3 The one column arrangement below the foundation (SG9)

FE analysis for SG9 is presented in this section considering a comparative evaluation with the results obtained in the centrifuge test. In this case, the dimensions of the original model were changed due to technique limitations previously analysed. The modified model considers a reduction in the stratum's length from 12.5 m to 15 m. The boundary condition considers the additional excess pore pressures in the free field; however, the comparative analysis between NM and CM during the dissipation stage is not considered for the free field as they do not represent the same location in the stratum.

Excess pore pressure generation

Figure 7.20 presents excess pore pressure time-histories for the soil at distances of 1.75 m, 5.25 m and in the free field, at depth of 2.1 m, for NM and CM. The r_u ratio reached a low value of 0.07 near the column in NM due to its proximity to the pillar and the significant confining pressure exerted by the foundation (Fig. 7.20a). A lower excess pore pressure was observed for the soil near the internal drain in NM compared with the CM, reaching 30% of the peak ratio obtained in the centrifuge test. This model presented a reduction in the original stratum length; however, the difference between the r_u ratios in CM and NM continued to be significant for the soil near the column. This behaviour occurred due to the greater permeability utilised in NM from the initiation of the "shaking", leading to higher control of excess pore pressures in the soil. On the other hand, the soil at further distances and near the boundaries of the stratum presented similar generation behaviour between NM and CM, showing complete liquefaction at 5.2 m and the free field (Fig. 7.20b and c). Similar to the physical model, the column in NM was unable to avoid complete liquefaction for distances

of at least 5.2 m due to the column's infinite spacing and the negligible influence of the pillar in controlling excess pore pressure generation at further locations.

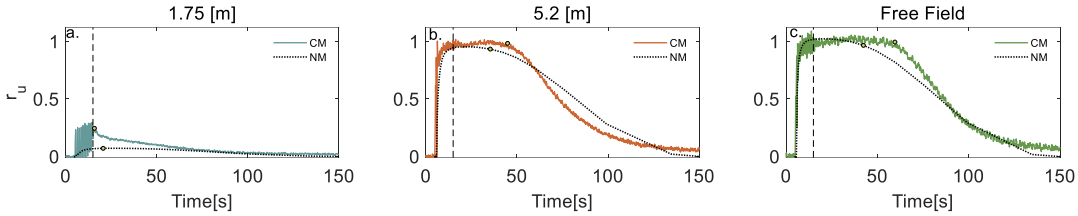

Fig. 7.20 Excess pore pressure ratios (r_u) time-histories for SG9 in NM and CM, at depth of 2.1m

Dissipation of excess pore pressures

Contours of excess pore pressure ratios for NM and CM are presented in Figure 7.19. Dissipation initiation times for distances of 1.75 m and 5.2 m from the foundation central axis were considered, including the end of the shaking and t=75 s. At t=15 s, lower excess pore pressure generation was observed near the column in NM, while greater ratios of r_u =1 were reached at a distance of 5.25 m (Fig. 7.21a). Meanwhile, similar behaviour was observed in CM, presenting a higher r_u magnitude near the rubble brick column compared with NM (Fig. 7.21b).

Dissipation close to the column started at t=20.6 s due to the fast fluid flow towards the column (Fig. 7.21c). This fast dissipation was generated as a response to the column's proximity and the great confining pressure. At this time, greater r_u values were registered in NM and CM at further locations, including the soil at 5.2 m and the free field. Similar to CM, dissipation in NM first occurred near the column, while the soil located further from it required a longer time to dissipate.

Dissipation at 5.25 m from the column began at t=35.5 s in NM, showing a slight drop of excess pore pressures near the column (Fig. 7.21e), while a significant rate of dissipation was observed in CM close to the pillar (Fig. 7.21f). Greater ratios were registered at 5.25 m in CM at this time, starting to dissipate at t=44.9 s. At t=75.6 s, a high r_u ratio of 0.5 was registered in NM from a radial distance of 5.2 m (Fig. 7.21g), while a value of 0.4 was observed at the same distance in CM. Moreover, the soil surrounding the foundation presented almost complete dissipation in CM at this time (Fig. 7.21h), while higher ratios were observed in NM. No increment in the rate of reconsolidation was observed in presence of the granular column in NM, contrasting with the behaviour observed in CM. Dissipation at shorter and further radial distances from the column required a longer time to finish reconsolidation in NM compared with CM.

The “infinite cell” behaviour of a single column during the generation and dissipation stages was possible to model using this simplified technique. The excess pore pressure generation and the following dissipation was highly influenced by the proximity of the column and the foundation confining pressure, as previously observed in the centrifuge test. Nevertheless, in addition to the limitations in terms of excess pore pressure generation, differences were raised during the dissipation stage due to the slower rate of reconsolidation, with greater evidence at further distances. The use of this numerical model provides accurate results for a limited area around the single column and could be applied for the estimation of the column’s radial influence during the generation and dissipation stages. On the other hand, the imprecise dissipation behaviour at farther distances, could represent an overestimation of the number of drains required for the soil mitigation.

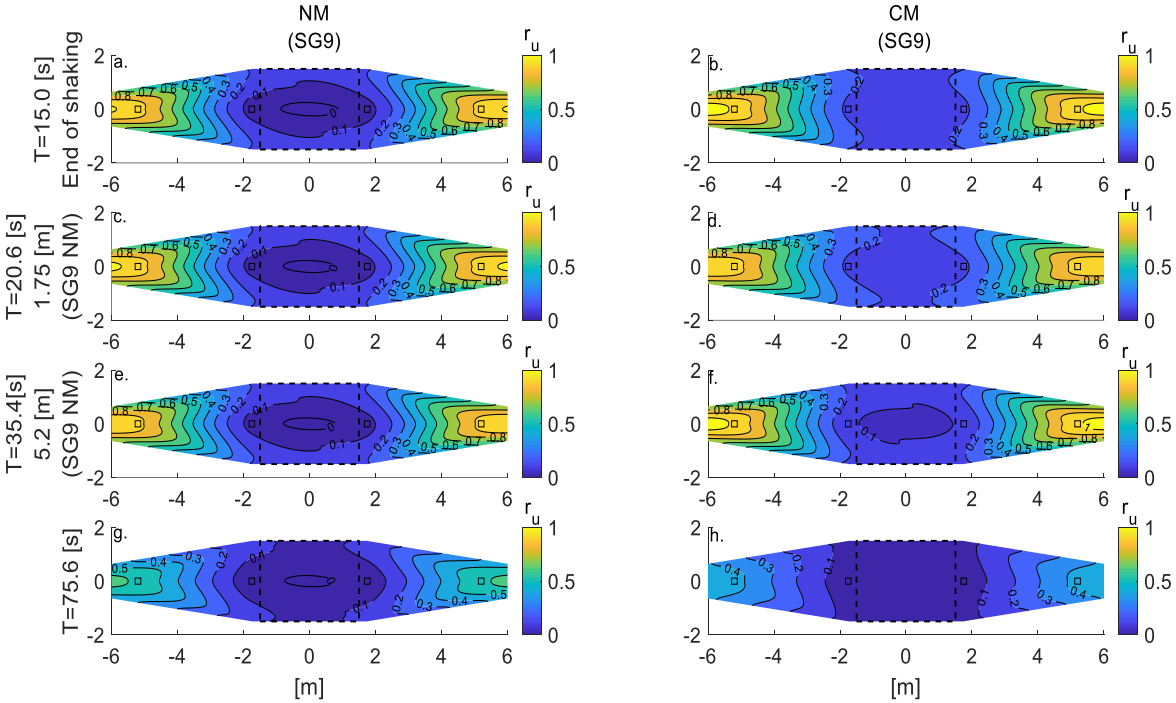

Fig. 7.21 Horizontal contours of excess pore pressure ratios (r_u) for SG9 in NM and CM, at depth of 2.1m

Settlement of the foundation

Figure 7.22 presents the foundation settlement obtained from NM and CM analysis for SG9. Settlement of the foundation reached a value of 373 mm in NM during the “shaking”, in response to the column’s minor stiffness and the additional excess pore pressures around the rubble brick, enabling greater volumetric and deviatoric strains. This value was similar to the settlement obtained in CM, suggesting an optimum match between the FE and the physical model in terms of the settlement response during the “shaking”. Settlement during

the dissipation stage reached 16 mm, only 2 mm greater compared with CM. The area surrounding the column in NM, which represented a high-risk zone, showed rapid fluid flow towards the column, reducing deformations below the foundation to a minimum value.

The foundation settlement reached a total value of 389 mm in the FE analysis. Similar to the previous cases, a good match in settlement response during the generation and dissipation stages was obtained in the numerical and physical models; however, the longer time needed for the excess pore pressure to dissipate in the soil surrounding the column in NM influenced the simulation of the foundation response.

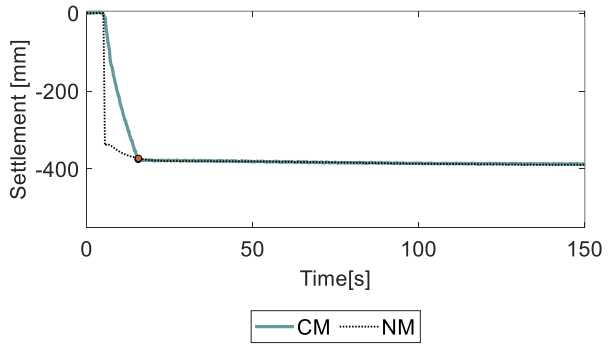

Fig. 7.22 Settlement time-histories of the foundation for SG9 in NM and CM

7.5 Arrangement of rubble brick perimeter drains below existing buildings

The performance of vertical perimeter drains below a foundation of 150 kPa (SG8) is evaluated using FE analysis in this section. The model considered a reduction in the original dimensions of the stratum, presenting a cross-sectional area of 9 m × 9 m. Similar to the previous case, the additional excess pore pressures, as a boundary condition were considered for the free field. The comparative analysis between NM and CM for SG8, considering EQ2 is developed in this section. The comparison of the free field behaviour in the numerical and physical modelling, during the reconsolidation stage is not presented as they represent different locations in the soil. The stiffness parameter utilised for the model was 1.1%*E*.

Excess pore pressure generation

Excess pore pressure time-histories at the top layer for NM and CM, are presented in Fig. 7.23. The soil below the foundation in NM reached a maximum r_u value of 0.04 (Fig. 7.23a), a lower ratio compared with the soil surrounding the perimeter drains due to the greater pressure exerted by the foundation and the effective control of the perimeter drains. Complete liquefaction was observed in the free field in NM (as in CM) due to the excess

pore pressure fluid boundary condition (Fig. 7.23c). The peak r_u values obtained in the soil below the foundation and near the perimeter drains represented 20% and 80% of the maximum values in CM. Although the model was shortened, the high initial constant permeability enabled significant control of the excess pore pressures under the foundation during the "shaking".

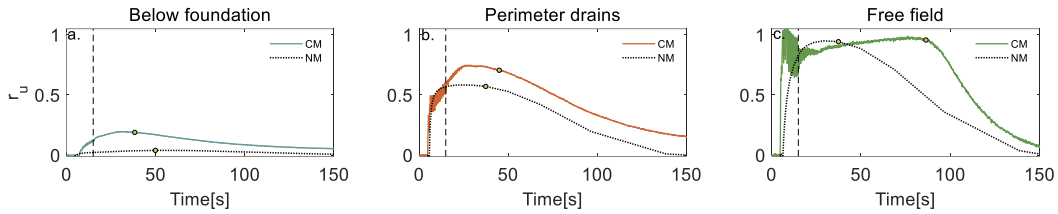

Fig. 7.23 Excess pore pressure ratios (r_u) time-histories for SG8 in NM and CM, at depth of 2.1m

Dissipation of excess pore pressures

Contours of excess pore pressures ratios are presented in Fig 7.24, considering the end of shaking, dissipation initiation times for the soil below the foundation and near the perimeter drains in NM and when t=87.1 s. At the end of the shaking, lower r_u values were generated in NM below the foundation, while greater ratios of 0.58 were reached in the soil near the perimeter drains (Fig. 7.24a). Contrastingly, similar r_u ratios were registered close to the perimeter drains in CM; however, a greater value was observed below the foundation compared with NM at this time (Fig. 7.24b).

The flowfront arrived in the soil around the perimeter drains at t=37.4 s in NM, after reaching a peak value of 0.6 (Fig. 7.24c), while no dissipation was observed at this layer in CM (Fig. 7.24d). Twelve seconds later, the excess pore pressures began to dissipate in the area below the foundation in NM (t=49.9 s) (Fig. 7.24e). Values of 0.04 and 0.5 near the perimeter drains and under the foundation were observed at this time in NM, while the soil at both locations in CM was already dissipating (Fig. 7.24f). Contrary to the soil dissipation behaviour in CM, which showed a faster flowfront arrival below the foundation compared with the perimeter drains, dissipation initially occurred around the perimeter drains in NM. The slower rate of reconsolidation in NM limited the radial fluid flow from the area below the foundation towards the perimeter drains, enabling a much more independent behaviour of the columns compared with CM and a faster dissipation near the vertical drains. At t= 87.1 s, a significant drop in excess pore pressures was observed in the physical model (Fig. 7.24g), while a slight decrease of pore pressures was registered in the entire layer of NM (Fig. 7.24h).

The influence of the constant radial distance from the drains to the foundation in the arrangement performance was observed in the FE analysis. The slower rate of reconsolidation presented in the soil reduced the drains' effective action compared with the

column's behaviour in the physical model. The accentuated, independent performance of the drains limited the rapid fluid flow from the area below the foundation, thus becoming a limitation for the dissipation simulation.

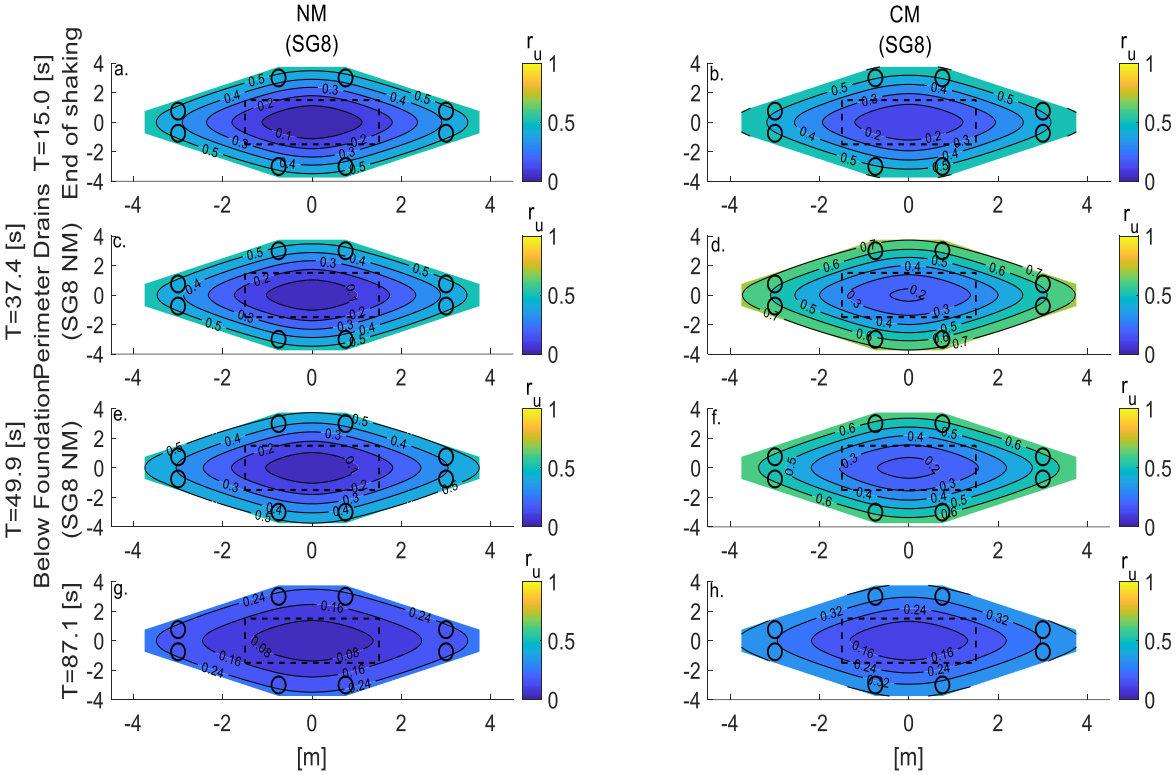

Fig. 7.24 Horizontal contours of excess pore pressure ratios (r_u) for SG8 in NM and CM at depth of 2.1m

Settlement of the foundation

Settlement of the foundation in NM during the generation stage reached a value of 405 mm, which represented 94% of the value obtained in CM (Fig. 7.25). In the absence of vertical drains below the foundation, complete dependence on the fine soil stiffness was observed, emphasising the lift of the foundation and the inaccurate settlement simulation of the foundation during the addition of excess pore pressures.

Settlement during the dissipation stage reached a value of 97 mm in NM. This limited settlement was generated due to the effective performance of the perimeter drains that decreased the time during which the high excess pore pressures were maintained and enabled only slight deviatoric and volumetric deformations below the foundation. However, this settlement represented a greater value compared with that registered in CM. Accurate results, to within 29% for the foundation settlement in NM and CM, were obtained; this is a noteworthy value when using the model. The slower rate of reconsolidation and the following major individual behaviour of the drains allowed a longer time for the foundation

to cease settlement in NM, although lower excess pore pressure ratios were reached during the “shaking”.

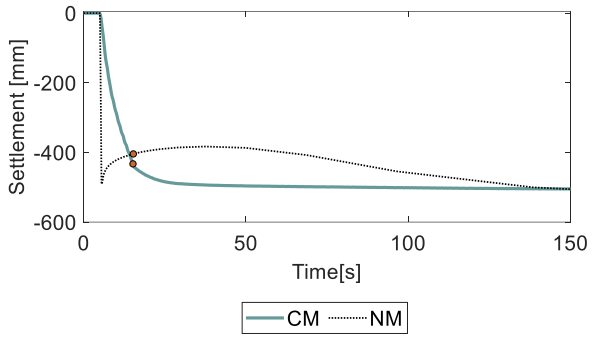

Fig. 7.25 Settlement time-histories of the foundation for SG8 in NM and CM

7.6 Limitations of the model

The simplified technique developed using ABAQUS software, based on the additional excess pore pressures as a boundary condition for liquefaction simulation in the free field presents certain limitations.

- The use of a constant soil stiffness represents the principal limitation for the soil reconsolidation simulation. The variation of E over time could not be modelled in the software, generating an imprecise soil behaviour during the dissipation stage. Additionally, permeability was considered to be a constant factor in the numerical model; nevertheless, this does not represent a major influential factor in the reconsolidation stage (Adamidis and Madabhushi, 2016). The constant permeability presents a considerable effect during the “shaking” stage, as a less accurate prediction in terms of excess pore pressure generation was observed.
- The technique provides less accurate results for larger volumes of soil as the simulation of excess pore pressure generation below the foundation is difficult to achieve.
- The use of a modified model with shorter dimensions to obtain precise results in terms of the generation and dissipation of excess pore pressures represents an attractive and effective option. However, this variation considers excess pore pressure ratios near the sub-perimeter ring as a boundary condition and avoids the evaluation of the perimeter drains performance.
- The addition of pore pressures as an edge condition in the stratum generates a foundation lift for soils with minor stiffness, leading to an imprecise simulation of the settlement response during the generation stage.

- A complete liquefaction behaviour is assumed for the free field in the model; nevertheless, this will not always be the case in real conditions.
- It must be noted that this numerical technique was developed using a foundation bearing pressure of 150 kPa. Therefore, the influence of using different surcharges needs to be studied in future work since there will be an effect of this parameter on other variables, such as stiffness and permeability, accentuating the limitations of this technique.

7.7 Calibration parameters

The numerical model of drain arrangements involved the calibration of soil stiffness (E) and permeability (k) as previously mentioned. These set of parameters were calibrated based on the results obtained in the physical models, considering the excess pore pressure dissipation and settlement response of the foundation. In order to explore the influence of these parameters (E and k) in the numerical model response, three stages of calibration were performed:

1) Calibration of numerical model SG2, and then modelling the other cases (SG3, SG3V, SG4, SG4V, SG9 and SG8) using the same SG2 set of parameters. It was found that parameters fitting SG2 did not fit the other numerical models.
2) Calibration of numerical models SG3, SG3V, SG4, SG4V, SG9 and SG8 (SG2 model was calibrated in the previous stage).
3) Finding an average set of parameters that provide as adequate fit to all the cases simultaneously. It was found that no single set of parameters could fit all the models at the same time.

Each stage is described in the following sections, including the main results and limitations.

7.7.1 Calibration of numerical model SG2

A set of calibrated parameters E and k was achieved for SG2, providing an optimal simulation of the soil and foundation response. It was found that a soil stiffness of 8.5%E and a permeability of k_d=0.045 m/s gave an adequate match compared to the physical model (CM). Nevertheless, the use of this same set of parameters for the analysis of the other six drain configurations (SG3, SG3V, SG4, SG4V, SG9 and SG8) led to a deficient simulation in terms of settlement of the foundation and dissipation behaviour of the soil. Table 7.3. presents results of foundation settlement and drains flowfront arrivals for the different models in which rubble brick drain arrangements were analysed, utilising the calibration parameters of SG2. Results obtained in CM are also presented.

Table 7.3. Chart of results obtained in CM and NM using calibration factor of 8.5%E and k_d=0.045 m/s (prototype scale).

Drain arrangement	Total settlement NM [m]	Total settlement CM [m]	Flowfront arrival time NM [s]				Flowfront arrival time CM [s]			
			Internal drain/1.75 [m]	Edge Drain	Sub perimeter Drains	Perimeter Drain/5.2 [m]	Internal drain/1.75 [m]	Edge Drain	Sub perimeter Drains	Perimeter Drain/5.2 [m]
SG2	0.258	0.258	45.0	—	—	46.4	44.8	—	—	47.5
SG3	0.065	0.456	20.3	—	28.1	35.1	25.6	—	26.0	40.9
SG3V	0.066	0.456	24.4	—	28.1	—	—	—	—	—
SG4	0.059	0.345	20.4	23.4	27.8	34.4	22.8	25.3	35.8	45.8
SG4V	0.053	0.345	20.1	20.1	26.6	—	—	—	—	—
SG9	0.033	0.387	19.7	—	—	26.6	15.8	—	—	44.9
SG8	0.068	0.505	28.4	—	—	35.4	38.3	—	—	49.8

From the results, it can be seen that the foundation settlement values for the rubble brick drain cases (SG3, SG3V,SG4,SG4V, SG9 and SG8) are significantly lower compared to the values obtained in the physical model, approximately 12% of the settlement obtained in CM. As previously stated, the soil stiffness (E) is the main parameter that controls the foundation settlement in the numerical model. Therefore, in order to model an accurate settlement response for SG3, SG3V, SG4, SG4V, SG9 and SG8, a lower value of soil stiffness (E) needs to be used. Moreover, although the flowfront arrivals obtained for SG3V and SG4V using k_d = 0.045 m/s, do not differ significantly from the flowfront arrivals obtained in the physical model, this parameter required to be variated as flowfront arrivals in the cases of single column (SG9) and perimeter drains below the foundation (SG8) present a significant variation. In order to find an adequate fit for the other cases, a calibration for each model is performed in the next section.

7.7.2 Calibration of models SG3, SG3V, SG4, SG4V, SG9 and SG8

In order to find an adequate fit for the other numerical models (SG3, SG3V, SG4, SG4V, SG9 and SG8), different sets of parameters E and k were calibrated taking to account the response compared to the CM. Table 7.4 summarises the set of calibrated parameters utilised for each drain configuration (E and k), and also includes applied excess pore pressure boundary condition, foundation settlement and flowfront arrivals for NM and CM. Details of soil stiffness reduction and drain permeability values are also indicated in the analysis developed for each arrangement in sections 7.3-7.5.

While these different set of parameters fitting accurately each numerical model could be useful in providing relevant information related to one single model at a time, it is also necessary to find average parameters that can give decent results for all the cases, or at least a greater number of cases simultaneously. In the next section, a sensitivity analysis of *E* and *k* is performed in order to explore the influence of each parameter in the response across numerical models.

Table 7.4. Chart of specific set of calibrated parameters per drain arrangement (prototype scale).

Drain arrangement	Reduced value of soil stiffness %E (fine and coarse material)	Permeability *k* [m/s]		Application of excess pore pressure boundary condition	Total settlement NM [m]	Total settlement CM [m]	Flowfront arrival time NM [s]				Flowfront arrival time CM [s]			
		Drain	Fine soil				Internal drain/1.75 [m]	Edge Drain	Sub perimeter Drains	Perimeter Drain/5.2 [m]	Internal drain/1.75 [m]	Edge Drain	Sub perimeter Drains	Perimeter Drain/5.2 [m]
SG2	8.5	0.07	0.001	Free field	0.258	0.258	45.0	—	—	46.4	44.8	—	—	47.5
SG3	1.3	0.35	0.001	Free field	0.458	0.456	12.3	—	32.0	39.0	25.6	—	26.0	40.9
SG3V	1.45	0.35	0.001	Sub-perimeter drain ring	0.455	0.456	25.6	—	31.8	—	—	—	—	—
SG4	2.1	0.35	0.001	Free field	0.343	0.345	9.4	10.7	37.2	41.6	22.8	25.3	35.8	45.8
SG4V	1.9	0.35	0.001	Sub-perimeter drain ring	0.342	0.345	22.5	26.6	32.8	—	—	—	—	—
SG9	1.1 coarse) 19% (fine)	0.35	0.001	Free field	0.389	0.387	20.6	—	—	35.4	15.8	—	—	44.9
SG8	1.1	0.35	0.001	Free field	0.506	0.505	49.9	—	—	37.4	38.3	—	—	49.8

7.7.3 Average set of parameters

A sensitivity analysis of *E* and *k* parameters was performed for all the different models of drain arrangements. Considering the calibrated values obtained for each case in the previous step, the sensitivity analysis was developed taking into account a soil stiffness reduction of 1.3%*E*, 1.6%*E*, 2%*E* and 4.5%*E* for the fine and coarse sand, while two permeability values (k_d =0.045 m/s and k_d =0.35 m/s) were considered for the column material. The aim was to find an average set of parameters that could fit the results obtained in all the numerical models at the same time. Average parameters could also be useful for modelling new drain configurations without the need of calibration using CM. Appendix B presents the results obtained in the sensitivity analysis.

Results shown in Table 7.5 showed that calibration parameters of 2%*E* and k_d =0.35 m/s allowed an optimal simulation of the foundation settlement and dissipation response of the

soil, particularly in the case of soil containing rubble brick drains below new buildings (Table 7.5).

Table 7.5. Chart of results obtained in CM and NM using calibration factors of 2%*E* and k_d=0.35 m/s (prototype scale).

Drain arrangement	Total settlement NM [m]	Total settlement CM [m]	Flowfront arrival time NM [s]				Flowfront arrival time CM [s]			
			Internal drain/1.75 [m]	Edge Drain	Sub perimeter Drains	Perimeter Drain/5.2 [m]	Internal drain/1.75 [m]	Edge Drain	Sub perimeter Drains	Perimeter Drain/5.2 [m]
SG2	0.52	0.258	37.4	—	—	44.4	44.8	—	—	47.5
SG3	0.306	0.456	8.4	—	30.1	37.9	25.6	—	26.0	40.9
SG3V	0.284	0.456	22.5	—	26.6	—	—	—	—	—
SG4	0.363	0.345	8.1	9.4	34.2	48.3	22.8	25.3	35.8	45.8
SG4V	0.302	0.345	22.5	26.6	32.8	—	—	—	—	—
SG9	0.361	0.387	40.8	—	—	54.1	15.8	—	—	44.9
SG8	0.286	0.505	37.4	—	—	29.1	38.3	—	—	49.8

Accurate simulation of the settlement foundation was obtained for SG4 and SG4V, reaching values close to those obtained in the physical model. In case of SG4, flowfront arrivals did not match the CM values as the early dissipation near the internal drain was influenced by excess pore pressures hardly arriving at this location (a limitation of the stratum geometry). On the other hand, a good match of flowfront arrivals was observed for SG4V. This accurate simulation in settlement and flowfront arrivals for SG4 and SG4V was expected as soil stiffness of 2%*E* and coarse material permeability of 0.35 m/s represents very close values to those obtained in the specific calibration of parameters performed in section 7.7.2.

In addition, the single column case (SG9) presents an optimal simulation in terms of settlement response. Nevertheless, the flowfront arrival times were longer compared to that attained in the physical model and in the validated numerical model developed in step 2 (Table 7.4). The significant drop in the calibrated parameter of the fine soil stiffness, enabled a delayed in the start of soil reconsolidation.

In contrast, in SG3 and SG3V, the foundation settlement reached 67% and 63% of the amount obtained in the physical model, respectively. The value of soil stiffness utilised was higher compared to the calibrated parameter that matched the physical model (Table 7.4), enabling greater soil deformation. The flowfront arrival times were very close to that of CM, particularly for SG3V. In SG8, the simulation of foundation settlement was highly managed by the stiffness of the fine soil as no drains were located below the structure. The soil stiffness of 2%*E* represents almost twice the calibrated value obtained for the model in the previous section (7.7.2); therefore, only half of the settlement reached in the physical model

was obtained. Similarly, the flowfronts in SG8 did not match the physical model behaviour, in which faster dissipation was observed below the foundation compared to the soil surrounding the perimeter drains. The slower rate of reconsolidation in the numerical model reduced the drains' effective action compared with the column's behaviour in CM, accentuating the independent performance of the perimeter drains and limiting the fast fluid flow from the area below the foundation. Finally, in SG2, although close values of flowfront arrival times between NM and CM were attained, the significant reduction of soil stiffness in the numerical model allowed a foundation settlement response of 520 mm, almost double the amount compared to that obtained using the original calibrated values that matched the physical model result.

Overall, the NM response in terms of foundation settlement and dissipation behaviour of the soil for the cases of rubble brick perimeter drains below existing buildings (SG8) and fraction B drains under new buildings (SG2) varied significantly compared to the CM results, when considering an average set of parameters (2%E and k_d =0.35 m/s). In contrast, in the case of rubble brick drain arrangements below new buildings (SG3, SG3V, SG4, SG4V and SG9), the set of average parameters provides an adequate simulation of the physical response.

Hence, the use of this average set of parameters could be suggested as a good starting point for practitioners developing new numerical models of high permeable drains under new buildings. However, the unfeasibility of using the same average set of parameters, mainly for SG2, needs to be studied in detail in future work. Possible additional CM could be required to recalibrate this model and to discard either experimental errors or numerical model limitations explained in section 7.6.

7.8 Parametric study: variation of permeability in the drains below new buildings

The coarse material permeability plays an important role in the adequate performance of vertical drains against liquefaction damage. Although a high permeability value guarantees the effectiveness of the technique, the evaluation of a range of magnitudes provides relevant information about the expected structural response prior to the liquefaction phenomenon. In addition, it enables the discovery of an optimal magnitude in terms of structural damage reduction, avoiding an overestimation of the permeability factor and reducing the risk of clogging in the drains.

The following section presents a parametric study for the SG2 FE model, considering a variation in the vertical drains permeability. Increments of 10, 100 and 1000 times the

original permeability were evaluated and a comparative analysis with the original numerical model (SG2NM) was elaborated for each permeability case.

7.8.1 Increment of 10*k* in the vertical drains material

Excess pore pressure generation

The analysis of SG2 considering an increment of ten times in the drains original permeability (SG2K10), is presented in this section. Figure 7.26 shows the excess pore pressure time-histories for the soil located near the internal and perimeter drains, and the free field in the original numerical model (SG2NM), centrifuge model (SG2CM) and the case with permeability variation (SG2K10). Results from SG2NM, SG2CM and SG2K10 are presented in grey, blue and dotted lines, respectively. Excess pore pressure ratios near the internal drain below the foundation showed a peak magnitude of 0.06, presenting a reduction of 60% from the ratio obtained in SG2NM (Fig. 7.26a). This decrease was generated as a result of the permeability increment, verifying the great effective control of excess pore pressure generation by employing a highly permeable material inside the vertical drains. This lower generation was also observed near the perimeter drains, presenting a decrease of 33% in the r_u ratio due to the rapid fluid flow from the surrounding soil (Fig. 7.26b). No significant variation in the peak r_u values was observed in the free field as no variation in the excess pore pressure boundary condition was utilised in the model (Fig. 7.26c).

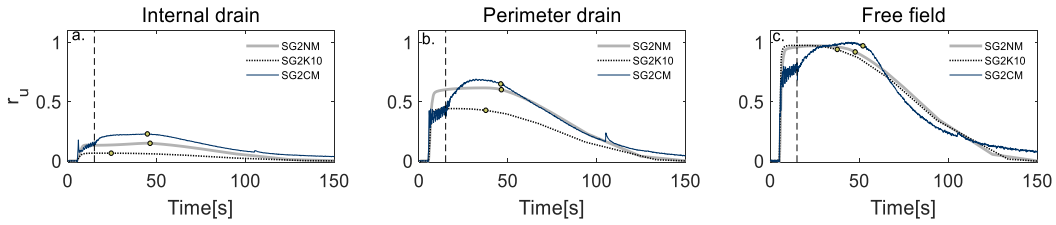

Fig. 7.26 Excess pore pressure ratios (r_u) time-histories for SG2K10, SG2NM and SG2CM, at depth of 2.1m

Dissipation of excess pore pressures

Figure 7.27 presents excess pore pressure contours for SG2K10 and SG2NM, considering dissipation initiation times for the soil near the drains in the arrangement with higher permeability, including the time at the end of the shaking and t =67 s. Ratios of 0.06 and 0.44 were observed near the internal and perimeter drains in SG2K10 at the end of the shaking (Fig. 7.27a). Meanwhile, in the original model (SG2NM), the r_u ratios were greater

at both locations because of the drains lower permeability that enabled a limited control of pore pressure generation in the soil (Fig. 7.27b). Complete liquefaction was observed in the free field for the original and the modified model at this time. Approximately ten seconds later, the flowfront arrived near the internal drain in SG2K10 (t=24.5 s) (Fig. 7.27c), while in the original model dissipation started twenty seconds later due to the central drain lower permeability.

At t=37.6 s, dissipation began close to the perimeter drains in SG2K10 after reaching a peak value of 0.44 (Fig. 7.27e). Similar to the soil adjacent to the internal drains in SG2K10, the flowfront arrived earlier compared with the same location in SG2NM. Thirty seconds later (t =67 s), a large amount of dissipation was registered below the foundation and around the perimeter drains in SG2K10, showing values of 0.05 and 0.3 (Fig. 7.27g) respectively, while higher r_u ratios were observed in SG2NM (Fig. 7.27h). The rise in the soil permeability increased the rate of reconsolidation, enabling a faster dissipation in the soil surrounding the drains.

In addition to the effective action of the drains during the generation stage, the increase in permeability of ten times accelerated the soil reconsolidation and enabled a reduction in the flowfront arrival times for the drain rings.

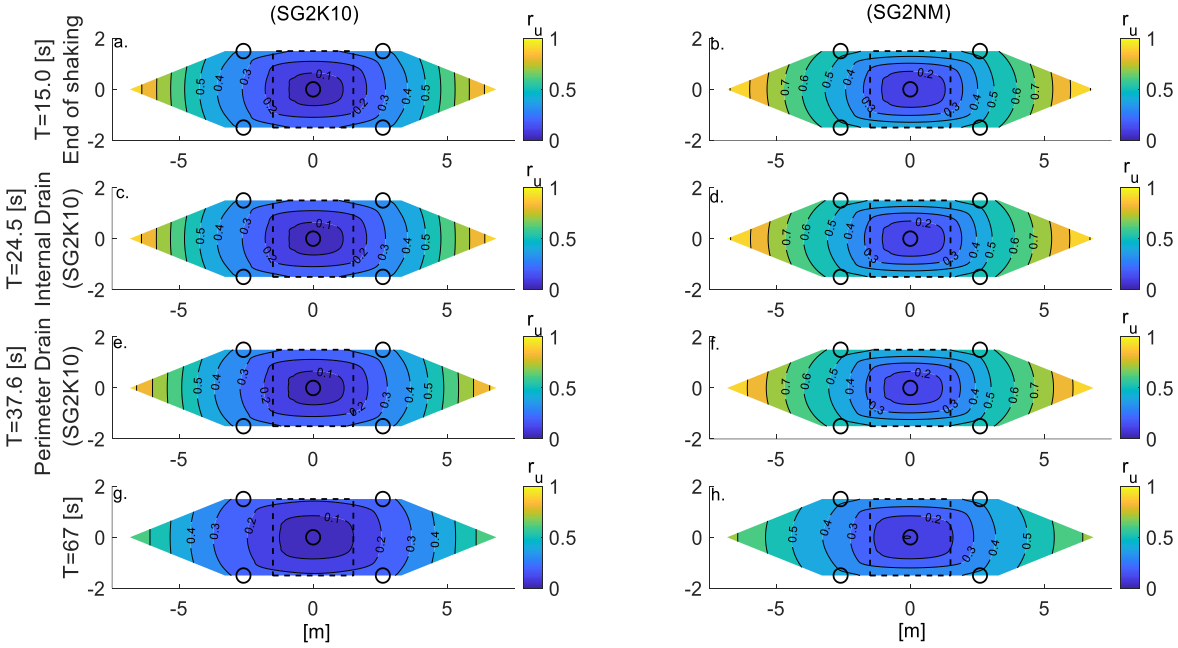

Fig. 7.27 Horizontal contours of excess pore pressure ratios (r_u) for SG2K10 and SG2NM at depth of 2.1m

Settlement of the foundation

Figure 7.28 presents the foundation settlement response for SG2NM, SG2CM and SG2K10. The foundation in SG2K10 reached a small value of 63 mm during the “shaking”

stage due to the improved control of excess pore pressure that limited the soil deformation below the foundation near the internal drain. This settlement amount represents a reduction of 50% of the magnitude obtained in the original numerical case, suggesting a significant improvement in the structural response during this stage by increasing the coarse material permeability by ten times.

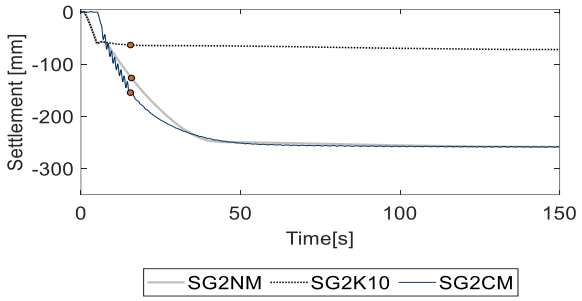

Fig. 7.28 Settlement time-histories of the foundation for SG2K10, SG2NM and SG2CM.

On the other hand, the high-permeable coarse material led to a reduction of 93% in the foundation settlement during dissipation. This minimal amount of 9 mm was obtained as a response to the rapid excess pore pressure dissipation induced by the vertical drains, reducing volumetric and deviatoric strains.

In comparison with the original case, SG2NM, the permeability of 10k led to a significant reduction of 72% in the total foundation settlement. Moreover, the significant reduction during the "shaking" stage verified the relevance of varying the permeability not only during the dissipation stage.

7.8.2 Increment of 100k and 1000k in the vertical drains material

The SG2 finite model considering increments of 100 (SGK100) and 1000 (SG2K1000) times in the permeability of the drains coarse material is presented in this section.

Excess pore pressure generation

Excess pore pressure time-histories for SG2K100 and SG2K1000 are presented, as well as SG2NM and SG2CM, in Figure 7.29, considering the soil near the drains and the free field. Significant reductions of 87% and 50% in the r_u peak ratios were observed close to the internal and perimeter drains by increasing the permeability factor 100 times in the numerical model (Fig. 7.29 a and b). In addition, using a permeability of 1000k, a negligible ratio was reached below the foundation, while a reduction of 51% in the r_u ratio was obtained for the soil adjacent to the drains (Fig. 7.29 d and e). Effective control of the excess pore pressure generation was achieved by the vertical drains in the soil.

Dissipation of excess pore pressures

Figure 7.30 presents excess pore pressure contours for SG2K100 and SG2NM considering dissipation initiation times near the internal and perimeter drains in the model with high-permeable material. At the end of the shaking, low r_u generation was observed below the foundation in SG2K100 due to the high-permeable central drain. The perimeter drains showed higher r_u values due to their "infinite cell" behaviour, while the free field still presented complete liquefaction (Fig. 7.30a). On the other hand, greater ratios were observed in SG2NM, presenting values of 0.13 and 0.6 below the foundation and close to the perimeter ring (Fig. 7.30b). This similar behaviour of lower excess pore pressure ratios due to the greater permeability was obtained for SG2K1000 at the end of the shaking, showing lower values compared with SG2NM and SG2K10 (Fig. 7.31a).

The flowfront arrived near the internal drain at t=20.3 s in SG2K10, while greater r_u values were registered close to the perimeter drains and the free field (Fig. 7.30c). Meanwhile, a greater ratio was observed below the foundation in SG2NM (Fig. 7.30d). In addition, dissipation started at t = 23.5 s near the perimeter drains in the model with high permeability, 25 seconds earlier compared with the similar location in the original case (Fig. 7.30e). Reductions of 55% and 50% in the flowfront arrival time for the internal and the perimeter drains were obtained by raising the permeability 100 times. Finally, at t = 85 s the faster fluid flow towards the drains allowed a significant reduction of pore pressures in the soil, showing complete dissipation below the foundation in SG2K100 (Fig. 7.30g). At the same time, greater values were still observed at this time for the entire layer in SG2NM (Fig. 7.30h).

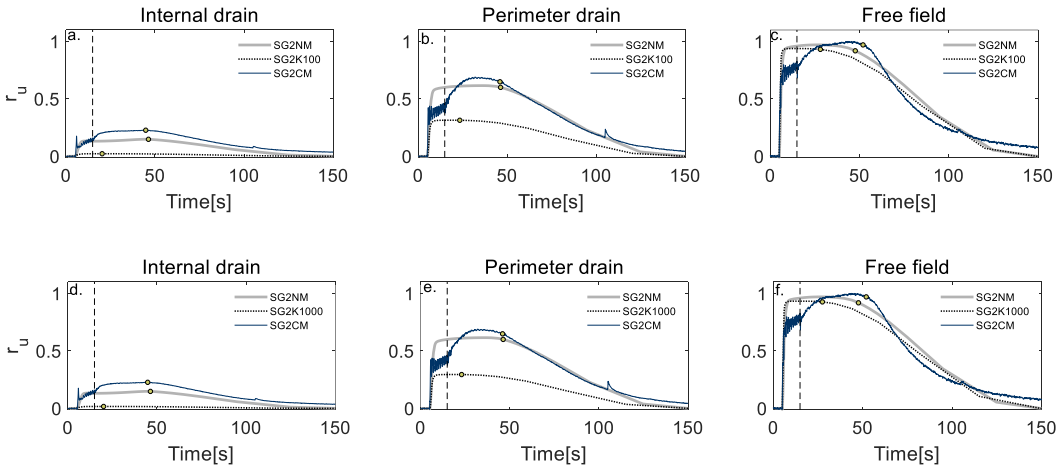

Fig. 7.29 Excess pore pressure ratios (r_u) time-histories for SG2K100, SG2K1000, SG2NM and SG2CM, at depth of 2.1m

Similar to SG2K100, the model with a permeability of 1000k presented a significant increment in the rate of reconsolidation compared with the original case. Dissipation near the internal drain began at t=20.1 s in SG2K1000, significantly earlier compared with SG2NM and marginally earlier than SG2K10 (Fig. 7.31c). Likewise, the flowfront arrived at t=23.1 s in the soil around the perimeter drains (Fig. 7.31e), showing a faster rate of reconsolidation compared with SG2NM (Fig. 7.31f). Flowfront arrival times near the internal and perimeter drains in SG2K1000 showed a significant reduction compared with the original case, and only a negligible reduction compared with SG2K100. At t=85 s lower r_u ratios were registered in SG2K1000 compared to SG2NM (Fig. 7.31g), presenting considerable dissipation below the foundation due to the faster dissipation enabled by the high level of permeability of the drains. Greater values were maintained near the drains and the free field in SG2NM at this time (Fig. 7.31h). The free field did not present a significant difference in dissipation behaviour as no influence of the drains was presented. Slightly lower r_u ratios were observed in SGK1000 compared with SGK100 at this time, following a similar reconsolidation behaviour, suggesting that the earliest flowfront arrival at this depth was approximately five seconds after the earthquake below the foundation and nine seconds for the soil near the perimeter drains.

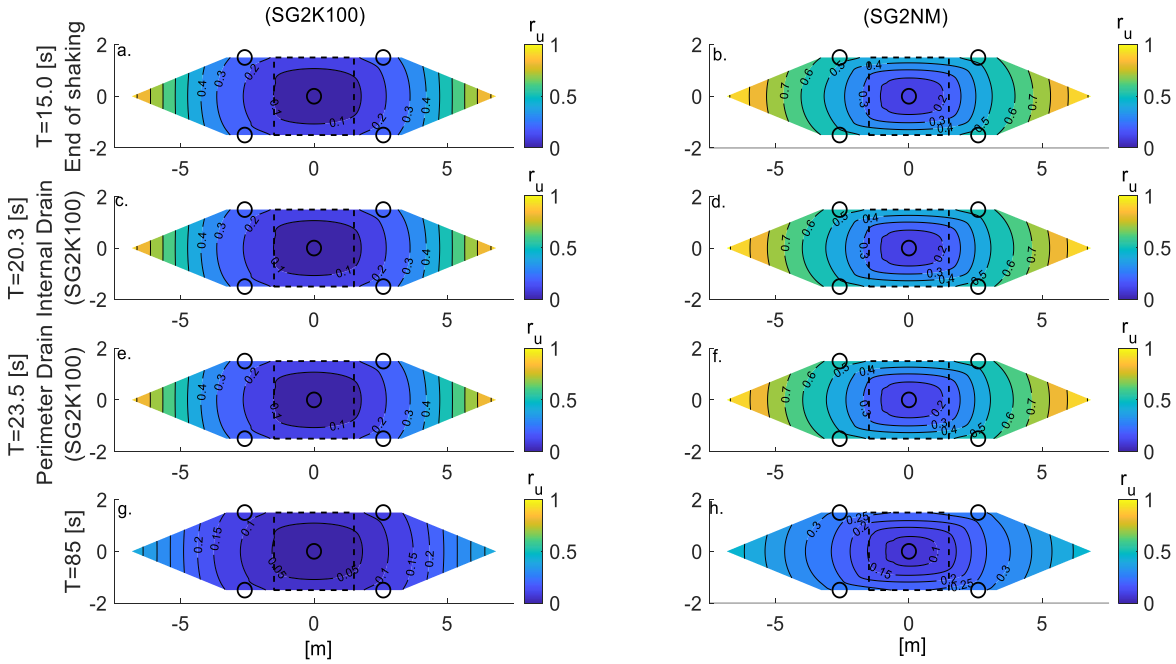

Fig. 7.30 Horizontal contours of excess pore pressure ratios (r_u) for SG2K100 and SG2NM at depth of 2.1m

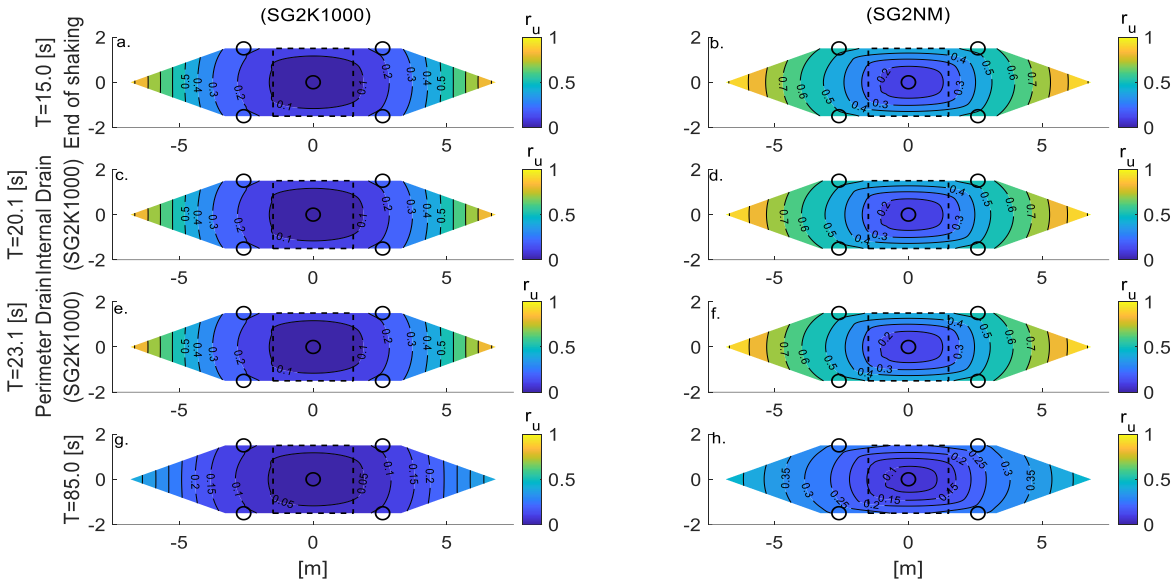

Fig. 7.31 Horizontal contours of excess pore pressure ratios (r_u) for SG2K1000 and SG2NM at depth of 2.1m

Permeability increments of 100 and 1000 times allowed for a significant improvement in the drains performance, enabling a faster reconsolidation in the soil and earlier flowfront arrivals near the central and external drain ring.

Settlement of the foundation

Figure 7.32 presents the foundation settlement response for SG2K100 and SGK1000, including the settlement obtained in SG2NM and SG2CM. During the shaking, a reduction of 52.8% in the settlement obtained in the original numerical model (SG2NM) was registered, by increasing permeability by 100 times, as a result of the enhanced control of excess pore pressures in the soil limiting deformations under the foundation. This settlement reduction was slightly higher in SG1000, representing a reduction of 53% compared with the original case.

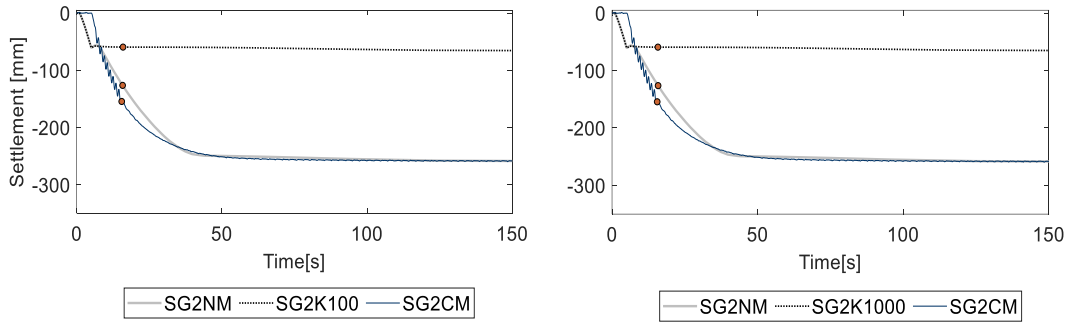

Fig. 7.32 Settlement time-histories of the foundation for SG2K100, SG2K1000, SG2NM and SG2CM

Increasing permeability improved the settlement response particularly during the dissipation stage. Negligible settlements of 10 mm and 5.8 mm were observed for the foundation in SG2K100 and SGK1000. The high-permeable coarse material inside the drains allowed for an almost complete reduction of the foundation settlement during the reconsolidation stage, preventing deviatoric and volumetric strains below the foundation. The minimal difference between the total settlement in SG2K100 and SG2K1000 was obtained due to the minor difference in the drains performance during the generation and particularly during the reconsolidation stage, indicating that the maximum settlement reduction expected using this arrangement of vertical drains is approximately 65 mm.

Figure 7.33 presents functions with the relationship between settlement and the permeability for a foundation of 150 kPa over a simplified arrangement of five vertical drains. The chart provides information for the expected foundation settlement during the "shaking" and the reconsolidation stage, together with the total permanent settlement. This graph can be useful for practitioners in determining the optimal permeability to obtain a tolerable structural settlement during the liquefaction phenomena. It also shows the risk of excessive settlements if the drains get clogged over a period of time and there is a drop in their effective permeability. It is important to know that this graph was elaborated based on a model with Hostun sand as fine material and foundation bearing pressure of 150 kPa; thus, further analyses with different soils and surcharges are recommended for future work.

Considering this vertical drain arrangement, an increase in permeability of 100 times would be sufficient to significantly reduce the foundation settlement to 65 mm, which represents a slightly higher value compared with the tolerable limit for the total seismic structural settlement (50 mm) (Lambe and Whitman, 1991).

In addition, this parametric study enabled avoidance of an overestimation of the drains permeability, reducing costs of installation as additional geomembranes are not required, and minimising the clogging effect.

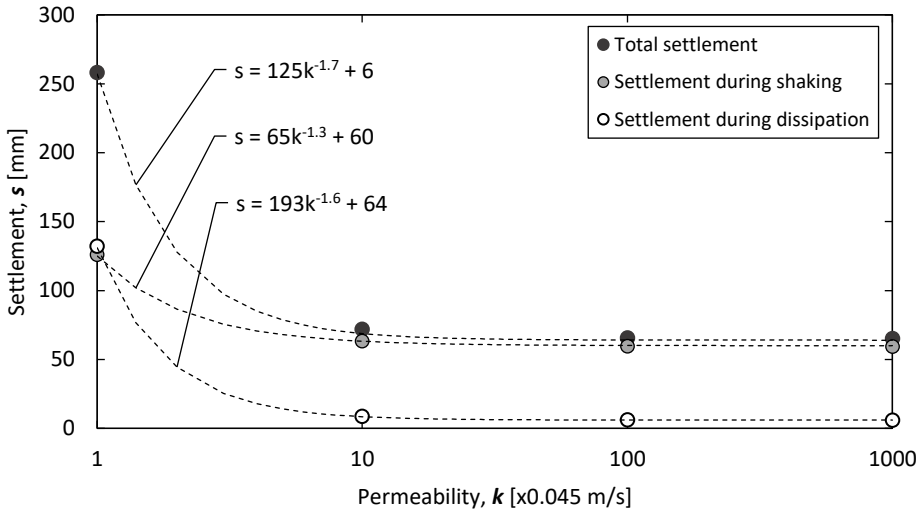

Fig. 7.33 Variation of settlement for different permeability values in the numerical model

Further analysis related to the shear strength provided by the vertical drains would be essential when utilising high-permeable material. Although a lower settlement response is guaranteed, the use of a coarser material suggests an increment in the shear reinforcement supplied by the columns, enabling a greater rotational response of the foundation during the shaking and representing a major risk of damage.

7.9 Conclusions

In this chapter, the simplified technique developed for soil reconsolidation and structural settlement simulation when using vertical drains against earthquake-induced liquefaction damage was utilised for the evaluation of a series of models previously evaluated using centrifuge modelling. The calibration of the model considered a reduction in the soil stiffness and an increment of the permeability factor for liquefaction simulation, while the validation of the method took into account the results obtained in centrifuge tests.

The FE model for SG2 presented an accurate simulation of the soil behaviour in terms of excess pore pressure generation. A faster rate of reconsolidation was observed in CM, although similar flowfront arrival times were obtained in the numerical and physical model. This behaviour occurred due to the variation of the C_v factor in the centrifuge test, involving a variation in the soil stiffness and permeability factors over time. This reconsolidation

behaviour was not observed in the FE analysis as constant values of E and k were retained permanently. Settlement of the foundation presented a small difference between CM and NM during the generation stage. A slightly lower ratio was registered in NM as lower excess pore pressures were generated. Moreover, strains due to the foundation rotation or ratcheting were omitted, enabling a reduced response in NM. On the other hand, a slightly higher settlement was obtained during the reconsolidation stage in NM as a consequence of the slower rate of reconsolidation in the soil leading to a longer time for the foundation to stop settlement compared with CM. The total settlement response reached similar values in both analyses validating the FE model.

Evaluation of the 13- and 17- drain arrangement, including the single column of rubble brick material, below new buildings were evaluated using this technique. A similar trend was observed in NM, of earlier dissipation initiation near the internal drain and later at the further drain rings as in CM for SG3. Nevertheless, the area below the foundation did not present accurate levels of r_u ratios. This was a limitation of the technique for stratums with large dimensions. After the "shaking", immediate dissipation was registered near the internal drain, illustrating a different behaviour to that observed in the physical model. Although the external drain rings in NM presented a good match in the flowfront arrival times with CM; limitations due to the rate of reconsolidation and the early start of dissipation below the foundation enabled an imprecise simulation of the soil reconsolidation. Similar foundation settlements were observed during the "shaking" stage for CM and NM; however, the settlement response in the FE analysis was mainly generated by the low initial soil stiffness rather than the influence of additional excess pore pressures. Moreover, the excess pore pressures as a boundary condition generated a lift of the foundation due to the applied condition in the soil with low stiffness. A difference of 18% in the settlement response was observed during the dissipation stage between NM and CM; nevertheless, a longer time for reconsolidation to finish was required in NM.

An alternative SG3 model was analysed to obtain more accurate excess pore pressure and dissipation behaviours of the soil, including an exact simulation of the settlement response during the reconsolidation stage. This variation implied the reduction of the stratum cross-section to obtain a greater presence of excess pore pressures below the foundation. This modification in the soil volume restricted the evaluated area to the soil encountered by the sub-perimeter drains. In this modified model, the peak excess pore pressures generated near the sub-perimeter drains were utilised as a boundary condition. The excess pore pressures at different depths along the stratum were calculated using a cubic polynomial function.

Using this modified model, an increment in the excess pore pressure ratios was registered near the internal and the sub-perimeter drains compared with the original

numerical model. Although the model dimensions were reduced, the peak ratios in the soil near the column continued to be lower compared with CM, due to the high constant initial permeability in the drains that allowed a high control of excess pore pressures from the initiation of the "shaking". Enhanced simulation of the dissipation behaviour near the internal drain was enabled due to the slightly faster rate of reconsolidation. In terms of settlement response, a continuous incremental value was obtained during the "shaking" stage, suggesting an upgraded simulation of the foundation response.

The analysis of the 17-drain arrangement using the FE model was presented in section 7.4.2. Similar to SG3, the model presented lower r_u ratios compared with the values obtained in the physical model, for the soil near the internal, edge and sub-perimeter drains. The improved control of high excess pore pressures below the foundation, due to the additional edge drains and the great area replacement ratio, was verified in the numerical model; however, the r_u ratios obtained close to the edge and internal drains did not represent realistic values. Inexact dissipation behaviour near the internal rings was observed as no significant differences in the flowfront arrival times were registered, suggesting an ineffective performance of the edge drains below the foundation. In addition, although a similar total settlement of the foundation was obtained in NM and CM, the significant influence of the soil minor stiffness, and the lift of the foundation during the "shaking" stage in NM, together with the slower rate of reconsolidation in the soil during the dissipation stage, provided an imprecise simulation of the foundation response.

Due to the limitations in excess pore pressure generation and the inaccurate soil dissipation behaviour principally below the foundation, an alternative model for SG4 was analysed considering similar variations as in SG3. In this modified model, the r_u ratios showed increased values near the internal and sub-perimeter drains compared with the original case, suggesting an improved simulation of the edge and internal drains performance. Moreover, during the dissipation stage, flowfront arrival times for the internal rings verified the effective action of the edge drains in NM, although the rate of reconsolidation continued to affect the behaviour of the soil. In addition, the soil behaviour near the sub-perimeter and perimeter drains, obtained in NM, enabled the verification of the delay in the flowfront arrival time for the outer drains, when considering an extra internal ring as previously observed in the physical model. A similar total settlement was obtained during the shaking and generation stages, showing an improved simulation, particularly during the initial stage in response to the raised excess pore pressures.

The single rubble brick column below the foundation was evaluated in section 7.4.3. This model considered a reduction in the original length for an improved simulation of the soil behaviour. The "infinite cell" behaviour during the generation and dissipation stages for a single column was observed in the FE analysis. In addition, the relevance of the bearing

pressure's influence and the proximity of the soil towards the rubble brick column was verified. Excess pore pressure ratios reached lower values in NM compared with CM, although a reduction in the stratum dimensions was utilised, due to the effective action of the rubble brick column. In addition, similar to CM, the numerical model was unable to prevent complete liquefaction behaviour at further radial distances. A more accurate dissipation modelling was observed for a limited radial distance close to the gravel column in the FE model. An excellent match in the amount of the foundation settlements was obtained between CM and NM; nevertheless, the different rate of reconsolidation in NM affected the dissipation simulation over time.

Finally, the performance of the vertical perimeter drains surrounding existing buildings was analysed using numerical modelling. Similar to SG9, this model considered a reduction in the original length of the stratum for an improved simulation of the soil performance. The excess pore pressure ratios reached lower values compared with CM, particularly in the area enclosed by the drains. The reduced fluid flow from below the foundation towards the drains, in response to the slow rate of reconsolidation, enabled a more individual behaviour of the drains compared with the physical model, becoming a limitation in the reconsolidation modelling. In terms of the settlement, the significant dependence of the foundation in the soil with a low level of stiffness induced a greater lift of the structure during the addition of the boundary condition and the consequent less accurate simulation of the settlement response during the "shaking". A difference of 29% in the total foundation settlement was obtained between CM and NM. The performance of the drains enabled the rapid dissipation of the area under the foundation; however, the slower dissipation led to a slightly higher settlement compared with CM.

This simplified technique exonerates the presence of the dynamic force that generates liquefaction in the soil and, therefore, a reduction in time and costs is anticipated using this numerical model. Moreover, this method provides practitioners with an effective procedure of estimating the required permeability for drains to minimise the structural settlement due to earthquake-induced liquefaction.

In section 7.8, a parametric evaluation for the simplified arrangement below new buildings considering a variation in the vertical drains permeability was performed.

An increment of ten times the original permeability value allowed an improved control of the excess pore pressure generation in the soil near the internal and perimeter drains and a faster rate of dissipation in the area enclosed by the perimeter drains, showing more rapid flowfront arrivals. Moreover, a significant reduction of 72% in the foundation total settlement was obtained by raising the coarse material permeability.

Permeability variation of 100k and 1000k in the drains material enabled a major difference in the excess pore pressure generation compared with the original case, presenting

significant r_u ratio reductions for the soil near the internal and perimeter drains. Moreover, the rapid rate of reconsolidation allowed earlier flowfront arrivals for the soil surrounding the drains. The maximum reduction in the flowfront arrival for the soil under the foundation and near the perimeter drains was nearly five and nine seconds after the shaking, as no significant variation was obtained during the dissipation stage between the vertical drains with 100*k* and 1000*k*. Total settlement reductions of 74.5% and 75 % of the settlement reached in the original case were obtained by increasing the permeability in 100 and 1000 times. This suggests there is a limiting threshold value for the vertical drain permeability beyond which the reduction in settlements is minimal.

Chapter 8

Conclusions

8.1 Research conclusions

8.1.1 Vertical drains performance in liquefaction mitigation under new buildings

The use of vertical drains in free field conditions and surrounding existing buildings has been evaluated using physical modelling in previous years. Nevertheless, the drains performance prior to the construction of buildings, (installed in the pre-construction stage), required further investigation to establish their performance in the presence of buildings, using experimental methods. In chapter 4, a centrifuge test considering the simplified arrangement of Fraction B vertical drains below a foundation of 150 kPa was conducted, to evaluate the performance of the technique and its effectiveness compared to an unimproved region. In addition, the influence of the bearing pressure on the arrangement performance was evaluated by considering foundations of different bearing pressure. The analysis of this and subsequent centrifuge tests was focused on the generation and dissipation of excess pore pressures in the soil and the foundation response in terms of settlement and dynamic behaviour.

In the improved soil, limited excess pore pressures were observed below the foundation near the internal drain, compared to the perimeter ring, in the presence of the greater confining pressure exerted by the foundation that enabled significant resistance for excess pore pressures to be generated. A bulb of low pressures below the foundation was observed in the treated and the untreated regions due to the significant confining pressure applied by the foundation, as previously observed by other authors (Ghosh, 2003; Adamidis, 2017). As

it was expected, following theoretical charts for the drain arrangement design, to reduce the possibility of complete liquefaction below a structure, would imply an overestimation of the r_u ratio in the soil. In addition, the faster dissipation obtained in the improved zone compared to the untreated region, allowed a reduction in the settlements, verifying the effectiveness of the technique. Moreover, the "unit cell" and "infinite cell" behaviour for the internal and perimeter drain, respectively, were emphasised in the presence of the bearing pressure influence. Although a reduction of the foundation settlement response was obtained by treating the soil, this decrease was not significant compared to the foundation response in the unimproved area, suggesting the inefficacy of drains in controlling high excess pore pressures and their negligible contribution to shear reinforcement. A low rotational response of the foundation was registered in the improved case, due to the level of soil softening generated which enabled a significant reduction in the soil acceleration.

The influence of the bearing pressure on the performance of the drain arrangement was corroborated during the shaking and consolidation stages. Lower excess pore pressure magnitudes were registered below the foundation of 150 kPa compared to the light foundation, in response to the significant confinement pressure and soil cyclic resistance during the shaking (Liu and Dobry, 1997; Ghosh, 2003; Dashti *et al.*, 2010a). In addition, the foundation significant confining stress enabled a rapid dissipation of excess pore pressures during the reconsolidation stage. The reconsolidation of soil particles will attempt to occur faster in the presence of a significant load. Therefore, the permanent settlement was lower in the case of the foundation of 150 kPa when compared to the lighter structure. The greater soil softening below the foundation of 50 kPa and the minor shear reinforcement provided by the Fraction B drains enabled a smaller transference of the input motion to the foundation and a consequent lower rotational response, compared to the foundation of 150 kPa.

8.1.2 Improved arrangement alternatives using sustainable materials as drains below new buildings

Different alternative drain arrangements were evaluated in chapter 5 to provide proper mitigation of the vulnerable area below the foundation, before the construction of buildings. The analysis considers rubble brick vertical drains as a sustainable and economical option.

The addition of edge drains below the foundation in an arrangement of 13 drains was analysed (17-vertical drain arrangement). The edge drains enabled improved control of excess pore pressures below the foundation, corroborating the effectiveness of the arrangement when a greater area replacement ratio (A_r) is considered. Furthermore, improved drainage was observed in the soil due to the effective action of the internal and edge drains. Nevertheless, negative effects arose, as the outer rings suffered a delay in the

flowfront arrivals. This resulted in a weak performance of the arrangement during the dissipation stage particularly in the area outside the foundation. A greater reduction of the foundation settlement was obtained by using the 17-vertical drain arrangement compared to the 13- drain arrangement due to the effective performance of the additional edge drains below the foundation, corroborating the arrangement's effectivity. Lower soil softening and faster regaining of the strength of the soil, in presence of the additional drains reduced deviatoric and volumetric strains under the foundation. Although the shear reinforcement provided by the arrangement was insufficient in both cases, a marginally larger acceleration and rotational response of the foundation over the 17-vertical drain arrangement was observed. The settlement improvement was unexpectedly minimal after considering four additional drains below the foundation, due to the bulging effect observed at the top of the drains due to loss of confinement with onset of liquefaction of surrounding soil. This enabled a significant loss of load carrying capacity in the gravel columns.

Encased internal and edge vertical drains below the foundation were utilised as an alternative to improve the performance of the original 17-vertical drain arrangement and the foundation response. Improved performance of this alternative arrangement was observed during the dissipation of excess pore pressures compared to the generation stage. Optimal control of high excess pore pressure during the shaking was impeded by the aluminium encasement, while the absence of the bulging effect in the drains improved the drainage performance of the arrangement, which maintained the original high permeability. Moreover, the stability of the internal and edge drains enabled a block performance of the columns below the foundation. The drains worked together exhibiting a "unit cell" behaviour with a greater potential to improve dissipation in the soil compared to the original 17- vertical drain arrangement. Significant settlement reduction was registered by using the encased drains below the foundation, mainly due to the reduction of the bulging effect that enabled the drains bearing capacity to remain unchanged. In addition, a great seismic demand was registered for the foundation over encased drains as expected, in response to the shear strength provided by the columns when the bulging effect in the drains was prevented.

As un upper bound to number of drains, a single column covering the entire footprint of the foundation was analysed. The evaluation included a comparison with the 17-vertical drain arrangement in which 45% of the base area of the foundation was covered by drains. The proximity of the soil to the single column and the influence of the foundation bearing pressure considerably affected the generation and dissipation behaviour of the surrounding soil. The foundation bearing pressure positively influenced the control and fast dissipation of excess pore pressures; however, during the shaking, the zero drain spacing presented by the column resulted in a weak performance of the arrangement. Moreover, enhanced performance of the 17-vertical drain arrangement was registered compared to the single

column during the shaking, as improved control of excess pore pressures in the area between the internal rings was enabled in the presence of the edge and sub-perimeter drains. In contrast, the single column presented faster dissipation in the entire soil, compared to the arrangement of 17 drains. This indicated the relevance of the edge and sub-perimeter drain rings in the soil during the shaking and their lower utility during the dissipation stage, if the entire foundation footprint was treated. The foundation over the single column showed greater settlement compared to the foundation over the 17- vertical drain arrangement. The external drain rings in the latter played an important role during the shaking, limiting the high levels of excess pore pressures and softening in the soil around the foundation. This behaviour limited the loss of drain stability and the consequent foundation settlement response, suggesting the relevance of considering external drains in an arrangement, around the structure, to diminish the column "infinite cell" behaviour. Optimal behaviour of the single column was expected as the entire footprint was treated; nevertheless, countereffects were observed. In addition to the greater foundation settlement, greater foundation acceleration was transferred to the foundation inducing a larger foundation rotational response, in response to the considerable shear reinforcement provided by the column.

Results obtained from the evaluation of the different arrangements indicate, that the arrangement with encased drains below the foundation represents the optimal alternative against structural damage in the case of earthquake-induced liquefaction, although a considerable rotational response is expected. In addition, the outcomes emphasise the necessity of designing the drain arrangements based on optimal performance during the earthquake, not only during the reconsolidation stage, as significant settlement was obtained during the shaking in all cases.

8.1.3 Performance of inclined perimeter drains below existing buildings

The utilisation of vertical drain arrangements is impractical in the case of existing buildings as the conventional design involves free field conditions and the possible demolition of the structure prior to the drains installation. Furthermore, the limitation of installing vertical drains implies constant radial proximity from the drains to the area below the foundation, which represents a high-risk zone. Therefore, the use of inclined perimeter drains is an optimal alternative that is, feasible to install around the foundation and inexpensive compared to other methods. In chapter 6, the performance of an inclined rubble brick drain arrangement located around existing buildings was assessed and compared to a vertical drain arrangement.

Excess pore pressures in the soil below the foundation and surrounding the perimeter drains were controlled by the inclined drains. A bulb of low pressures was generated in the soil enclosed by the drains and quickly dissipated after the shaking, due to the drains radial

proximity to the foundation central axis. The rapid dissipation of excess pore pressures limited deviatoric and volumetric deformations in the soil and resulted in faster recovery of soil strength, enabling a lower settlement of the foundation compared to the foundation over vertical rubble brick drains. A less effective performance was observed in the case of the vertical drain arrangement during the shaking and reconsolidation stages in response to the constant radial distance from the drains to the foundation, along the stratum depth. Excess pore pressures started to dissipate later compared to the inclined drains, showing greater reconsolidation volumetric strains and deviatoric deformations in the soil. Larger settlement response of the foundation over vertical drains was obtained compared to that of the inclined arrangement case, corroborating the effectiveness of this alternative. However, the greater softening generated in the soil with vertical drains during the shaking allowed a reduction of the soil acceleration and a minor transference of the input motion to the foundation, resulting in a lower rotational response of the structure, compared to the foundation over inclined drains.

The bearing pressure influence in the inclined arrangement performance was also evaluated as a relevant mechanism of settlement, by analysing a similar drain configuration below a foundation of 50 kPa. Effective performance of the inclined drains below the light foundation was not managed principally due to the drain's radial proximity to the structure. The effective action of the inclined drains was controlled by the high confining pressure applied by the foundation in the soil. A more rapid dissipation of excess pore pressures was observed in the case of the heavy foundation compared to the light foundation, which induced a faster regaining of stiffness in the soil and lower reconsolidation induced volumetric and deviatoric strains. This behaviour enabled a similar settlement response between the heavy and light foundation. In addition, a greater transference of the input motion to the heavy foundation was registered, enabling a superior dynamic response of the structure compared to the light foundation.

8.1.4 Numerical modelling of drain arrangements below new and existing buildings

The use of physical and numerical methodologies for geotechnical solutions implies great expenditure of resources; thus, evaluation of a significant number of models is not frequently conducted. Moreover, the inefficacy of different software in liquefaction simulation has been verified in the last few decades, particularly in terms of settlement. Due to these shortcomings, the creation of a simplified 3D FE technique using a standard ABAQUS software was proposed in this work, centred on the reconsolidation of the soil containing a vertical drain arrangement. Similar models evaluated using centrifuge

modelling for new and existing buildings were assessed. The proposed technique was validated considering results obtained from the physical modelling.

Limitations in the soil properties were presented principally due to the simulation of the "shaking", as coupled pore fluid and dynamic analysis cannot be conducted in ABAQUS software. The numerical model must be calibrated for accurate simulation of the soil liquefaction behaviour. The rate of reconsolidation at low soil effective stresses during liquefaction, involves a reduction in the soil stiffness and an increase in soil permeability parameter.

The SG2 numerical model presented an accurate simulation of the soil behaviour during the shaking. The excess pore pressure generation showed similar results to the physical modelling. In contrast, although similar flowfront arrivals were observed for the drains during the dissipation in the numerical and centrifuge models, the rate of reconsolidation was faster in the centrifuge model due to the variation of C_v. While both factors remained constant in the numerical model, the soil stiffness and permeability presented a variation in the physical model during dissipation. The foundation settlement showed similar results in the numerical and centrifuge models, with a slight variation in the numerical simulation during the shaking as a lower generation of excess pore pressures was registered in the soil, causing less softening. However, a slightly larger settlement was registered during the dissipation stage in the numerical model compared to the centrifuge model, as a result of the slower rate of reconsolidation. Overall, the total foundation settlement achieved the same value in both cases, validating the numerical model.

In SG3, the generation of excess pore pressures was not accurately simulated, particularly below the foundation, due to the limitation of excess pore pressures applied as a boundary condition in a large volume of soil. In contrast, the soil dissipation behaviour showed a similar trend in the numerical and centrifuge models, in which the internal drain enabled a faster dissipation initiation compared to the external drains. Nevertheless, an imprecise simulation of the reconsolidation stage was obtained in the numerical model as an early flowfront arrival near the internal drain below the foundation was attained. Although the foundation settlement in both cases was similar during the shaking, the response in the numerical model was principally caused by the minor level of soil stiffness rather than the excess pore pressure effect. Moreover, the application of excess pore pressures as a boundary condition in the soil with minor stiffness generated a lift of the foundation. Also, the foundation settlement response showed a difference between the numerical and centrifuge models during the dissipation stage, as more time was required for the soil in the numerical model to complete reconsolidation.

A variation in the SG3 original numerical model was assessed (SG3V), to obtain a more exact simulation of excess pore pressure generation and dissipation in the soil and of the

foundation response. A variation in the dimensions of the soil cross-section was considered. In this way, there would be a higher presence of excess pore pressures below the foundation. Nevertheless, by considering this change in the soil volume, the area of analysis was limited to the zone enclosed by the sub-perimeter drains. The peak excess pore pressure obtained from the centrifuge test in the soil surrounding the sub-perimeter drains was considered as boundary condition in this case, and a polynomial function was utilised to estimate the excess pore pressure magnitudes per one metre depth in the stratum. In this model, greater excess pore pressure ratios were registered close to the drain rings compared to the SG3 original case. The r_u ratios in the soil near the drains still remained lower compared to the values obtained in the centrifuge model, as the initial permeability was considerably high in the numerical model, enabling good control of excess pore pressure generation since the start of the "shaking". In addition, a more accurate dissipation behaviour of the soil below the foundation was obtained due to the faster rate of reconsolidation presented in this modified model. The foundation settlement was more accurately modelled, due to the reduction of the foundation uplift effect.

In SG4, where the 17-vertical drain arrangement was modelled, low values of r_u in the soil surrounding the drain rings were also obtained due to the limitation of the excess pore pressure boundary condition. Although an enhanced control of excess pore pressures was presented below the foundation due to the effective action of the additional edge drains, the level of r_u reached around the internal drain rings was negligible. In addition, an inaccurate performance of the edge and internal drains was registered during the dissipation stage, showing the same flowfront arrival times for both rings, behaviour that differed from that obtained in the physical model. However, the foundation settlement obtained during the shaking matched in the numerical and physical model; and similar as in the previous arrangement, the low stiffness of the soil and the slow rate of reconsolidation in the soil, caused an imprecise simulation of the foundation response.

The SG4 original model was also altered (SG4V). Results in this variated model presented an enhanced simulation of the edge and internal drain rings performance in response to the more accurate simulation of excess pore pressure generation. Higher values around the drain rings were registered compared to the original model. In addition, the flowfront arrival times for the edge and internal drains were more similar to the values obtained in the physical model, suggesting an improved simulation of the edge drains performance during the reconsolidation stage. The delay of the flowfront arrival in the soil surrounding the external drain rings due to the presence of an extra ring, observed in the physical model, was corroborated using numerical modelling. Improved simulation of the foundation settlement response compared to the original SG4 numerical model was obtained during the shaking and dissipation stages.

The single column of rubble brick material below the foundation of 150 kPa was modelled in section 7.4.3. A reduction of the original stratum cross-section was considered at first instance. Similar to the physical model, the “infinite cell” behaviour of the single column was observed, together with the significant relevance in the arrangement performance of the bearing pressure influence and soil proximity to the column. Lower magnitudes of excess pore pressures were presented in the numerical model compared with the centrifuge model, because of the significant input permeability. The drain performance reduced its effectivity at further distances, where complete liquefaction was registered, similar to the behaviour obtained in the physical model. Moreover, accurate simulation of the soil reconsolidation was obtained in the numerical model for a limited radial distance. The foundation settlement showed similar outcomes in the numerical and physical models, although the different rate of reconsolidation enabled an imprecise simulation of the dissipation behaviour of the soil in the numerical model.

The arrangement of vertical perimeter drains around a foundation of 150 kPa was also modelled considering a reduction of the stratum dimensions. The behaviour of the soil enclosed by the drains under the foundation in the numerical model presented a considerable difference with the physical model results, due to the lower excess pore pressures reached below the foundation in the first case. In addition, during the dissipation stage, the slow rate of reconsolidation in the numerical model enabled a decreased fluid flow from the zone below the foundation towards the vertical drains, suggesting an independent behaviour of the drains in the FE model. The foundation response depended significantly on the below soil behaviour rather than the effective performance of the drains. An inexact simulation of the foundation settlement was obtained in the numerical model, particularly during the shaking, due to the significant lift of the foundation attained. Although the drains enabled an improved dissipation of excess pore pressures below the foundation in the numerical model, the slower rate of reconsolidation let to a slightly greater settlement compared to the centrifuge model during the dissipation stage.

The proposed simplified method provides the engineers with a useful and efficient method for the estimation of an adequate coarse material permeability that would allow minor structural settlement in case of earthquake-induced liquefaction. The developed numerical models are expected to provide benefits in terms of time and costs as the dynamic analysis is omitted. Nevertheless, this simplified procedure presents limitations, the principal being that the soil stiffness and permeability remained constant during and after the “shaking”, obscuring the correct simulation of the soil behaviour. In addition, it was difficult to attain the correct simulation of excess pore pressure generation under the foundation in case of large soil volumes; therefore, a solution to this issue was proposed, reducing the stratum dimensions. Although an improved simulation in the excess pore pressure generation was obtained, it was not possible to analyse the external drain rings

located far from the foundation. Another limitation was the foundation lift obtained in the models with low soil stiffness, in response to the pore pressure applied at the edges of the stratum. This enabled an inexact settlement response in the foundation during the "shaking". Moreover, the assumption of complete liquefaction in the free field as excess pore pressure boundary condition in the soil, and the limitation of the model having been validated for a bearing pressure of 150 kPa, represents another restriction.

A parametric analysis was developed in the last section, considering variations in drain permeability in the simplified arrangement of five vertical drains below a foundation of 150 kPa. A significant reduction of the total settlement was achieved when the drains permeability was multiplied by ten. Enhanced control of excess pore pressures and fast dissipation was observed below the building; therefore, faster flowfront arrival was enabled near the drain rings. Moreover, increments of 100 and 1000 times the drains original permeability were also analysed. This variation allowed limited r_u values near the drains compared to the original case. The improved rate of consolidation facilitated a rapid flowfront arrival in the soil surrounding the internal and perimeter drains. No considerable variation was observed in the flowfront arrivals by increasing the permeability from 100 to 1000 times. In addition, significant settlement reduction was obtained in both cases, with a difference of 0.5% between them, suggesting that there was a maximum permeability value for which no further reduction of the foundation settlement should be expected. The developed parametric analyses prevent the over requirement of the drains permeability, which is highly beneficial in terms of costs. Functions relating the predicted settlement for a specific drain permeability were proposed for practitioners.

8.2 Recommendations for designing engineers

Recommendations for designing engineers are given in this section, in consideration of the results obtained in this research. The different analyses developed in this work were carried out using physical and numerical modelling and took specific parameters into account. For this reason, the following recommendations should be carefully considered within these limitations and should not be extrapolated.

8.2.1 Assessment of buildings in liquefiable prone areas

The drain arrangement, as a countermeasure technique, should involve an adequate design before its installation in the field, which should focus particularly on two points. First, it should centre on the reduction of the building settlement, caused by the soil softening presented below and surrounding the structure. The second point to focus on is the adequate control of the structural dynamic response when soil softening is reduced, in response to the

drainage mitigation. Due to the reduction of the excess pore pressure generation in the presence of drains and the consequent transfer of higher accelerations, the foundation may suffer adverse effects in terms of acceleration response. The principal objective is to achieve an adequate and secure design.

Design charts that are frequently used to estimate structural settlement do not take into consideration deformations in the soil due to deviatoric strains, nor the influence of drainage mitigation techniques on settlement mechanisms. Therefore, the building settlement response may not be accurately estimated based on empirical charts. The numerical technique proposed in this work gives a validated tool for relatively quick estimation of soil deformation during the reconsolidation stage using a standard FE software package. However, deviatoric strains due to ratcheting are omitted as dynamic analysis is not considered. Particular attention should be given to the soil behaviour and the foundation dynamic response during the shaking.

8.2.2 Design of treated soil beneath new and existing buildings

Theoretical charts utilised for the design of drain arrangements, which have the aim of reducing the occurrence of complete liquefaction, omit the presence of a structure, and an overestimation of the r_u ratio should therefore be expected. This suggests that inaccurate design of the treated area below buildings should be anticipated. The design practice for structures that have low bearing pressure and are located in liquefiable areas should be planned more carefully in comparison to buildings with greater bearing pressure, as greater generation and slower dissipation of excess pore pressures in the soil is expected under such conditions.

In addition, if there was a significant presence of drains below the foundation footprint, the use of a large area replacement ratio in the soil could be highly beneficial for the structural response. Nevertheless, mitigating the foundation base area alone would not be sufficiently effective, particularly during the shaking. In the design for the treated zone, the improved area should be extended significantly beyond the plan area where the structure is located, thus including the use of external drain rings in the configuration. In the same way, when peripheral drain rings located outside the foundation are considered in the drain arrangement, the addition of internal drains below the foundation base area should be carefully considered in the design; a delay in the effective performance of the external drains is expected.

The drain arrangement design must consider significant radial proximity from the drains to the foundation, particularly when inclined perimeter drains are employed as countermeasure technique for existing buildings. The accurate selection of an inclination angle subject to the directional drilling capability of the stone column rig, that sufficiently

covers the foundation footprint is highly advantageous. However, in this case, relevant attention should be given to the dynamic response of the structure. Furthermore, the utilisation of an effective drain encasement, such as high-permeability, high-strength geosynthetics, is vitally important for the optimal performance of the drains as it prevents a bulging effect in the drains and a high risk of clogging. Nevertheless, the significant transference of the input motion to the structure should be taken into account in the structural design.

Numerical tools currently being used to solve geotechnical problems, particularly those involving earthquake-induced liquefaction analysis, are not highly effective for complex 3D analyses required for this problem, as has previously been stated. The simulation of soil-structure interaction during and after the earthquake, considering drainage mitigation techniques in the soil, may provide an inaccurate settlement response. Therefore, the use of this popular tool could provide imprecise details in the design of drain arrangements.

The method developed in this work can be widely beneficial for design engineers. The simplified FE technique is optimal for the simulation of structural settlement during the reconsolidation stage, considering the specific arrangement of drains, bearing pressure and soil properties. The technique provides reasonably validated results, particularly in simulating the performance of drain arrangements below new buildings, in which various drain rings are presented in the configuration, significantly covering the area under the foundation. Designers should consider this efficient method when estimating the coarse material permeability for obtaining a minor structural settlement in the case of liquefaction; however, limitations of the technique previously detailed require some improvement.

8.2.3 Improvement of the technique

The evaluated drain arrangements were optimal alternatives for the mitigation of new and existing buildings, as drains were able to improve control and dissipation of excess pore pressures in the soil. Nevertheless, it was not possible to achieve complete settlement reduction in any of the cases. Considerable co-seismic settlement was found during the shaking, suggesting the need for an improved performance of the drain arrangement particularly for during the shaking. Enhanced control of the fluid flow and sufficient shear reinforcement would reduce soil softening and, consequently, structural settlement. For this reason, the use of mixed mitigation techniques is essential to the design practice. For instance, the installation of extra inclined shallow drains between the drains in the original arrangement (significantly close to the structure) could be an optimal alternative that would enable an effective control of excess pore pressures beneath the structure. In addition, the use of stone column walls, together with the drain arrangement, would provide greater shear reinforcement to the soil, thus reducing the settlement response. These mixed techniques

should be thoroughly designed, as counteracting effects in the structure would be expected in both cases.

8.3 Future work

Limitations presented in the physical and numerical analysis emphasise the relevance of continued research focused on the performance of vertical drains and highlight the need for further work in particular areas.

Although the evaluated drain arrangements in this work presented an improved response of the foundation, a complete reduction of the settlement response was not obtained; therefore, the assessment of novel arrangement designs for damage mitigation of new and existing buildings is still required. For instance, the evaluation of inclined drains considering different inclination angles below the foundation is attractive. In addition, the assessment of mixed techniques using other countermeasure methods together with drains should be considered to obtain an enhanced structural response. The use of additional stone columns in the soil or lowering the ground water level would represent a significant improvement in terms of soil shear strength.

The variation of specific drain parameters in the centrifuge and numerical models should be taken into account. Models with different drain radius and drain spacing should be assessed to obtain an improved foundation response and to enhance novel design charts for drain arrangements. Furthermore, the use of different recycled material as coarse sand inside drains should be considered in future work, as it would be highly economical and environmentally beneficial.

All the drain arrangements were analysed considering uniform soil, which is not an exact representation of the field. Modelling different soil layers and considering a higher soil density could be of interest as a variation in the drain rings dissipation performance and flowfront arrivals could be presented.

The analysis of prefabricated vertical drains considering geosynthetic and geomembrane as drain coating represent an interesting alternative. This evaluation could be highly attractive to the manufacturing and production industry.

In addition, foundations with different bearing pressures should be analysed. This would provide a trend of expected settlement for specific bearing pressure, useful for practitioners. Furthermore, modelling the foundation as a rigid structure or building in the thesis may have resulted over-exaggerated structural accelerations. Therefore, the evaluation of the foundation plus a superstructure is required to obtain results in terms of transfer of accelerations to the building and dynamic response on each floor. This would provide a more

realistic representation of the building performance over the improved soil. Moreover, the evaluation of various foundation bearing pressure, particularly in the numerical model, is highly relevant as this has significant influence in the soil stiffness and permeability variables, which emphasise the limitations of the proposed technique.

Numerical modelling is a useful and accessible methodology for practitioners and is greatly relevant for improving existing numerical techniques. The simplified FE technique proposed in this work was validated considering results from experimental tests; nevertheless, the developed numerical models still present certain shortcomings in the accurate simulation of the soil and structure behaviour during and after the "shaking".

Improved simulation of the soil and foundation response requires mainly a variation in the soil stiffness and permeability during the "shaking" and reconsolidation stages. Continuous research on the development of new numerical codes and software focused on this issue is needed. In addition, a comparative analysis between the existing software utilised for liquefaction simulation in which the dynamic analysis is considered, and the proposed simplified technique developed in this work should be carried on. In this way, differences in the soil and structural behaviour due to deviatoric strains during the dynamic simulation could be recognised.

Assuming free field liquefaction for the excess pore pressure boundary condition in the soil represents an unreal context. A parametric evaluation considering different levels of excess pore pressure generation (r_u) as boundary condition along the stratum depth should be developed. This could be useful to provide the expected settlement response for different degrees of soil softening.

The soil liquefaction simulation and dynamic behaviour could be a complex task to achieve in numerical modelling. The use of an accurate constitutive model in the numerical simulation is a relevant factor. In this work, the Mohr Coulomb constitutive model provides a reasonable simulation of the soil behaviour by considering specific parameters and load conditions. The use of other constitutive models may provide slightly different results compared with this work; however, a significant variation in the principal findings is not expected. In addition, the estimation of the parameters utilised in the model requires to be improved. The friction angle used for the drain materials was obtained from direct shear box tests; however, this may be improved using triaxial element tests, considering cyclic loading.

The smear zone around drains should be considered in future models, as this would imply a variation in the arrangement performance and foundation response. Evaluating different levels of permeability degradation around the drains could be of interest, as this is a expected behaviour in the field. Moreover, the permeability anisotropy of the soil and its effects in the excess pore pressure generation and dissipation should be considered in the numerical analysis.

Further parametric studies using all the validated numerical models presented in this work should be undertaken to provide additional functions, in which the settlement response of the structure could be predicted considering specific bearing pressure and drain material. In this way, practitioners would have accessible tools to select the optimal mitigation arrangement to diminish the risk of significant damage in structures, in case of earthquake-induced liquefaction. Such studies would need to include detailed cost-benefit analyses.

References

Abdullah, A. and Hazarika, H. (2016) 'Improvement of Shallow Foundation Using Non-Liquefiable Recycle Materials'. *Japanese Geotechnical Society Special Publication*, 2(54), pp. 1863–1867.

Adamidis, O. (2017) *Earthquake-Induced Liquefaction of Sand and Response of Structures with Shallow Foundations*. PhD Thesis, University of Cambridge, United Kingdom.

Adamidis, O. and Madabhushi, G.S.. (2015) 'Use of Viscous Pore Fluids in Dynamic Centrifuge Modelling'. *International Journal of Physical Modelling in Geotechnics*, 15(3), pp. 141–149.

Adamidis, O. and Madabhushi, G.S.P. (2018) 'Deformation Mechanisms under Shallow Foundations on Liquefiable Layers of Varying Thickness'. *Géotechnique*, 68(7), pp. 1–13.

Adamidis, O. and Madabhushi, G.S.P. (2016) 'Post-Liquefaction Reconsolidation of Sand'. *Proceedings of the Royal Society A: Mathematical, Physical and Engineering Sciences*, 472(2186), p. 20150745.

Arulanandan, K. and Scott, R.F. (1993) 'Verification of Numerical Procedures for the Analysis of Soil Liquefaction Problems'. *International Conference on the Verification of Numerical Procedures for the Analysis of Soil Liquefaction Problems (1993: Davis, Calif.). AA Balkema.*

Arulanandan, K. and Sybico, J. (1992) 'Post-Liquefaction Settlement of Sand-Mechanism and in Situ Evaluation'. *Technical Report NCEER*, 1(92–0019), pp. 239–53.

ASTM. (2016) 'D4254: Standard Test Methods for Minimum Index Density and Unit Weight of Soils and Calculation of Relative Density.' *West Conshohocken, PA, USA: ASTM International.*

ASTM. (2014) 'D854: Standard Test Methods for Specific Gravity of Soil Solids by Water Pycnometer.' *West Conshohocken, PA, USA: ASTM International.*

Badanagki, M., Dashti, S., Paramasivam, B. and Tiznado, J.C. (2019) 'How Do Granular Columns Affect the Seismic Performance of Non-Uniform Liquefiable Sites and Their Overlying Structures?' *Soil Dynamics and Earthquake Engineering*, 125, p. 105715.

Badanagki, M., Dashti, S. and Kirkwood, P. (2018) 'Influence of Dense Granular Columns on the Performance of Level and Gently Sloping Liquefiable Sites'. *Journal of*

Geotechnical and Geoenvironmental Engineering, 144(9), p. 04018065.

Baez, J.I. and Martin, G.R. (1993) 'Advances in the Design of Vibro Systems for the Improvement of Liquefaction Resistance'. *Symposium Ground Improvement*, pp. 1–16.

Bahadori, H., Farzalizadeh, R., Barghi, A. and Hasheminezhad, A. (2018) 'A Comparative Study between Gravel and Rubber Drainage Columns for Mitigation of Liquefaction Hazards'. *Journal of Rock Mechanics and Geotechnical Engineering*, 10(5), pp. 924–934.

Balakrishnan, A. (2000) *Liquefaction Remediation at a Bridge Site*.

Bertalot, D., Brennan, A. and Villalobos, F. (2013) 'Influence of Bearing Pressure on Liquefaction-Induced Settlement of Shallow Foundations'. *Géotechnique*, 63(5), pp. 391–399.

Bertalot, D. and Brennan, A.J. (2015) 'Influence of Initial Stress Distribution on Liquefaction-Induced Settlement of Shallow Foundations'. *Géotechnique*, 65(5), pp. 418–428.

Bhuiyan, M. Z. I., Ali, F. H. and Salman, F. A. (2015). Application of recycled concrete aggregates as alternative granular infills in hollow segmental block systems. *Soils and Foundations*, 55(2), 296-303.

Boussinesq, J. (1883) *Application Des Potentiels à L'étude de L'équilibre et Du Mouvement DesSolides Élastiques*. Paris: Gauthier-Villars.

Brennan, A. (2004) *Vertical Drains as a Countermeasure to Earthquake-Induced Soil Liquefaction.* PhD Thesis, University of Cambridge, United Kingdom.

Brennan, A. and Madabhushi, G.S.P. (2011) 'Measurement of Coefficient of Consolidation during Reconsolidation of Liquefied Sand'. *Geotechnical Testing Journal*, 34(2), pp. 139–146.

Brennan, A.J., Madabhushi, G.S.. and Houghton, N.E. (2006) 'Comparing Laminar and Equivalent Shear Beam (ESB) Containers for Dynamic Centrifuge Modelling'. *Proceedings of the 6th International Conference ICPMG*, 6, pp. 171–176.

Brennan, A.J. and Madabhushi, G.S.P. (2002) 'Effectiveness of Vertical Drains in Mitigation of Liquefaction'. *Soil Dynamics and Earthquake Engineering*, 22(9–12), pp. 1059–1065.

BSI. (1990) 'BS 1377-4: Methods of Test for Soils for Civil Engineering Purposes. Part 4: Compaction-Related Tests'.

Castro, G. (1975) 'Liquefaction and Cyclic Mobility of Saturated Sands'. *Journal of the Geotechnical Engineering Division*, 101(6), pp. 551–569.

Castro, J. and Sagaseta, C. (2011) 'Deformation and Consolidation around Encased Stone Columns'. *Geotextiles and Geomembranes*, 29(3), pp. 268–276.

Coelho, P., Haigh, S., Madabhushi, G.S.P. and O'Brien, T. (2004) 'Centrifuge Modeling of the Use of Densification as a Liquefaction Resistance Measure for Bridge Foundations'. *In 13th World Conference on Earthquake Engineering*, p. 15.

Dashti, S., Bray, J.D., Pestana, J.M., Riemer, M. and Wilson, D. (2010a) 'Centrifuge Testing

to Evaluate and Mitigate Liquefaction-Induced Building Settlement Mechanisms'. *Journal of Geotechnical and Geoenvironmental Engineering*, 136(7), pp. 918–929.

Dashti, S., Bray, J.D., Pestana, J.M., Riemer, M. and Wilson, D. (2010b) 'Mechanisms of Seismically Induced Settlement of Buildings with Shallow Foundations on Liquefiable Soil'. *Journal of Geotechnical and Geoenvironmental Engineering*, 136(1), pp. 151–164.

Florin, V.A. and Ivanov, P.L. (1961) 'Liquefaction of Saturated Sandy Soils.' *The 5th International Conference on Soil Mechanics and Foundation Engineering.*, pp. 107–111.

Franzius, J. (2003) *Behaviour of Buildings Due to Tunnel Induced Subsidence*. PhD Thesis, Imperial College of Science, Technology and Medicine.

Garala, T.K., Madabhushi, G.S.P. and Di Laora, R. (2020) 'Experimental Investigation of Kinematic Pile Bending in Layered Soils Using Dynamic Centrifuge Modelling'. *Géotechnique*, pp. 1–16.

García-Torres, S. and Madabhushi, G.S.P. (2020) 'Inclined Perimeter Drains Performance as Liquefaction Countermeasure Techniques Below Existing Buildings'. *Journal of Earthquake and Tsunami*, p. 2050015.

García-Torres, S. and Madabhushi, G.S.P. (2019).

Geng, L., Tang, L., Cong, S.Y., Ling, X.Z. and Lu, J. (2017) 'Three-Dimensional Analysis of Geosynthetic-Encased Granular Columns for Liquefaction Mitigation'. *Geosynthetics International*, 24(1), pp. 45–59.

Ghajj, K., Dilrukshi, A.L.A. and Subasinghe, N.N. (2008) 'Study on Advantages of Using Coir Dust in Vertical Drains for the Improvement of Soft Clay'. *Women's Career Advancement and Training & Development in the Construction Industry*, p. 1343.

Ghosh, B. (2003) *Behaviour of Rigid Foundation in Layered Soils during Seismic Liquefaction.* PhD Thesis, University of Cambridge, United Kingdom.

Gunaratne, M. (2006) *The Foundation Engineering Handbook*. Taylor & Francis - Boca Raton, Florida.

Haigh, S.K., Eadington, J. and Madabhushi, G.S.P. (2012) 'Permeability and Stiffness of Sands at Very Low Effective Stresses'. *Géotechnique*, 62(1), pp. 69–75.

Haji, T. (2017) *Evaluating the Effects of Tunnel Construction on Buildings*. PhD Thesis, University of Nottingham.

Hamada, M. and Wakamatsu, K. (1996) 'Liquefaction, Ground Deformation and Their Related Damage to Structures'. *The 1995 HyogokenNanbu Earthquake—Investigation into Damage to Civil Engineering Structures, JSCE, Tokyo.*

Hardin, B. and Drnevich, V. (1972) 'Shear Modulus and Damping in Soils: Design Equations and Curves'. *Journal of Soil Mechanics and Foundations Division*, 98(sm7).

Hausler, E. and Sitar, N. (2001) 'Dynamic Centrifuge Testing of Improved Ground'. *15th Intern. Conf. on Soil Mechanics and Geotechnical Engineering, Istanbul, Turkey.*

Hausler, E.A. and Sitar, N. (2001) 'Performance of Soil Improvement Techniques in Earthquakes'. *Proc. Fourth Int. Conf. on Recent Advances in Geotechnical Earthquake Engineering and Soil Dynamics San Diego, CA, USA.*

Hazarika, H., Sugano, T., Kikuchi, Y., Yasuhara, K., Murakami, S., Takeichi, H., Karmokar,

A.K., Kishida, T. and Mitarai, Y. (2007) ‘Sandwiched Backfilling Technique for Earthquake Protection of Geotechnical Structures’.

Hazen, A. (1892) *Some Physical Properties of Sands and Gravels: With Special Reference to Their Use in Filtration, Publisher Not Identified*.

Heron, C.M. (2013) *The Dynamic Soil Structure Interaction of Shallow Foundations on Dry Sand Beds*. PhD Thesis, University of Cambridge, United Kingdom.

Howell, R., Rathje, E.M., Kamai, R. and Boulanger, R. (2012) ‘Centrifuge Modeling of Prefabricated Vertical Drains for Liquefaction Remediation’. *Journal of Geotechnical and Geoenvironmental Engineering*, 138(3), pp. 262–271.

Howell, R. (2013) *The Performance of Lateral Spread Sites Treated with Prefabricated Vertical Drains: Physical and Numerical Models.* PhD Thesis, The University of Texas at Austin.

Howell, R., Rathje, E.M. and Boulanger, R.W. (2015) ‘Evaluation of Simulation Models of Lateral Spread Sites Treated with Prefabricated Vertical Drains’. *Journal of Geotechnical and Geoenvironmental Engineering*, 141(1).

Idriss, I. and Boulanger, R. (2004) ‘Semi-Empirical Procedures for Evaluating Liquefaction Potential during Earthquakes.’ *The 11th ICSDEE & 3rd ICEGE. Berkeley, CA, USA.*, pp. 32–56.

Ishihara, K. (1993) ‘Liquefaction and Flow Failure during Earthquakes’. *Geotechnique*, 43(3), pp. 351–451.

Ishihara, K. (1985) ‘Stability of Natural Deposits during Earthquakes’. *International Conference on Soil Mechanics and Foundation Engineering*, 11, pp. 321–376.

Ishihara, K., Tatsuoka, F. and Yasuda, S. (1975) ‘Undrained Deformation and Liquefaction of Sand under Cyclic Stresses’. *Soils and Foundations*, 15(1), pp. 29–44.

Ishihara, K. and Yoshimine, M. (1992) ‘Evaluation of Settlements in Sand Deposits Following Liquefaction during Earthquakes’. *Soils and Foundations*, 32(1), pp. 173–188.

Kawasaki, K., Sakai, T., Yasuda, S. and Satoh, M. (1998) ‘Earthquake-Induced Settlement of an Isolated Footing for Power Transmission Tower’. *Centrifuge*, 98, pp. 271–276.

Kirmani, S.M.H. (2004) ‘CONSOLIDATION OF SOIL FOR FOUNDATION BY USING SAND DRAINS’. *IEP-SAC Journal 2005*.

Kutter, B., Carey, T., Hashimoto, T., Zeghal, M., Abdoun, T., Kokkali, P., Madabhushi, G.S.P., Haigh, S.K., D’Arezzo, F.B., Madabhushi, S.S.C., Hung, W.Y., Lee, C.J., Cheng, H.C., Iai, S., Tobita, T., Ashino, T., Ren, J., Zhou, Y.G., Chen, Y.M. *et al.* (2018) ‘LEAP-GWU-2015 Experiment Specifications, Results, and Comparisons’. *Soil Dynamics and Earthquake Engineering*, 113, pp. 616–628.

Lambe, T. and Whitman, R. (1991) *Soil Mechanics*. John Wiley & Sons.

Ledesma, E., Jiménez, J. and Ayuso, J. (2015) ‘Maximum Feasible Use of Recycled Sand from Construction and Demolition Waste for Eco-Mortar Production–Part-I: Ceramic Masonry Waste’. *Journal of Cleaner*, 87, pp. 692–706.

Lee, F.H. (1985) *Centrifuge Modelling of Earthquake Effects on Sand Embankments and Islands*. PhD Thesis, University of Cambridge, United Kingdom.

Liu, K.W. and Rowe, R.K. (2015) 'Numerical Modelling of Prefabricated Vertical Drains and Surcharge on Reinforced Floating Column-Supported Embankment Behaviour'. *Geotextiles and Geomembranes*, 43(6), pp. 493–505.

Liu, L. and Dobry, R. (1997) 'Seismic Response of Shallow Foundation on Liquefiable Sand'. *Journal of Geotechnical and Geoenvironmental Engineering*, 123(6), pp. 557–567.

Luong, M.P. and Sidaner, J.F. (1981) 'Undrained Behaviour of Cohesionless Soils under Cyclic and Transient Loading'. *In 1st International Conference on Recent Advances in Geotechnical Earthquake Engineering and Soil Dynamics. University of Missouri-Rolla, St. Louis, USA.*, pp. 215–220.

Madabhushi, S. P. G., Houghton, N.E. and Haigh, S.K. (2006) 'A New Automatic Sand Pourer for Model Preparation at University of Cambridge'. In *Proceedings of the 6th International Conference on Physical Modelling in Geotechnics*. Taylor & Francis Group, London, UK., pp. 217–222.

Madabhushi, G. and Haigh, S. (2012) 'How Well Do We Understand Earthquake Induced Liquefaction?' *Indian Geotechnical Journal*, 42(3), pp. 150–160.

Madabhushi, G.S.P. (2014) *Centrifuge Modelling for Civil Engineers*. Taylor & Francis, London.

Madabhushi, G.S.P., Haigh, S.K., Houghton, N.E. and Gould, E. (2012) 'Development of a Servo-Hydraulic Earthquake Actuator for the Cambridge Turner Beam Centrifuge'. *International Journal of Physical Modelling in Geotechnics*, 12(2), pp. 77–88.

Mitchell, J.K., Baxter, C.D. and Munson, T.C. (1995) 'Performance of Improved Ground during Earthquakes'. *Soil Improvement for Earthquake Hazard Mitigation*, pp. 1–36.

Mitrani, H. (2006) *Liquefaction Remediation Techniques for Existing Buildings*. PhD Thesis, University of Cambridge, United Kingdom.

Mitrani, H. and Madabhushi, G.S.P. (2005) 'Centrifuge Tests Investigating Inclined Grout Micro-Piles as a Method of Liquefaction Remediation for Existing Buildings'. *In Earthquake Engineering and Soil Dynamics*, pp. 1–12.

Mitrani, H. and Madabhushi, G.S.P. (2012) 'Rigid Containment Walls for Liquefaction Remediation'. *Journal of Earthquake and Tsunami*, 6(4).

Mizutani, T., Towhata, I., Shinkawa, N., Ibi, S. and Komatsu, T. (2001) 'Shaking Table Tests on Mitigation of Liquefaction-Induced Subsidence of River Dikes'. *International Conference on Soil Mechanics and Geotechnical Engineering*, pp. 1207–1210.

Murugesan, S. and Rajagopal, K. (2010) 'Studies on the Behavior of Single and Group of Geosynthetic Encased Stone Columns'. *Journal of Geotechnical and Geoenvironmental Engineering*, 136(1), pp. 129–139.

Nataatmadja, A. and Tan, Y.L. (2001) 'Resilient Response of Recycled Concrete Road Aggregates'. *Journal of Transportation Engineering*, 127(5), pp. 450–453.

Okamura, M., Tomida, Y., Okamoto, T. and Yasuhara, H. (2012) 'Remedial Measure for Highway Embankments on Liquefaction Prone Foundation'. *Second International Conference on Performance-Based Design in Earthquake Geotechnical Engineering*.

Olarte, J., Paramasivam, B., Dashti, S., Liel, A. and Zannin, J. (2017) 'Centrifuge Modeling

of Mitigation-Soil-Foundation-Structure Interaction on Liquefiable Ground'. *Soil Dynamics and Earthquake Engineering*, 97, pp. 304–323.

Olarte, J.C., Dashti, S., Liel, A.B. and Paramasivam, B. (2018) 'Effects of Drainage Control on Densification as a Liquefaction Mitigation Technique'. *Soil Dynamics and Earthquake Engineering*, 110, pp. 212–231.

Onoue, A. (1988) 'Consolidation by Vertical Drains Taking Well Resistance and Smear into Consideration.' *Soils and Foundations*, 28(4), pp. 165–174.

Onoue, A., Mori, N. and Takano, J.U.N. (1987) 'In-Situ Experiment and Analysis on Well Resistance of Gravel Drains.' *Soils and Foundations*, 27(2), pp. 42–60.

Orense, R.P., Morimoto, I., Yamamoto, Y., Yumiyama, T., Yamamoto, H. and Sugawara, K. (2003) 'Study on Wall-Type Gravel Drains as Liquefaction Countermeasure for Underground Structures'. *Soil Dynamics and Earthquake Engineering*, 23(1), pp. 19–39.

Paramasivam, B., Dashti, S. and Liel, A. (2018) 'Influence of Prefabricated Vertical Drains on the Seismic Performance of Structures Founded on Liquefiable Soils'. *Journal of Geotechnical and Geoenvironmental Engineering*, 144(10).

Pestana, J.M., Hunt, C. and Goughnour, R. (1997) 'FEQDrain: A Finite Element Computer Program for the Analysis of the Earthquake Generation and Dissipation of Pore Water Pressure in Layered Sand Deposits with Vertical Drains'. *EERC Research Rep. No. 97*, (17).

Port and Harbour Research Institute. (1997) *Handbook on Liquefaction Remediation of Reclaimed Land*. AA Balkema.

Rasouli, R., Towhata, I., Rattez, H. and Vonaesch, R. (2018) 'Mitigation of Nonuniform Settlement of Structures Due to Seismic Liquefaction'. *Journal of Geotechnical and Geoenvironmental Engineering*, 144(11).

Rasouli, R., Hayashida, T. and Towhata, I. (2012) 'Experimental Study on Subsidence of Surface Structures Due to Liquefaction and Its Mitigation'. *Proceedings of 1st International Symposium on Earthquake Engineering,Tokyo, Japan*, 1, pp. 8–10.

Rasouli, R., Towhata, I. and Akima, T. (2016) 'Experimental Evaluation of Drainage Pipes as a Mitigation against Liquefaction-Induced Settlement of Structures'. *Journal of Geotechnical and Geoenvironmental Engineering*, 142(9).

Rasouli, R., Towhata, I. and Hayashida, T. (2014) '1-g Shaking Table Tests on Mitigation of Seismic Subsidence of Structures'. *Proceedings of the International Conference on Physical Modeling in Geotechnics.*

Rollins, K.M. and Seed, H.B. (1990) 'Influence of Buildings on Potential Liquefaction Damage'. *Journal of Geotechnical Engineering*, 116(2), pp. 165–185.

Roylance, D. (2001) *Finite Element Analysis*.

Schofield, A.N. (1980) 'Cambridge Geotechnical Centrifuge Operations'. *Géotechnique*, 30(3), pp. 227–268.

Schofield, A.N. (1981) 'Dynamic and Earthquake Geotechnical Centrifuge Modelling'. *Report No. D-SOILS/TR104, Technical Report, Cambridge University Engineering Department, UK.*

Schofield, A.N. and Wroth, C.P. (1968) *Critical State Soil Mechanics*. McGraw-Hill.

Scott, R. (1986) 'Solidification and Consolidation of a Liquefied Sand Column'. *Soils and Foundations*, 26(4), pp. 23–31.

Seed, H.B. (1981) 'Earthquake-Resistant Design of Earth Dams Earthquake-Resistant Design of Earth Dams'. *In First International Conference on Recent Advances in Geotechnical Earthquake Engineering & Soil Dynamics*, pp. 1157–1173.

Seed, H.B. (1979) 'Soil Liquefaction and Cyclic Mobility Evalution for Level Ground during Earthquakes'. *Journal of Geotechnical and Geoenvironmental Engineering*, 105(ASCE 14380).

Seed, H.B. and Booker, J.R. (1977) 'Stabilisation of Potentially Liquefiable Sand Deposits Using Gravel Drains'. *Journal of Geotechnical and Geoenvironmental Engineering*, 103(ASCE 13050), pp. 757-768.

Seed, H.B. and Idriss, I.M. (1971) 'Simplified Procedure for Evaluating Soil Liquefaction Potential'. *Journal of Soil Mechanics & Foundations Division*, 97(7), pp. 1249–1273.

Seed, H.B. and Lee, K.L. (1966) 'Liquefaction of Saturated Sands during Cyclic Loading'. *Journal of the Soil Mechanics and Foundations Division*, 92(6), pp. 105–134.

Shahir, H., Pak, A., Taiebat, M. and Jeremić, B. (2012) 'Evaluation of Variation of Permeability in Liquefiable Soil under Earthquake Loading'. *Computers and Geotechnics*, 40, pp. 74–88.

SIMULIA, A. (2014) '6.14.' *ABAQUS Analysis User's Manual.*

Sonu, C., Ito, K. and Oishi, H. (1993) 'Harry Seed, Liquefaction and the Gravel Drain'. *Civil Engineering*, 63(12), p. 58.

Stringer, M.E. and Madabhushi, S.P.G. (2009) 'Novel Computer-Controlled Saturation of Dynamic Centrifuge Models Using High Viscosity Fluids'. *Geotechnical Testing Journal*, 32(6), pp. 559–564.

Tajudin, A., Azhar, S., Yusof, F., Bakar, I., Marto, A., Zakaria, M.N. and Abdullah, M.E. (2015) 'Numerical Modeling of Prefabricated Vertical Drain for Soft Clay Using ABAQUS'. *Applied Mechanics and Materials*, 773, pp. 1502–1507.

Tang, L., Cong, S., Ling, X., Lu, J. and Ahmed, E. (2015) 'Numerical Study on Ground Improvement for Liquefaction Mitigation Using Stone Columns Encased with Geosynthetics'. *Geotextiles and Geomembranes*, 43(2), pp. 190–195.

Tatsuoka, F., Tomita, Y. I., Iguchi, Y. and Hirakawa, D. (2013). Strength and stiffness of compacted crushed concrete aggregate. *Soils and foundations*, 53(6), 835-852.

Tokimatsu, K., Tamura, S., Suzuki, H., Foundations, K.K.-S. and. and 2012, U. (2012) 'Building Damage Associated with Geotechnical Problems in the 2011 Tohoku Pacific Earthquake'. *Soils and Foundations*, 52(5), pp. 956–974.

Tokimatsu, K. and Seed, H.B. (1987) 'Evaluation of Settlements in Sands Due to Earthquake Shaking'. *Journal of Geotechnical Engineering*, 113(8), pp. 861–878.

Towhata, I. (2008) *Geotechnical Earthquake Engineering*. Springer, Berlin.

Towhata, I. and Rasouli, R. (2013) 'Attempts to Protect Personal Houses from Seismic Liquefaction Problem'. *Proc., 4th Int. Seminar on Forensic Geotechnical Engineering*,

pp. 191–209.

Vermeer, P. and Borst, D. (1984) ‘Non-Associated Plasticity for Soils, Concrete and Rock’. *HERON*, 29(3).

Vickers, C. (2001) *An Investigation of the Pore Size of Bone Graft as Used in Impaction Grafting Total Hip Arthoplasty*. MEng Project, University of Cambridge Department of Engineering.

Vytiniotis, A. (2009) *Numerical Simulation of the Response of Sandy Soils Treated with Pre-Fabricated Vertical Drains*. PhD Thesis, Massachusetts Institute of Technology.

Widiyanto, W., Santoso, P.B., Hsiao, S.-C. and Imananta, R.T. (2019) ‘Post-Event Field Survey of 28 September 2018 Sulawesi Earthquake and Tsunami’. *Nat. Hazards Earth Syst.*, 1, pp. 1–23.

Yasuda, S., Morimoto, I., Kiku, H. and Tanaka, T. (2004) ‘Reconnaissance Report on the Damage Caused by Three Japanese Earthquakes in 2003’. *Proceedings of 11th ICSDEE and 3rd ICEGE, Berkeley, CA, USA*, 1, pp. 14–21.

Yasuda, S. (2007) *Remediation Methods against Liquefaction Which Can Be Applied to Existing Structures*. Springer, Dordrecht.

Ye, G.B., Zhang, Z., Han, J., Xing, H.F., Huang, M.S. and Xiang, P.L. (2013) ‘Performance Evaluation of an Embankment on Soft Soil Improved by Deep Mixed Columns and Prefabricated Vertical Drains’. *Journal of Performance of Constructed Facilities*, 27(5), pp. 614–623.

Yoshimi, Y. and Tokimatsu, K. (1977) ‘Settlement of Buildings on Saturated Sand during Earthquakes’. *Soils and Foundations*, 17(1), pp. 23–38.

Youd, T.L. and Idriss, I.M. (2001) ‘Liquefaction Resistance of Soils: Summary Report from the 1996 NCEER and 1998 NCEER/NSF Workshops on Evaluation of Liquefaction Resistance of Soils’. *Journal of Geotechnical and Geoenvironmental Engineering*, 127(4), pp. 297–313.

Zeybek, A., Madabhushi, G. and Pelecanos, L. (2020) ‘Seismic Response of Partially Saturated Soils beneath Shallow Foundations under Sequential Ground Motions Offshore Wind Foundations View Project Buildings View Project Seismic Response of Partially Saturated Soils beneath Shallow Foundations under Sequent’. *Bulletin of Earthquake Engineering*, 18(5), pp. 1987–2002.

Zeybek, A. and Madabhushi, G.S.P. (2017) ‘Influence of Air Injection on the Liquefaction-Induced Deformation Mechanisms beneath Shallow Foundations’. *Soil Dynamics and Earthquake Engineering*, 97, pp. 266–276.

Appendix A.

Symmetry axes of the arrangement in SG3, SG4, SG5, SG6 and SG9 (top layer).

Test SG3

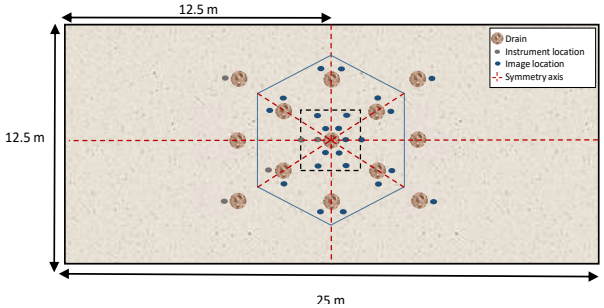

Test SG6, SG7 and SG8

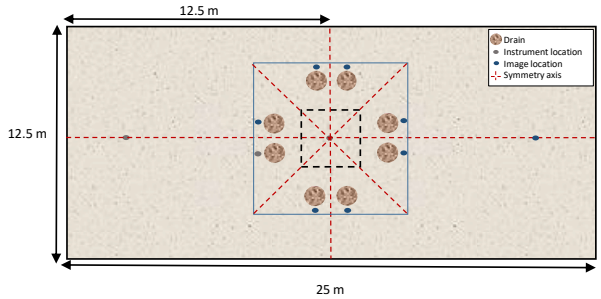

Test SG9

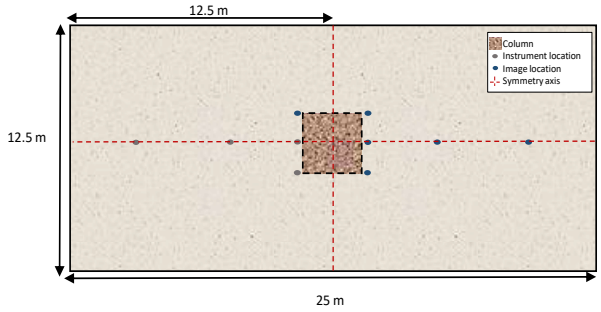

Appendix B.

Sensitivity analysis of *E* and *k* parameters for the seven different models of drain arrangements.

- Chart of results obtained in CM and NM using calibration factor of 1.3%*E* and k_d= 0.045m/s and 0.35 m/s (prototype scale).

Drain arrangement	Permeability*k* [m/s]	Total settlement NM [m]	Total settlement CM [m]	FF arrival times NM [s]				FF arrival times CM [s]			
				Internal drain/1.75 [m]	Edge Drains	Sub perimeter Drains	Perimeter Drain/5.2 [m]	Internal drain/1.75 [m]	Edge Drains	Sub perimeter Drains	Perimeter Drain/5.2 [m]
SG2	0.045 0.35	0.939 0.834	0.258	50.7 44.4	— —	— —	55.4 49.9	44.8	—	—	47.5
SG3	0.045 0.35	0.466 0.456	0.456	56.2 12.3	— —	77.2 32.0	56.2 39.0	25.6	—	26.0	40.9
SG3V	0.045 0.35	0.464 0.39	0.456	40.2 30.0	— —	50.2 38.3	— —	—	—	—	—
SG4	0.045 0.35	0.555 0.542	0.345	50.5 10.7	64.5 12.8	85.5 40.6	64.5 65.5	22.8	25.3	35.8	45.8
SG4V	0.045 0.35	0.488 0.453	0.345	37.4 26.6	37.4 32.8	49.9 42.2	— —	—	—	—	—
SG9	0.045 0.35	0.538 0.534	0.387	56.2 49.9	— —	— —	61.8 67.7	15.8	—	—	44.9
SG8	0.045 0.35	0.462 0.427	0.505	44.9 41.2	— —	— —	33.8 31.8	38.3	—	—	49.8

- Chart of results obtained in CM and NM using calibration factor of 1.6%E and k_d= 0.045m/s and 0.35 m/s (prototype scale).

Drain arrangement	Permeability$k$ [m/s]	Total settlement NM [m]	Total settlement CM [m]	FF arrival times NM [s]				FF arrival times CM [s]			
				Internal drain/1.75 [m]	Edge Drains	Sub perimeter Drains	Perimeter Drain/5.2 [m]	Internal drain/1.75 [m]	Edge Drains	Sub perimeter Drains	Perimeter Drain/5.2 [m]
SG2	0.045 0.35	0.787 0.678	0.258	52.2 37.4	— —	— —	54.8 49.9	44.8	—	—	47.5
SG3	0.045 0.35	0.392 0.382	0.456	49.6 9.1	— —	67.3 30.3	49.6 38.2	25.6	—	26.0	40.9
SG3V	0.045 0.35	0.391 0.355	0.456	44.9 26.6	— —	44.9 32.8	— —	—	—	—	—
SG4	0.045 0.35	0.467 0.452	0.345	43.8 9.3	54.9 10.2	71.8 37.2	54.9 53.8	22.8	25.3	35.8	45.8
SG4V	0.045 0.35	0.409 0.378	0.345	30.0 26.6	30.0 32.8	49.9 42.2	— —	—	—	—	—
SG9	0.045 0.35	0.449 0.447	0.387	56.2 46.1	— —	— —	56.2 61.8	15.8	—	—	44.9
SG8	0.045 0.35	0.387 0.356	0.505	44.9 38.3	— —	— —	33.8 31.8	38.3	—	—	49.8

- Chart of results obtained in CM and NM using calibration factor of 2%E and k_d= 0.045m/s and 0.35 m/s (prototype scale).

Drain arrangement	Permeability$k$ [m/s]	Total settlement NM [m]	Total settlement CM [m]	FF arrival times NM [s]				FF arrival times CM [s]			
				Internal drain/1.75 [m]	Edge Drains	Sub perimeter Drains	Perimeter Drain/5.2 [m]	Internal drain/1.75 [m]	Edge Drains	Sub perimeter Drains	Perimeter Drain/5.2 [m]
SG2	0.045 0.35	0.643 0.520	0.258	46.8 37.4	— —	— —	46.8 44.4	44.8	—	—	47.5
SG3	0.045 0.35	0.316 0.306	0.456	41.8 8.4	— —	55.8 30.1	55.8 37.9	25.6	—	26.0	40.9
SG3V	0.045 0.35	0.318 0.284	0.456	38.3 22.5	— —	50.7 26.6	— —	—	—	—	—
SG4	0.045 0.35	0.376 0.363	0.345	38.2 8.1	50.0 9.4	67.7 34.2	67.7 48.3	22.8	25.3	35.8	45.8
SG4V	0.045 0.35	0.330 0.302	0.345	30.0 22.5	30.0 26.6	38.3 32.8	— —	—	—	—	—
SG9	0.045 0.35	0.364 0.361	0.387	42.2 40.8	— —	— —	56.2 54.1	15.8	—	—	44.9
SG8	0.045 0.35	0.314 0.286	0.505	38.3 37.4	— —	— —	30.0 29.1	38.3	—	—	49.8

- Chart of results obtained in CM and NM using calibration factor of 4.5%E and k_d= 0.045m/s and 0.35 m/s (prototype scale).

Drain arrangement	Permeability$k$ [m/s]	Total settlement NM [m]	Total settlement CM [m]	FF arrival times NM [s]				FF arrival times CM [s]			
				Internal drain/1.75 [m]	Edge Drains	Sub perimeter Drains	Perimeter Drain/5.2 [m]	Internal drain/1.75 [m]	Edge Drains	Sub perimeter Drains	Perimeter Drain/5.2 [m]
SG2	0.045 0.35	0.366 0.195	0.258	5.0 5.0	— —	— —	45.8 35.1	44.8	—	—	47.5
SG3	0.045 0.35	0.144 0.136	0.456	37.4 6.9	— —	49.9 28.6	49.9 35.6	25.6	—	26.0	40.9
SG3V	0.045 0.35	0.148 0.127	0.456	24.4 19.8	— —	30.0 22.4	— —	—	—	—	—
SG4	0.045 0.35	0.171 0.162	0.345	27.6 6.9	45.1 7.5	60.9 32.0	60.9 36.9	22.8	25.3	35.8	45.8
SG4V	0.045 0.35	0.15 0.135	0.345	26.6 19.7	26.6 22.3	32.8 26.6	— —	—	—	—	—
SG9	0.045 0.35	0.167 0.164	0.387	38.3 37.1	— —	— —	50.7 48.9	15.8	—	—	44.9
SG8	0.045 0.35	0.144 0.128	0.505	29.9 29.9	— —	— —	29.9 24.4	38.3	—	—	49.8